TECHNISCHE UNIVERSITÄT MÜNCHEN

Fakultät für Chemie

Lehrstuhl für Biotechnologie

Investigation of the Hsp90 co-chaperone machinery in eukaryotes

Maximilian Michael BIEBL

Vollständiger Abdruck der von der Fakultät für Chemie der Technischen Universität München zur Erlangung des akademischen Grades eines Doktors der Naturwissenschaften (Dr. rer. nat.) genehmigten Dissertation.

Vorsitzende/-r:	Prof. Dr. Matthias Feige
Prüfende/-r der Dissertation:	1. Prof. Dr. Johannes Buchner
	2. Prof. Dr. Michael Sattler
	3. Prof. Dr. Ursula Jakob

Die Dissertation wurde am 22.09.2020 bei der Technischen Universität München eingereicht und durch die Fakultät für Chemie am 18.11.2020 angenommen.

Contents

List of Figures

List of Tables

Abbreviations

β-ME β-Mercaptoethanol
ADH Alcohol Dehydrogenase
ADP Adenosine-5′-diphosphate
Aha1 Activator of Hsp90 ATPase homolog 1
AMP-PNP Adenosine-5′-(β, γ-imido)-triphosphate
AP Antarctic Phosphatase
APS Ammonium Persulfate
AR Androgen Receptor
ATP Adenosine-5′-triphosphate
ATPγS Adenosine-5′-(γ-thio)-triphosphate
aUC Analytical Ultracentrifugation
BFP Blue Fluorescent Protein
CFTR Cystic Fibrosis Transmembrane Conductance Regulator
CNPY3 Canopy Fibroblast Growth Factor Signaling Regulator 3
Co-IP co-immunoprecipitation
CRISPR Clustered Regularly Interspersed Short Palindromic Repeats
CS CHORD-Sgt1
CSP Chemical Shift Perturbation
CST Cytometer Setup and Tracking
CTD C-terminal Domain
CV Column Volume
DAmP Decreased Abundance by mRNA Perturbation
DBD DNA Binding Domain
DEX Dexamethason
DMEM Dulbecco's Modified Eagle Medium
DNA Deoxyribonucleic acid
DOL Degree of Labeling
DTT 1,4-Dithiotreitol
DUF Domain of Unknown Function
E. coli Escherichia coli
EDTA Ethylendiamintetraacetic acid
eEF2 Eukaryotic Elongation Factor 2
ERAD ER-Associated Degradation

F-DEX Dexamethasone Fluorescein
FACS Fluorescence-Activated Cell Sorting
FANCA Fanconi Anaemia, Complementation Group A
FBS Fetal Bovine Serum
FKBP FK506 binding protein
FLCN Folliculin
FNIP1/2 Folliculin-Interacting Protein 1/2
FRET Förster Resonance Energy Transfer
gDNA Genomic DNA
GR Glucocorticoid Receptor
GRE Glucocorticoid Response Element
GR-LBD Glucocorticoid Receptor Ligand Binding Domain
Grp94 94 kDa Glucose-Regulated Protein
HAT Hydroxyapatite
Hop Hsc70-Hsp90 Organizing Protein
Hsp Heat Shock Protein
Hsp70 Heat Shock Protein 70
Hsp90 Heat Shock Protein 90
HSR Heat Shock Response
HtpG High Temperature Protein G
IPTG Isopropyl-β-D-thiogalactopyranoside
KD Knockdown
KO Knockout
LB Lysogeny Broth
MD Middle Domain
MR Mineralocorticoid Receptor
NAC Nascent Polypeptide-Associated Complex
NEF Nucleotide Exchange Factor
NMR Nuclear Magnetic Resonance
NTD N-terminal Domain
NudC Nuclear Migration Protein C
PBS Phosphate Buffered Saline
PCR Polymerase Chain Reaction
PDI Protein Disulfide Isomerase
PIE Pulsed Interleaved Excitation
PMSF Phenylmethylsulfonyl fluoride
Pp5 Protein Phosphatase 5
PPIase Peptidyl-prolyl-cis/trans-isomerase
Ppt1 Serine/Threonine Protein Phosphatase T
PTM Post-Translational Modification
pTyr Phosphotyrosine
PVDF Polyvinylidene Fluoride

RAC Ribosome-Associated complex
S. cerevisiae Saccharomyces cerevisiae
SD Synthetic Defined
SDS Sodium Dodecyl Sulfate
SDS-PAGE Sodium Dodecyl Sulfate Polyacrylamide Gel Electrophoresis
SEC Size Exclusion Chromatography
SEC-MALS Size Exclusion Chromatography with Multi Angle Light Scattering
SGA Synthetic Genetic Array
sgRNA single guide RNA
SHR Steroid Hormone Receptor
SLIC Sequence and Ligation Independent Cloning
STAT-1 Signal Transducer and Activator of Transcription 1
Sti1 Stress-Inducible 1
TAE Tris-Acetate-EDTA
TBE-PAGE Tris-Borat-EDTA Polyacrylamide Gel Electrophoresis
TBS Tris-Buffered Saline
TCA Trichloroacetic Acid
TEMED N,N,N′,N′-Tetramethylethylendiamin
TF Trigger Factor
TLR Toll-like Receptor
TPR Tetratricopeptide Repeat
Trap1 tumor necrosis factor receptor associated protein 1
Tsc1/2 Tuberculosis Sclerosis Complex 1/2

Summary

1.1 The Epistatic Network of Hsp90 Co-Chaperones in Yeast

Hsp90 is an ATP-dependent molecular chaperone conserved from bacteria to man. By aiding the folding, maturation and assembly of a large variety of substrates ('clients'), including steroid hormone receptors (SHRs) and protein kinases, it is considered a central hub of proteostasis in the cell. For its function, Hsp90 is assisted by a cohort of co-chaperones. Previous studies have shown that different clients require the function of distinct subsets of co-chaperones. Yet, how the co-chaperones co-operate has remained unknown. Here, we generated a library of 110 Hsp90 co-chaperone double mutants and analyzed them concerning viability and the maturation of the gluococorticoid receptor (GR), mineralocorticoid receptor (MR) and v-Src kinase. Within a network of loose genetic interactions, we identified central epistatic modules regulating protein translation, kinase maturation and SHR activation. For kinase maturation, the bridging of Hsp70 and Hsp90 by the co-chaperone Sti1/Hop is essential for maturation, while for SHRs the regulation of the dwell time on Hsp90 by Aha1 and Hch1 is important, stressing the specific requirements of clients. Hence, the Hsp90 co-chaperome is characterized by plastic genetic networks that are fine-tuned for the specific needs of each client.

1.2 Screening for Novel Hsp90 Co-Factors in Mammalian Cells

While yeast Hsp90 is assisted by 12 known co-chaperones, the co-chaperome expanded from yeast to man where more than 25 co-chaperones are known and new co-chaperones are still being identified. For many of these co-chaperones, the influence on Hsp90 function and client maturation has remained elusive. To comprehensively study the effect of known Hsp90 modulators and to identify novel Hsp90 co-factors, we here developed a CRISPRi (clustered regularly interspersed short palindromic repeats interference)-based screening platform using a fluorescent reporter system for SHR activity. Screening a library biased for proteostasis factors, we identified several known modulators of SHRs as well as novel Hsp90 co-chaperone candidates. Individual knockdown of several hits confirmed the influence on client

maturation and validated the screening system. The modulators identified for different SHRs in the same cell line were similar, whereas significant differences of the SHR regulation became evident between cell lines, suggesting a cell line-specific regulation of SHRs. Together, a powerful screening system for Hsp90-associated modulators was developed that could be extended for different classes of clients.

1.3 The Hsp90 Co-Chaperone NudC

Several Hsp90 clients require the initial processing by the Hsp40-Hsp70 system and the subsequent transfer of the client to Hsp90 for activation. While it is known that Sti1/Hop functions as an adapter between Hsp70 and Hsp90 and facilitates client transfer, the mechanistic details and the regulation of this process are currently unknown. We found NudC as a for an Hsp90-dependent SHR modulator during CRISPRi screening. Similarities of the interactome of NudC and Hop that were detected in high-throughput interactome studies, this prompted us to investigate the effect of NudC on Hsp90 client maturation. Loss of NudC affects the maturation of GR in *in vitro* and *in vivo* and is important for cellular viability. NudC forms a stable dimer and binds to Hsp40 and Hsp90. Binding of NudC to client-bound Hsp40:Hsp70 complexes facilitates the release of Hsp70 and accelerates the transfer of clients to Hsp90. Taken together, NudC is a *bona fide* co-chaperone of Hsp40 and Hsp90 and to our best knowledge the first known accelerator of client handover from Hsp70 to Hsp90.

1.4 Das Epistatische Netzwerk der Hsp90 Co-Chaperone in Hefe

Hsp90 ist ein ATP-abhängiges molekulares Chaperon, das von Prokaryoten bis zum Menschen konserviert ist. Durch die Unterstützung der Faltung, Reifung und Assemblierung einer Vielzahl von Substraten ('Klienten'), einschließlich Steroidhormonrezeptoren (SHRs) und Proteinkinasen, gilt es als zentraler Knotenpunkt der Proteostase in der Zelle. In seiner Funktion wird Hsp90 von einer Vielzahl an Co-Chaperonen unterstützt. Frühere Studien hatten gezeigt, dass verschiedene Klienten die Funktion unterschiedlicher Kombinationen von Co-Chaperonen benötigen. Wie die Co-Chaperone zusammenarbeiten, ist weitgehend unerforscht. In dieser Arbeit wurde eine Bibliothek von 110 Hsp90-Co-Chaperon-Doppelmutanten generiert und diese wurden hinsichtlich Lebensfähigkeit und der Reifung des Glukokortikoidrezeptors, des Mineralokortikoidrezeptors und der v-Src Kinase analysiert. Innerhalb eines Netzwerks schwacher genetischer Interaktionen wurden zentrale epistatische Module identifiziert, die die Proteintranslation, Kinase-Reifung und SHR-Aktivierung regulieren. Für die Kinase-Reifung ist die Verbindung von Hsp70 und Hsp90 durch das Co-Chaperon Sti1/Hop essentiell für die Reifung, während für die SHRs die Regulation der Verweildauer der Rezeptoren an Hsp90 durch Aha1

und Hch1 wichtig ist. Diese Ergebnisse unterstreichen die spezifischen Anforderungen von Klienten. Folglich zeichnet sich das Hsp90-Co-Chaperom durch plastische genetische Netzwerke aus, die auf die spezifischen Bedürfnisse von Klienten abgestimmt sind.

1.5 Screening Nach Hsp90 Co-Faktoren in Säugetierzellen

Während Hsp90 in Hefe von 12 bekannten Co-Chaperonen unterstützt wird, expandierte das Co-Chaperom von der Hefe zum Menschen, bei dem mehr als 25 Co-Chaperone bekannt sind und noch immer neue Co-Chaperone identifiziert werden. Für viele dieser Co-Chaperone ist der Einfluss auf die Funktion von Hsp90 und die Reifung der Klienten noch nicht charakterisiert. Um die Wirkung bekannter Hsp90 Modulatoren zu untersuchen und neue Hsp90 Co-faktoren zu identifizieren, wurde eine CRISPRi (clustered regularly interspersed short palindromic repeats interference) basierte Screening Plattform entwickelt, die ein Fluoreszenz-basiertes Reportersystem für die SHR-Aktivität verwendet. Beim Screening einer CRISPRi Bibliothek für Proteostase-assoziierte Proteine konnten mehrere bekannte Modulatoren von SHRs sowie neue Hsp90-Co-Chaperon Kandidaten gefunden werden. Der individuelle Knockdown mehrerer Hits bestätigte den Einfluss auf die Reifung der Klienten und validierte das Screeningsystem. Die für verschiedene SHRs in derselben Zelllinie identifizierten Modulatoren waren ähnlich, während zwischen den Zelllinien signifikante Unterschiede in der SHR-Regulation deutlich wurden, was auf eine Zelllinien-spezifische Regulation der SHRs schließen lässt. Zusammengefasst wurde ein leistungsfähiges Screeningsystem für Hsp90-assoziierte Modulatoren entwickelt, das auf verschiedene Klientenfamilien erweitert werden kann.

1.6 Das Hsp90 Co-Chaperon NudC

Mehrere Hsp90 Klientenproteine erfordern zunächst die Einflussnahme des Hsp40-Hsp70-Systems und die anschließende Übergabe des Klienten an Hsp90 zur Aktivierung. Während bekannt ist, dass Sti1/Hop als Adapter zwischen dem Hsp70- und dem Hsp90-System fungiert und die Übergabe des Klienten erleichtert, sind die mechanistischen Details und die Regulation des Prozesses noch unbekannt. Durch CRISPRi-Screening identifizierten wir NudC als einen Kandidaten für einen Hsp90-abhängigen SHR-Modulator. Zusammen mit Ähnlichkeiten des Interaktoms von NudC und Hop, die in Hochdurchsatz-Interaktom-Studien entdeckt wurden, veranlasste uns dies, die Wirkung von NudC auf die Reifung der Klienten zu untersuchen. Der Verlust von NudC beeinträchtigt die Reifung von GR *in vitro* und *in vivo* und NudC ist wichtig für das zelluläre Überleben. NudC bildet ein stabiles Dimer und bindet an Hsp40 und Hsp90. Die Bindung von NudC an Klienten-gebundene Hsp40:Hsp70 Komplexe erleichtert die Freisetzung von Hsp70 und beschleunigt den Transfer von Klienten zu Hsp90. Zusammengenommen zeigen die Ergebnisse, dass

NudC ein *bona fide* Co-Chaperon von Hsp40 und Hsp90 ist und der erste bekannte Beschleuniger für die Übergabe von Klienten von Hsp70 an Hsp90 ist.

Introduction

2.1 Protein Folding and Misfolding

Cellular integrity is maintained by proteins, ranging from cellular stability conferred by cytoskeletal proteins, over intracellular transport by highly sophisticated molecular motors to metabolic processes catalyzed by extremely versatile enzymes. A mammalian cell expresses between 10,000 and 20,000 different proteins (Balchin et al., 2016), which are all synthesized as linear macromolecules, with a length of up to more than 1000 amino acids. While 20% to 30% of proteins remain in a largely unfolded state, referred to as intrinsically disordered proteins (Dunker et al., 2002), the majority of proteins needs to acquire a unique three-dimensional fold to be functional.

Due to the astronomical number of possible protein backbone orientations, sampling of all conformations to find the best state would exceed the age of the universe for most proteins. Yet, proteins usually fold on short timescales. This apparent paradox has been coined 'Levinthal's paradox' (Levinthal, 1968; Levinthal, 1969). In our modern view, the thermodynamics of protein folding are represented as energy landscapes and the 'folding funnel' model (Figure 1) (Bryngelson et al., 1995; Onuchic et al., 1997). In this model the free energy of protein conformations is shown on the z-axis whereas the lateral axes reflect the different possible conformations. A large number of unfolded protein conformations with high free energy exist. Based on the idea of stochastic sampling of conformational states (Dobson, 2004; Zwanzig et al., 1992), different folding trajectories down the 'folding funnel' are possible that lead to a smaller number of possible states and lower free energy conformations at the bottom of the funnel (Onuchic and Wolynes, 2004). Intermediate folding states may occur and manifest as local kinetic traps along the funnel surface (Dill and Chan, 1997).

Small proteins may fold rapidly on smooth free-energy surfaces without intermediates (Jackson, 1998). By contrast, rate-limiting steps such as prolyl *cis/trans* isomerization or disulfide bond formation pose substantial kinetic barriers during

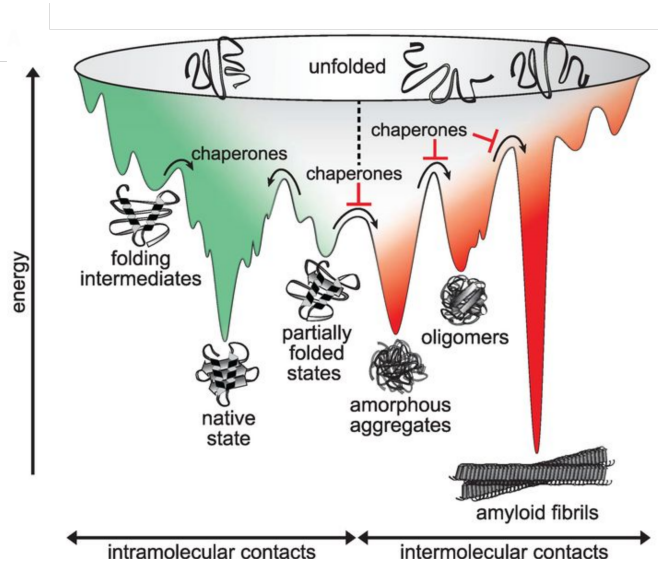

FIGURE 1 | **Folding Funnel Model for Protein Folding and Aggregation.**
The free-energy surface is depicted showing possible fates of an unfolded protein with the z-axis representing the enthalpy and the x- and y-axes showing the entropy (not depicted). During folding, proteins follow downhill trajectories to reach a low free-energy state with low entropy. Proteins can populate intermediates of the rugged free-energy surface, in which hydrophobic stretches may be exposed, increasing the risk of off-pathway aggregation. Aggregation can be suppressed by chaperones and productive folding is generally facilitated by chaperones. From Balchin et al., 2016.

the folding especially of large proteins. Hence, these proteins usually populate intermediates and require several steps to reach the native fold (Brockwell and Radford, 2007). One of the key driving forces of protein folding is the burial of hydrophobic residues into the core of the protein (Ohgushi and Wada, 1983; Pace et al., 1996; Baldwin and Rose, 2013). Yet, in folding intermediates hydrophobic stretches may be partly exposed posing the risk of forming non-native intramolecular contacts and in particular intermolecular interactions leading to aggregation. Some aggregated proteins like Alzheimer's-associated tau protein or α-synuclein implicated in Parkinson's disease may form very stable amyloid fibers, characterized by β-sheets stacked perpendicular to the long axis of the fibril (Chiti and Dobson, 2006). The concentration-dependent nature of protein aggregation exacerbates the problem in cells due to the high physiological protein concentration of approximately 200-300 mg mL^{-1} (Kiefhaber et al., 1991; Ellis and Minton, 2006). Excluded volume effects due to molecular crowding and thus, reduced entropic freedoms of proteins favor the formation of compact, aggregated states over the generally less compact native folds (Ellis and Minton, 2006; Hong and Gierasch, 2010). Molecular chaperones (Section 2.3) evolved to prevent the formation of aggregates and promote native folding *in vivo* (Pelham, 1986; Ellis, 1990).

To retain the high conformational dynamics required for their function, most native proteins are only 5-10 kcal mol^{-1} more stable than their denatured state (Ghosh and Dill, 2010). Consequently, even under physiological conditions and especially

under stress conditions, a substantial fraction of the proteome may transiently become partially unfolded and prone to deleterious aggregation. The detrimental effects of protein aggregation affect cytoskeletal integrity, organelle localization, intracellular transport, metabolic changes and nuclear processes, ultimately leading to cell cycle arrest and potentially cell death (Richter et al., 2010; Verghese et al., 2012). Besides the apparent loss of activity of aggregated proteins, the toxicity of aggregates seems to be caused by disruption of membrane integrity and perturbation of calcium homeostasis (Janson et al., 1999; Chiti and Dobson, 2006). Of note, it has been suspected that toxicity is caused by smaller oligomers and aggregates species rather than mature high molecular weight complexes (Holmes et al., 2014; Verma et al., 2015; Xie and Jakob, 2019). To counteract these harmful consequences of protein unfolding especially under stress, cells orchestrate a cellular response termed the Heat Shock Response (HSR) (Lindquist, 1986; Richter et al., 2010).

2.2 The Heat Shock Response

The HSR was first identified as puffing patterns of *D. busckii* chromosomes after stress in the 1960s (Ritossa, 1962). The HSR is initiated by a variety of different stressors including heat stress to protect the cell (Lindquist and Craig, 1988; Richter et al., 2010). It has been shown that the induction of the HSR, independent of the nature of the stressor, is particularly important to protect the cell against subsequent stress by conferring 'acquired stress resistance' (Parsell et al., 1993). To that end, the HSR governs a transcriptional program regulating more than 3000 genes under severe heat shock in yeast including genes responsible for stress protection and genes counterbalancing the increased protein aggregation and degradation during stress (Gasch et al., 2000; Larkindale and Vierling, 2008; Matsuura et al., 2010; Mühlhofer et al., 2019). The affected genes contain regulators of cellular metabolism, DNA repair, transcription factors and proteins responsible to sustain cellular structure (Richter et al., 2010). Yet, the predominant class of stress-inducible genes across different species are the initially discovered heat shock proteins (Hsps), also referred to as molecular chaperones (Section 2.3) (Ellis, 1990; Gething and Sambrook, 1992; Jakob and Buchner, 1994; Buchner, 1996).

Primarily, the HSR in yeast is regulated by two transcription factors, Hsf1 and Msn2/4 that have partially overlapping target spectra (Martinez-Pastor et al., 1996; Morimoto, 1998; Gasch et al., 2000). Vertebrates express four members of the Hsf family, from which Hsf1 plays the predominant role in regulating the expression of Hsps. In yeast, only Hsf1 is present and essential for survival under all conditions, while it seems to be dispensible in mammalian cells in the absence of stress (Sarge et al., 1993; Solis et al., 2016). Different models for the regulation of Hsf1 have been proposed. In the 'titration model', Hsf1 is kept inactive by molecular chaperones under physiological conditions. It becomes active, when the chaperones have to deal with the increased load of unfolded proteins under stress conditions (Guo

et al., 2001; Voellmy and Boellmann, 2007). In unstressed mammalian cells, Hsf1 is monomeric and trimerizes upon stress to become active, while in yeast, Hsf1 is present in a constitutively trimerized, active state (Sorger et al., 1987; Jakobsen and Pelham, 1988; Sorger and Pelham, 1988; Clos et al., 1990; Rabindran et al., 1993). In line with this notion it was found that Hsf1 is essential even under physiological conditions in yeast due to its simulating effect on the expression of the molecular chaperones Hsp70 and Hsp90 (Solis et al., 2016). Yet, the core function of Hsf1 is conserved between mammals and yeast since a constitutively active form of human Hsf1 can rescue the loss of yeast Hsf1 (Liu et al., 1997). Subsequent to trimerization, phosphorylation of Hsf1 is required to efficiently regulate gene expression (Cotto et al., 1996; Zheng et al., 2016). Of note, a role of Hsp90 in controlling Hsf1 dynamics by removing it from heat shock elements in DNA has been reported as a negative feedback mechanism (Kijima et al., 2018).

2.3 Molecular Chaperones and Protein Folding

Exposure of cells to stress increases the load of unfolded, misfolded and aggregated proteins. Yet, even under non-stress conditions, proteins may unfold and thus mechanisms to maintain proteostasis are required. Two systems act in synergism to maintain cellular proteostasis - the ubiquitin-proteasome system that clears damaged, short-lived proteins and the molecular chaperone system capturing folding intermediates to prevent misfolding and aggregation (Jolly and Morimoto, 2000). Importantly, both systems are connected, ensuring that terminally unfolded proteins are poised for proteosomal degradation (Hayes and Dice, 1996; Shiber and Ravid, 2014).

Molecular chaperones are defined as proteins aiding in protein folding or the assembly of protein complexes without being part of the final conformation (Laskey et al., 1978; Schopf et al., 2017; Balchin et al., 2020). Some chaperones are stress-induced, while others are constitutively expressed and they can be ATP-dependent or act independently of ATP. Historically, chaperones have been classified according to their molecular weight - Hsp40s, Hsp60s, Hsp70s, Hsp90s, Hsp100s and small heat shock proteins (sHsps) (Gething and Sambrook, 1992; Buchner, 1996). Interestingly, recently it was shown that throughout evolution the complexity of the proteome increased exponentially, while the core-chaperones such as Hsp60, Hsp70, Hsp90 and Hsp100 expanded linearly (Rebeaud et al., 2020). The needs of the increased proteome complexity are met by the increased cellular abundance of the core-chaperones and most importantly by the emergence of new co-factors and expansion of existing co-factor families regulating the core-chaperones (Rebeaud et al., 2020)

The first set of chaperones a nascent chain encounters at the ribosome exit tunnel are ribosome-associated chaperones including the Ribosome-Associated Complex (RAC) and the Nascent Polypeptide Associated Complex (NAC) in eukaryotes (Balchin et al., 2016; Deuerling et al., 2019). In the cytosol, the Hsp40/Hsp70

system binds nascent chains and coordinates handover to downstream folding machineries such as the chaperonins (Hsp60s) and Hsp90. Chaperonins (GroEL/ES in *E. coli*, TRiC/CCT in humans) form barrel-shaped cavities trapping substrates to fold in a secluded environment shielded from the cellular proteome (Kim et al., 2013; Hayer-Hartl et al., 2016). Hsp90 represents a central hub in the cell responsible for the maturation of a variety of clients, that will be discussed in detail in Section 2.5. Other chaperone systems include the Hsp40-Hsp70 system (Section 2.4) and the Hsp70-Hsp100 bi-chaperone system in prokaryotes and yeast that has evolved as a disaggregase in the cell (Parsell et al., 1994; Rosenzweig et al., 2013; Saibil et al., 2013; Mogk et al., 2015). By contrast, sHsps form heterogeneous oligomer assemblies usually comprising 2 to 40 monomers and act as holdases of early-unfolded substrates, which rely on other ATP-dependent chaperones such as Hsp70 to refold trapped susbtrates (Mogk and Bukau, 2017; Mogk et al., 2019; Haslbeck et al., 2019; Janowska et al., 2019). Additionally, chaperones that catalyze certain rate-limiting steps during the folding process are in place to prevent aggregation. Most importantly, they include Peptidyl-Prolyl *cis/trans* Isomerases (PPIases) and Protein Disulfide Isomerases (PDIs) (Wilkinson and Gilbert, 2004; Schmidpeter and Schmid, 2015).

In summary, an elaborate proteostasis system comprising a variety of different chaperones has evolved to ensure the maturation of nascent proteins, but also to keep folded substrates in an active state. Within the scope of this work, only the Hsp70 and Hsp90 systems will be discussed. The other chaperone systems have been reviewed in detail elsewhere (Wilkinson and Gilbert, 2004; Horwich et al., 2007; Kim et al., 2013; Saibil et al., 2013; Schmidpeter and Schmid, 2015; Balchin et al., 2016; Hayer-Hartl et al., 2016; Mogk et al., 2018; Dahiya and Buchner, 2019; Deuerling et al., 2019; Haslbeck et al., 2019; Janowska et al., 2019).

2.4 The Hsp40/Hsp70 System

Hsp70 is one of the most versatile chaperones in the cell, fulfilling several stress-related and housekeeping activities. They include *de novo* protein folding, membrane translocation, prevention of aggregation, the disaggregation and refolding of substrates and the disassembly of protein complexes (Mayer and Bukau, 2005; Kampinga and Craig, 2010; Young, 2010; Rosenzweig et al., 2019). To that end, Hsp70s associate with a variety of different cellular systems: Hsp70 binds to the ribosome as part of the RAC system, with Hsp100s as a bi-chaperone disaggregase system, with small Hsps (sHsps) for the disassembly of aggregates and they hand over substrates to downstream processing chaperone systems such as chaperonins and most importantly Hsp90.

In yeast, four cytosolic Hsp70 homologs (Ssa1-4) are found that are highly homologous and differ mainly in their expression levels (Boorstein et al., 1994) (Table 1). Ssa2 is constitutively expressed at high levels, Ssa1 has a low basal expression

that is increased during stress and the expression of Ssa3 and Ssa4 is entirely stress-induced (Kabani and Martineau, 2008). Additionally, yeasts harbor three ribosome-associated Hsp70 isoforms (Ssb1, Ssb2 and Ssz1) (Boorstein et al., 1994). The homologue Ssc1 is restricted to mitochondria and Ssd1/Kar2 is localized in the ER (Werner-Washburne and Craig, 1989). In humans, 13 Hsp70 homologues are expressed, differing in their expression levels and cellular localization (Rosenzweig et al., 2019). The most important members of this family comprise six cytosolic Hsp70 isoforms (HspA1A, HspA1B, HspA1L, HspA2, HspA6, HspA8/Hsc70) and an additional ribosome-associated isoform (HspA14/Hsp70L1) (Daugaard et al., 2007) (Table 1). The localization of binding protein (Bip) / glucose-regulated protein (Grp78) and mtHsp70/Grp75 are confined to the ER and the mitochondrial matrix, respectively (Tavaria et al., 1996).

TABLE 1: Hsp70 Homologs in Yeast and Humans

Subcellular Localization	**Hsp70 Homolog**	
	Yeast	*Human*
Cytosol	Ssa1	HspA1A
	Ssa2	HspA1B
	Ssa3	HspA1L
	Ssa4	HspA2
		HspA6
		HspA8/Hsc70
Ribosome-associated	Ssb1	HspA14/Hsp70L1
	Ssb2	
	Ssz1	
ER	Ssd1/Kar2	Grp78/Bip/HspA5
Mitochondria	Ssc1	mtHsp70/Grp75

References: Kabani and Martineau, 2008; Radons, 2016; Rosenzweig et al., 2019

2.4.1 The Structure and Allosteric Cycle of Hsp70

Most Hsp70 homologs share common structural features with the archetypal bacterial Hsp70 orthologue DnaK (Bertelsen et al., 2009; Kityk et al., 2012). These include the N-terminal 45 kDa nucleotide binding domain (NBD), which is attached via a short linker to the substrate binding domain (SBD) and a flexbile C-terminal tail of variable length (Figure 2A) (Radons, 2016). The SBD is split into a 15 kDa substrate binding part (SBDβ) and a 10 kDa α-helical lid domain (SBDα) (Figure 2B). In eukaryotic, cytsolic Hsp70, the C-terminal tail contains a terminal EEVD motif that interacts with different tetratricopeptide repeat (TPR)-containing co-factors (Section

2.5) (Zuiderweg et al., 2017). Of note, isoforms confined to mitochondria and the ER contain an N-terminal localization motif and lack the C-terminal EEVD motif (Daugaard et al., 2007). Instead, the ER-resident Hsp70 contains the KDEL ER-retention motif (Munro and Pelham, 1987).

2.4.1.1 Structural Features of Hsp70s

The NBD is composed of four subdomains forming a two-lobed structure with a deep cleft (Figure 2B) (Flaherty et al., 1990). The binding of ATP to the bottom of the cleft leads to the coordination of all subdomains (Mayer and Bukau, 2005; Woo et al., 2009; Alderson et al., 2016; Rosenzweig et al., 2019). The SBDβ contains a β-sandwich structure that forms a peptide binding cavity (Zhu et al., 1996). C-terminal to the substrate binding part of the SBD lies the Hsp70 lid (SBDα) comprising five α-helices that interact with the β-sandwich SBD through hydrogen-bonds and ionic interactions (Sharma and Masison, 2009). The interaction of the SBDα and SBDβ domains is ATP-dependent, with the peptide binding cavity being enclosed in the ADP- and apo-state and the lid being undocked in the ATP-bound state.

2.4.1.2 The Conformational Cycle of Hsp70

The controlled binding and release of substrate polypeptides is a prerequisite of chaperones to promote the spontaneous folding of target proteins. The Hsp70 allosteric cycle is driven by nucleotide binding and hydrolysis (Szabo et al., 1994; McCarty et al., 1995; Laufen et al., 1999; Jiang et al., 2005). Additionally, Hsp70s never function alone and are further modulated by J-domain proteins (JDPs) and nucleotide exchange factors (NEFs) (Figure 2C) (Laufen et al., 1999; Cyr, 2008). In the ATP-bound state, the SBD has a low affinity (K_D = 1 - 10 µM) for substrates that interact with high association and dissociation rates (Swain et al., 2007; Kityk et al., 2012; Qi et al., 2013b; Rosenzweig et al., 2019). In this state, the SBDα and SBDβ domains separate and clamp to opposing faces of the the NBD due to the linker being able to dock into a crevice formed by the NBD after structural rearrangements in response to ATP binding (Figure 2B) (Kityk et al., 2012; Qi et al., 2013b). As a consequence, the ATPase activity is efficiently blocked leading to the low overall ATPase rate of approximately $6 \times 10^{-4}\,s^{-1}$ (Mayer and Bukau, 2005). Binding of a substrate peptide into the SBDβ cavity releases the SBD from the NBD promoting ATP hydrolysis and the subsequent closing of the SBDα lid resulting in a 10-fold increase in substrate binding affinity and drastic decrease of association and dissociation rates (Figure 2C) (Ha et al., 1997; Mayer et al., 2000; Jiang et al., 2005). Notably, in addition to the release of the SBD from the NBD, also the linker slips out of the NBD cavity resulting in a sub-optimal conformation for ATP hydrolysis, resulting in only moderate activation of the ATPase rate by substrate binding (Mayer and Gierasch, 2019). Intriguingly, it has been suggested that J-domains stimulate the ATPase by modulating linker positioning (Section 2.4.3). The exchange of ADP for ATP to close the

conformational cycle is promoted by NEFs (Section 2.4.4). In summary, ATP hydrolysis in Hsp70s is modulated by co-factors as well as substrate binding and entails large conformational changes that affect the substrate binding characteristics.

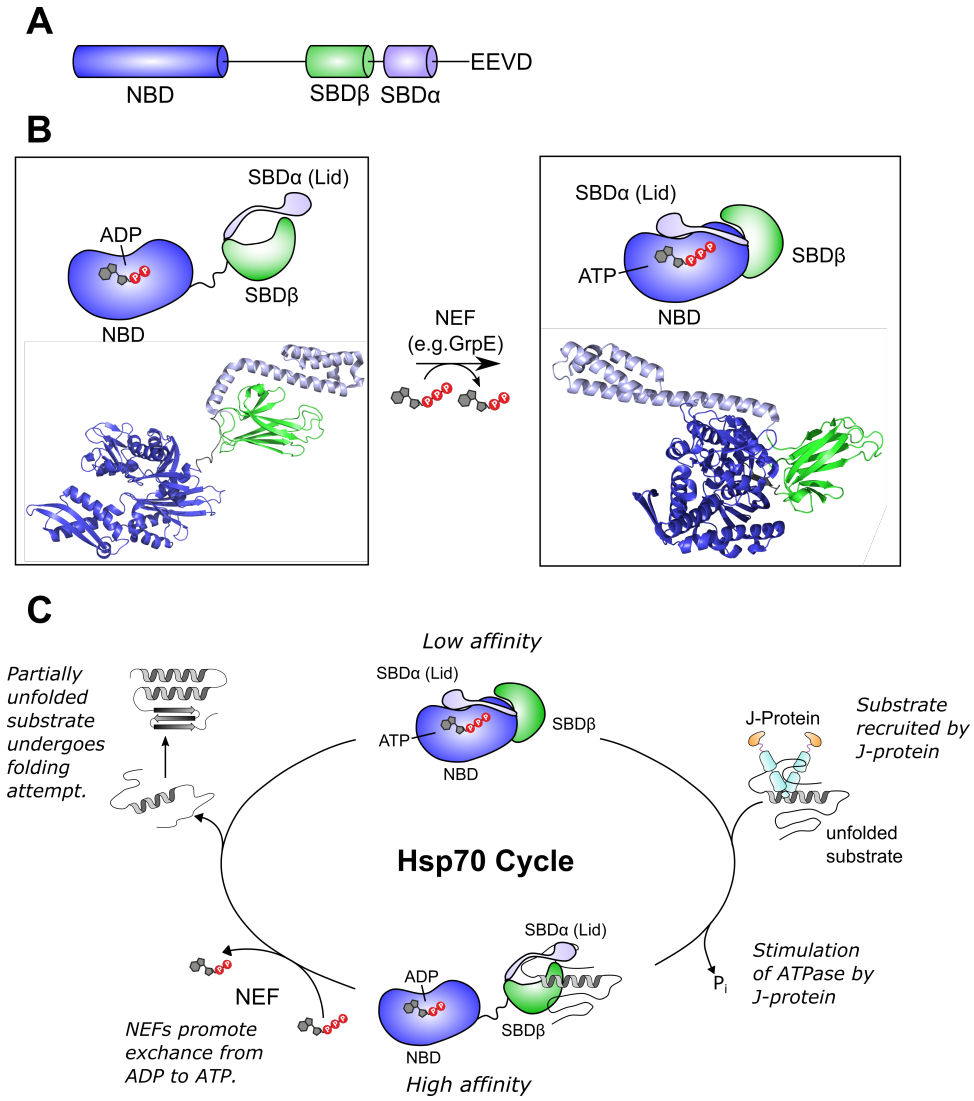

FIGURE 2 | **The Structure and Allosteric Cycle of Hsp70.**
A Schematic domain architecture of cytosolic Hsp70. Hsp70 confined to the ER or mitochondria additionally harbor N-terminal localization motifs. The C-terminal EEVD motif is not present in ER-localized and mitochondrial Hsp70. ER Hsp70 contains the KDEL ER-retention signal at the C-terminus.
B The conformations of ADP-bound and ATP-bound Hsp70 are shown as schematic models (top) and as crystal structures of *E. coli* DnaK (bottom) (ADP-bound, PDB: 2KHO; ATP-bound, PDB: 4B9Q).
C The nucleotide-dependent conformational cycle of Hsp70 is shown in the presence of partially unfolded substrate. J-domain proteins (Section 2.4.3) recruit substrate proteins to ATP-bound Hsp70 and facilitate ATP hydrolysis, switching Hsp70 to the high affinity ADP-bound state. Nucleotide exchange factors promote the exchange of ADP to ATP entailing the release of partially unfolded substrate. The substrate can then undergo a folding attempt and may either reach a native state or be fed into the Hsp70 cycle again.
[NBD: nucleotide binding domain; SBD: substrate binding domain; NEF: nucleotide exchange factor]

2.4.2 Hsp70 Substrate Recognition

Analysis of peptide binding to members of the Hsp70 family showed, that Hsp70 binds extended, five-residue stretches that contain hydrophobic amino acids typically buried in the hydrophobic core and only exposed in partially unfolded proteins (Figure 3) (Flynn et al., 1989; Knarr et al., 1995; Knarr et al., 1999; Zhu et al., 1996; Rüdiger et al., 1997). The hydrophobic peptide binds into the hydrophobic groove of the SBDβ and is additionally stabilized by hydrogen bonds to the substrate backbone and interactions with the SBDα lid (Zhu et al., 1996; Pellecchia et al., 2000; Stevens et al., 2003). Different studies hint towards substrates in an at least partially unfolded state when bound to Hsp70, in particular by the disruption of long-range tertiary contacts (Sekhar et al., 2015; Mashaghi et al., 2016; Sekhar et al., 2016; Rosenzweig et al., 2017). Importantly, for some substrates such as the glucocorticoid receptor (GR) and p53 the transient unfolding by Hsp40/Hsp70 is important to maintain their function (Kirschke et al., 2014; Morán Luengo et al., 2018; Dahiya et al., 2019). In conclusion, Hsp70 binds exposed hydrophobic stretches and exerts unfolding pressure on proteins, thus enabling the substrate to escape from kinetic traps in the folding pathway and reshaping the energy surface (Mashaghi et al., 2016; Sekhar et al., 2016; Rosenzweig et al., 2017).

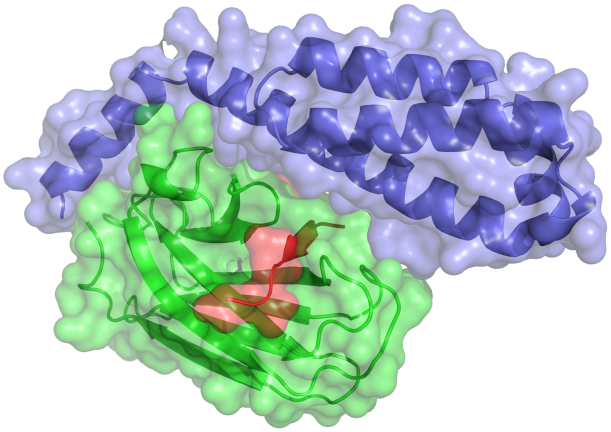

FIGURE 3 | **The Structure of Substrate Peptide Bound to Hsp70.**
The binding of a NRLLLTG peptide (red) to the Hsp70 SBDα (blue) and SBDβ (green) is shown (PDB: 1DKX).

2.4.3 The Regulation of Hsp70 by J-proteins

2.4.3.1 Three J-Domain Protein Classes

One of the major families of Hsp70 regulators are JDPs often referred to as Hsp40s. JDPs expand the functional diversity of Hsp70s for example by tethering Hsp70 to membranes or ribosomes and delivering substrates to Hsp70, thus affecting substrate specificity (Kampinga and Craig, 2010). In humans, 41 structurally and functionally diverse JDPs are known, contrasting the rather high conservation of Hsp70s

and stressing the multifunctionality conferred by JDPs (Craig et al., 2006). The class-defining feature of JDP is a common approximately 70 residue long α-helical hairpin domain, named J-domain after the archetype bacterial DnaJ (Greene et al., 1998; Kelley, 1998; Jiang et al., 2007). Depending on the identity and presence of additional domains, JDPs have been divided into the more closely related classes A and B and the very diverse class C (Figure 4A) (Cheetham and Caplan, 1998; Ohtsuka and Hata, 2000; Hageman and Kampinga, 2009; Rosenzweig et al., 2019). Class A JDPs (e.g. yeast Ydj1, human DNAJA1) comprise the J-domain at the N-terminus, followed by a G/F-rich linker, two C-terminal β-sandwich domains (CTD-I and CTD-II) and a C-terminal dimerization domain (DD) (Figure 4A,B) (Cheetham and Caplan, 1998; Walsh et al., 2004; Wu et al., 2005; Barends et al., 2013). A zinc-finger-like region is embedded into the CTD-I region (Linke et al., 2003; Fan et al., 2005). Class B JDPs (e.g. yeast Sis1, human DNAJB1) have a similar architecture, yet lack the zinc-finger-like region and in some cases carry different subdomains (Cheetham and Caplan, 1998; Walsh et al., 2004). Lastly, class C JDPs share only the J-domain but have high variation in length and domain architecture (Kampinga and Craig, 2010).

2.4.3.2 The Allosteric Effects of J-Domain Proteins on Hsp70

The ability of JDPs to bind Hsp70 and activate its ATPase lies within the J-domain, in particular in the conserved HPD-motif located in the loop between the two main helices (Figure 4) (Kelley, 1998; Suh et al., 1998; Jiang et al., 2007). In the currently accepted model, substrate triggers the dissociation of the SBDβ from the NBD, which allows the NBD to transition to its ATPase-competent state (Swain et al., 2007; Kityk et al., 2018). Binding of the J-domain prevents the linker from slipping out of the crevice in the NBD, which would lead to a NBD conformation that is less efficient for ATP hydrolysis (Suh et al., 1998; Vogel et al., 2006; Kityk et al., 2018). Additionally, interaction of the HPD motif with a hydrogen bond network positions the catalytic residues in a better position for ATP hydrolysis (Kityk et al., 2018). As a consequence, substrate and JDPs synergistically activate the Hsp70 ATPase activity (Mayer and Gierasch, 2019). Of note, the JDP-induced conformation of Hsp70 seems to be very dynamic (Wu et al., 2020). Intriguingly, while the HPD motif is strictly conserved, JDPs known to interact with specialized Hsp70s (e.g. ribosome-associated isoforms) exhibit modifications in adjacent regions of the J-domain that bind the concomitant non-classical interaction sites on the cooperating Hsp70 (Kityk et al., 2018; Mayer and Gierasch, 2019; Rosenzweig et al., 2019). To summarize, JDPs act in synergism with substrates, keeping the Hsp70 NBD in an ATPase-competent state, thus stimulating the Hsp70 ATPase.

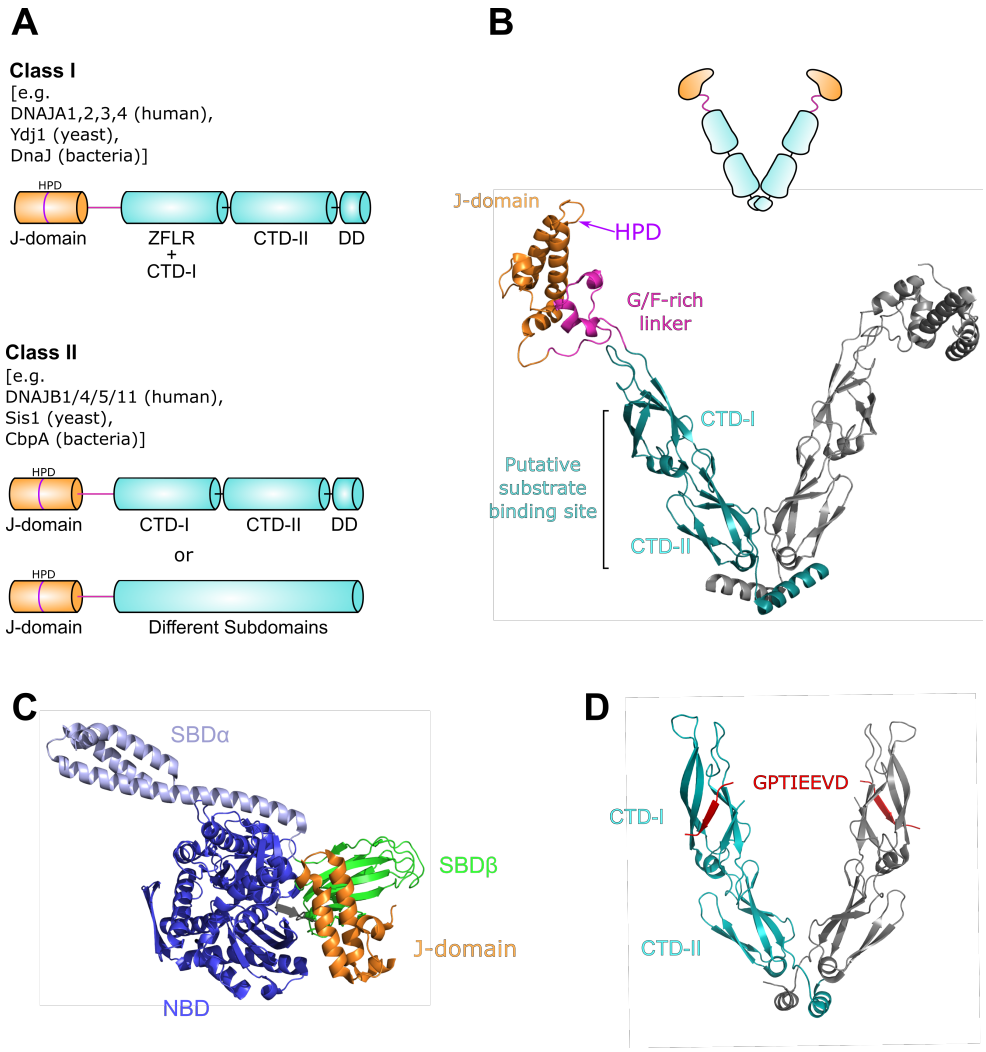

FIGURE 4 | **The Structure of J-Domain Proteins.**
A The domain organization of class A and class B J-domain proteins (JDPs) is shown. Well known members of each class are included.
B A schematic representation (top) and crystal structure (bottom) of *Thermus thermophilus* (PDB: 4J80) DnaJ is shown.
C The structure of a complex between the *E. coli* DnaJ J-domain and DnaK (PDB: 5NRO). The J-domain binds Hsp70 via the HPD motif interacting with the interface between the Hsp70 NBD and SBDβ on top of the linker that connects both domains.
D The crystal structure of DNAJB1 complexed with the C-terminal Hsp70 peptide (PDB: 3AGY) is depicted. The peptide forms a single β-strand that binds a groove in the CTD-I domain.
[CTD: C-terminal domain; DD: Dimerization domain; SBD: Substrate binding domain; NBD: Nucleotide binding domain]

2.4.3.3 J-Domain Independent Contacts to Hsp70

Additional contacts outside of the J-domain further modulate the function Hsp70 in some JDPs. In particular, the C-terminal EEVD motif of cytosolic Hsp70 was shown to form secondary contacts with some JDPs (e.g. yeast Sis1, human DNAJB1, DNAJA2) while other JDPs have been reported to not bind the Hsp70 EEVD motif (e.g. yeast Ydj1, human DNAJA1) (Freeman et al., 1995; Aron et al., 2005; Li et al., 2006; Yu et al., 2015b). It was found that the interaction of Hsp70-EEVD with Sis1 is

crucial for *in vitro* model substrate refolding, suggesting that Sis1 is less efficient in transferring substrate to Hsp70s bound to downstream processing factors due to the blocked EEVD motif (Yu et al., 2015b). Sis1, as opposed to Ydj1 forms a salt bridge between the J-domain and the G/F-linker that is responsible for the observed effects, even though the exact mechanism is not clear (Yu et al., 2015b). Similar results have also been obtained for the human paralogs (Yu et al., 2015a). Taken together, these results show that binding of the Hsp70 C-terminus to Hsp40s provides an additional regulatory layer.

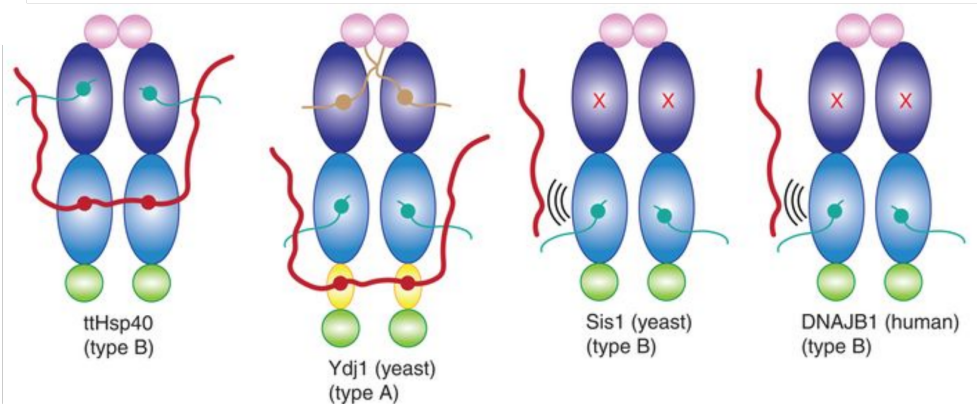

FIGURE 5 | **The Competitive Binding of the Hsp70 C-tail and Substrates to JDPs.** The binding of substrate (red) and the Hsp70 C-terminal EEVD motif (cyan) to different JDPs is shown. Substrate and the C-tail may bind simultaneously or compete for binding depending on the type of JDP. In *Thermus thermophilus* Hsp40 (ttHsp40), substrate is bound to CTD-I (light blue) while the EEVD stretch attaches to CTD-II (purple). In Ydj1, inter-protomer autoinhibition (brown) blocks CTD-II, but substrate can bind the zinc-finger-like domain (yellow). In Sis1 and DNAJB1, C-tail peptide and substrate compete for CTD-I (indicated by three bent lines). From (Jiang et al., 2019). Reprinted with permission from AAAS.
[J-domain (green), zinc-finger-like-domain (yellow), CTD-I (light blue), CTD-II (purple), dimerization domain (pink), Hsp70 C-tail peptide (cyan), substrate (red), autoinhibitory tail (brown)].

The proposed binding site of the EEVD motif lies in the CTD-I or CTD-II region and EEVD binding competes with substrate binding (Figure 4D, 5) (Li et al., 2003; Li et al., 2006; Jiang et al., 2019). Of note, recently it was shown that EEVD binds distinct CTDs in different JDPs and the degree of competition with substrate varies between different JDPs (Jiang et al., 2019). For example, the Ssa1 C-tail binds the Ydj1 CTD-I domain, but substrate can still be bound in the zinc-finger-like domain of Ydj1 (Figure 5) (Jiang et al., 2019). By contrast, the Ssa1 C-tail competes with substrate binding to CTD-I in Sis1 (Figure 5) (Jiang et al., 2019). In *Thermus thermophilus* Hsp40, CTD-II binds the Hsp70 C-tail, while substrate is bound to the CTD-I domain (Figure 5) (Jiang et al., 2019). In summary, a complex interplay of simultaneous and competitive binding between Hsp40, Hsp70 and substrate has evolved to meet the needs of different substrates.

2.4.3.4 The Interaction of JDPs with Substrates and the Transfer to Hsp70

Since JDP-mediated transfer of substrates initiates the Hsp70 chaperone cycle to a large degree, JDPs define the Hsp70 substrate spectrum (Craig et al., 2006; Clerico et al., 2015; Craig and Marszalek, 2017). For DnaJ, an eight residue stretch enriched in hydrophobic and aromatic amino acids has been proposed as the recognition motif (Rüdiger et al., 2001; Jiang et al., 2019). Yet, differences in the substrate spectrum have become evident. For example, differences between the binding sites within a substrate protein have become evident for ERdj3, ERdj4 and ERdj5, which is important for the regulated degradation of terminally unfolded proteins (Behnke et al., 2016). As mentioned, the primary binding sites of substrates on JDPs lie within the CTD-I and CTD-II domains that expose a large hydrophobic cleft, in which the substrate can form an anti-parallel β-strand with the CTD-I/II β-sheets (Lee et al., 2002; Li et al., 2003; Li and Sha, 2005; Jiang et al., 2019). Additionally, a role of the G/F linker in regulating substrate binding is evident in some cases (Yan and Craig, 1999; Perales-Calvo et al., 2010). Intriguingly, distinct binding sites on a substrate show preference for one CTD or another, suggesting subtle differences in substrate binding between the CTDs (Jiang et al., 2019). Hence, the binding of Hsp40s to clients seems to be highly dynamic using multivalent binding sites. In such, the folding properties of substrates are altered by Hsp40 binding and unfolded stretches are presented to Hsp70. When Hsp40 associates with Hsp70, the C-terminal EEVD motif occupies potential substrate binding sites, thus decreasing the affinity of the substrate for Hsp40 (Li et al., 2003; Suzuki et al., 2010; Jiang et al., 2019). Some JDPs may stay associated with substrate and Hsp70 forming a trimeric complex (e.g. Ydj1) while others leave the complex (e.g. Sis1, DNAJB1) (Figure 2C, 5). In conclusion, JDPs bind exposed hydrophobic sequences with the CTD regions. Competition with the Hsp70 EEVD motif modulates JDP affinity for substrate and poises polypeptides for transfer from the JDP to Hsp70.

2.4.4 The Regulation of Hsp70 by Nucleotide-Exchange Factors

To function efficiently, the timed association and release of substrates to and from Hsp70 are crucial. After ATP hydrolysis and the concomitant transition of Hsp70 to the high-affinity state, release of substrate requires the exchange of ADP with ATP, which is facilitated by NEFs (Craig et al., 2006; Bracher and Verghese, 2015b; Mayer and Gierasch, 2019; Rosenzweig et al., 2019). Prokaryotes, mitochondria and chloroplasts rely on GrpE for nucleotide exchange (Bracher and Verghese, 2015a; Bracher and Verghese, 2015b). GrpE dimerizes via a long α-helical domain and wedges open the Hsp70 NBD with its β-sheet domain facilitating nucleotide release (Harrison et al., 1997). In the eukaryotic cytosol, NEFs belonging to the Bag, Hsp110 and Armadillo families are responsible for nucleotide exchange, from which the Bag family members increase the nucleotide exchange rate most efficiently (approx. 100-fold) (Gassler et al., 2001; Kampinga and Craig, 2010; Rosenzweig et al., 2019). Despite

lacking homology between the classes, they all stabilize a partially open Hsp70 NBD conformation, thus accelerating nucleotide exchange. To this end, Bag family members (e.g. yeast Snl1; human Bag1) use a conserved three-helix bundle BAG domain (Sondermann et al., 2001; Höhfeld and Jentsch, 1997; Takayama et al., 1999). Hsp110/Grp170 NEFs (e.g. yeast Sse1, Lhs1; human Hsp110, Grp170) belong to the Hsp70 superfamily and resemble the open Hsp70 state. They form NBD-to-NBD interactions with Hsp70s to promote nucleotide exchange (Polier et al., 2008). In Armadillo-type NEFs (e.g. yeast Fes1, Sil1; human HspBP1, Sil1/BAP), the Armadillo repeats mediate Hsp70 binding (Yan et al., 2011). For Armadillo-type NEFs, additionally an N-terminal substrate-mimicking domain has been found that facilitates substrate release from Hsp70 (Gowda et al., 2018). Taken together, despite structural differences of Hsp70 NEFs, they all rely on a conserved mechanism of stabilizing an open NBD state to promote nucleotide exchange and in addition by a second domain interacting with the SBD accelerate the release of substrates to allow spontaneous refolding, re-feeding into another cycle on Hsp70 or handover to downstream chaperone systems like the Hsp90 system.

2.5 The Hsp90 System

Hsp90 is central molecular chaperone and one of the most abundant proteins in the cell constituting 1-2% of the cellular proteome under non-stress conditions (Wiech et al., 1992; Taipale et al., 2010). Historically, Hsp90 was first discovered in complexes with steroid hormone receptors (SHRs) and protein kinases (Brugge and Erikson, 1977; Brugge et al., 1981; Pratt and Toft, 1997). While Hsp90 is upregulated during stress, it is essential also under physiological conditions, highlighting its central role in maintaining cellular proteostasis (Borkovich et al., 1989). Hsp90 may affect clients by facilitating folding and activation, promoting assembly of protein complexes or enhancing ligand binding (Figure 6) (Schopf et al., 2017). By now, hundreds of diverse clients have been found that affect central cellular pathways, including targets involved in cell growth and proliferation making Hsp90 a potential target for cancer treatment (Taipale et al., 2010; Trepel et al., 2010; Echeverría et al., 2011; Biebl and Buchner, 2019; Jaeger and Whitesell, 2019). Besides cancer, Hsp90 has also been associated with neurodegenerative diseases such as Alzheimer's, Parkinson's and Huntington's disease since some of the disease-driving proteins are Hsp90 clients (Bohush et al., 2019; Ferrari and Rüdiger, 2019; Gupta et al., 2020). Additionally, it was shown that Hsp90 and co-chaperones are involved in psychiatric disease (Baker et al., 2018; Criado-Marrero et al., 2018; Sabbagh et al., 2018). Consequently, much effort has been made to find biocompatible Hsp90 inhibitors (Neckers and Workman, 2012; Zuehlke et al., 2018). Notably, eukaryotic Hsp90 is the central part of a cellular machinery comprising several additional factors, so-called co-chaperones establishing Hsp90 as a flexible unit to meet the needs of its diverse client spectrum (Cox and Johnson, 2018). Since some co-chaperones have also been associated with disease

formation, inhibitors targeted against co-chaperones are also in development (Wang et al., 2006; Patwardhan et al., 2013; Shelton et al., 2017; Stiegler et al., 2017; Li et al., 2018; Sabbagh et al., 2018).

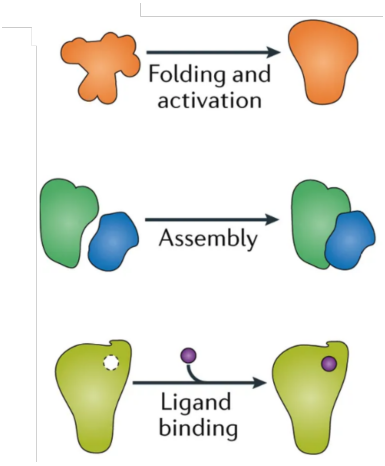

FIGURE 6 | **How Hsp90 Affects Clients.**
A schematic representation of ways in which Hsp90 can affect clients is shown. From (Schopf et al., 2017).

2.5.1 Hsp90 Evolution and Isoforms

Hsp90 is highly conserved from bacteria to humans (Chen et al., 2006). Archaea lack Hsp90, whereas bacteria usually contain one copy of Hsp90 such as *E. coli* high temperature protein G (HtpG) (Chen et al., 2006). *S. cerevisiae* contains a constitutively expressed Hsp90 paralogue, 82 kDa heat shock cognate (Hsc82), and a stress inducible isoform, 82 kDa heat shock protein (Hsp82), which are homologous to the constitutively expressed and heat-induced Hsp90β and Hsp90α in *Homo sapiens*, respectively (Chen et al., 2006; Johnson, 2012). The constitutive and heat-induced Hsp90 isoforms substantially overlap functionally, yet some distinct functions have been identified in yeast and humans (Morano et al., 1999; Millson et al., 2007; Girstmair et al., 2019; Reidy and Masison, 2020). While *E. coli* HtpG is not essential even under heat-stress conditions, at least one copy of *S. cerevisiae* Hsp90 is required for viability, stressing the increased importance of the Hsp90 system from prokaryotes to eukaryotes (Bardwell and Craig, 1988; Borkovich et al., 1989).

Additionally, organelle-specific Hsp90 family members have evolved in higher eukaryotes. In humans, tumor necrosis factor receptor associated protein 1 (Trap1) is present in the mitochondrial matrix and 94 kDa glucose-regulated protein (Grp94) is located in the ER (Johnson, 2012). Moreover, extracellular and cell surface-associated Hsp90α has sparked interest in the past due to its interaction with matrix metalloproteinases, thus modulating cell migration and cancer cell invasiveness (Sidera et al., 2004; Clayton et al., 2005; Li et al., 2007; Wong and Jay, 2016). Mitochondrial TRAP1 has been linked to Parkinson's disease and cancer formation (Song et al.,

1995; Im, 2016; Masgras et al., 2017). It has been shown to antagonize the generation of reactive oxygen species (ROS), regulate mitochondrial permeability and may promote growth by suppressing apoptosis (Masuda et al., 2004; Hua et al., 2007; Im et al., 2007; Kang et al., 2007; Im, 2016). Furthermore, TRAP1 seems to regulate the balance between oxidative phosphorylation and aerobic glycolysis, emphasizing its role in cancerogenesis (Yoshida et al., 2013). ER-localized Grp94 is considerably better understood than TRAP1 and has also been implicated in different diseases (Biebl and Buchner, 2019). Grp94 is involved in the maturation of integrins, toll-like receptors (TLRs) and other secretory or membrane-associated targets (Randow and Seed, 2001; Yang et al., 2007; Staron et al., 2010; Liu et al., 2010). Interestingly, no general defects of cell-surface receptors have been found upon loss of Grp94, suggesting a rather specific function of Grp94 (Randow and Seed, 2001). A potential role in the maturation of immunoglobulins has been suggested, but is still discussed (Melnick et al., 1994; Liu and Li, 2008). While cytosolic Hsp90 function is modulated by a cohort of co-chaperones, no co-chaperones are known for TRAP1 and only a single co-chaperone, canopy fibroblast growth factor signaling regulator 3 (CNPY3) has been identified for Grp94 (Wakabayashi et al., 2006; Liu et al., 2010). In summary, evolution expanded the Hsp90 spectrum from bacteria to humans, providing an elaborate chaperone system regulating a variety of cellular pathways.

Intriguingly, Susan Lindquist and co-workers suspected that Hsp90 could also act as a driver of evolution by buffering the potentially detrimental effects of mutations in proteins by rescuing protein instability. Data from different species support this hypothesis, since loss of Hsp90 revealed masked phenotypes in model organisms (Rutherford and Lindquist, 1998; Queitsch et al., 2002; Jarosz and Lindquist, 2010; Rohner et al., 2013). Interestingly, in humans, Hsp90 has been shown to buffer genetic variation of Fanconi anaemia, complementation group A (FANCA) proteins, which are causative for Fanconi anemia (Karras et al., 2017). In this case, environmental stress unmasks detrimental phenotypes by engaging Hsp90 away from the disease-related protein and as a result leads to phenotypic variability in patients carrying the same mutations (Karras et al., 2017).

2.5.2 The Structure and Conformational Cycle of Hsp90

Despite different functions, all Hsp90 homologs have a conserved domain architecture consisting of three domains (Figure 7A,B) (Ali et al., 2006; Pearl and Prodromou, 2006): The N-terminal domain (NTD) responsible for ATP binding (Prodromou et al., 1997), the middle domain (MD) implicated in client binding and the C-terminal domain (CTD) mediating constitutive dimerization of Hsp90, which is essential *in vivo* (Harris et al., 2004; Wayne and Bolon, 2007). In cytosolic Hsp90 (and Grp94) the NTD and MD are connected via a flexible, charged linker, which is essential *in vivo*. Truncation of the linker affects client maturation by Hsp90 (Hainzl et al., 2009; Jahn et al., 2014; Zuehlke and Johnson, 2012; Tsutsumi et al., 2012).

The ATP binding site of Hsp90 shares homology with the Bergerat fold found in other members of the GHKL superfamily (gyrase subunit B, histidine kinase, DNA mismatch repair protein MutL) (Bergerat et al., 1997). ATP is bound in a unique, kinked fashion in the NTD, which allowed the discovery of selective inhibitors of the Hsp90 ATPase such as the ansamycin geldanamycin and radicicol (Figure 7C) (Roe et al., 1999; Soga et al., 2003). Hsp90 binds ATP with very low affinity (K_D = 400 µM) whereas the affinity for ADP is considerably higher (K_D = 10 µM), suggesting that a favorable cellular ATP:ADP ratio is required for Hsp90 function (Prodromou et al., 1997; Scheibel et al., 1997; Rowlands et al., 2004). The MD consists of two $\alpha\beta\alpha$ motifs that form a hydrophobic patch and an amphipathic protrusion (Figure 7B) (Sato et al., 2000; Meyer et al., 2003; Shiau et al., 2006). Early mutational studies and recent structural research has confirmed that the MD mediates client interactions (Bohen and Yamamoto, 1993; Nathan and Lindquist, 1995; Ali et al., 2006; Kirschke et al., 2014; Lorenz et al., 2014; Karagöz and Rüdiger, 2015; Verba et al., 2016). The constitutive C-terminal dimerization is mediated by two helices in the CTD of each protomer forming a four-helix bundle (Figure 7B) (Harris et al., 2004; Ali et al., 2006). Cytosolic Hsp90 in eukaryotes also contains the MEEVD motif at the C-terminal end of a approx. 35 residue unstructured tail, allowing the interaction with TPR containing co-chaperones (Schopf et al., 2017; Biebl and Buchner, 2019). Taken together, the structural features of Hsp90 yield a dynamic, V-shaped structure of the Hsp90 dimer that is predominantly open in the absence of ATP, but can undergo transient N-terminal dimerization (Prodromou et al., 2000; Shiau et al., 2006).

2.5.2.1 The ATPase Cycle of Cytosolic Hsp90

The binding of ATP to the Hsp90 NTD initiates a series of large, rate-limiting conformational rearrangements throughout the molecule (Weikl et al., 2000; Shiau et al., 2006; Cunningham et al., 2008; Hessling et al., 2009). Consequently, Hsp90 ATP turnover is extremely slow with a hydrolysis rate of approximately 0.1 ATP min^{-1} in humans and 1 ATP min^{-1} in yeast (Panaretou et al., 1998; Weikl et al., 2000; McLaughlin et al., 2002; Richter et al., 2008). Binding of ATP first induces the closing of the ATP lid, a helical structure within the NTD that closes over the nucleotide binding pocket in the ATP-bound, but not in the ADP-bound state (Figure 8) (Prodromou et al., 1997; Ali et al., 2006; Richter et al., 2006; Taipale et al., 2010). The ATP lid precludes stable N-terminal dimerization in the absence of ATP and is required for ATP hydrolysis (Richter et al., 2006). Subsequently, N-terminal dimerization yields the closed 1 state. For ATP hydrolysis, the contact of the ATP γ-phosphate to an arginine (Arg380 in yeast) in a loop of the Hsp90 MD establishes the so-called closed 2 state in which the two domains of the Hsp90 'split ATPase' are joined (Figure 7C, Figure 8) (Meyer et al., 2003; Cunningham et al., 2008). β-strand swapping between the N-terminal segments additionally stabilizes N-terminal dimerization (Ali et al., 2006; Richter and Buchner, 2006). After ATP hydrolysis, the NTDs dissociate, ADP and phosphate are released and Hsp90 reverts to its open state (Hessling et al.,

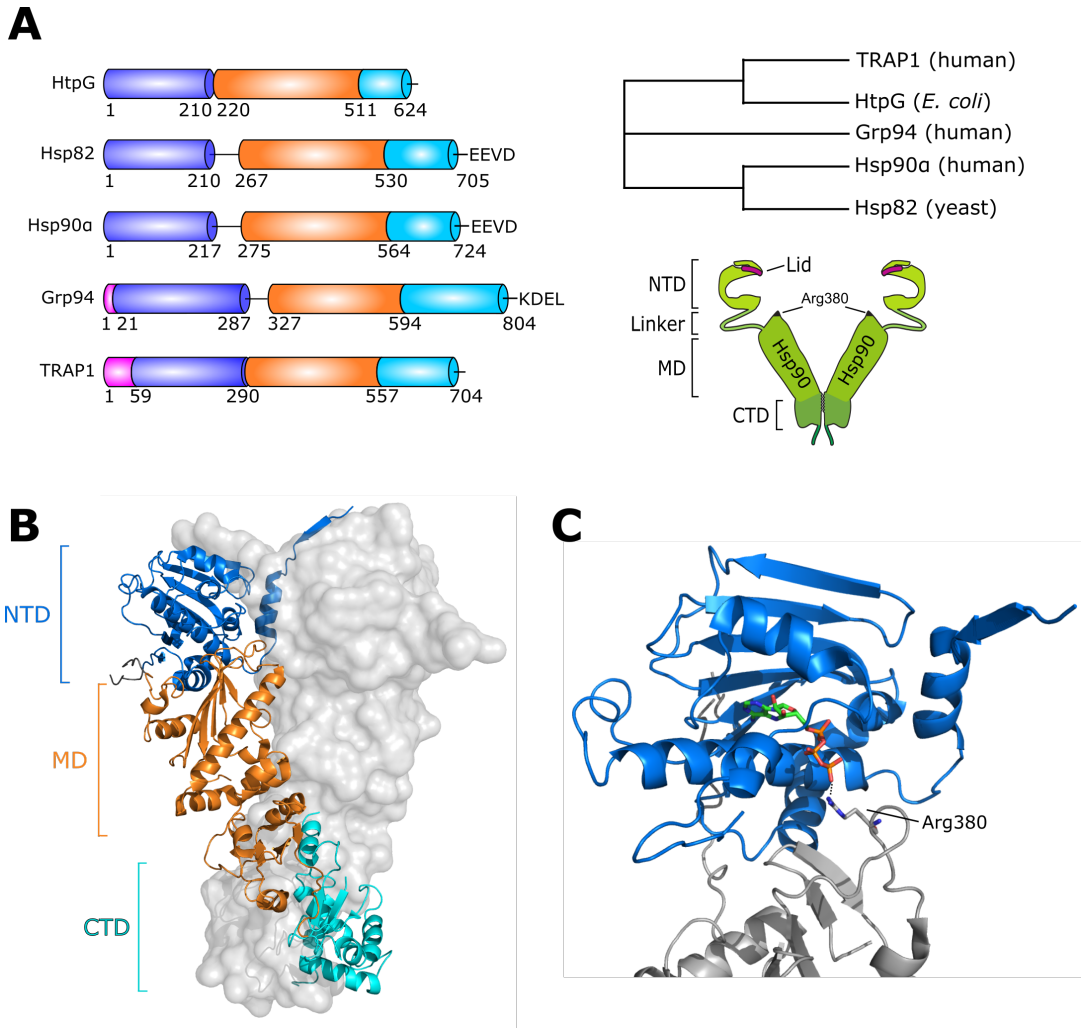

FIGURE 7 | **The Structure of Hsp90.**
A The domain architecture (left panel) and the evolutionary distance (right) of different Hsp90 family members are shown. The N-terminal domain (NTD) is depicted in blue, the middle domain (MD) in orange and the C-terminal domain (CTD) in cyan. Targeting sequences for miochondria (TRAP1) and the ER (Grp94) are shown in pink. Note the different lengh of the charged linker between the NTD and the MD. The presence of functionally important C-terminal sequences is indicated. A schematic model of the Hsp90 dimer is shown (right panel).
B The crystal structure of yeast Hsp82 in the N-terminally closed state is shown and color-coded as in (A) (PDB: 2CG9).
C The NTD of Hsp90 with bound ATP is depicted. The Arg380 residue of the MD required for hydrolysis is shown as sticks (PDB: 2CG9).
[NTD: N-terminal domain; MD: Middle domain; CTD: C-terminal domain]

2009). Despite the low enzymatic activity, the ability to hydrolyze ATP has long been deemed essential for survival (Obermann et al., 1998; Panaretou et al., 1998), yet a more recent study suggested that rather the dwell time of different conformations is essential *in vivo* (Figure 8) (Zierer et al., 2016).

While the general Hsp90 cycle is conserved across species, subtle differences between homologs have been reported. While bacterial HtpG is considered to undergo a deterministic, ratchet-like, nucleotide-driven Hsp90 cycle, eukaryotic Hsp90 has been described as a stochastic machinery, in which all states are accessible in nucleotide-free conditions and nucleotides merely shift the equilibrium (Southworth and Agard, 2008; Mickler et al., 2009; Ratzke et al., 2012). The expansion of the Hsp90 co-chaperome from bacteria, lacking co-chaperones via yeast having 12 co-chaperones to humans with more than 25 co-chaperones raises the speculation that co-chaperones confer directionality to the Hsp90 cycle in eukaryotes and convey additional functions (Ratzke et al., 2014; Mayer and Le Breton, 2015). Interestingly, the presence of ATP shifts human Hsp90 much less to the closed state than yeast and bacterial Hsp90 (Southworth and Agard, 2008).

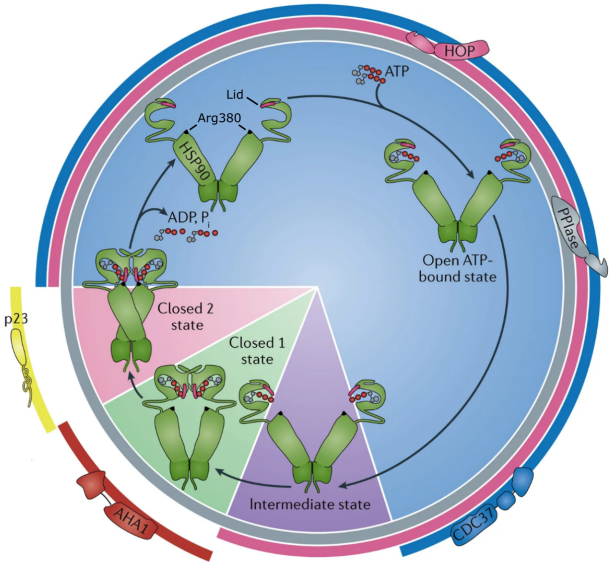

FIGURE 8 | **The Conformational Cycle of Hsp90.**
The conformational cycle of Hsp90 is depicted. Hsp90 is predominantly found in an open state. Binding of ATP leads to the closing of the ATP lid (pink), N-terminal dimerization (closed 1 state) and twisting of the protomers (closed 2 state) and positioning the catalytic Arg380 (in yeast) of the MD (black dot) towards the ATP γ-phosphate. Co-chaperones associate with specific Hsp90 conformations. Hsc70/Hsp90 organizing protein (Hop) associates with the open state and prevents closing. Cdc37 is thought to bind early in the cycle to recruit kinases, but it has also been found in a closed Hsp90:Cdc37:kinase complex. Peptidyl-prolyl *cis/trans* isomerases (PPIases) associate with different conformations of Hsp90. Activator of Hsp90 ATPase homolog 1 (Aha1) promotes dimer closing and accelerates the Hsp90 ATPase activity. p23 selectively binds to the N-terminally dimerized Hsp90 closed 2 conformation and inhibits ATPase function, thereby modulating cycle progression. From (Schopf et al., 2017).
[Hop: Hsc70/Hsp90 organizing protein; PPIase: Peptidyl-prolyl *cis/trans* isomerase; Aha1:Activator of Hsp90 ATPase homolog 1]

2.5.2.2 The Structural Differences Between Hsp90 Homologs

The main difference between different Hsp90 homologs lies within the length of an N-terminal, unstructured extension called the N-terminal strap, the length of the charged linker and the presence or absence of a functionally relevant C-terminal motif for ER retention or TPR domain binding (Figure 9) (Johnson, 2012). The closely related TRAP1 and HtpG both lack the charged linker between the NTD and MD (Chen et al., 2006). By contrast, Grp94 possesses a truncated linker that is important for ATP hydrolysis and calcium binding (Schulte et al., 1999; Biswas et al., 2007; Huck et al., 2017). Additionally, *E. coli* HtpG and TRAP1 lack the C-terminal EEVD motif, consistent with the lack of known co-chaperones for these Hsp90 homologs (Figure 7A) (Chen et al., 2006). By contrast, Grp94 contains the ER-retention sequence KDEL to ensure ER-localization. Cytosolic Hsp90 in yeast and higher eukaryotes contains the MEEVD motif that mediates the interaction with several co-chaperones. *E. coli* HtpG and yeast Hsp82 lack the N-terminal strap, whereas human cytsolic Hsp90 encodes a short strap and TRAP1 and Grp94 both harbor long N-terminal straps (Figure 9) (Chen et al., 2006; Partridge et al., 2014). In Grp94 the pre-N domains swap across the dimer and form loose contacts with the opposing protomer (Huck et al., 2017). A suppressive effect on the Grp94 ATPase and a regulatory role on dimerization have been proposed (Dollins et al., 2007; Huck et al., 2017). In TRAP1, the N-terminal strap forms tighter *trans* contacts stabilizing the closed conformation (Lavery et al., 2014). Additionally, the pre-N straps act as a thermosensor for TRAP1 and regulate ATPase activity (Partridge et al., 2014).

While the general conformational cycle of Hsp90 is conserved among different species, some species-specific features have been found. In particular, TRAP1 shares the common cycle intermediates of an open, N-terminally dimerized and closed state (Leskovar et al., 2008; Lavery et al., 2014; Partridge et al., 2014; Elnatan et al., 2017). However, a unique asymmetry between the protomers as part of a sequential, deterministic ATP hydrolysis mechanism has been proposed. In the TRAP1 cycle, one protomer takes a buckled conformation and hydrolyzes ATP first (Figure 9) (Elnatan et al., 2017). Symmetry then flips and the second monomer is poised for hydrolysis (Elnatan et al., 2017). In summary, these results prove the generality of the Hsp90 conformational cycle, yet they also indicate homolog-specific details that seem to fine-tune Hsp90 to meet the requirements of each homolog.

2.5.3 The Regulation of Hsp90

Hsp90 expression and function is tightly regulated by several levers: Transcriptional regulation controls Hsp90 levels; nucleotides affect the Hsp90 conformation; post-translational modifications (PTMs) have diverse effects on Hsp90; clients may affect the Hsp90 conformation and ATPase; and a plethora of co-chaperones regulate different aspects of the Hsp90 machinery in eukaryotes (Mollapour and Neckers, 2012; Mayer and Le Breton, 2015; Prodromou, 2016; Sima and Richter, 2018).

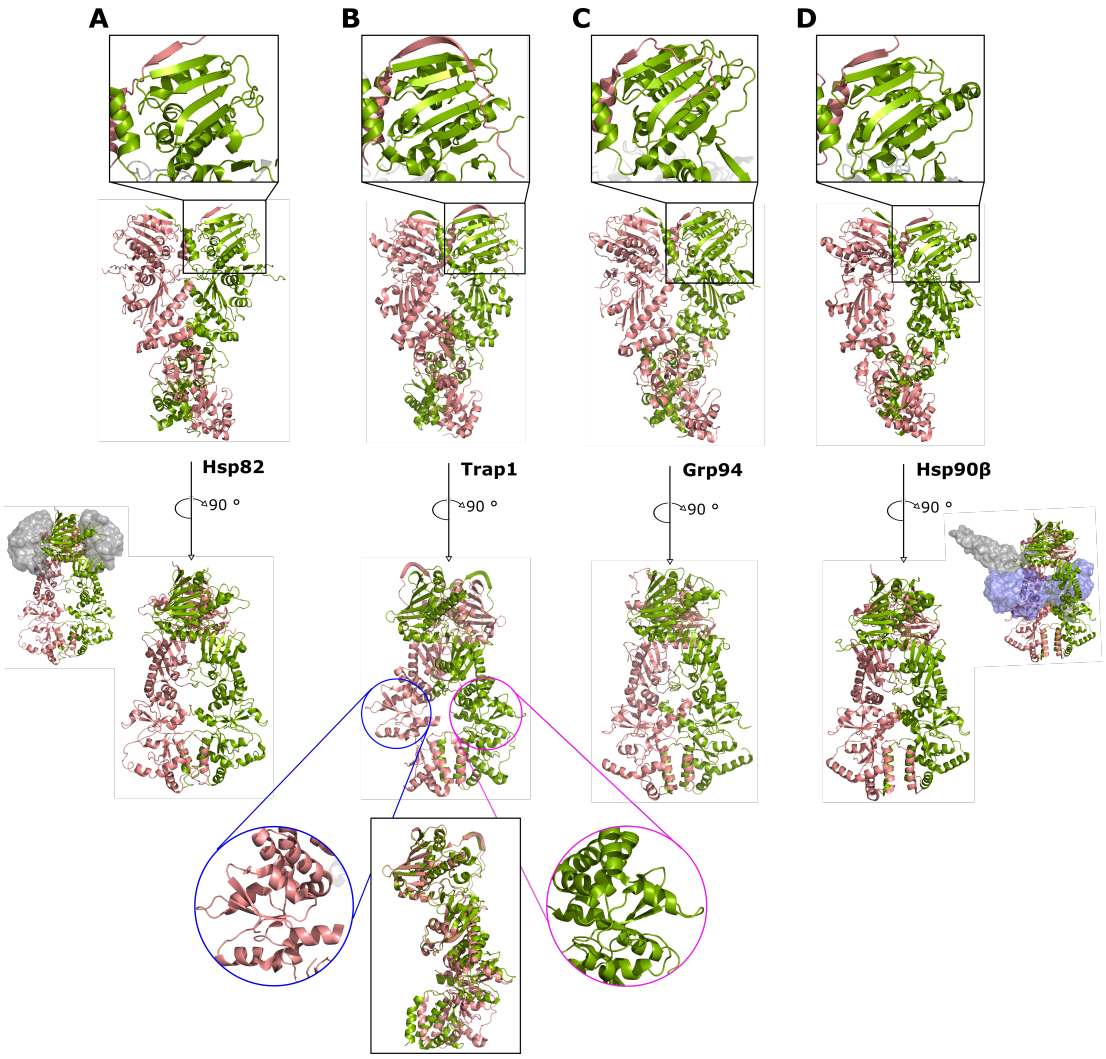

FIGURE 9 | **Structural Variability Between Hsp90 Homologs.**
(**A-D** The structure models of **A** Hsp82 (PDB: 2CG9), **B** TRAP1 (PDB: 4IPE), **C** Grp94 (PDB: 5ULS) and **D** Hsp90β (PDB: 5FWL) are shown. In the top panel, insets highlight the orientation of the N-terminal strap. In the bottom panel, an overlay of the TRAP1 is shown illustrating the buckled conformation of the green protomer. Since Hsp82 and Hsp90β structures were solved in complex with Sba1/p23 and Cdk4+Cdc37, respectively, the full structures are depicted next to the isolated Hsp90 dimer (from Biebl and Buchner, 2019).

2.5.3.1 The Transcriptional Regulation of Hsp90

Despite the high basal expression of Hsp90, the levels of heat-inducible isoforms of Hsp90 are further increased during stress conditions. As described, Hsp90 expression as many other Hsps is primarily regulated by Hsf1 and interestingly is also dependent on Hsf1 during non-stress conditions in yeast (Section 2.2) (Solis et al., 2016). In turn, Hsp90 (and Hsp70) also regulate Hsf1 activity. Beside Hsf1 regulation, other transcription factors for Hsp90 have been identified. In humans, they include nuclear factor-κB (NF-κB), NF-IL6 and signal transducer and activator of transcription 1 (STAT-1) and STAT-3 (Stephanou et al., 1997; Ammirante et al., 2008; Prodromou, 2016). Of note, some transcriptional regulators have synergistic or antagonistic functional relationships (Taipale et al., 2010). Together, they increase overall Hsp90 abundance by approximately 2-fold under stress (Taipale et al., 2010; Prodromou, 2016). Intriguingly, Hsp90 itself also regulates transcription by ensuring the maturation of some transcription factors and controlling chromatin accessibility (Sawarkar et al., 2012; Echtenkamp et al., 2016; Gvozdenov et al., 2019).

2.5.3.2 Post-Translational Modifications of Hsp90

As a central hub of an elaborate chaperone machinery, Hsp90 is modified by PTMs, but importantly also affected by the PTMs of co-chaperones (discussed in Section 2.5.4) (Mollapour and Neckers, 2012). PTMs affect the chaperone cycle, association with clients and co-chaperones as well as nucleotide binding. A large variety of PTMs on Hsp90 have been reported, including phosphorylation, acetylation, methylation, S-nitrosylation, oxidation, and SUMOylation (Scroggins and Neckers, 2007). They may affect Hsp90 locally, but implications in long-range inter-domain communication have been found (Morra et al., 2009; Retzlaff et al., 2009; Soroka et al., 2012; Rehn et al., 2020). For example, dephosphorylation of serine 485 in yeast Hsp90 or nitrosylation of a cysteine 597 in Hsp90α or methylation of lysine 607 in Hsp90β in the MD or CTD affect N-terminal dimerization and the ATPase of Hsp90 (Retzlaff et al., 2009; Soroka et al., 2012; Rehn et al., 2020). Due to the wealth of PTMs and the complex individual effects each modification can have, only an overview is provided here. Hsp90 PTMs have been extensively reviewed elsewhere (Mollapour and Neckers, 2012; Woodford et al., 2016a; Backe et al., 2020).

A plethora of phosphorylation sites on Hsp90 have been identified in all three domains of Hsp90, which include serine, threonine and tyrosine residues (Mollapour et al., 2010; Soroka et al., 2012). While each phosphorylation site may individually affect Hsp90, hyperphosphorylation has generally been associated with decreased Hsp90 ATPase and altered association with co-chaperones and clients (Mimnaugh et al., 1995; Wandinger et al., 2006). Interestingly, Serine/Threonine Protein Phosphatase T in yeast (Ppt1) and Serine/Threonine Protein Phosphatase 5 (PP5) in humans are Hsp90 co-chaperones that dephosphorylate Hsp90 and thus regulate the Hsp90 phosphorylation status (Wandinger et al., 2006). Additionally, many Hsp90

clients are kinases that in turn phosphorylate Hsp90 (Mollapour and Neckers, 2012; Taipale et al., 2012). Hence, the regulation of Hsp90 phosphorylation is very complex and considered to fine-tune Hsp90 function.

Acetylation and deacetylation of Hsp90 occurs by p300 and histone deacetylases (HDAC), in particular HDAC1, HDAC6 and HDAC10 (Bali et al., 2005; Murphy et al., 2005; Kekatpure et al., 2009). Similar to hyper-phosphorylation, acetylation on many sites has been associated with decreased binding of clients and co-chaperones (Scroggins et al., 2007).

S-nitrosylation of Cys597 in Hsp90β inhibits the activation of endothelial nitric oxide synthase (eNOS), inhibits the ATPase and shifts the conformational equilibrium of Hsp90 (García-Cardeña et al., 1998; Martínez-Ruiz et al., 2005; Retzlaff et al., 2009). Hence, nitrosylation establishes a negative feedback mechanism for eNOS activation. As mentioned, this also highlights that PTMs can have long-distance effects since Cys597 is located in the CTD of Hsp90 and it affects ATP hydrolysis in the N/M domains.

In summary, Hsp90 is subject to a variety of different PTMs that can affect Hsp90 locally or via long-range allosteric interactions and thus allows the rapid and temporary regulation of the association of Hsp90 with clients and co-chaperones. Intriguingly, also co-chaperones are regulated by PTMs, adding yet another layer of regulation to the Hsp90 system (Vaughan et al., 2008; Mollapour and Neckers, 2012; Röhl et al., 2015a).

2.5.4 The Hsp90 Co-Chaperome

While transcriptional regulation and regulation via PTMs are universal to most cellular proteins, Hsp90 function is also modulated by a plethora of co-chaperones (Table 2). Per definition, co-chaperones assist Hsp90 in its function but do not rely on Hsp90 for their own stability. While bacteria lack co-chaperones, yeast contains 12 and humans at least 25 co-chaperones, yet new human co-chaperones are still discovered, suggesting that only a fraction of Hsp90 modulators are known to date (Taipale et al., 2014; Woodford et al., 2016b; Woodford et al., 2017). Additionally, for several potential co-chaperones only high-throughput data is available, but detailed knowledge about their function is lacking. Binding sites for co-chaperones are distributed over all three Hsp90 domains (Figure 10). Some co-chaperones bind Hsp90 simultaneously while others compete with each other. Additionally, co-chaperones my associate with Hsp90 in a conformation-specific manner. Despite functional and structural differences among co-chaperones, two categories have historically been distinguished: TPR-containing co-chaperones and co-chaperones lacking TPR domains.

TABLE 2: Hsp90 co-chaperones

Co-Chaperone		**Function**	**Interaction Site on Hsp90**
Yeast Homolog	*Mammalian Homolog*		
Sti1	Hop	Hsp90 ATPase inhibitor; Adapter between Hsp70 and Hsp90	MEEVD; MD and CTD
Cdc37	Cdc37	Essential in yeast; Recruitment-factor for kinases; Inhibitor of Hsp90 ATPase	NTD and MD
Cns1	Ttc4	Essential in yeast; Regulator of translation elongation via eEF2	MEEVD
Tah1	Rpap3	Part of the Rvb1-Rvb2-Tah1-Pih1 complex	MEEVD
Pih1	Pih1	Part of the Rvb1-Rvb2-Tah1-Pih1 complex	Binds Tah1
Cpr6	Cyp40	TPR-containing Peptidyl-prolyl-*cis/trans*-isomerase (PPIase)	MEEVD
Cpr7	Cyp40	TPR-containing PPIase; Epistatic module with Cns1 in yeast	MEEVD
Sba1	p23	Inhibitor of Hsp90 ATPase; Binds closed Hsp90 conformation	NTD, MD
Aha1	Aha1	Strong accelerator of the Hsp90 ATPase	NTD, MD
Hch1	-	Homolog of Aha1; Weak accelerator of the Hsp90 ATPase	MD
Ppt1	PP5	TPR-containing protein phosphatase; Modulates the phosphorylation state of Cdc37 and Hsp90	MEEVD
Sgt1	Sgt1	Essential in yeast; Involved in kinetochore assembly in yeast, and innate immunity in plants	NTD
-	CHIP	TPR-containing E3 ubiquitin ligase; Involved in the degradation of misfolded clients	MEEVD, NTD, MD
-	FKBP51	TPR-containing PPIase; Implications in SHR maturation	MEEVD, NTD, MD, CTD
-	FKBP52	TPR-containing PPIase; Implications in SHR maturation	MEEVD
-	NudC	Largely unknown; Interacts with Hsp90 via a p23-like domain	unknown

References: Li et al., 2012; Mayer and Le Breton, 2015; Schopf et al., 2017; Biebl and Buchner, 2019

2.5.4.1 TPR-Containing Co-Chaperones

TPR-domains contain a 34-residue motif forming a pair of anti-parallel α-helices. Adjacent TPR motifs pack to each other creating a groove for MEEVD binding (Das et al., 1998; Scheufler et al., 2000). One of the best studied TPR co-chaperones is Hsc70-Hsp90 organizing protein (Hop) (stress-inducible protein 1 [Sti1] in yeast), acting as an adapter between the Hsp70 and Hsp90 system (Johnson et al., 1998; Wegele et al., 2006). The multidomain protein contains three TPR domains (TPR1, TPR2A and TPR2B) allowing the simultaneous interaction with Hsp70 and Hsp90 (Figure 10) (Chen and Smith, 1998; Johnson et al., 1998; Scheufler et al., 2000; Schmid et al., 2012; Röhl et al., 2015b). Sti1/Hop binds to the MEEVD motif of Hsp90, yet additional contacts with the CTD and MD are formed, keeping Hsp90 in an open client-accessible conformation and hence allosterically inhibiting the Hsp90 ATPase (Figure 10) (Prodromou et al., 1999; Richter et al., 2003; Schmid et al., 2012; Reidy et al., 2018). Interestingly, occupation of one TPR domain affects the binding behavior of the others, suggesting a complex cooperativity between Hsp70, Sti1/Hop and Hsp90, which is poorly understood (Röhl et al., 2015b). Additionally, while it is generally accepted that Sti1/Hop facilitates client handover, the regulation and mechanism of this process is largely unknown. Interestingly, in bacteria and yeast direct contacts between Hsp70 and Hsp90 have been reported expanding the possibilities for client transfer (Genest et al., 2015; Kravats et al., 2018).

The phosphatase Ppt1/Pp5 (in yeast and humans, respectively) is a TPR co-chaperone (Figure 10) that requires binding to Hsp90 to relieve auto-inhibition of the phosphatase activity by the C-terminal αJ helix (Chen and Cohen, 1997; Swingle et al., 2004). In turn, Ppt1/Pp5 dephosphorylates Hsp90 as discussed, but it also dephosphorylates the co-chaperone cell division control 37 (Cdc37) and folliculin-interacting protein 1 (FNIP1) (Wandinger et al., 2006; Vaughan et al., 2008; Sager et al., 2019). Additionally, dephosphorylation of Hsp90 client proteins such as tau protein involved in Alzheimer's disease has been reported (Salminen et al., 2011; Shelton et al., 2017; Bohush et al., 2019).

PPIases catalyze the isomerization of prolyl-peptide bonds. Several PPIases are also Hsp90 co-chaperones, including FKBP51, FKBP52 and cyclophilin 40 (Cyp40) in vertebrates. They bind the C-terminal MEEVD motif in Hsp90, but for FKBP51 additionally an extended interaction surface spanning all three Hsp90 domains has been proposed (Oroz et al., 2018). While they display Hsp90-independent chaperone activity *in vitro*, the PPIase enzyme activity seems to be dispensable for Hsp90-dependent client activation (Bose et al., 1996; Freeman et al., 1996; Duina et al., 1998; Riggs et al., 2003; Riggs et al., 2007). *S. cerevisiae* harbors two PPIases, homologous to Cyp40, named Cpr6 and Cpr7. Despite significant similarities between Cpr6 and Cpr7 as well as FKBP51 and FKBP52, distinct functions have been proposed (Hutchison et al., 1993; Duina et al., 1996; Mayr et al., 2000; Zuehlke and Johnson, 2012; Schopf et al., 2019). For FKBP51 and FKBP52 even opposing effects on GR maturation have been proposed, and surprisingly, the differences seem to be due to

structural differences in the PPIase domain (Riggs et al., 2007; Storer et al., 2011).

The TPR co-chaperone cyclophilin 7 suppressor (Cns1) in yeast (tetratricopeptide repeat protein 4 (Ttc4) in humans) is one of three essential co-chaperones in yeast. The human homolog has largely remained unstudied, whereas we know that yeast Cns1 forms a genetic module with Cpr7 to maintain eukaryotic elongation factor 2 (eEF2) (Tesic et al., 2003; Tenge et al., 2015; Schopf et al., 2019). To this end, Cns1 directly binds eEF2, the co-factor Hgh1 and Hsp90 to form a quarternary complex (Schopf et al., 2019).

Suppressor of G2 allele of S-phase kinase-associated protein 1 (Sgt1) is also essential in yeast. Despite the presence of a TPR domain, Sgt1 interacts with the Hsp90 NTD via its CHORD-Sgt1 (CS) domain (Zhang et al., 2008). While its function in mammals is largely unknown, it has been implicated in kinetochore assembly in yeast and maturation of leucin-rich-repeat (LRR) receptors of the innate immune response in plants (Kitagawa et al., 1999; Catlett and Kaplan, 2006; Mayor et al., 2007).

To shuttle terminally unfolded substrates to the proteasome, the TPR-containing E3 ligase C-terminus of Hsc70-interacting protein (CHIP) associates with Hsp70 and Hsp90 functioning as a specialized co-chaperone (Connell et al., 2001; Xu et al., 2002; Quintana-Gallardo et al., 2019). Despite being able to bind Hsp90, the association of CHIP to Hsp70 seems to be more important for the degradation of clients in the cellular environment (Kundrat and Regan, 2010; Theodoraki and Caplan, 2012).

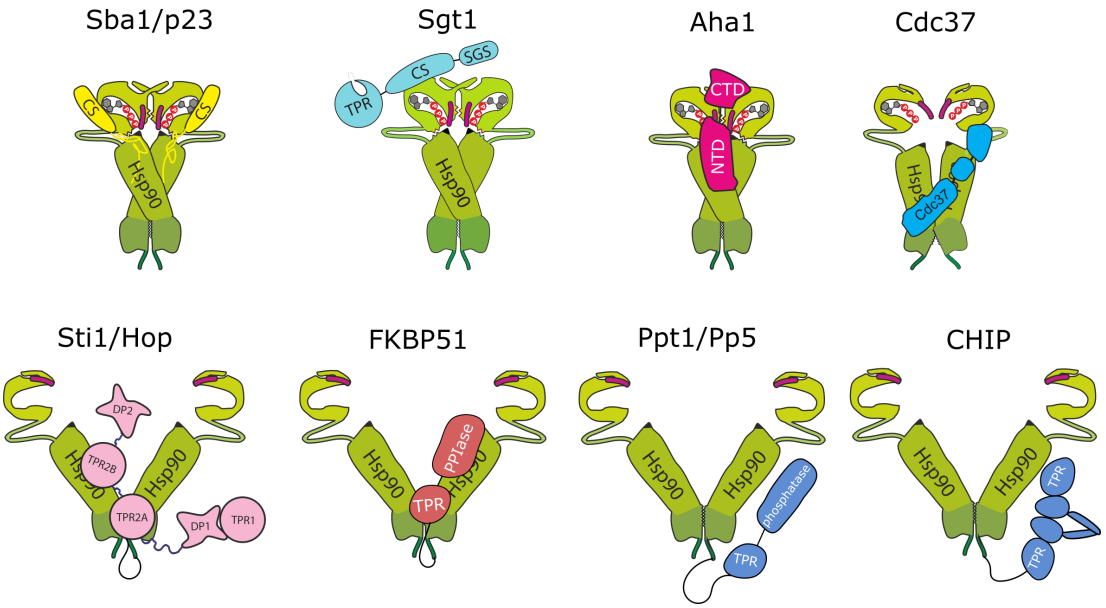

FIGURE 10 | **The Interactions Between Co-Chaperones and Hsp90.**
Schematic models for the interaction of different co-chaperones with Hsp90 are shown. The CS domain of Sba1/p23 interacts with the Hsp90 NTD. Sgt also associates with Hsp90 via the CS domain. The Aha1 N-terminal domain (NTD) interacts with the Hsp90 MD, whereas the Aha1 C-terminal domain interacts with the Hsp90 NTD in a dynamic fashion. Cdc37 has been found to interact with the Hsp90 NTD, but another structure showed that Cdc37 wraps around the Hsp90 MD in the client-bound state. The multimodular Sti1/Hop co-chaperone interacts with the MEEVD motif with its TPR2A domain and the TPR2B domain binds to MD of Hsp90. PPIases and Ppt1/Pp5 interact with Hsp90 via the TPR domain.

2.5.4.2 Co-Chaperones Lacking TPR-Domains

Cdc37 is a non-TPR containing Hsp90 co-chaperone that is essential in yeast. While Sti1/Hop is considered to be important for transfer of diverse clients to Hsp90, Cdc37 is dedicated to the recruitment of kinases (Grammatikakis et al., 1999; Citri et al., 2006). In humans, up to 60% of kinases are recruited to Hsp90 via Cdc37 (Taipale et al., 2012). In that context is has been found that Cdc37 samples the stability of kinases and thus is responsible for the selection of unstable kinases (Falsone et al., 2004; Boczek et al., 2015; Keramisanou et al., 2016). Early studies suggested binding to the Hsp90 N-terminus and an inhibitory effect on Hsp90 ATPase (Siligardi et al., 2002; Roe et al., 2004; Eckl et al., 2013). A recent cryo-EM structure of a trimeric Hsp90:Cdc37:kinase complex displayed Cdc37 wrapped around the MD of one Hsp90 monomer (Verba et al., 2016), suggesting that Cdc37 undergoes large conformational transitions on Hsp90 during the Hsp90 cycle (Figure 10).

Late in the Hsp90 cycle Sba1/p23 (yeast/human) selectively binds the dimerized NTDs of the closed Hsp90 conformation. Theoretically, two molecules can bind per Hsp90 dimer (Figure 10), even though this scenario is unlikely in the cellular environment in which Hsp90 is about 10 times more abundant than Sba1/p23 (Sullivan et al., 2002; Ghaemmaghami et al., 2003; Richter et al., 2004; Siligardi et al., 2004; Ali et al., 2006; McLaughlin et al., 2006; Karagöz et al., 2011). Consequently, the N-terminally associated state of Hsp90 is stabilized by Sba1/p23. Despite ATP binding in the presence of Sba1/p23, the ATPase activity inhibited, indicating a non-competitive mechanism (Sullivan et al., 1997; McLaughlin et al., 2002; Panaretou et al., 2002; Richter et al., 2004). Structurally, Sba1/p23 harbors a folded CS domain that mediates Hsp90 binding and an unfolded tail that is important for chaperone function (Weikl et al., 1999; Weaver et al., 2000; Ali et al., 2006). Importantly, Sba1/p23 also has Hsp90-independent chaperone activity and has been found to take part in several cellular processes in an Hsp90-independent manner (Bose et al., 1996; Freeman et al., 1996): These include chromatin remodeling, ribosome biogenesis and the direct interaction with the tumor suppressor p53 (Echtenkamp et al., 2011; Echtenkamp et al., 2016; Wu et al., 2018).

Aha1 is the only known potent activator of the Hsp90 ATPase (Panaretou et al., 2002). Aha1 binds the Hsp90 MD with its N-terminal domain and forms dynamic interactions with the Hsp90 NTD with its C-terminal domain (Figure 10) (Oroz et al., 2019; LaPointe et al., 2020). The molecular mechanism for Hsp90 ATPase activation lies in the ability of Aha1 to accelerate N-terminal dimerization of Hsp90 *in trans* and to increase the dynamics of nucleotide binding (Meyer et al., 2004; Retzlaff et al., 2010; Mercier et al., 2019). The binding site of Aha1 on Hsp90 overlaps with the proposed client binding site, suggesting that Aha1 may bind competitively with clients (Koulov et al., 2010; Lorenz et al., 2014; Verba et al., 2016). Yeast expresses an Aha1 homolog, Hch1. Hch1 shares homology with the Aha1 N-terminal domain, but lacks the C-terminal part and has a considerably lower potency to activate the Hsp90 ATPase (Panaretou et al., 2002; Armstrong et al., 2012). Interestingly, it has

been proposed that the loss of Hch1 in humans has been functionally complemented by a reversible phosphorylation on Tyr627 (Zuehlke et al., 2017).

Besides classical co-chaperones that affect a vast array of clients, some more specialized co-chaperones are known: The TPR-containing protein associated with Hsp90 1 (Tah1; RNA polymerase II associated protein 3 [Rpap3] in humans) acts as an adapter for protein interacting with Hsp90 1 (Pih1), which itself associates with RuvB-like protein 1 (Rvb1) and Rvb2, and thus links Hsp90 to the R2TP complex (Zhao et al., 2005; Zhao et al., 2008; Rivera-Calzada et al., 2017). Notably, mammalian Rpap3 is much larger than yeast Tah1 and additionally associates with subunits of the prefoldin module (Boulon et al., 2010; Cloutier et al., 2017; Houry et al., 2018). Alanyl-tRNA synthetase domain-containing protein (Aarsd1) is a tissue specific homolog of p23 in myoblasts (Echeverría et al., 2016). Tuberculosis sclerosis complex 1 (Tsc1) has been found to associate with Hsp90 and Tsc2, which is stabilized in this complex (Woodford et al., 2017; Sager et al., 2018). In analogy to Tsc1 specifically stabilizing Tsc2, FNIP1/2 were found as specific co-chaperones mediating the contact to Hsp90 for the stabilization of the tumor suppressor folliculin (FLCN) (Woodford et al., 2016a; Sager et al., 2019).

2.5.4.3 Nuclear Migration Protein NudC

For other potential co-chaperones high-throughput data suggest the role as a co-chaperone but functional insight is lacking (Taipale et al., 2014). Nuclear migration protein NudC is a factor that formed complexes with the Hsp70 and Hsp90 system similar to Sti1/Hop in a large-scale interactome study (Taipale et al., 2014). However, the cellular function of NudC is not well understood. While it is present in mammals and fission yeast, it is not found in *S. cerevisiae*. As part of the Nud family of proteins, it regulates nuclear migration in cells and it associates with the dynein motor-associated protein lissencephaly protein 1 (Lis1) (Zhu et al., 2010). Roles in the immune response, neuronal migration and thrombopoiesis have been suggested (Fu et al., 2016). Additionally, an Hsp90-independent chaperone function on model substrates has been reported and an inhibitory effect on Hsp90 ATPase has been discussed (Zhu et al., 2010; Zheng et al., 2011). NudC contains a CS domain similar to Sba1/p23 and Sgt1 (Zheng et al., 2011), making it a promising suspect for an Hsp90 co-chaperone, yet if and how NudC affects client maturation by Hsp90 has not been investigated so far.

2.5.4.4 The Co-Chaperone-Assisted Hsp90 Cycle

Due to the dimeric nature of Hsp90 for many co-chaperones simultaneous binding in a 2:2 stoichiometry has been shown *in vitro* and is theoretically possible *in vivo* (Prodromou et al., 1999; Ebong et al., 2011). However, given the *in vivo* ratios between Hsp90 and co-chaperones, symmetric Hsp90:co-chaperone complexes are unlikely (Figure 11A). Even the most abundant Hsp90 co-chaperones such as

Sti1/Hop, Sba1/p23 and PPIases each constitute usually less then 10% of the Hsp90 levels (Ghaemmaghami et al., 2003; Finka and Goloubinoff, 2013). This fits the findings that binding of a single co-chaperone to the Hsp90 dimer may be sufficient to reach its biological effects: For example, binding of a single Sti1/Hop molecule suffices to inhibit Hsp90 and a single Aha1 monomer activates the Hsp90 ATPase (Retzlaff et al., 2010; Schmid et al., 2012). Consequently, mixed co-chaperone complexes have been reported and seem to be important for cell cycle progression such as Hsp90:Sti1:Cpr6 (Ebong et al., 2011; Li et al., 2011). For many co-chaperones we know at which point in the Hsp90 cycle they come into play in the yeast system (Figure 11B) (Li et al., 2011). Unfortunately, a comprehensive knowledge of the cooperation of co-chaperones in the Hsp90 cycle is largely lacking and co-chaperones have mostly been studied in isolation. Additionally, our understanding of co-chaperone interactions throughout the Hsp90 cycle has almost exclusively been obtained in studies in the yeast system (Li et al., 2012).

In the emerging model, Sti1/Hop binds Hsp90 early in the cycle to inhibit ATP hydrolysis and dimer closing (Figure 11B) (Prodromou et al., 1999; Richter et al., 2003; Schmid et al., 2012). Simultaneously, client-loaded Hsp70 can associate with another TPR domain of Sti1/Hop forming a Hsp90:Sti1/Hop:Hsp70:client complex (Wegele et al., 2006). Some types of Hsp40 may remain bound, while others may dissociate after Hsp70 binding to the substrate (Pratt and Toft, 2003; Jiang et al., 2019). From this complex, the client is transferred to the open Hsp90 dimer in a still unknown mechanism. For kinases, a Sti1/Hop-independent recruitment mechanism via Cdc37 has been proposed in which kinase-bound Cdc37 first attaches to the Hsp90 NTD and then transitions to a state in which the kinase and Cdc37 are bound to the MD of closed Hsp90 (Roe et al., 2004; Eckl et al., 2015; Verba et al., 2016). Yet, also for kinases, Sti1/Hop is important for maturation (Lee et al., 2004; Taipale et al., 2014; Sahasrabudhe et al., 2017). After client transfer, Hsp70 dissociates. How the Hsp70 release is regulated is not entirely understood. Binding of Sti1/Hop to one Hsp90 monomer facilitates the binding of a PPIase such as Cpr6 to the second MEEVD motif (Figure 11B) (Li et al., 2011). Aha1 and ATP binding compete with Sti1/Hop binding and accelerates closure to the closed 1 state (Figure 8, Figure 11) (Li et al., 2013). Subsequently, Hsp90 transitions to the closed 2 state which is selectively bound and stabilized by Sba1/p23. Following ATP hydrolysis, Hsp90 opens up and bound co-chaperones, ADP, phosphate and the client dissociate from Hsp90.

How other co-chaperones are integrated in the Hsp90 cycle is unknown. Previously, the Buchner lab found that co-chaperones affect client activity in a client-specific way and different co-chaperones were required for the maturation of closely related clients (Sahasrabudhe et al., 2017). Surprisingly, even clients that only differed by point mutations affected the co-chaperone landscape that regulated client activity, suggesting that co-chaperones are selectively recruited to fine-tune Hsp90 to meet the requirements of different Hsp90 clients (Sahasrabudhe et al., 2017). This

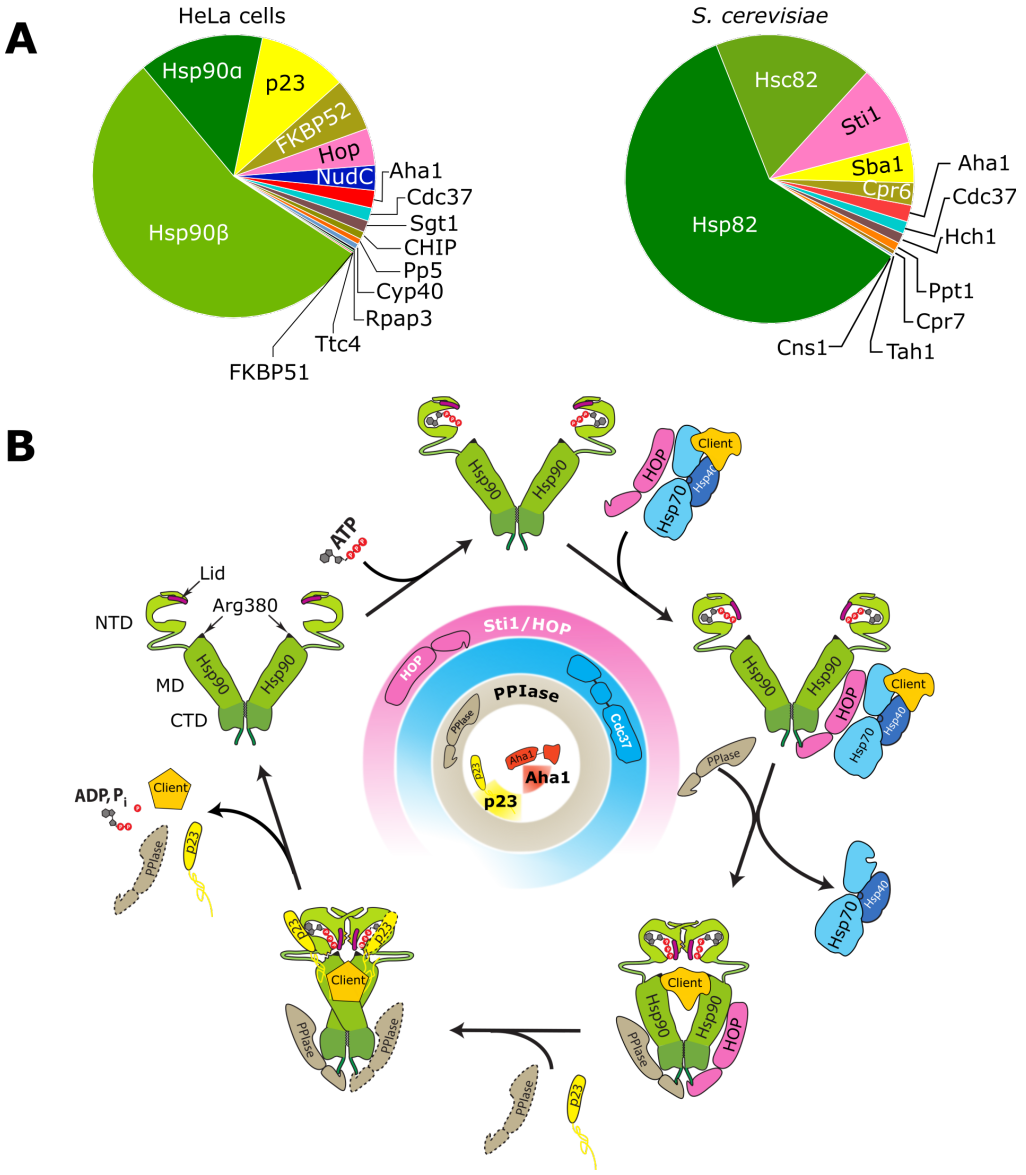

FIGURE 11 | **The Co-Chaperone-Assisted Hsp90 Cycle.**
A The relative cellular abundance of cytosolic Hsp90 and co-chaperones in HeLa cells (left) and *S. cerevisiae* (right). Abundance data for yeast and HeLa cells were taken from Ghaemmaghami et al., 2003 and Finka and Goloubinoff, 2013, respectively.
B The co-chaperone-assisted Hsp90 cycle is shown. Some co-chaperones associate with specific Hsp90 conformations, indicated by the colored circles in the middle. Comprehensive knowledge of the sequential action of all co-chaperones is not available. The sequential interactions of Sti1/Hop transferring client from the Hsp70 system, PPIases and Sba1/p23 are shown. Note that our understanding of the co-chaperone assisted Hsp90 cycle is almost exclusively derived from the yeast system. From Biebl and Buchner, 2019.

leaves us with the hypothesis that there is not a comprehensive Hsp90 cycle including all co-chaperones. In a cell, we suspect the presence of a heterogenous ensemble of Hsp90 complexes modulated by different subsets of co-chaperones. Yet, how the co-chaperones co-operate in this process in a client-dependent manner is entirely unknown.

2.5.5 The Hsp90 Client Spectrum

Hsp90 is responsible for the maturation of a broad spectrum of structurally and functionally unrelated client proteins (Figure 12A). More than 300 clients are known to date and an updated list is maintained by the Picard lab (Echeverría et al., 2011). Protein kinases and SHRs have been extensively studied (Brugge et al., 1981; Xu and Lindquist, 1993; Picard et al., 1990; Dittmar and Pratt, 1997; Dittmar et al., 1997; Pratt and Toft, 1997; Pratt and Dittmar, 1998). About 60% of the human kinome are Hsp90 clients, whereas only about 7% of transcription factors are Hsp90 clients (Taipale et al., 2012). This is surprising since transcription factors have long been considered a classical group of Hsp90 clients. In particular, the tumor suppressor p53 has been studied in detail concerning the interaction with Hsp90 due to its implication in cancer (Blagosklonny et al., 1996; Sepehrnia et al., 1996; Whitesell et al., 1998; Nagata et al., 1999; Rudiger et al., 2002; Hagn et al., 2011; Alexandrova et al., 2015; Dahiya et al., 2019). E3 ubiquitin ligases recently found interest as an emerging class of Hsp90 clients that is poorly understood so far (Taipale et al., 2012). Besides the Hsp90-associated E3 ubiquitin ligase CHIP, cullin 5 (Cul5) has been identified as an Hsp90-associated E3 ubiquitin ligase that regulates the degradation of client proteins and hence functions more as an Hsp90 co-chaperone than a client (Ehrlich et al., 2009). Ubiquitin-like PHD and RING finger domain-containing protein 1 (UHRF1) has been described as a *bona fide* Hsp90 client that relies on Hsp90 function on its stability (Ding et al., 2016). Generally, proteins are considered Hsp90 clients if they continuously require Hsp90 to remain active (Karagöz and Rüdiger, 2015). As mentioned, different clients may require Hsp90 assistance in different ways, reaching from folding over complex assembly to ligand binding (Figure 6). The role of Hsp90 during *de novo* folding of substrates that do not constitutively require Hsp90 function is still under discussion. Notably, using a mass-spectrometry-based approach it has been found that a large number of proteins require Hsp90 only transiently during *de novo* folding, which has found little attention in the past due to the inherent short-lived character of these interactions (Savitski et al., 2018). This contradicts early findings form the Lindquist lab, postulating that Hsp90 is not involved in the *de novo* folding of a majority of cellular proteins.

2.5.5.1 Client Recognition by Hsp90

The structural or sequence determinants that define a client have remained largely elusive for Hsp90. While defined commonalities between substrates are known

for example for Hsp70, common features among Hsp90 clients are largely lacking (Karagöz and Rüdiger, 2015). In addition, the dichotomous classification into client and non-client has been questioned, since a continuous distribution of binding affinities for Hsp90 has been observed for kinases (Taipale et al., 2012). In this context, comparison of cellular c-Src with oncogenic v-Src has provided valuable insight into the selection determinants of Hsp90. Despite 97% sequence identity, c-Src requires Hsp90 only for *de novo* folding, while v-Src is a stringent Hsp90 client (Xu et al., 1999). In depth analysis of these kinases and the step-wise transformation of c-Src into v-Src by introducing individual mutations suggested that a combination of overall stability, folding cooperativity and compactness define Hsp90 clients rather than discrete binding motifs (Falsone et al., 2004; Taipale et al., 2012; Boczek et al., 2015; Keramisanou et al., 2016; Savitski et al., 2018). This is also in line with the finding that the kinase-specific co-chaperone Cdc37 seems to exert mild unfolding pressure on kinases to select for metastable kinases in order to recruit them to Hsp90 (Keramisanou et al., 2016).

2.5.5.2 The Hsp90 Client Binding Site

Pinpointing the client binding site on Hsp90 has been challenging due to the transient nature of the Hsp90:client interaction, the instability of the clients and the size of the complex (Karagöz and Rüdiger, 2015). The binding affinity of clients to Hsp90 is generally rather low and in some cases dependent on the Hsp90 conformation (Karagöz et al., 2014; Lorenz et al., 2014). Early mutational studies suggested that hydrophobic residues in the C-terminal part of the MD mediate client binding (Bohen and Yamamoto, 1993; Nathan and Lindquist, 1995; Genest et al., 2013). By now, structural models and structures of Hsp90:client complexes have been obtained, confirming that the Hsp90 MD is pivotal for the binding of most clients, but additional contacts with the CTD and NTD may be formed in some cases (Figure 12B) (Shiau et al., 2006; Lorenz et al., 2014; Verba et al., 2016; Radli and Rüdiger, 2018).

The combined approach using NMR, small-angle X-ray scattering (SAXS) and electron microscopy (EM) allowed mapping the binding of the GR ligand binding domain (GR-LBD) to the Hsp90 MD, with minor contacts formed with the NTD and CTD (Figure 12B) (Lorenz et al., 2014). Of note, in this model, one GR-LBD could bind each face of the Hsp90 dimer and affinity was highest when Hsp90 was not entirely closed (Lorenz et al., 2014). Notably, similar to long-range information transfer observed for PTMs on Hsp90, binding of the GR-LBD to Hsp90 has been found to act as a switch point inducing long-distance conformational changes in Hsp90 as reflected in the influence on the ATPase (Rutz et al., 2018)

This is in line with a cryo-EM structure of the Hsp90β:Cdc37:Cdk4 complex, in which the β4-β5 strands of the kinase were ripped apart and threaded through the closed Hsp90 dimer orifice leaving the N-lobe and C-lobe of the kinase bound to the opposing Hsp90 interfaces (Figure 12B) (Verba et al., 2016). The interaction

surface on Hsp90 overlaps significantly for the GR-LBD and Cdk4 and the overall structure resembles that of the two GR-LBD monomers bound to the opposing Hsp90 interfaces (Lorenz et al., 2014; Verba et al., 2016). The structure of the trimeric Hsp90β:Cdc37:Cdk4 also provided insight into the role of Cdc37 which wraps around the MD of one of the Hsp90 monomers and seems to mimic native contacts in the kinase N-lobe that are natively formed between the N- and C-lobes (Verba et al., 2016). Why kinases would be bound in such an open conformation is not entirely clear but it is speculated that nucleotide binding in this conformation is facilitated (Eckl et al., 2016; Verba et al., 2016). Additionally, the contradictory results of Cdc37 bound to the Hsp90 NTD in earlier studies (Roe et al., 2004; Eckl et al., 2013) and the cryo-EM structure showing binding to the MD (Verba et al., 2016) suggests significant conformational transitions on Hsp90 throughout the kinase maturation cycle.

While the binding sites of Cdk4 and GR-LBD largely overlap, other clients contact a less restricted surface on Hsp90. Tau protein has been reported to form transient contacts to the NTD and MD (Figure 12B) (Karagöz et al., 2014). The p53 DNA binding domain (p53-DBD) was found to interact with yeast Hsp90 on the 90 MD and CTD, while binding to human Hsp90α was proposed to occur in all three domains (Hagn et al., 2011; Park et al., 2011b; Park et al., 2011a). Interestingly, from previous studies it had remained unclear, whether p53-DBD binds Hsp90 in a native-like state, a molten-globule or entirely unfolded conformation, but more recent investigations hint towards a partially folded state of the p53-DBD when it is received form Hsp70 and a native conformation after release from Hsp90 (Rudiger et al., 2002; Hagn et al., 2011; Park et al., 2011b; Boysen et al., 2019; Dahiya et al., 2019).

In conclusion, the Hsp90 MD plays a crucial role in the interaction with clients, yet contacts to the NTD and CTD may be important for some clients. How Hsp90 affects a client seems to be client-specific and depend on the stage during the folding trajectory at which the client interacts with Hsp90. Even though the affinity of a client to Hsp90 most likely changes throughout the Hsp90 cycle, the interaction is generally of low affinity (e.g. 1-5 µM for GR-LBD, about 3 µM for v-Src and about 1µM for p53-DBD) to allow the association and timely dissociation of a client that is required for folding (Müller et al., 2004; Lorenz et al., 2014; Boczek et al., 2015).

2.5.5.3 The Client Maturation Cascade

The abundance of cellular chaperone systems that are in place to ensure the folding of the proteome rises the question how these connect to each other. It is suspected that approximately 70% of nascent chains associate with the ribosome-associated RAC/NAC complex and may then fold spontaneously (Hartl et al., 2011; Balchin et al., 2016). This scenario especially holds true for smaller proteins, whereas larger multi-domain proteins are subsequently bound by the Hsp70 system. Three scenarios for polypeptides are possible starting from the Hsp70 hub: 1) Polypeptides may fold after one or several folding cycles on Hsp70. 2) Proteins may be shuttled

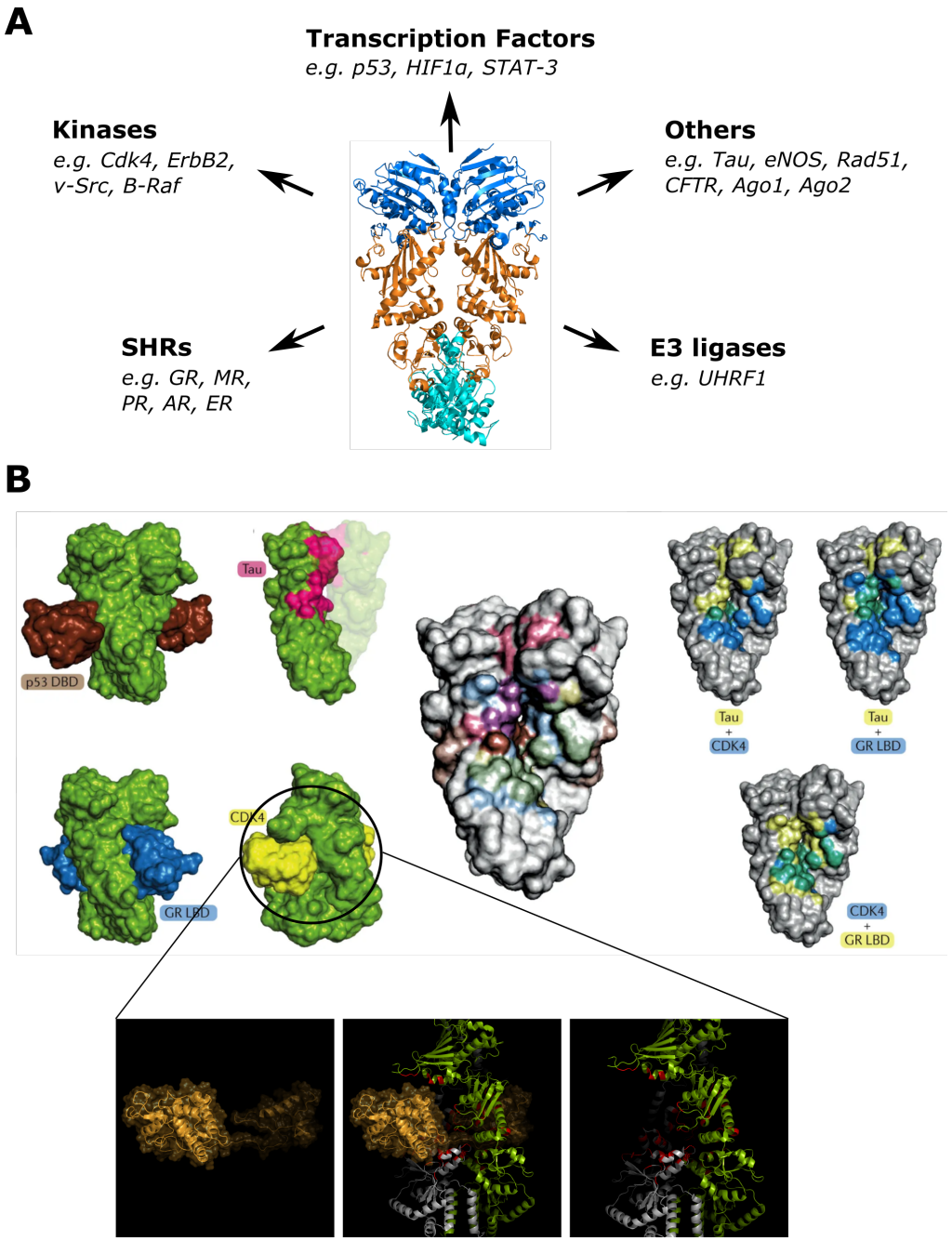

FIGURE 12 | **The Hsp90 Client Spectrum.**
A The structure of yeast Hsp90 (PDB: 2CG9) and important clients are shown.
B The interaction of Hsp90 with the clients p53 DNA binding domain (p53-DBD), the GR ligand binding domain (GR-LBD), tau protein and Cdk4 is shown. The p53-DBD and GR-LBD are bound to yeast Hsp82 (PDB: 2CG9) (Hagn et al., 2011; Lorenz et al., 2014). The tau binding site was mapped on yeast Hsp82 (Karagöz et al., 2014). Cdk4 is bound to human Hsp90β (Verba et al., 2016). An overlay of the binding sites of all shown clients mapped on yeast Hsp82 is depicted in the center, individual overlays are shown on the right. The colors of the overlaid binding sites are the product of the overlay of the blue, yellow, brown and purple client interaction sites as shown on the left. A close-up view of Cdk4 threaded through the Hsp90 protomers is shown in the inset. Residues of Hsp90 in proximity to Cdk4 are highlighted in red. Adapted from Schopf et al., 2017.
[Cdk4 = Cyclin dependent kinase 4; ErbB2 = Human epidermal growth factor receptor 2; B-Raf = B rapidly accelerated fibrosarcoma; HIF1α = hypoxia-inducible factor α; STAT-3 = Signal transducer and activator of transcription 3; eNOS = endothelial nitric oxide synthase; CFTR = Cystic fibrosis transmembrane conductance regulator; Ago1/2 = Protein argonaute 1/2; MR = mineralocorticoid receptor; PR = progesterone receptor; AR = androgen receptor; ER = estrogen receptor; UHRF1 = Ubiquitin-like PHD and RING finger domain-containing protein 1]

to the TRiC/CCT complex, which seems to be the case for about 10% of the cellular proteins. 3) Approximately 10-20% of proteins will be transferred to Hsp90 via Sti1/Hop (Zhao and Houry, 2007; Taipale et al., 2010; Wu et al., 2012). The relay between Hsp70 and Hsp90 is particularly well studied (Morán Luengo et al., 2019). Hsp90 is generally considered to bind near-native proteins late in their folding pathway (Jakob et al., 1995; Mayer and Le Breton, 2015). At least for some Hsp90 clients such as the GR, p53 and firefly luciferase, Hsp70 acts as a trap that keeps a client in an inactive, partly unfolded state and Hsp90 is required to release the deadlock on these clients (Kirschke et al., 2014; Morán Luengo et al., 2018; Boysen et al., 2019; Dahiya et al., 2019). This suggests that Hsp70 and Hsp90 closely collaborate and depend on each other for the maturation of clients.

In summary, life has developed an elaborate, inter-dependent chaperone system to ensure the maturation of diverse substrates under physiological conditions and under stress. In this network, Hsp90 plays a crucial role in the maturation of a diverse spectrum of clients and the combined, sequential activity of Hsp70 and Hsp90 seems to be crucial for many clients to reach their native state.

2.6 Objective of this Thesis

2.6.1 The Yeast Co-Chaperome

As outlined, the function of Hsp90 is tightly regulated by a cohort of co-chaperones in eukaryotes. In the yeast system, 12 co-chaperones regulate Hsp90. For some co-chaperones we know at which point in the conformational cycle they associate with Hsp90 and structural information granted insight into the binding mechanisms between co-chaperones and Hsp90. For a long time only anecdotal information about the influence co-chaperones have on client maturation was available. The Buchner lab for the first time studied the effect of yeast co-chaperones on Hsp90 clients in a comprehensive manner and found that yeast co-chaperones affect Hsp90 client maturation in a client-specific way (Sahasrabudhe et al., 2017). Yet, this also raises the question how the co-chaperones that affect client maturation co-operate for their function and how the large set of co-chaperones is coordinated. The genetic interactions between co-chaperones in yeast have primarily been studied in high-throughput studies using the synthetic genetic array (SGA) technology pioneered by Charles Boone and coworkers (Costanzo et al., 2016; Rizzolo et al., 2017; Kuzmin et al., 2018; Rizzolo et al., 2018). All previous large-scale SGA screens were done based on fitness measurements. Hence, these studies can not be used to predict the functional relationship between co-chaperones during the maturation of clients. In this thesis, yeast is used as a model system to specifically analyze the co-operation of co-chaperones in the maturation of heterologous clients such as SHRs and v-Src kinase. The yeast Hsp90 system faithfully recapitulates the Hsp90 dependence of mammalian clients as pioneered by the Yamamoto and Lindquist labs (Picard et al., 1990; Bohen and Yamamoto, 1993; Xu and Lindquist, 1993; Chang and Lindquist,

1994; Fang et al., 1996). Hsp90 co-chaperones are well conserved between mammals and yeast. In many cases it has also been shown that human co-chaperones behave similarly to their yeast homologs (Panaretou et al., 2002; Richter et al., 2004; McLaughlin et al., 2006; Vaughan et al., 2008; Koulov et al., 2010; Retzlaff et al., 2010; Röhl et al., 2015a). Hence, yeast provides a suitable platform to study the Hsp90 system using human client proteins. Furthermore, mechanisms that could interfere with reporter activity are absent: These include the endogenous expression of the same client, expression of client isoforms, transcriptional and post-translational modifications and downstream effects of client activation that may entail substantial effects on client activity.

To analyze genetic interactions between Hsp90 co-chaperones on the level of client activation, double knockouts/knockdowns (KOs/KDs) of all possible yeast Hsp90 co-chaperones are generated. In the resulting double mutant strains the effects of the KOs/KDs on the ability of Hsp90 to fold and activate GR, MR and v-Src are systematically analyzed. This allows to obtain a comprehensive picture of genetic networks underlying client maturation. By choosing the closely related GR and MR as model clients along with the unrelated v-Src kinase, information about the client-specificity of the underlying genetic networks can be extracted. High-scoring genetic interactors are selected for follow-up studies to determine the nature of the genetic interaction.

Together, this project expands our current knowledge on the coordinated action of co-chaperones by comprehensively analyzing the epistatic co-chaperone networks underlying client maturation *in vivo*.

2.6.2 The Human Co-Chaperome

The co-chaperome expanded from yeast with 12 co-chaperones to more than 25 co-chaperones in humans (Taipale et al., 2014). Yet, new co-chaperones are still identified in the human system, suggesting that the known co-chaperones only represent a part of the factors that modulate Hsp90 in humans. In addition, many of the known co-chaperones have been identified in high-throughput studies and were only classified as Hsp90 co-chaperones based on their interaction profile and homology. For those co-chaperones, only little in-depth knowledge about their function is available. In this thesis, we set out to investigate the human co-chaperome systematically. Due to the notorious weak interaction of co-chaperones and clients with Hsp90, we sought to screen for Hsp90 modulators in the context of client maturation. By employing client activity-based screening, also short-lived but functionally important interactions of Hsp90 and SHRs with modulators can be identified. To this end, Clustered Regularly Interspersed Short Palindromic Repeat Interference (CRISPRi) technology is employed to screen in mammalian cell lines in cooperation with the Kampmann lab at the University of California, San Francisco (Qi et al., 2013a; Gilbert et al., 2013; Kampmann, 2018). A screening library biased for proteostasis factors is used to screen for modulators that affect the activation of GR,

MR and PR in an Hsp90-dependent way. Screens performed in different cell lines reveal potential cell line-specific differences in the co-chaperone-assisted client maturation. High-scoring hits need to be further validated in follow-up experiments. In summary, this work establishes and employs a screening system for Hsp90 client maturation regulators in mammalian cells. This expand our knowledge about the Hsp90-dependent and Hsp90-independent factors required for Hsp90 client maturation in mammalian cells, including client-specific and cell line-specific differences. A thorough understanding of the Hsp90 co-chaperome is required to further understand for example the rewiring of the cellular proteostasis network during cancer formation (Rodina et al., 2016).

2.6.3 The Hsp90 Co-Chaperone NudC

NudC has been identified in high-throughput interaction studies to be associated with Hsp90, yet the function and the role in the Hsp90 system is entirely unknown (Zhu et al., 2010; Zheng et al., 2011; Taipale et al., 2014). Its role as a potential Hsp90 co-chaperone needs to be defined. To that end, purified NudC from *E. coli* is analyzed *in vitro* concerning its interaction with Hsp70 and Hsp90 in the context of client maturation using a variety of biochemical and biophysical methods including analytical ultracentrifugation (auC), NMR, mass spectrometry, fluorescence anisotropy and Förster Resonance Energy Transfer (FRET). In addition, *in vitro* findings are validated in the cellular environment. In conclusion, this project provides an understanding of how NudC interacts with Hsp70 and Hsp90 and the implications this has for client maturation.

Material and Methods

3.1 Materials

3.1.1 Technical Devices

The technical devices used during this work are summarized in Table 3. Cell counting and cell sorting equipment was used at the UCSF (San Francisco, USA).

TABLE 3: Technical Devices

Device	**Origin**
Spectrophotometers	
Chriascan-plus	Applied Photophysics (Leatherhead, UK)
Jasco FP-8500	Jasco (Groß-Umstadt, Germany)
Nanodrop ND-1000 UV-VIS Spectrophotometer	Peqlab (Erlangen, Germany)
Pherastar Plus Microplate Reader	BMG Labtech (Ortenberg, Germany)
Tecan Sunrise Plate Reader	Tecan Group Ltd. (Männedorf, Switzerland)
Ultrospec 1100 pro UV/Visible Spectrophotometer	Amersham Biosciences (Buckinghamshire, England)
Varian Cary 50 & Varian Cary 100	Varian (Palo Alto, USA)
Centrifuges	
Avanti J-25, J-26 XP and JXN-26 Rotors JA-10 and JA-25.50	Beckman Coulter (Brea, USA)
Beckmann Coulter XL-A analytical ultracentrifuge	Beckman Coulter (Brea, USA)
Fluorescence detection unit	AVIV Biomedical (Lakewood, USA)
Benchtop Centrifuge 5418	Eppendorf (Hamburg, Germany)

Universal 320 R	Hettich (Tuttlingen, Germany)
Mikro 200R	Hettich (Tuttlingen, Germany)
Chromatography Systems	
Äkta FPLC	GE Helathcare (Buckinghamshire, UK)
UPC-900 monitor	
P-920 pump	
Frac-900 fraction collector	
Shimadzu HPLC system	Shimadzu (Munich, Germany)
LC-20AC pump	
DGU 20A3 degasser	
SIL-20AC autosampling system	
SPD-20A UV detector	
RF-10AXL fluorescence detector	
Incubators and Hoods	
Heidolph Inkubator 1000 with Unimax 1010	Heidolph Instruments (Schwabach, Germany)
Heracell 150i CO_2 incubator	Thermo Scientific (Waltham, USA)
Herasafe	Thermo Scientific (Waltham, USA)
Incubator Binder KB 115	Binder GmbH (Tuttlingen, Germany)
Incubator Certomat BS-1	Sartorius (Göttingen, Germany)
Incubator Mytron WB	Mytron (Heiligenstadt, Germany)
Cell Counting and Cell Sorting	
BD Aria II FACS cytometer	BD Biosciences (Franklin Lakes, USA)
BD LSRFortessa X-14	BD Biosciences (Franklin Lakes, USA)
BD High Throughput Sampler	BD Biosciences (Franklin Lakes, USA)
Countess II Automated Cell Counter	Thermo Fisher (Waltham, USA)
Gel Electrophoresis and Western Blot	
Electrophoresis Power Supply - EPS 3501 XL& EPS 601 & EPS 1001	GE Healthcare (Buckinghamshire, UK)
Fastblot B44	Biometra (Göttingen, Germany)

Hoefer Mighty Small dual gel caster	Hoefer (Holliston, USA)
Mighty Small II SE 250 & SE 260	Hoefer (Holliston, USA)
Mini Gel Tank	Thermo Fisher (Waltham, USA)
Detection Systems	
ImageScanner III	GE Healthcare (Buckinghamshire, UK)
ImageQuant LAS 4000	GE Healthcare (Buckinghamshire, UK)
Typhoon 9200	GE Healthcare (Buckinghamshire, UK)
Chromatography Columns	
HiLoad 16/60 Superdex 75 pg	GE Healthcare (Buckinghamshire, UK)
HiPrep Desalting column G-25 resin	GE Healthcare (Buckinghamshire, UK)
HisTrap HP, 5 ml	GE Healthcare (Buckinghamshire, UK)
Hydroxyapatite (HAT)	Bio-Rad (Hercules, USA)
Resource-Q, 6 ml	GE Healthcare (Buckinghamshire, UK)
Q-Sepharose, Fast Flow	GE Healthcare (Buckinghamshire, UK)
Superdex 200 Increase 10/300 GL	GE Healthcare (Buckinghamshire, UK)
Other Equipment	
Bandelin Sonoplus HD2200	Bandelin (Berlin, Germany)
Cell Disruption System Basic Z	Constant Systems (Warwick, UK)
Certomat RM	Sartorius (Göttingen, Germany)
Certomat SII, GFL 3005	Sartorius (Göttingen, Germany)
Eppendorf Thermomixer compact	Eppendorf (Hamburg, Germany)
Freezer Ultra-low temperature C760, -80 °C	New Brunswick Scientific (Nürtingen, Germany)
Gel Dryer MGD-5040	VWR (Radnor, USA)
Gene Pulser Xcell Electroporation Systems	Bio-Rad (Hercules, USA)

Homogenizer Silent Crusher M	Heidolph Instruments (Schwabach, Germany)
Magnetic stirrer Heidolph MR 3001	Heidolph Instruments (Schwabach, Germany)
Mixer Mill MM400	Retsch (Haan, Germany)
pH-Meter 538 MultiCal	WTW (Weilheim, Germany)
Phosphor storage screen BAS-IP	GE Healthcare (Buckinghamshire, UK)
Platform shaker Heidolph Polymax 2040	Heidolph Instruments (Schwabach, Germany)
Sartorius 1409 MP	Sartorius (Göttingen, Germany)
Sartorius BL 310	Sartorius (Göttingen, Germany)
Sartorius BP 121 S	Sartorius (Göttingen, Germany)
T100 Thermal Cycler	Bio-Rad (Hercules, USA)
Ultra-Micro fluorescence cuvette	Hellma Analytics (Müllheim, Germany)
Ultra-Micro quartz absorption cuvette	Hellma Analytics (Müllheim, Germany)
Vortex Heidolph REAX top	Heidolph Instruments (Schwabach, Germany)

3.1.2 Software

The software used during this thesis is shown in Table 4. Additionally, device-specific software programs were used to operate different machines.

TABLE 4: Software and Online Tools

Software/Tool	**Origin/Reference**
Programs	
Astra 5.3.4.20	Wyatt Technology (Santa Barbara, USA)
BD FACSDiva Software	BD Biosciences (Franklin lakes, USA)
ConSurf Tool	Open Source https://consurf.tau.ac.il/
Cytoscape 3.6.1	Shannon et al., 2003

DichroWeb	Whitmore and Wallace, 2008
Endnote X7.5	Thomson Reuters (New York City, USA)
Enthought Canopy	Enthought (Austin, USA)
FlowJo 10.3	BD Life Sciences (Franklin Lakes, USA)
Gimp 2.6	Open Source (www.gimp.org)
ImageJ 1.50i	Schneider et al., 2012
Inkscape 0.48.5	Open Source (www.inkscape.org)
JabRef 4.3.1	Open Source (www.jabref.org)
LaTeX	Open Source (www.latex-project.org)
MAGeCK-iNC	Open Source (www.kampmannlab.ucsf.edu)
Microsoft Office 2010	Microsoft (Redmond, USA)
Origin Pro 9.1 (64-bit)	OriginLab (Northampton, USA)
Perseus 1.6.2.1	Tyanova et al., 2016
Pymol 1.1	Schrödinger, LLC (New York City, USA)
SedFit 14.1	Schuck, 2000
Sednterp	Laue et al., 1992
Serial Cloner 2.6.1	Open Source (www.serialbasics.free.fr)
SedView 1.1	Hayes and Stafford, 2010
Online Tools	
Clustal Omega	www.ebi.ac.uk
NCBI Blast	https://blast.ncbi.nlm.nih.gov
NEBaseChanger	https://nebasechanger.neb.com
NEBuilder Assembly Tool	https://nebuilder.neb.com
ProtParamTool	https://web.expasy.org/protparam
STRING 11.0	https://string-db.org/

3.1.3 Consumables

Consumable equipment used throughout this thesis is summarized in Table 5.

TABLE 5: Consumables

Equipment	Origin
Amicon pressure based sample concentration cell (50 ml)	Merck Millipore (Billerica, USA)
Amicon Ultra-15 Centrifugal Filter Units	Merck Millipore (Billerica, USA)
Amicon Ultra-4 Centrifugal Filter Units	Merck Millipore (Billerica, USA)
Corning 100 mm TC-Treated Culture Dish	Corning (Corning, USA)
Corning Falcon Test Tube with Strainer Snap Cap	Corning (Corning, USA)
Dialysis tubes Spectra/Por (6-8 kDa)	Spectrum (New Brunswick, USA)
PD-10 Desalting Column	GE Healthcare (Buckinghamshire, UK)
PVDF membrane	Carl Roth (Karlsruhe, Germany)
Sigma cell culture plate 6-well, 24-well, 48-well, 96-well	Sigma-Aldrich (St. Louis, USA)
Serological Pipette 1 ml, 5 ml, 10 ml, 25 ml, 50 ml	Sarstedt (Nümbrecht, Germany)
ServaGel TG Prime 4-20%	Serva (Heidelberg, Germany)
TC-Flask T25, T75	Sarstedt (Nümbrecht, Germany)
Ultracel Ultrafiltration disc 10 kDa NMWL 76 mm and 44.5 mm	Merck Millipore (Billerica, USA)
Xpress Micro-Dialyzer MD100, MWCO 3.5 kDa	Serva (Heidelberg, Germany)

3.1.4 Chemicals, Media and Solutions

TABLE 6: Chemicals, Media and Solutions

Chemical	Origin
Cell Culture	
Dulbecco's Modified Eagle Medium (DMEM)	Sigma-Aldrich (St. Louis, USA)
Dulbecco's Phosphate Buffered Saline	Sigma-Aldrich (St. Louis, USA)

Fetal Bovine Serum (FBS)	Sigma-Aldrich (St. Louis, USA)
Lipofectamine 2000	Thermo Fisher (Waltham, USA)
OPTI-MEM	Thermo Fisher (Waltham, USA)
Penicillin-Streptomycin (10,000 U mL^{-1})	Thermo Fisher (Waltham, USA)
RPMI-1640	Sigma-Aldrich (St. Louis, USA)
Trypan Blue Solution	Sigma-Aldrich (St. Louis, USA)
Trypsin-EDTA Solution	Sigma-Aldrich (St. Louis, USA)
Growth Media	
Agar Agar	Serva (Heidelberg, Germany)
Bacto Peptone	BD Biosciences (Franklin Lakes, USA)
Bacto Tryptone	BD Biosciences (Franklin Lakes, USA)
Bacto Yeast Extract	Serva (Heidelberg, Germany)
D-Galactose	Sigma-Aldrich (St. Louis, USA)
D-Glucose	Carl Roth (Karlsruhe, Germany)
LB-Medium Powder	Serva (Heidelberg, Germany)
Raffinose pentahydrate	Merck (Darmstadt, Germany)
Yeast Nitrogen Base	BD Biosciences (Franklin Lakes, USA)
YPD-Medium Powder	Carl Roth (Karlsruhe, Germany)
Antibiotics and Hormones	
Ampicillin sodium salt	Carl Roth (Karlsruhe, Germany)
Kanamycin sulfate	Carl Roth (Karlsruhe, Germany)
Hygromycin B	Roche (Basel, Switzerland)
Nourseothricin sulfate	Jena Biosciences (Jena, Germany)
Gentamicin (G418) disulfate salt	Sigma-Aldrich (St. Louis, USA)
Puromycin dihydrochloride	Sigma-Aldrich (St. Louis, USA)
L-Canavanine sulfate	Sigma-Aldrich (St. Louis, USA)
L-4-Thialysine hydrochloride	Sigma-Aldrich (St. Louis, USA)
11-Deoxycorticosterone	Sigma-Aldrich (St. Louis, USA)
Dexamethasone	Sigma-Aldrich (St. Louis, USA)
Dexamethasone Fluorescein (F-DEX)	Sigma-Aldrich (St. Louis, USA)

Aldosterone	Sigma-Aldrich (St. Louis, USA)
Progesterone	Sigma-Aldrich (St. Louis, USA)
Amino Acids, Nucleic Acids and Nucleotides	
Adenine	Sigma-Aldrich (St. Louis, USA)
Deoxyribonucleotide triphosphates (dNTP)	Roche (Basel, Switzerland)
Adenosine-5′-diphosphate (ADP) disodium salt	Roche (Basel, Switzerland)
Adenosine-5′-triphosphate (ATP) disodium salt trihydrate	Roche (Basel, Switzerland)
Adenosine-5′-(γ-thio)-triphosphate (ATPγS) tetralithium salt	Roche (Basel, Switzerland)
Adenosine-5′-(β, γ-imido)-triphosphate (AMP-PNP) lithium salt hydrate	Roche (Basel, Switzerland)
L-Arginine	Sigma-Aldrich (St. Louis, USA)
L-Aspartate	Sigma-Aldrich (St. Louis, USA)
L-Histidine	Sigma-Aldrich (St. Louis, USA)
L-Leucine	Sigma-Aldrich (St. Louis, USA)
L-Lysine	Sigma-Aldrich (St. Louis, USA)
L-Methionine	Sigma-Aldrich (St. Louis, USA)
L-S^{35}-Methionine	Hartmann Analytics (Braunschweig, Germany)
L-Threonine	Sigma-Aldrich (St. Louis, USA)
L-Tryptophan	Sigma-Aldrich (St. Louis, USA)
L-Tyrosine	Sigma-Aldrich (St. Louis, USA)
L-Phenylalanine	Sigma-Aldrich (St. Louis, USA)
Uracil	Sigma-Aldrich (St. Louis, USA)
Fluorophores and Stains	
Alexa647-maleimide	Thermo Fisher (Waltham, USA)
ATTO488-maleimide	ATTO-TEC (Siegen, Germany)
SERVA DNA Stain G	Serva (Heidelberg, Germany)
Miscellaneous reagents	
Acetic Acid	Carl Roth (Karlsruhe, Germany)
Acetone	Carl Roth (Karlsruhe, Germany)

Acrylamide (38%, 2% Bisacrylamide)	Serva (Heidelberg, Germany)
Accudrop Beads	BD Biosciences (Franklin Lakes, USA)
Agarose, ultra pure	Carl Roth (Karlsruhe, Germany)
Ammonium Persulfate (APS)	Roche (Basel, Switzerland)
Ammonium sulfate	Sigma-Aldrich (St. Louis, USA)
Benzonase nuclease	Sigma-Aldrich (St. Louis, USA)
Bromphenolblue S	Serva (Heidelberg, Germany)
Cytometer Setup and Tracking (CST) Beads	BD Biosciences (Franklin Lakes, USA)
cOmplete His-Tag Purification Resin	Roche (Basel, Switzerland)
Coomassie Brilliant Blue R-250	Serva (Heidelberg, Germany)
Dimethylsulfoxide (DMSO)	Sigma-Aldrich (St. Louis, USA)
1,4-Dithiotreitol (DTT)	Carl Roth (Karlsruhe, Germany)
Ethylendiamintetraacetic acid (EDTA)	Merck (Darmstadt, Germany)
GFP-Trap	Chromotek (Planegg-Martinsried, Germany)
Glycerol	Carl Roth (Karlsruhe, Germany)
Glycine	Carl Roth (Karlsruhe, Germany)
GlycoBlue Co-Precipitant	Thermo Fisher (Waltham, USA)
Hydrochloric acid	Carl Roth (Karlsruhe, Germany)
N-(2-Hydroxyethyl)-piperazin-N'-2-ethansulfonic acid (HEPES)	Serva (Heidelberg, Germany)
Isopropyl-β-D-thiogalactopyranoside (IPTG)	Carl Roth (Karlsruhe, Germany)
Lithium acetate	Carl Roth (Kalrsruhe, Germany)
Magnesium chloride-hexahydrate	Merck (Darmstadt, Germany)
Methanol	Merck (Darmstadt, Germany)
β-Mercaptoethanol (β-ME), pure	Merck (Darmstadt, Germany)
Milk Powder (blotting grade)	Carl Roth (Karlsruhe, Germany)
Nicotinamideadenine dinucleotide (NADH)	Roche (Basel, Switzerland)
ortho-Nitrophenyl-β-galactoside (ONPG)	Sigma-Aldrich (St. Louis, USA)

Phenylmethylsulfonyl fluoride (PMSF)	Sigma-Aldrich (St. Louis, USA)
Phosphoenolpyruvate (PEP)	Roche (Basel, Switzerland)
1,4-Piperazinediethanesulfonic acid (PIPES)	Sigma-Aldrich (St. Louis, USA)
Polybrene	Sgima-Aldrich (St. Louis, USA)
Polyethylene glycol-3350	Sigma-Aldrich (St. Louis, USA)
Polyethylene glycol-4000	Sigma-Aldrich (St. Louis, USA)
Potassium acetate	Merck (Darmstadt, Germany)
Potassium chloride	Carl Roth (Karlsruhe, Germany)
Protease Inhibitor Mix HP	Serva (Heidelberg, Germany)
Protease Inhibitor Mix G	Serva (Heidelberg, Germany)
Salmon Sperm (single-strand DNA)	Sigma-Aldrich (St. Louis, USA)
Serva DNA Stain G	Serva (Heidelberg, Germany)
SpeedBeads magnetic carboxylate modified particles	GE Healthcare (Buckinghamshire, UK)
Sodium chloride	Merck (Darmstadt, Germany)
Sodium deoxycholate	Sigma-Aldrich (St. Louis, USA)
Sodium dodecyl sulfate (SDS)	Carl Roth (Karlsruhe, Germany)
Sodium hydroxide	Merck (Darmstadt, Germany)
N,N,N',N'-Tetramethylethylendiamin (TEMED)	Carl Roth (Karlsruhe, Germany)
Trichloroacetic acid (TCA)	Merck (Darmstadt, Germany)
Tris-(Hydroxymethyl)-aminomethane (Tris)	Carl Roth (Karlsruhe, Germany)
Triton X-100	Merck (Darmstadt, Germany)
Tween-20	Merck (Darmstadt, Germany)
Urea	Merck (Darmstadt, Germany)
Westernbright ECL Spray	Advansta (Menlo Park, USA)

3.1.5 Antibodies and Enzymes

Antibodies and Enzymes used during this work are shown in Table 7.

TABLE 7: Antibodies and Enzymes

Equipment	Origin
Antibodies	
Anti-pTyr (clone: P-Tyr-01)	antikörper-online.de (Aachen, Germany)
Anti-PGK1 (clone: 22C5D8)	Thermo Fisher (Waltham, USA)
Anti-NudC (polyclonal)	antikörper-online.de (Aachen, Germany)
Anti-yAha1 (custom-made)	Pineda (Berlin, Germany)
Anti-yHch1 (custom-made)	Pineda (Berlin, Germany)
Anti-yCpr6 (custom-made)	Pineda (Berlin, Germany)
Anti-yCpr7 (custom-made)	Pineda (Berlin, Germany)
Anti-yCdc37 (custom-made)	Pineda (Berlin, Germany)
Anti-yCns1 (custom-made)	Pineda (Berlin, Germany)
Anti-Gfp (clone: 7.1 and 13.1)	Roche (Basel, Switzerland)
Anti-GR (custom-made)	Pineda (Berlin, Germany)
Anti-HA (clone: HA-7)	Sigma-Aldrich (St. Louis, USA)
Anti-yHsp26 (custom-made)	Pineda (Berlin, Germany)
Anti-Hsp70 (custom-made)	Pineda (Berlin, Germany)
Anti-Hsp82/Hsc82 (custom-made)	Pineda (Berlin, Germany)
Anti-Hsp90 α/β (clone: AC88)	Abcam (Cambridge, UK)
Anti-Hop (custom-made)	Pineda (Berlin, Germany)
Anti-yPpt1 (custom-made)	Pineda (Berlin, Germany)
Anti-ySba1 (custom-made)	Pineda (Berlin, Germany)
Anti-ySti1 (custom-made)	Pineda (Berlin, Germany)
Anti-mouse IgG-Peroxidase (from rabbit)	Sigma-Aldrich (St. Louis, USA)
Anti-rabbit IgG-Peroxidase (from goat)	Sigma-Aldrich (St. Louis, USA)
Enzymes	
Antarctic phosphatase	New England Biolabs (Ipswich, USA)

DNase I	Roche (Basel, Switzerland)
GoTaq DNA Polymerase	Promega (Madison, USA)
Lactate dehydrogenase suspension	Roche (Basel, Switzerland)
Polynucleotide kinase	New England Biolabs (Ipswich, USA)
Pyruvate kinase suspension	Roche (Basel, Switzerland)
Q5 High-Fidelity DNA Polymerase	New England Biolabs (Ipswich, USA)
T4 DNA Ligase	New England Biolabs (Ipswich, USA)
T4 DNA Polymerase	New England Biolabs (Ipswich, USA)
TEV-Protease	in-house production
ULP1 catalytic unit (Sumo-Protease)	in-house production

All restriction enzymes were obtained from New England Biolabs (Ipswich, USA). All enzymes were used with the recommended buffers according to the manufacturer's protocol.

3.1.6 Kits and Calibration Standards

TABLE 8: Kits

Kits and Standards	**Origin**
GeneRuler 50 bp DNA Ladder	Thermo Fisher (Waltham, USA)
Wizard Plus SV Minipreps DNA Purification System	Promega (Madison, USA)
Wizard Plus SV Midipreps DNA Purification System	Promega (Madison, USA)
Wizard SV Gel and PCR Clean-Up System	Promega (Madison, USA)
NucleoSpin Blood	Macherey-Nagel (Düren, Germany)
Qiagen Plasmid Plus Midi Kit	Qiagen (Venlo, Netherlands)
Serva Dual Color Protein Standard III	Serva (Heidelberg, Germany)
Serva FastLoad 1 kb DNA Ladder	Serva (Heidelberg, Germany)
Serva Triple Color Protein Standard III	Serva (Heidelberg, Germany)

3.1.7 Oligonucleotides

TABLE 9: Oligonucleotides

No.	Oligonucleotide Sequence[a]	Application
CRISPR Screening		
1	F: tccatttcaggtgtcgtgagctagccaccATGGACTCCAAAGAATCATTAAC R1: actgcggttggcgaccggtggatcccCTTTTGATGAAACAGAAGTTTTTTG R2: gttcaactctaggtttacttgtacaTCACTTTTGATGAAACAGAAG	GR into pMK1253 Clover-tagged untagged
2	F: tccatttcaggtgtcgtgagctagccaccATGGAAACCAAAGGCTAC R1: actgcggttggcgaccggtggatcccCTTTCTGTGAAAGTAAAGGG R2: gttcaactctaggtttacttgtacaTCACTTTCTGTGAAAGTAAAG	MR into pMK1253 Clover-tagged untagged
3	F: tccatttcaggtgtcgtgagctagccaccATGACTGAGCTGAAGGCA R1: actgcggttggcgaccggtggatcccCTTTTTATGAAAGAGAAGGGGTTTC R2: gttcaactctaggtttacttgtacaTCACTTTTTATGAAAGAGAAGGG	PR into pMK1253 Clover-tagged untagged
4	F: gatcgataagcttgatatcgaattcGTTTTCCCAGTCACGACG R: ctcgcccttgctcaccatggcgcgccTTTACCAACAGTACCGGAATG	300bp reporter into pXG207
5	F: TCCAATAACGTCGTACGGC R: CGTCGGGCTTATGAAAGTG	CRISPRi library amplification
6	Forward Sequencing: GTGTGTTTTGAGACTATAAGTATCCCTTGGAGAACCACCTTGTTG	Next-Gen. Seq. (Forward Indices)
	Mirror Sequencing: CCACTTTTTCAAGTTGATAACGGACTAGCCTTATTTAAACTTGCTATGCTGT	Next-Gen. Seq. (Mirror Indices)

Yeast Double Mutant Screening

7	F: CAGACCGATACCAGGATCTT	Colony-PCR fw. primer for KanMX4 cassette
	R: GAAACAACTCTGGCGCATCG	Colony-PCR rev. primer for KanMX4 cassette
	F: TCTACATGAGCATGCCC	Colony-PCR fw. primer for NatMX cassette
	R: ACGCCGAGTACGAGATGA	Colony-PCR rev. primer for NatMX cassette
8	F: ACTGTTCGTGATCGTCATCCAT	Colony-PCR for *tah1*Δ
	R: ATGGCTTTGTTGCTGTACCC	
9	F: TCTTAGAAAACGAGAAAGACTTTC	Colony-PCR for *cdc37**
	R: AGGTACAAAACCTCTGCTGT	
10	F: ACTGACATTTCACGATATCTTGA	Colony-PCR for *cns1**
	R: CCCAAAAGGTCTTGAATTCGAT	
11	F: gacggattctagaactagtggatccATGGACTCCAAAGAATCATTAAC	GR into p415GPD
	R: gacataactaattacatgactcgagTCACTTTTGATGAAACAGAAG	
12	F: gacggattctagaactagtggatccATGGAAACCAAAGGCTAC	MR into p415GPD
	R: gacataactaattacatgactcgagTCACTTTCTGTGAAAGTAAAG	
13	F1: gacggattctagaactagtggatccATGGTCGTGAATAACCCAAATAAC	Generation of Aha1 D53K
	R1: cttcacacttACCTTCAATGGACGAAAC	
	F2: cattgaaggtAAGTGTGAAGTTAATCAGC	
	R2: gacataactaattacatgactcgagTTATAATACGGCACCAAAG	
14	F: CATCACCGGTAAGTCCAACGTATC	Generation of Hch1 D53K
	R: CTACTCACCTGGGTTAAC	
15	F1: gacggattctagaactagtggatccATGGGTTACCCATACGATGTTCCTGACTATGCG	HA-tagged v-Src into p416GAL1
	R1: tactccccatACCAGCACCGGCACCGGC	
	F2: cggtgctggtATGGGGAGTAGCAAGAGC	

	R2: gacataactaattacatgactcgagCTACTCAGCGACCTCCAAC	
16	F1: gacggattctagaactagtggatccATGTCATTGACAGCCGATG R1: ataaaacatgtgcTGGAGTTTCAGAAACTTCAATAG F2: tgaaactccagcaCATGTTTTATATTCTAACAGGTC R2: gtgcagcagctcttgcAGAATATCCTCTAGCATCTTC F3: aggatattctgcaAGAGCTGCTGCACTAGCG R3: gacataactaattacatgactcgagTTAGCGGCCAGTCCGGATG	Generation of Sti1 N39A/N435A
17	F1: gacggattctagaactagtggatccATGTCATTGACAGCCGATG R1: cattaccaatagcCGCAAATGATTTGGAAATGAC F2: atcatttgcggctATTGGTAATGCCTATCACAAATTGGGTG R2: gacataactaattacatgactcgagTTAGCGGCCAGTCCGGATG	Generation of Sti1 R341A
Characterization of NudC		
18	F: tcacagagaacagattggtggatccATGGGTGGTGAACAAGAAG R: agtggtggtggtggtggtgctcgagTTAATTGAATTTGGCTTTGCTAAAATC	NudC into pET-SUMO
19	F1: aagatctgaattcttcgaactcgagATGGGTGGTGAACAAGAAG R1: gcagcgtacgATTGAATTTGGCTTTGCTAAAATC F2: caaattcaatCGTACGCTGCAGGTCGAC R2: atcttatcatgtctggccagctagcTTACTTGTACAGCTCGTCCATG	NudC-GFP into pVitroII-Hygro-MCS2
20	F1: aagatctgaattcttcgaactcgagatggaaaccggtgcagcag R1: gcagcgtacgaaactgcacggcacccgg F2: cgtgcagtttcgtacgctgcaggtcgac R2: atcttatcatgtctggccagctagcttacttgtacagctcgtccatg	NudCD3-GFP into pVitroII-Hygro-MCS2
21	F: aagatctgaattcttcgaactcgagATGGGTGGTGAACAAGAAG R: atcttatcatgtctggccagctagcTTAATTGAATTTGGCTTTGCTAAAATC	NudC into pVitroII-Hygro-MCS2

22	F: aagatctgaattcttcgaactcgagCGTACGCTGCAGGTCGAC R: atcttatcatgtctggccagctagcTTACTTGTACAGCTCGTCCATG	GFP into pVitroII-Hygro-MCS2
23	F: tggacagcaaatgggtcgcggatccATGAAGCTGAAACCGAATTTAG R: agtggtggtggtggtggtgctcgagCTAGCTGTTCTCGGGATTAATC	NudC$^{158-274}$ into pET28b
24	F: tggacagcaaatgggtcgcggatccATGGGTGGTGAACAAGAAG R: agtggtggtggtggtggtgctcgagCTAGCTGTTCTCGGGATTAATC	NudC$^{1-274}$ into pET28b
25	F: tggacagcaaatgggtcgcggatccATGGGTGGTGAACAAGAAG R: agtggtggtggtggtggtgctcgagCTAACCCGGACTATCCAG	NudC$^{1-141}$ into pET28b
26	F: tggacagcaaatgggtcgcggatccATGAAGCTGAAACCGAATTTAG R: agtggtggtggtggtggtgctcgagTTAATTGAATTTGGCTTTGC	NudC$^{158-331}$ into pET28b
27	F: TCTGGTTCTTTCAGGGCATTGCTATTTATTC R: ACCAGAACCAGAAAAGTGCTTGACTGC	Generation of Hsp90$\beta^{322-328GS}$ mutant

[a] 'F' and 'R' denote the forward and the reverse primers, respectively.

3.1.8 Plasmids

TABLE 10: Plasmids

Plasmid Backbone	Insert	Origin
Yeast Vectors		
p415GPD	GR	This work
p415GPD	MR	This work
p413GPD	GR	Sahasrabudhe et al., 2017
p413GPD	MR	Sahasrabudhe et al., 2017
p413GPD	HA-GR	Sahasrabudhe et al., 2017
p413GPD	HA-MR	Sahasrabudhe et al., 2017
p413GAL1	v-Src	Boczek et al., 2015
p416GAL1	v-Src	This work
p416GAL1	HA-v-Src	This work
p416GAL-S	v-Src	This work
p415GPD	yAha1	This work
p415GPD	yAha1^{D53K}	This work
p415GPD	yCdc37	This work
p415GPD	yHch1	This work
p415GPD	yHch1^{D53K}	This work
p415GPD	ySba1	This work
p415GPD	ySti1	This work
p415GPD	ySti1$^{N39A/N435A}$	This work
p425GAL1	yAha1	This work
p425GAL1	yAha1^{D53K}	This work
p425GAL1	yHch1	This work
pFA6-NatNT2	NatNT2	(Janke et al., 2004)
pFA6-NatMX4	NatMX4	(Janke et al., 2004)
pUCΔSS-26X	GRE, mCyc, lacZ	Sahasrabudhe et al., 2017
Vectors for Human Cell Lines		
pDLO	2xGal4, 2xGRE, mADH, Luciferase	Brian Freeman, University of Illinois

pLG15	sgRNAs for individual Knockdowns	This work
pMDL	Lentiviral Packaging	Addgene no. 12251
pMK1253	GR-WT	This work
pMK1253	GR-Clover	This work
pMK1253	MR-WT	This work
pMK1253	MR-Clover	This work
pMK1253	PR-WT	This work
pMK1253	PR-Clover	This work
pRSV	Lentiviral Packaging	Addgene no. 12253
pSLQ1371	CRISPRi/a library	This work
pXG207	2xGal4, 2xGRE, mADH mCherry	This work
pVitroII-Hygro-MCS	NudC	This work
pVitroII-Hygro-MCS	NudC-GFP	This work
pVitroII-Hygro-MCS	GFP	This work
pVSVG	Lentiviral Packaging	Addgene no. 12259
Vectors for Protein Purification		
pET28a	NudC	GeneArt (Thermo Fisher, Waltham, USA)
pET28b	$NudC^{1-141}$	This work
pET28b	$NudC^{1-274}$	This work
pET28a	$NudC^{50-331}$	GeneArt (Thermo Fisher, Waltham, USA)
pET28b	$NudC^{158-274}$	This work
pET28b	$NudC^{158-331}$	This work
pET28b	$NudC^{I104A/L107A}$	This work
pET28b	Hsp90α	Joanna Soroka, TU Munich
pET28b	Hsp82	Alina Röhl, TU Munich
pET28	Hop (tagless)	Klaus Richter, TU Munich
pET28b	Hch1	Jing Li, TU Munich

pET28b	hAha1	Sandrine Stiegler, TU Munich
pET-Halo	GR-LBDm	Lorenz et al., 2014
pET-SUMO	NudC	This work
pET-SUMO	Hsp70	Eva Kriehuber, TU Munich
pET-SUMO	Hsp70-ΔEEVD	This work
pET-SUMO	Hsp90β	Franziska Tippel, TU Munich
pET-SUMO	Ydj1	Andreas Schmid, TU Munich
pET-SUMO	Hop^{TPR1}	Daniel Rutz, TU Munich
pET-SUMO	Hop^{TPR2A}	Daniel Rutz, TU Munich
pET-SUMO	Hop^{TPR2B}	Daniel Rutz, TU Munich
pET-SUMO	Hop$^{TPR2A-2B}$	Daniel Rutz, TU Munich
pET-SUMO	Hop$^{TPR2A-2B-DP2}$	Daniel Rutz, TU Munich
pET-SUMO	Hsp90$\beta^{322-328GSsub}$	This work
pETM-11	Hsp90β^{NM}	Florent Delhommel, TU Munich
pETM-11	Hsp90β^{MC}	Florent Delhommel, TU Munich

3.1.9 Organisms

3.1.9.1 Bacterial Strains

For cloning purposes *Escherichia coli (E. coli)* Mach1, *E. coli* XL-1 blue and *E. coli* DH5α were used (Table 11). Notably, all lentiviral vectors were maintained in *E. coli* DH5α cells. The *E. coli* BL-21 strain was used for protein expression.

TABLE 11: Bacterial Strain Genotypes

Strain Name	Genotype	Origin
E. coli BL21-CodonPlus(DE3)-RIL	F$^-$ *ompT hsdS*($r_B{}^-$ $m_B{}^-$) dcm$^+$ Tet^r *gal* λ(DE3) *endA* Hte [*argU ileY leuW* Cam^r]	Agilent (Santa Clara, USA)
E. coli Mach1	F$^-$ φ80(*lacZ*)ΔM15 Δ*lacX*74 *hsdR*($r_K{}^-m_K{}^+$) Δ*recA1398 endA1 tonA*	Thermo Fisher (Waltham, USA)
E. coli XL-1 blue	*recA1 endA1 gyrA96 thi-1 hsdR17 supE44 relA1 lac* [F′ *proAB lacI^q*ZΔM15 Tn10 (Tet^r)]	Agilent (Santa Clara, USA)
E. coli DH5α	*fhuA2* Δ(*argF-lacZ*)*U169 phoA glnV44* φ*80*Δ(*lacZ*)M15 *gyrA96 recA1 relA1 endA1 thi-1 hsdR17*	New England Biolabs (Ipswich, USA)
E. coli MegaX DH10B T1^R	F$^-$ *mcrA* Δ(*mrr-hsd*RMS-*mcr*BC) φ80*lacZ*ΔM15 Δ*lacX74 recA1 endA1 araD*139 Δ(*ara, leu*)7697 *galU galK* λ^- *rpsL nupG tonA*	Thermo Fisher (Waltham, USA)

3.1.9.2 Yeast Strains

The wild-type *Saccharomyces cerevisiae (S. cerevisiae)* BY4741 strain (MATa; *his3*Δ*1*; *leu2*Δ*0*; *met15*Δ*0*, *ura3*Δ*0*) and single knockout mutations in the BY4741 genetic background were obtained from Euroscarf (Oberusel, Germany). In these strains, the respective genes were replaced by the KanMX4 antibiotic resistance cassette. For essential co-chaperones, Decreased Abundance by mRNA Perturbation (DAmP) strains (Schuldiner et al., 2005) were obtained from Dharmacon (Lafayette, USA) as diploids. The Synthetic Genetic Array (SGA) strain Y8205 (MATα; *can1*Δ*::STE2pr-Sp_his5*; *lyp1*Δ*::STE3pr-LEU2*; *his3*Δ*1*; *leu2*Δ*0*; *ura3*Δ0) was obtained from the Boone lab (Toronto, Canada). All double mutants contain knockouts or knockdowns of two genes encoding for Hsp90 co-chaperones in the same genetic background. Strains containing the *tet07-CNS1* mutation (*tet07-CNS1 R1158 pCNS1::kanR-tet07-TATA*) were a kind gift from Florian Schopf and Christopher Dodt (TU Munich, Germany). Table 12 contains the genotypes of yeast strains generated and used during this thesis.

TABLE 12: Yeast Strain Genotypes

Strain Name[a]	**Genotype**[b]
Wild-Type Strains	
BY4741	MATa; *his3Δ1*; *leu2Δ0*; *met15Δ0*, *ura3Δ0*
Y8205	MAT*α*; *can1Δ::STE2pr-Sp_his5*; *lyp1Δ::STE3pr-LEU2*; *his3Δ1*; *leu2Δ0*; *ura3*Δ0
BY4741 *x* Y8205	MATa; *can1Δ::STE2pr-Sp_his5*; *his3Δ1*; *leu2Δ0*; *ura3Δ0*
Single Knockout/Knockdown Strains	
yfg1Δ	MATa; *can1Δ::STE2pr-Sp_his5*; *his3Δ1*; *leu2Δ0*; *ura3Δ0*; *yfg1Δ::NatMX*
*yfg1**	MATa; *can1Δ::STE2pr-Sp_his5*; *his3Δ1*; *leu2Δ0*; *ura3Δ0*; *yfg1::DAmP-NatMX*
Double Knockout/Knockdown Strains	
yfg1Δ/yfg2Δ	MATa; *can1Δ::STE2pr-Sp_his5*; *his3Δ1*; *leu2Δ0*; *ura3Δ0*; *yfg1Δ::NatMX*; *yfg2Δ::KanMX4*
yfg2Δ/yfg1Δ	MATa; *can1Δ::STE2pr-Sp_his5*; *his3Δ1*; *leu2Δ0*; *ura3Δ0*; *yfg2Δ::NatMX*; *yfg1Δ::KanMX4*
yfg1/yfg2Δ*	MATa; *can1Δ::STE2pr-Sp_his5*; *his3Δ1*; *leu2Δ0*; *ura3Δ0*; *YFG1::DAmP-NatMX*; *yfg2Δ::KanMX4*
yfg2/yfg1Δ*	MATa; *can1Δ::STE2pr-Sp_his5*; *his3Δ1*; *leu2Δ0*; *ura3Δ0*; *YFG2::DAmP-NatMX*; *yfg1Δ::KanMX4*
yfg1/yfg2**	MATa; *can1Δ::STE2pr-Sp_his5*; *his3Δ1*; *leu2Δ0*; *ura3Δ0*; *YFG1::DAmP-NatMX*; *YFG2::DAmP-KanMX4*
yfg2/yfg1**	MATa; *can1Δ::STE2pr-Sp_his5*; *his3Δ1*; *leu2Δ0*; *ura3Δ0*; *YFG2::DAmP-NatMX*; *YFG1::DAmP-KanMX4*

[a] yfg: your favorite gene; To be replaced by one of the genes encoding for an Hsp90 co-chaperone

[b] DAmP-NatMX/KanMX4: DAmP by insertion of the NatMX/KanMX4 antibiotic resistance cassette

3.1.9.3 Human Cell Lines

TABLE 13: Human Cell Lines

Cell Line Name	Description	Origin
Hek293T	Lentivirus packaging cell line, CRL-3216	ATCC (Manassas, USA)
Hek293T-CRISPRi	Monoclonal Hek293T cell line stably transfected with the CRISPRi machinery	Kampmann lab (UCSF, USA)
Hek293T-GRWT-A1m	Monoclonal Hek293T-CRISPRi cell line encoding the GR-WT gene in the genome	This work
Hek293T-MRWT-B12m	Monoclonal Hek293T-CRISPRi cell line encoding the MR-WT gene in the genome	This work
Hek293T-PRWT-B4m	Monoclonal Hek293T-CRISPRi cell line encoding the PR-WT gene in the genome	This work
Hek293T-GR-Clover	Monoclonal Hek293T-CRISPRi cell line encoding the GR-Clover gene in the genome	This work
K562-CSISPRi	Monoclonal K562 cell line stably transfected with the CRISPRi machinery	Kampmann lab (UCSF, USA)
K562-GRWT-A1m	Monoclonal K562-CRISPRi cell line encoding the GR-WT gene in the genome	This work

3.1.10 Media and Buffers

3.1.10.1 Growth Media for Bacteria and Yeasts

Table 14 summarizes media used for the growth of bacterial and yeast cells during this work. Bacterial cultures were supplemented with either $100\,\mu g\,mL^{-1}$ ampicillin, $50\,\mu g\,mL^{-1}$ kanamycin or $100\,\mu g\,mL^{-1}$ hygromycin B. Yeast growth media were supplemented with $100\,\mu g\,mL^{-1}$ Nourseothricin, $200\,\mu g\,mL^{-1}$ gentamicin or $200\,\mu g\,mL^{-1}$ hygromycin B to select for the genomic insertion of resistance cassettes. For agar plates, $20\,g\,L^{-1}$ agar agar were added to the media. Glucose was autoclaved separately and added to the media after autoclaving.

TABLE 14: Growth Media

Growth Medium	**Composition**
Bacterial growth media	
Lysogeny Broth (LB)	20 g L^{-1} LB powder
2xYT medium	3.5% bacto tryptone 2.0% yeast extract 0.5% NaCl
ZYM-5052 auto-induction medium (Studier, 2005)	
ZY	10 g L^{-1} bacto tryptone 5 g L^{-1} yeast extract
M	25 mM Na_2HPO_4 25 mM KH_2PO_4 50 mM NH_4Cl 5 mM Na_2SO_4
5052	0.5% glycerol 0.05% D(+)-glucose 0.2% lactose monohydrate
trace elements (1000x)[a]	0.2x
SOB / SOC medium	2% bacto tryptone 0.5% yeast extract 8.56 mM NaCl 2.5 mM KCl 10 mM $MgCl_2$ 10 mM $MgSO_4$ for SOC: + 20 mM glucose
Yeast Growth Media	
YPD	1% yeast extract 2% bacto peptone 2% glucose
Synthetic Defined (SD) medium	6.7 g L^{-1} YNB 20 g L^{-1} glucose 2 g L^{-1} amino acid mix[b]
Enriched Sporulation Medium	10 g L^{-1} potassium acetate 1 g L^{-1} yeast extract 0.5 g L^{-1} glucose 0.1 g L^{-1} sporulation amino acid mix[c]

Haploid Selection Medium	1.7 g L^{-1} YNB without ammonium sulfate 1 g L^{-1} glutamate natrium salt 2 g L^{-1} -His/Arg/Lys amino acid mix 100 µg mL^{-1} L-canavanine 100 µg mL^{-1} thialysine antibiotics as applicable

[a] The 1000x trace elements mix contained 50 mM $FeCl_3$, 20 mM $CaCl_2$, 10 mM $MnCl_2$, 10 mM $ZnSO_4$, 2 mM $CoCl_2$, 2 mM $CuCl_2$, 2 mM $NiCl_2$, 2 mM Na_2MoO_4, 2 mM Na_2SeO_3, 2 mM H_3BO_3 in 60 mM HCl.

[b] The SD amino acid mix contained 0.5 g adenine, 2 g arginine, 2 g aspartate, 2 g histidine, 10 g leucine, 2 g lysine, 2 g methionine, 2 g threonine, 2 g tryptophan, 2 g tyrosine, 2 g phenylalanine and 2 g uracil.

[c] The sporulation amino acid mix contained 2 g histidine, 10 g leucine, 2 g lysine and 2 g uracil.

3.1.10.2 Human Cell Growth Media

To maintain human cells, DMEM or RPMI-1640 were supplemented with 10% Fetal Bovine Serum (FBS) and 1x penicillin-streptomycin mix. K562 cell lines were maintained in RPMI-1640-based medium and Hek293T cells were grown in DMEM-based medium.

3.1.10.3 Purification Buffers

GR-LBD purification buffers

- **Ni-NTA A** (50 mM Tris-HCl, 2 M urea, 100 mM NaCl, 5 $MgCl_2$, 10 mM imidazole, 2 mM β-ME, 50 µM dexamethasone, pH 7.9)
- **Ni-NTA B/C** (50 mM Tris-HCl, 500 mM NaCl, 10 mM/350 mM imidazole, 10% glycerol, 2 mM β-ME, 50 µM dexamethasone, pH 7.9)
- **TEV-Buffer** (50 mM Tris-HCl, 100 mM NaCl, 10% glycerol, 2 mM β-ME, 0.5% CHAPS, 50 µM dexamethasone, pH 7.9)
- **SEC Buffer** (25 mM Tris-HCl, 100 mM NaCl, 10% clycerol, 2 mM DTT, 50 µM dexamethasone, pH 7.9)

Hch1 Purification Buffers

- **Ni-NTA A/B** (40 mM NaH_2PO_4, 500 mM NaCl, 1 mM $MgCl_2$ 20 mM/300 mM imidazole, 1 mM DTT, pH 7.5)
- **SEC**(40 mM Hepes, 150 mM KCl, 5 mM $MgCl_2$, 1 mM DTT, pH 7.5)

Hop Purification Buffers

- **Q-Sepharose A/B** (25 mM Hepes, 5 mM $MgCl_2$, 500 mM KCl (only in Q-Sepharose B), 1 mM DTT, pH 7.6)

- **HAT A/B** (10 mM/400 mM potassium phosphate, pH 7.5)
- **SEC** (40 mM Hepes, 150 mM KCl, 5 mM $MgCl_2$, 1 mM DTT, pH 7.5)

Hsp40 Purification Buffers

- **Ni-NTA A/B** (40 mM NaH_2PO_4, 500 mM NaCl, 20 mM/500 mM imidazole, 2 mM β-ME (+10% glycerol for DNAJA1), pH 8.0)
- **SEC** (40 mM Hepes, 150 mM KCl, 5 mM $MgCl_2$, 1 mM DTT, pH 7.5)

Hsp70 Purification Buffers

- **Ni-NTA A/B** (40 mM Hepes, 150 mM KCl, 350 mM NaCl, 20 mM $MgCl_2$, 5% glycerol, 10 mM/300 mM imidazole, 2 mM β-ME, 0.5 mM ATP (only Ni-NTA A), pH 7.5)
- **SEC** (40 mM Hepes, 150 mM KCl, 5 mM $MgCl_2$, 1 mM DTT, pH 7.5)

Hsp90 Purification Buffers

- **Ni-NTA A/B** (50 mM Na_2HPO_4, 300 mM NaCl, 10 mM/500 mM imidazole, 1 mM DTT, pH 7.8)
- **ResQ A/B** (40 mM Hepes, 20 mM/1000 mM KCl, 1 mM EDTA, 1 mM DTT, pH 7.5)
- **SEC** (40 mM Hepes, 150 mM KCl, 5 mM $MgCl_2$, 1 mM DTT, pH 7.5)

NUDC Purification Buffers

- **Ni-NTA A/B** (10 mM Tris-HCl, 50 mM KCl, 50 mM NaCl, 5 mM $MgCl_2$, 10 mM/300 mM imidazole, 1 mM DTT, pH 7.5)
- **SEC** (40 mM Hepes, 150 mM KCl, 5 mM $MgCl_2$, 1 mM DTT, pH 7.5)

3.2 Methods

3.2.1 Molecular Cloning Techniques

3.2.1.1 Maintenance of Bacterial Cells

Bacterial cultures were generally grown at 37 °C while shaking. For short-term storage, bacteria on agar plates were stored at 4 °C.

3.2.1.2 Generation of Chemically Competent *E. coli*

Fresh *E. coli* colonies were used to inoculate 25 mL of SOB medium and grown for 6-8 h at 37 °C while shaking. From this culture, 10 mL were used to inoculate 250 mL of SOB medium. The cultures were grown over-night at 18 °C until one of them reached an OD_{600} of 0.55 to 0.6. Cells were then placed on ice for 10 min before cells were harvested at 2,500 xg at 4 °C for 10 min. The pellet was resuspended in 50 mL ice-cold TB buffer (10 mM Pipes, 55 mM $MnCl_2$, 15 mM $CaCl_2$, 250 mM KCl, pH 6.7) and incubated on ice for 10 min. Cells were then pelleted again as described, resuspended in 20 mL TB buffer supplemented with DMSO to a final concentration of 7% and flash-frozen in liquid nitrogen.

3.2.1.3 Plasmid Transformation into *E. coli*

For transformation into chemically competent *E. coli*, 100 ng of plasmid DNA or an entire Sequence and Ligation Independent Cloning (SLIC) reaction (Section 3.2.1.7) were mixed with 100-200 µL of chemically competent cells. The reaction was incubated on ice for 20 min and then heat-shocked at 42 °C for 45 s. The reaction was then immediately cooled on ice for 2-5 min and diluted in 1 mL of LB^0 medium and incubated at 37 °C while shaking for 1 h. Subsequently, the suspension was pelleted at 7000 xg for 30 s and plated on selective LB agar plates.

3.2.1.4 Plasmid Digestion and Purification

Plasmid DNA was transformed into *E. coli* and a 5 mL culture was grown over-night in LB with the respective antibiotic at 37 °C. Plasmid DNA was then extracted using the Wizard Plus SV Minipreps DNA Purification System according to the manufacturer's protocol.

Plasmids were digested using approximately 1 µg of DNA mixed with 20-50 units of each restriction enzyme in the recommended buffer in a final reaction volume of 50 µL. The reaction took place at 37 °C for at least 1 h. The digested DNA was then treated with 5 units of Antarctic Phosphatase (AP) at 37 °C for 1 h. Subsequently, the vector was purified using the Wizard SV Gel and PCR Clean-Up System according to the manufacturer's protocol.

3.2.1.5 Polymerase Chain Reaction

Polymerase Chain Reaction (PCR) was used to amplify insert DNA for SLIC (Section 3.2.1.7). The PCR conditions for standard PCRs is shown in Table 15. After the reaction, the sample was subjected to DpnI digest (0.5 U/µL) at 37 °C for 1 h and then purified using the Wizard SV Gel and PCR Clean-Up kit.

TABLE 15: Standard PCR Conditions for Cloning

Component	Final Concentration
Template	1-10 ng
dNTPs (10 mM per dNTP)	200 µM
Forward Primer	1 µM
Reverse Primer	1 µM
Q5 reaction buffer	1x
Q5 High-Fidelity DNA Polymerase	0.02 units/µL
H_2O	*ad* 50 µL

A general temperature cycle program is shown in Table 16.

TABLE 16: Temperature Cycle Program for Standard PCRs

Step	Temperature	Time
Initial Denaturation	98 °C	30 s
35 Cycles		
Denaturation	98 °C	15 s
Annealing	X °C[a]	30 s
Extension	72 °C	30 s per kb
Final Extension	72 °C	10 min

[a] X indicates the primer-specific annealing temperature as determined by the NEBuilder or NEBaseChanger tools.

3.2.1.6 Agarose and Polyacrylamid Gel Electrophoresis for DNA Analysis

To analyze the success of PCR reactions, confirm the purity and to select DNA fragments of the desired size, we employed agarose gel electrophoresis and Tris-Borat-EDTA Polyacrylamide Gel Electrophoresis (TBE-PAGE). For agarose gels, 0.8% - 2% agarose gels in Tris-Acetate-EDTA (TAE) buffer (40 mM Tris, 20 mM acetic acid, 1 mM EDTA) were prepared. The suspension of agarose in TAE buffer was boiled until the agarose was dissolved, the gel was mixed with Serva DNA Stain G (1:50,000) and cast into a chamber. Gels were then run at a constant voltage of 120 V for 20 min

and DNA was visualized by UV irradiation. To recover DNA, a gel slice containing the desired product was excised and purified using the Wizard SV Gel and PCR Clean-Up System.

For the analysis of small DNA fragments, TBE-PAGE with 15% -20 % acrylamide in 0.5x TBE buffer (Stock: 89 mM Tris, 89 mM boric acid, 20 mM EDTA) were used. Polymerization was induced by the addition of 100 µL of 10% APS and 10 µL of TEMED to 10 mL TBE-acrylamide solution. Samples were mixed with 6x Purple Loading Dye and run in 0.5x TBE buffer at 200 V until the dye front reached approximately 1/3 of the gel. The gel was then soaked in a Stain G bath (1:10,000 in TBE) while shaking for 15 min at room temperature. Subsequently, DNA was visualized by UV irradiation. To recover DNA from TBE gels, we used the *'Crush and Soak'* protocol. Briefly, the gel piece was placed in a 0.5 mL non-stick Eppendorf tube, which was pierced with a needle at the bottom. The tube was placed in a 1.5 mL tube and centrifuged until the gel was crushed through the hole. The gel pieces were then incubated with 200 µL of nuclease-free water and heated to 70 °C for 10 min. The slurry was transferred to a spin-column and the solution was separated from the gel debris by centrifugation. For precipitation, 2 µL GlycoBlue and 25 µL of 3 M NaCl were added and mixed before addition of 750 µL of isopropanol. The sample was placed at -20 °C for 30 min and then centrifuged at 20,000 xg at 4 °C for 30 min to pellet DNA. The pellet was washed with 80% ethanol, air-dried and DNA was dissolved in nuclease-free water.

3.2.1.7 Sequence and Ligation Independent Cloning

For SLIC, the vector was obtained by restriction digest and the inserts were generated by standard PCR (Table 15). The primers for the PCR reaction were designed using the NEBuilder tool (Table 4). For the SLIC reaction, 100 ng of digested vector were mixed with a two-fold molar excess of insert DNA and 1x NEB Buffer 2.1 in a 10 µL reaction volume. The reaction was initiated by the addition of 1.5 units of T4 DNA Polymerase and incubated for 2.5 min at room temperature. The reaction was then placed on ice for 10 min before the entire reaction mixture was used for transformation into *E. coli* XL-1 blue, DH5α or Mach1 cells (Section 3.2.1.3).

3.2.1.8 Site-Directed Mutagenesis

The Site-Directed Mutagenesis Protocol was used to introduce point mutations into plasmid DNA, following the manufacturer's protocol. PCR primers were designed using the NEBaseChanger tool (Table 4). Briefly, plasmid DNA was amplified with primers containing the mutation with a standard PCR protocol using 5-25 ng of template (Table 15, Table 16). Subsequently, 1 µL of the PCR reaction were mixed with 0.5 µL DpnI, 0.5 µL T4 DNA Ligase and 0.5 µL Polynucleotide Kinase with 1x T4

DNA Ligase Buffer in a 10 µL reaction volume. The reaction occurred at room temperature for 5 min, was then transferred on ice and the entire reaction was used for transformation into *E. coli* XL-1 blue, DH5α or Mach1 cells (Section 3.2.1.3).

3.2.1.9 Genomic DNA Extraction

Genomic DNA was extracted from yeast following a modified Bust n' Grab protocol (Harju et al., 2004). Briefly, an over-night culture was harvested and resuspended in lysis buffer (2% Triton X-100, 1% Sodium Dodecyl Sulfate (SDS), 100 mM NaCl, 10 mM Tris-HCl, 1 mM EDTA, pH 8.0). The suspension was then subjected to 3 freeze-thaw cycles comprising freezing at -80 °C for 20 min and boiling at 95 °C for 5 min. The suspension was then mixed with 200 µL of phenol-chloroform-isoamyl alcohol. The sample was centrifuged at full speed at room temperature for 10 min and the aqueous phase was aspirated. The DNA was precipitated by addition of 400 µL -20 °C cold ethanol. The sample was then pelleted and washed with 70% ethanol as described. Subsequently, the pellets were air-dried at 30 °C and resuspended in H_2O.

3.2.1.10 Determination of DNA Concentration and Quality

DNA concentration was quantified by UV-spectroscopy. Absorbance was measured at 260 nm in a Nanodrop ND-100 UV/Vis spectrophotometer and the concentration was calculated using the Lambert-Beer Law (Equation 3.1).

$$A_{260} = \epsilon \times c \times d \tag{3.1}$$

with A_{260} representing the absorption at 260 nm, ϵ denoting the extinction coefficient (0.02 mL µg^{-1} cm^{-1} for DNA), c being the DNA concentration [ng µL^{-1}] and d being the layer thickness [cm]. DNA purity was determined by ensuring the A_{260}/A_{280} ratio was between 1.8 and 2.0. H_2O was measured to correct for background absorption.

3.2.2 Heterologous Protein Expression

All proteins that were used for this thesis were purified as part of the study except for the following exceptions: Hop^{TPR1}, Hop^{TPR2A}, Hop^{TPR2B}, Hop$^{TPR2A-2B}$ and Hop$^{TPR2A-2B-DP2}$ were kind gifts from Daniel Rutz (TU Munich). p53-DBD and labeled variants were kindly provided by Vinay Dahiya (TU Munich). p23 was a gift from Jannis Lawatscheck (TU Munich). A summary of the proteins used during this thesis and the respective purification procedure overview is found in Table 17.

3.2.2.1 Cell Growth and Lysis

Proteins were expressed in *E. coli* BL21-Codon Plus (DE3)-RIL cells from pET28 or pET-SUMO plasmids. Cells were grown in LB media for most purifications and in

TABLE 17: Protein Purification Summary

Protein	Expression Conditions	Purification Steps
hAha1	4 h at 37 °C	Ni-NTA, ATP wash, SEC
GR-LBD	over-night at 16-18 °C	Ni-NTA, Dilution with TEV-Buffer, TEV-protease digest, reverse Ni-NTA, SEC
Hch1	4 h at 37 °C	Ni-NTA, ATP wash, SEC
hHsp70	4 h at 37 °C	Ni-NTA, Dialysis/Buffer exchange into Ni-NTA A, SUMO-protease digest, reverse Ni-NTA, SEC
hHsp90 & yHsp82	4 h at 37 °C	Ni-NTA, Dilution with ResQ A buffer, Resource Q, SEC
Hop	4 h at 37 °C	Q-Sepharose, HAT, SEC
NudC & NudC mutants	4 h at 37 °C	Ni-NTA, ATP wash, SEC
NudC (tagless)	4 h at 37 °C	Ni-NTA, ATP wash, Dialysis/Buffer exchange into Ni-NTA A, SUMO-protease digest, reverse Ni-NTA, SEC
Ydj1 & DNAJA1	4 h at 37 °C & 20 °C over-night	Ni-NTA, ATP wash, Dialysis/Buffer exchange into Ni-NTA A, SUMO-protease digest, reverse Ni-NTA, SEC
Sti1 & Sti1 mutants	4 h at 37 °C	Ni-NTA, ATP wash, Dialysis/Buffer exchange into Ni-NTA A, SUMO-protease digest, reverse Ni-NTA, SEC

2xYT media for the purification of Hsp90. Cells were grown to an OD_{600} of 0.5-0.8 and were then induced by the addition of 1 mM IPTG. Proteins were expressed at 37 °C for 4 h or at 30 °C over-night yielding comparable results. DNAJA1 was expressed at 20 °C over-night.

The Glucocorticoid Receptor Ligand Binding Domain (GR-LBD) was expressed in *E. coli* BL21-Codon Plus (DE3)-RIL using a previously published auto-induction system (Studier, 2005). Briefly, ZYM-5052 medium (Table 14) was inoculated by addition of 0.1% of the culture medium of an over-night LB culture and then grown at 37 °C for 4 h. The cells were shifted to 16-18 °C, incubated for 1 h and then supplemented with 50 µM dexamethasone. Protein expression then took place at 16-18 °C over-night.

Cells were harvested at 7,000 rpm in a JA-10 rotor at 4 °C for 12 min. For GR-LBD expression, the pellet was then washed with cold Phosphate Buffered Saline (PBS) once before lysis. The pellet was resuspended in the respective Ni-NTA A buffer supplemented with 1x Protease Inhibitor Mix HP, 1 mM PMSF and DNase I and lysed by pressure at 2 kbar in a cell disruption system. Afterwards, the lysate

was cleared by centrifugation at 48,000 xg in a JA-25.50 rotor at 4 °C for 45-60 min.

3.2.2.2 Protein Purification

All protein constructs expressed with a His_6-tag (His_6 only, His_6-SUMO or His_6-Halo) were purified using affinity chromatography with nickel resin (Ni-NTA) and Size Exclusion Chromatography (SEC). Due to the special requirements of the GR-LBD, the nickel affinity chromatography step was adapted. Hsp90 was additionally subjected to anion-exchange chromatography on a Resource Q column before SEC. Tagless HOP was purified using a combination of ion exchange columns and SEC.

Hsp90, Hsp70 and Co-Chaperone Purification
Lysate in the respective Ni-NTA A buffer (Section 3.1.10.3) was loaded onto the column and the bound protein was washed with at least 5 column volumes (CV) of Ni-NTA A buffer. For Hsp90 co-chaperones, an ATP wash with 10 mL of a 2 mM ATP solution in Ni-NTA A was done to dissociate DnaK. Bound proteins were eluted by washing with Ni-NTA B buffer. Sumo-tagged proteins were then either subjected to dialysis into Ni-NTA A buffer or the buffer was changed into Ni-NTA A buffer using a HiPrep desalting column according to the manufacturer's protocol. Digest with SUMO-protease took place at 4 °C over-night or at 15 °C for 4 h. To separate the cleaved SUMO-tag and SUMO-protease, the digest was then subjected to Nickel affinity chromatography and the flow-through was collected.

Hsp90 constructs were additionally subjected to Resource Q anion-exchange chromatography following tag removal. The protein was dialyzed into ResQ A buffer, loaded onto the column and washed with at least 5 Column Volume (CV) of ResQ A buffer. A gradient from ResQ A buffer to ResQ B buffer was applied to elute Hsp90 from the Resource Q column.

Subsequently, all proteins were purified by SEC on a HiLoad 16/60 Superdex column. To this end, protein-containing fractions were pooled and concentrated to a volume of 5 mL and injected onto the column. The protein was eluted by washing with SEC buffer.

GR-LBD Purification
GR-LBD was purified as previously described (Lorenz et al., 2014). Briefly, GR-LBD was unfolded in Ni-NTA A buffer (Section 3.1.10.3) and loaded onto nickel resin. The GR-LBD was then refolded on-column by gradient buffer exchange into Ni-NTA B buffer (2% per mL). The protein was eluted with Ni-NTA C buffer and diluted into TEV-Buffer in a ratio of 1:10. Cleavage of the His_6-Halo tag was performed with TEV-protease at 4 °C over-night. The Halo-tag was then separated as described above for the SUMO tag and the GR-LBD was concentrated to approximately 20 mL using a N_2-pressured Amicon concentration cell. The GR-LBD was then further purified with 4 SEC cycles, each injected with a sample volume of 5 mL.

Hop Purification
For the purification of tagless HOP, the lysate in Q-Sepharose A buffer was loaded onto a Q-Sepharose column and the column was washed with Q-Sepharose A buffer until baseline was reached. A 400 mL gradient to Q-Sepharose B buffer was applied and Hop-containing fractions were pooled and dialyzed into HAT A buffer overnight. The dialyzed protein was loaded onto a HAT column and eluted by running a 200 mL gradient to HAT B buffer. The protein-containing fractions were pooled and subjected to SEC as described.

Protein Purity and Concentration
Throughout all purification steps, protein-containing fractions were identified and protein purity was monitored by SDS-PAGE (Section 3.2.2.3). Proteins were usually purified until at least 95% purity was reached. The purified proteins were concentrated by ultrafiltration and protein concentration was determined by UV/Vis spectrophotometry at 280 nm (Equation 3.1). The buffer alone was measured and the signals were subtracted to account for absorption of the buffer. The extinction coefficient of proteins was determined using the ProtParam tool (Table 4). Generally, all proteins were flash-frozen in liquid N_2 and stored at -80 °C.

3.2.2.3 SDS-PAGE and Western Blot

Sodium Dodecyl Sulfate Polyacrylamide Gel Electrophoresis (SDS-PAGE) was used to separate proteins according to their molecular weight to monitor the protein purification process, prepare samples for Western Blot and for co-immunoprecipitation or pulldown experiments. Protein samples were mixed with 1x Laemmli buffer (Laemmli, 1970) and boiled at 95 °C for 5 min. Samples were then run on SDS-PA gels with an acrylamide concentration between 10-20% (Table 18). The gels were run in SDS running buffer (0.1% SDS, 25 mM Tris, 200 mM glycine) at a current of 35 mA for 45 min. For Western Blot, a Polyvinylidene Fluoride (PVDF) membrane was activated by incubation in methanol for 15 s, washing with H_2O for 2 min and equilibrating in transfer buffer (25 mM Tris, 192 mM glycine, 20% methanol, 0.012% SDS, pH 8.3) for 5 min. Transfer took place at 72 mA per gel for 1.5 h - 2 h. Blocking was done with 5% milk or 5% BSA in Tris-Buffered Saline with Tween (TBS-T) (TBS with 0.1% Tween-20) at 4 °C over-night. The primary antibody was either incubated with the membrane at 4 °C over-night or at room-temperature for 1 h. Unbound antibodies were separated by washing with TBS-T for 10 min thrice before the secondary antibody was added at a 1:10,000 dilution and incubated with the membrane at room temperature for 1 h. After washing with TBS-T for 10 min thrice, the luminescence of the conjugated secondary antibody was detected after treatment of the membrane with the Westernbright ECL Spray according to the manufacturer's protocols in an ImageQuant LAS 4000 system.

TABLE 18: Composition of SDS-PA Gels

Component	Final Concentration
Resolving Gel	
Acrylamide (40%)	3.13 mL
Tris (1.5 M)	2.5 mL
H_2O	4.27 mL
APS	100 µL
N,N,N′,N′-TEMED	15 µL
Stacking Gel	
Acrylamide (40%)	0.5 mL
Tris (1.5 M)	1.25 mL
H_2O	3.18 mL
APS	100 µL
N,N,N′,N′-TEMED	15 µL

3.2.3 *In Vitro* Protein Analysis

3.2.3.1 Protein Labeling

The target protein was dialyzed into buffer lacking thiol-based reducing agents. The dye was dissolved in DMSO and added to the protein in a 2-fold molar excess so that the final DMSO concentration did not exceed 1%. The reaction occurred at room temperature for 60 min, before quenching by placing on ice and addition of 5 mM DTT. To separate unbound label, the solution was subjected to gel filtration using a PD-10 desalting column following the manufacturer's protocol. The target fractions were then concentrated and the protein concentration and labeling efficiency were determined by UV/Vis-spectrophotometry. The Degree of Labeling (DOL) was calculated following equation 3.2.

$$DOL = \frac{c_{dye}}{c_{protein}} = \frac{A_{dye} \times {\epsilon_{dye}}^{-1}}{(A_{280} - CF \times A_{dye,max}) \times {\epsilon_{protein}}^{-1}} \tag{3.2}$$

with A_{280} as the absorption at 280 nm, ϵ as the extinction coefficient and CF as the correction factor (provided by the manufacturer).

3.2.3.2 Fluorescence Anisotropy

Fluorescence anisotropy was used to measure the binding of the apo GR-LBDm to dexamethasone fluorescein (F-DEX). The measurements were performed with a protocol adapted from a previously published study (Kirschke et al., 2014). To this end, 1 µM of apo GR-LBDm dialyzed into TEV-buffer (Section 3.2.2.2) was mixed with 2 µM Ydj1, 12 µM Hsp70 and 2 mM ATP in anisotropy buffer (30 mM Hepes, 50 mM

KCl, 5 mM $MgCl_2$, 5 mM DTT, pH 7.5). The reaction was incubated at 25 °C for 60 min - 70 min to ensure sequestration of GR-LBD by Hsp40/70. The reaction was induced by addition of 50 nM F-DEX (in DMSO) and hormone binding was monitored by excitation at 490 nm and emission detection at 520 nm with 5 nm bandwidth and medium sensitivity on a Jasco FP-8500 instrument. Fluorescence anisotropy was detected in 5 s intervals until the reaction had reached equilibrium. Data was fitted using an exponential increase function, yielding data for hormone binding kinetics and equilibrium.

3.2.3.3 CD spectroscopy

To determine the secondary structure composition, proteins were subjected to circular dichroism (CD) spectroscopy on a Chirascan device. Proteins were diluted to a concentration of 0.1 - 0.3 mg mL^{-1} in PBS or SEC buffer. For proteins prone to aggregation in the absence of reducing agents, 100 µM TCEP were added. For Far-UV CD spectra, five scans from 200 nm to 280 nm were recorded and averaged after subtraction of the buffer background signal. Secondary structure predictions were done using the DichroWeb software with the K2D algorithm. The mean residue ellipticity θ_{MRW} was calculated following equation 3.3 with θ_{MRW} defined as the molar ellipticity per amino acid in [deg cm^2 $dmol^{-1}$], θ as the observed ellipticity at a wavelength in [mdeg], MW as the molecular weight in [g mol^{-1}], N_{AA} as the number of amino acids in the protein, d as path length of the cuvette in [cm] and c as the concentration in [g mL^{-1}].

$$[\theta]_{MRW} = \frac{\theta \times MW}{N_{AA} \times 10^4 \times d \times c} \tag{3.3}$$

3.2.3.4 Single-Pair FRET spectroscopy

Single molecule Förster Resonance Energy Transfer (FRET) spectroscopy measurements were performed to investigate the folding status of the p53-DNA Binding Domain (DBD) under different conditions. Experiments were conducted in collaboration with the lab of Don Lamb at the Ludwig-Maximilians-Universität (LMU) (Munich, Germany) following a previously published protocol (Dahiya et al., 2019). Adjustments and operation of the spFRET setup were performed together with Ganesh Agam (Don Lamb Lab, LMU, Germany). Briefly, the p53-DBD was randomly labeled with the Atto532 and Alexa647 dyes on Cys182 and Cys229, while other exposed cysteines were mutated to serine. We incubated 10 nM of labeled p53-DBD with 3 µM of Hsp40, 20 µM of Hsp70 and 5 mM ATP at 37 °C for 1 h in 20 mM Hepes, 50 mM KCl, 5 mM $MgCl_2$, 1 mM TCEP at pH 7.4. Then, the solution was diluted in a solution containing Hsp40, Hsp70 and ATP to reach a concentration of approximately 70 pM of p53-DBD. Before measurement 20 µM of Hsp90, Hop or NudC were added.

The measurement was performed on a custom-made confocal microscope. Pulsed Interleaved Excitation (PIE) with a 532 nm laser (PicoTA 530; Topica) and a 640 nm

laser (LDH-D-C-640; PicoQuant) synchronized at a repetition rate of 26.7 MHz with a 18 ns delay were used for alternating excitation of donor and acceptor dyes. The laser power was measured at 100 µW. Collection of fluorescence was done with a 60x water immersion objective (Plan Apo IR 60x1.27 WI; Nikon) and a 75 µm diameter pinhole to cut off extrafocal signals. Fluorescence was then separated with a polarizing beam-splitter (PBS3; Thorlabs) and a dichroic mirror (DualLine z532/635, AHF Analysetechnik). Emission filters were used and fluorescence was detected on single-photon-counting avalanche photobodies (Perkin-Elmer). Custom-written MATLAB software was used to analyze Multi-Parameter Fluorescence Detection (MFD) data (Schrimpf et al., 2018).

Briefly, molecules with a stoichiometry of approximately 0.5 were selected, representing molecules carrying both dyes. Then, photo-bleaching and blinking events were excluded and signals were corrected for spectral crosstalk between donor and acceptor channel and direct acceptor excitation by the donor-exciting laser. Additionally, differences in the quantum yields of the fluorophores were accounted for before calculation of the FRET efficiencies. The FRET efficiency and fluorescence lifetime correlation was calculated to detect conformational changes within a burst (Kalinin et al., 2010).

3.2.3.5 Analytical Ultracentrifugation

Analytical ultracentrifugation (aUC) was used to investigate complex formation of proteins. All experiments were performed in aUC buffer (20 mM Hepes, 20 mM KCl, 5 mM $MgCl_2$, 5 mM DTT, pH 7.5). For fluorescence-based aUC measurements, proteins contained the Atto488 label randomly attached to cysteine residues. The labeled protein was used at a concentration of 500 nM, Hsp90 was usually used at a dimer concentration of 2 µM, Hsp40 and Hsp70 at a concentration of 4 µM and co-chaperones were used at a concentration of 6 µM unless specified otherwise. In competition experiments, a 20-fold molar excess of unlabeled species was added. If applicable, nucleotides were used at a concentration of 2 mM. Measurements containing GR-LBD were done in the presence of 50 µM dexamethasone. Data analysis was performed using Sedview, SedFit (Schuck, 2000) and Origin Pro 2016G.

3.2.3.6 Nuclear Magnetic Resonance Spectroscopy

Nuclear Magnetic Resonance (NMR) was done to determine the interaction of NudC with Hsp40 and Hsp90. We conducted NMR experiments in cooperation with the Michael Sattler Lab (TU Munich, Munich, Germany) and the Rina Rosenzweig Lab (Weizmann Institute of Science, Rehovot, Israel).

3.2.3.7 ATPase Measurement

We employed a regenerative ATPase assay based on a previously published protocol (Ali et al., 1993) to determine the effect of NudC on the Hsp90 ATPase activity. 2x

premix (5.17 mM phosphoenol pyruvate, 0.43 mM NADH, 6 units of pyruvate kinase and 30.25 units of lactate dehydrogenase in 20 mM Hepes, 20 mM KCl, 5 mM $MgCl_2$, 5 mM DTT, pH 7.5) were prepared. The final protein concentration was 4 µM for Hsp90 (monomer concentration) and 6 µM for NudC; the buffer was added to keep salt concentration constant between samples. The reaction was induced by addition of 2 mM ATP and NADH absorption was measured at 340 nm over the course of approximately 60 min. 5 mM radicicol were then added to control for background activity of contaminant ATPases. The ATPase activity was calculated by the slope of the 340 nm signal after subtraction of background ATPase activity.

3.2.3.8 *In Vitro* Pulldown Analysis

In vitro pulldowns with purified proteins was used to determine protein binding. We used His_6-tagged bait proteins and different prey proteins at a concentration of 5 µM in 100 µL binding buffer (30 mM Hepes, 50 mM KCl, 5 mM $MgCl_2$, 1 mM DTT and 0.05% Tween-20). cOmplete His-Tag Purification Beads were washed thrice with binding buffer and an equivalent of approximately 25 µL of beads in binding buffer were added to each sample. Binding was allowed to occur at 4 °C while shaking for 1 h. The beads were then washed twice with binding buffer and the bound proteins were eluted by addition of 60 µL binding buffer containing 300 mM imidazole. The eluted proteins were mixed with Laemmli buffer and then subjected to SDS-PAGE.

3.2.3.9 Size Exclusion Chromatography with Multi Angle Light Scattering

Size Exclusion Chromatography with Multi Angle Light Scattering (SEC-MALS) was used to monitor complex formation and to measure complex size. Hsp90, Ydj1 and NudC concentrations were 35 µM in a volume of 50 µL. To stabilize the complex between NudC and Hsp90, glutardialdehyde was added to a final concentration of 0.025% and incubated at 37 °C for 5 min while shaking. The crosslinking reaction was quenched by addition of Tris-HCl (pH 7.5) at a final concentration of 130 mM. The sample was analyzed on a Superdex 200 Increase 10/300 column that had been pre-equilibrated with 40 mM Hepes, 150 mM KCl, 5 mM $MgCl_2$, 1 mM TCEP, 0.05% NaN_3, pH 7.5 for about 24 h to ensure stable background detector signal. Chromatography and signal detection was performed on a Shimadzu HPLC system. Data was analyzed using the Astra 5.3.4.20 software.

3.2.4 Genetic Modification of *S. cerevisiae*

3.2.4.1 Maintenance of Yeast

Yeast cells were generally grown at 30 °C on suitable agar plates or as liquid cultures that were shaken rapidly to maximize aeration. Centrifugation of liquid cultures was performed at room temperature or at 4 °C at a maximum of 3000 xg. For short-term storage, agar plates were stored at 4 °C. For long-term storage, a stationary

yeast culture was mixed with glycerol to a final concentration of 15% and kept at -80 °C.

3.2.4.2 Plasmid Transformation into Yeast

Single and double plasmid transformation was performed following a a previously published protocol (Elble, 1992). Briefly, cells were grown to stationary phase and 200 µL of the suspension were harvested by centrifugation at 4220 xg. The supernatant was discarded so that approximately 50 µL of the supernatant remained. The cells were resuspended by shaking at 1,400 rpm for approximately 30 s. Then, 150 µL of the PLATE-Mix (90 mL 45% PEG-4000, 10 mL lithium acetate (1 M), 1 mL Tris-HCl (1 M), 0.2 mL EDTA (0.5 M)), 6 µL of 1 M DTT, 0.8 µL single-strand DNA from salmon testes and 300 ng - 500 ng of DNA were added. The suspension was mixed thoroughly by vortexing and incubated at room-temperature over-night. The samples were then centrifuged at 4220 xg for 30 s, the supernatant was aspirated, cells were resuspended in H_2O and plated on selective agar.

3.2.4.3 Linear Gene Knockout

We used the Knop toolbox to generate linear knockouts in *S. cerevisiae* (Janke et al., 2004). Knockout primers were designed to contain 60 bp overhangs with the 5′ and 3′ flanking regions of the target gene fused to the S1 and S2 primers of the Knop toolbox (Janke et al., 2004). The primers were used either with the pFA6a-NatNT2 or pFA6a-NatMX4 templates following a published amplification protocol (Janke et al., 2004) (Table 19, 20).

TABLE 19: Reaction Setup for Knockout Cassette PCR

Component	**Final Concentration**
Template	100 ng
dNTPs (10 mM per dNTP)	200 µM
Forward Primer	1 µM
Reverse Primer	1 µM
KNOP 2 Buffer	1x
Q5 High-Fidelity DNA Polymerase	0.02 units/µL
GoTaq Polymerase	0.05 units/µL
H_2O	*ad* 50 µL

Based on Janke et al., 2004.

The amplified PCR product was transformed into yeast using a previously published protocol (Gietz and Schiestl, 2007). Briefly, 50 mL of YPD medium were inoculated with an over-night culture to a final OD_{600} of 0.15. The cells were grown to log-phase by shaking at 30 °C for 4 h, harvested at 3000 xg for 5 min and washed

TABLE 20: Amplification Program for Knockout Cassettes

Step	Temperature	Time
Initial Denaturation	97 °C	4 min
10 Cycles		
Denaturation	97 °C	1 min
Annealing	54 °C	30 s
Extension	68 °C	1 min
20 Cycles		
Denaturation	97 °C	1 min
Annealing	54 °C	30 s
Extension	68 °C	2 min 40 s + 20 s per cycle

Based on Janke et al., 2004.

with H_2O. The pellet was then resuspended in 0.1 M lithium acetate and briefly pelleted by centrifugation and resuspended in 500 µL of 0.1 M lithium acetate. For each transformation, 50 µL of the suspension were pelleted and mixed with 240 µL of 50% PEG-3350, 10 µL of single-stranded DNA from salmon testes, 36 µL of 1 M lithium acetate and the entire PCR reaction of the resistance cassette filled *ad* 72 µL with H_2O. The reaction was vortexed thoroughly, incubated at 30 °C for 30 min and then heat-shocked at 42 °C for 30 min. Subsequently, the cells were centrifuged at 4420 xg and the supernatant was aspirated. The pellet was resuspended in pre-warmed YPD and incubated at 30 °C while shaking for 2-3 h. The cells were then pelleted at 4420 xg for 30 s and resuspended in H_2O for plating on selective agar plates.

3.2.5 Genetic Modification of Human Cell Lines

3.2.5.1 Maintenance of Tissue Culture Cells

All tissue cultures were maintained at 37 °C with 5% CO_2 atmosphere and checked for mycoplasm contamination regularly. Cells were kept at a confluency between 20% and 90% by periodic cell splitting. Suspension cell lines were split by diluting in fresh medium. For adherent cell lines, the supernatant was discarded, cells were washed with PBS and then incubated with trypsin at 37 °C for 5 min. The cells were then resuspended in fresh medium and diluted appropriately. For long-term storage, at least 1×10^6 cells were resuspended in freezing medium (FBS with 10% DMSO) and slowly cooled to -80 °C at a rate of 1 °C min^{-1}.

3.2.5.2 Transient Transfection

For transient transfection of cell lines we used the Lipofectamine 2000 kit with an adapted protocol. Approximately 0.1×10^6 cells were seeded into a 24-well plate. For reverse transfection protocols, cells were immediately mixed with transfecting

agent, while for standard transfections, cells were incubated over-night before transfection. In one tube 25 µL of Opti-MEM were mixed with plasmid DNA, and in a second tube, 25 µL of Opti-MEM were mixed with 1 µL of Lipofectamine 2000. The tubes were combined, incubated at room temperature for 5 min and added onto the cells in a drop-wise manner. After 48 h the medium was exchanged with fresh medium. The amount of DNA used for transfection ranged between 20 ng and 500 ng depending on the plasmid. For larger transfection reactions the amounts of reagents were scaled accordingly.

3.2.5.3 Lentiviral Transduction

To generate stable cell lines for genomically encoding target genes, we used lentiviral transduction. To this end, Hek293T cells were seeded at 20% confluency in DMEM complete (DMEM + FBS) in 15 cm dishes (7.5×10^6 cells seeded), 10 cm dishes (2.4×10^6 cells seeded) or in a 6-well plate (0.3×10^6 cells seeded) depending on the required amount of virus. In the following, the requirements for 15 cm dishes are shown and values have to be adapted for smaller reactions. After 24 h, medium was changed to pre-warmed transfection medium (5 mL DMEM complete, 15 mL DMEM only, 20 µL of 25 mM chloroquine). For each transfection 5 µg of the lentiviral vector, 5 µg of the lentiviral packaging plasmid mix (Kampmann et al., 2014) composed of the pRSV, pMDL and pVSVG plasmids at a concentration of 250 ng µL^{-1} each, 125 µL of 2 M $CaCl_2$ and 1000 µL H_2O were mixed in a Fluorescence-Activated Cell Sorting (FACS) tube. Under constant bubbling 1000 µL of 2x HBS (270 mM NaCl, 10 mM KCl, 40 mM HEPES, 10 mM glucose, 1.5 mM Na_2HPO_4, pH 7.10 exactly) were drop-wise added to the solution. The reaction was incubated at room temperature for 10 min and then added drop-wise onto the cells. After 7 h - 11 h, the medium was removed from the cells and replaced with prewarmed DMEM complete. After 48 h, the supernatant was harvested and filtered through a syringe-driven 0.45 µm filter. If required, virus was then concentrated at 3,000 rpm using Amicon Ultra-15 centrifuge filters with a 100 kDa cutoff.

To infect Hek293 cells with packaged lentivirus, 60,000 cells were seeded into a 24-well plate and 500 µL of concentrated virus per plasmid were added immediately. The cells were then incubated for 2 d - 3 d before the infection rate was assessed. To infect K562 cells, 1.5×10^6 cells were seeded in 1.5 mL of medium in a 6-well plate. Subsequently, 500 µL of concentrated virus were added and polybrene was added to a final concentration of 8 µg mL^{-1} to enhance infection rates. Cells were spun in the plate at 700 xg for 2 h at room temperature. Afterwards, cells were incubated at 37 °C for at least 3-4 h, cells were harvested at room temperature at 500 xg, washed with PBS and resuspended in fresh media. The suspension was then split into T25 flasks at a cell density of approximately 0.5×10^6 cells mL^{-1}.

3.2.6 Protein Analysis in the Cellular Context

3.2.6.1 *In Vivo* S^{35}-Methionine Incorporation

We used S^{35}-methionine incorporation to measure protein biosynthesis rates in yeast cells of different genetic backgrounds. To that end, we adapted a published protocol (Esposito and Kinzy, 2014). Yeast cells were grown at 30 °C to log-phase in SD -Met medium and 1 OD_{600} unit was harvested by centrifugation at 3000 xg for 5 min and resuspended in 1 mL pre-warmed SD -Met medium. Incorporation was induced by the addition of hot L-methionine mix (6 µL L-methionine (10 mM) and 0.37 MBq of S^{35}-L-methionine) to the sample. At the indicated time points, protein biosynthesis was stopped by addition of 100 µg mL^{-1} cycloheximide. The sample was washed once with H_2O supplemented with 100 µg mL^{-1} cycloheximide and then lysed by a published alkali lysis protocol (Kushnirov, 2000). Briefly, cells were resuspended in 0.1 M NaOH and incubated at room-temperature for 3 min. Cells were then spun down, the supernatant was discarded and the pellet was resuspended in 25 µL of 2.5x Laemmli buffer. The samples were boiled at 95 °C for 5 min and then subjected to SDS-PAGE. The gel was dried and used to expose a phosphor storage screen over-night before detection on a Typhoon4000 phosphoimager system.

3.2.6.2 Cycloheximide Chase

Cycloheximide chase analysis was used to measure protein stability *in vivo*. Cells were grown to log-phase before cycloheximide was added at a concentration of 100 µg mL^{-1} for yeast or 10 µg mL^{-1} for mammalian cells. To quench the reaction, we added trichloroacetic acid to a final concentration of 20% and allowed protein precipitation to occur at -80 °C over-night. The samples were then thawed, centrifuged at 17000 xg for 1 min at room temperature and the supernatant was discarded. After washing twice with -20 °C cold 80% acetone, the samples were air-dried. The dried pellet was resupsended in buffer (1% SDS in 0.1 M NaOH), 1x Laemmli buffer was added and the samples were boiled at 95 °C for 5 min before SDS-PAGE.

3.2.6.3 Aggregated Protein Isolation

To measure the solubility of target proteins in the cellular environment, we separated supernatant and pellet fractions. To that end, we grew cells to log-phase and harvested between 15 and 60 OD_{600} units at 3000 xg at room temperature before flash-freezing in liquid N_2. The pellet was then thawed and resuspended in 500 µL of lysis buffer (50 mM Tris-HCl, 150 mM NaCl, 5 mM $MgCl_2$, 5% glycerol, pH 8.0) with 1x Protease Inhibitor Mix G, 1 mM PMSF, 5 mM EDTA and 2 µg mL^{-1} of puromycine. To each sample 12.5 U of benzonase were added. The cells were then lysed by glass-bead disruption with four cycles of 2 min at 30 Hz and 2 min off-time between cycles. The lysate was pre-cleared by centrifugation at 500 xg for 1 min at

4 °C. The protein concentration of the cleared lysate was normalized and 50 µL of the sample volume were centrifuged at 18000 xg at 4 °C for 20 min. The pellet was then washed twice with lysis buffer and was then resuspended in resuspension buffer (50 mM Tris-HCl, 1% SDS, 6 M urea, 1 mM EDTA, pH 7.5). The samples were then analyzed by SDS-PAGE and Western-Blot.

3.2.6.4 Pulldown Analysis

In vivo pulldowns coupled with mass spectrometry (MS) were done with C-terminally GFP-tagged proteins and the GFP-Trap Agarose system according to the manufacturer's manual. Briefly, 3 million HEK293 cells were transfected with pVITRO2-MCS-NudC-GFP or pVITRO2-MCS-GFP as control and incubated for 2 d with the transfecting agent before lysis. Cells were washed with PBS and then lysed in lysis buffer (20 mM Hepes, 100 mM NaCl, 1 mM $MgCl_2$, 0.1% NP-40, pH 7.0) by gentle shaking for 10 min at 4 °C. The lysate was incubated with the beads at 4 °C for 25 min in an overhead shaker before washing thrice with lysis buffer and thrice with PBS before preparation for MS. The preparation, measurement and raw data analysis for MS were conducted by Moritz Mühlhofer (TU Munich) as described elsewhere (Mühlhofer et al., 2019). Briefly, proteins were subjected to on-bead tryptic digestion, alkylation and desalting. The peptides were then measured on a Q Exactive Plus instrument coupled to an Ultimate3000 Nano-HPLC via an electrospray easy source (Thermo Fisher, Waltham, USA). MS/MS data was analyzed using MaxQuant (version 1.6.2.6) (Cox et al., 2014; Cox and Mann, 2008) and then further analyzed using Perseus (version 1.6.2.1).

3.2.7 Investigation of Hsp90 Co-Chaperone Double Mutants in Yeast

3.2.7.1 Generation of a Double Mutant Library

To analyze the co-operation between Hsp90 co-chaperones in yeast, we generated double mutants of all possible combinations of Hsp90 co-chaperones. The genotypes of all original and mutant strains are summarized in Table 12. To generate the double mutant library, first the KanMX4 resistance cassette was swapped to the Nourseothricin resistance cassette NatMX using the Knop toolbox (Janke et al., 2004). The resulting strains were mated with the Y8205 strain on YPD plates at 30 °C for 20 h. Diploids were sporulated on Enriched Sporulation Medium (Table 14) for 5 d at 20 °C. Then, haploids with the Mat α genotype were selected by incubation on Haploid Selection Medium (Table 14) prepared with -Leu/Arg/Lys amino acid mix instead of -His/Arg/Lys amino acid mix. Additionally, the plates contained Nourseothricin to select for genotypes containing the deleted or knocked-down co-chaperone gene. The resulting haploid Mat α strains carrying Nourseothricin resistance were then mated with the original haploid Mat a strains carrying the G418 resistance from the KanMX4 cassette in all possible combinations. Subsequently, haploid double mutants were selected using the SGA screening workflow (Tong et

al., 2001; Tong and Boone, 2006). In brief, the diploids were duplicated on Enriched Sporulation Medium plates and then transferred to Haploid Selection Medium supplemented with either Nourseothricin or G418 or both antibiotics, to detect the potential synthetic lethality of the double mutant. The identity of all double mutants was confirmed by Colony-PCR and/or by the loss/depletion of protein determined by Western-Blot.

3.2.7.2 Viability Screening

The fitness of double mutant strains at 30 °C, 37 °C and 42 °C was evaluated by drop-dilution assay on YPD medium. To this end, the strains were grown to stationary phase over-night at 30 °C, 5 OD_{600} units were harvested at 4220 xg, washed with H_2O and resuspended in 500 µL H_2O. From these stocks, for each strain a 10-fold dilution series starting from $OD_{600} = 1$ was prepared and spotted on a YPD plate. Cells were then incubated at the indicated temperatures for 48 h. Spot density was quantified using the ImageJ software. Each plate contained the wild-type strain and the relevant single mutant strain as controls and only strains spotted on the same plate were compared to each other to exclude experiment-to-experiment errors.

3.2.7.3 Yeast Reporter Assays

Steroid Hormone Receptor (SHR) Activity Screening

The activity of the GR and the MR in yeast were determined using a previously published protocol (Sahasrabudhe et al., 2017). Yeast cells were transformed with the SHR-expressing plasmid and the pUCΔSS-26X reporter plasmid. Deep-wells in a 96-well format were inoculated and the cultures were grown to stationary phase in selective medium while shaking at 30 °C over-night. The cultures were then diluted in a 1:10 ratio in medium supplemented with 11-deoxycorticosterone (DOC) for GR or aldosterone for MR at a concentration of 10 µM. The cultures were then grown for approximately 24 h at 30 °C. For the measurement, 50 µL of the cell suspension were pelleted in a clear-bottom, black 96-well plate by centrifugation at 4000 xg for 10 min. The pellet was resuspended in 150 µL assay buffer (82 mM Na_2HPO_4, 12 mM NaH_2PO_4, 0.1% SDS, pH 7.5) and cells were permeabilized by shaking for 15 min at 900 rpm. The reaction was initiated by addition of 50 µL ONPG (4 mg mL^{-1}) and the absorption at 420 nm was measured for 45 min. The slope of the linear region of the A_{420} signal was used to calculate the β-galactosidase activity. In all measurements, the wild-type and the suitable single mutant strain were measured on the same plate and activities were normalized to the wild-type activity.

v-Src Toxicity Screening

Viral Src kinase is toxic in yeast and leads to cell death (Kornbluth et al., 1987). To analyze the effect of Hsp90 co-chaperones on v-Src maturation, we conditionally expressed v-Src from the p416GAL1 or the weaker p416GAL-S plasmid in the Hsp90

co-chaperone double mutant backgrounds. Cells were grown to stationary phase over-night. For each strain, 5 OD_{600} units were harvested at 4220 xg, washed with H_2O and the resuspended in 500 µL H_2O. As described in Section 3.2.7.2, dilutions were prepared and spotted on selective agar plates containing either 2% D-glucose as control or 2% D-galactose to induce v-Src expression. Cell growth was quantified by measuring the spot density with ImageJ after 48 h or 72 h of incubation at 30 °C. The growth on D-galactose containing plates was normalized to the growth on D-glucose containing plates prepared during the same experiment. Each plate contained the wild-type and the respective single mutant strain as controls and growth rates of different strains were only compared for spots grown on the same plate.

v-Src Activity Analysis
Since yeast express only one endogenous tyrosine kinase, the activity of v-Src could be measured by quantifying phophotyrosine (pTyr) levels. To this end, cultures transformed with the p416GAL1-vSrc plasmid were grown to late log-phase at 30 °C over-night in selective medium containing 2% raffinose as the only carbon source. The cells were then diluted to a final OD_{600} of approximately 0.15 (or 0.2 - 0.3 for slow-growing strains) and grown over-night to log-phase. In the morning, pre-warmed selective medium with a volume of at least 25 mL supplemented with 2% raffinose was inoculated to a density of 0.3 OD_{600} and grown for approximately 5 h while shaking vigorously at 30 °C. The cell densities were determined to ensure even doubling rates across all strains under investigation. v-Src expression was then induced by the addition of pre-warmed D-galactose at a final concentration of 2%. Protein expression was allowed to occur for 5 h - 6 h before 10 OD_{600} units were harvested at 4000 xg. The pellet was resuspended in 30% TCA and frozen over-night at -80 °C. TCA precipitation and sample preparation was then performed as described previously.

3.2.7.4 Genetic Interaction Quantification

Genetic interactions were quantified using the ϵ-Score. For fitness analysis, the ϵ-Score was defined as

$$\epsilon = f_{ab} - f_a \times f_b \tag{3.4}$$

where f_{ab} indicates the fitness of the double mutant and f_a and f_b represent the fitness of the individual mutants (Elena and Lenski, 1997; Mani et al., 2008). To provide a measure of v-Src activity, which is inversely correlated to viability, the ϵ-Score was defined as

$$\epsilon = f_a \times f_b - f_{ab} \tag{3.5}$$

with f_{ab} indicating double mutant fitness and f_a and f_b denoting the fitness of the individual mutants. For SHR activity measurements, the ϵ-Score was used as stated

in the respective Results and Discussion section due to the more complex possible combinations of deactivating, activating and neutral effects. For normalization, the ϵ-Score was divided by the expected activity

$$\epsilon_{norm} = \epsilon - Score/(f_a \times f_b). \tag{3.6}$$

3.2.8 Screening Human Cell Lines for Hsp90 Modulators

3.2.8.1 Flow Cytometry and Fluorescence-Activated Cell Sorting

To analyze and sort human cells with respect to fluorescence markers, we used flow cytometry and FACS. For flow cytometry, adherent cell lines were trypsinized and thoroughly resuspended before use to form singlet cell populations. To further prevent coagulation of cells, adherent cell lines were pushed through a cell strainer into a FACS tube. Suspension cell lines were subjected to flow cytometry after thorough resuspension. Samples were then analyzed on a BD LSRFortessa X-14 flow cytometer with the FACSDiva software according to the manufacturer's protocol (BD Biosciences, Franklin Lakes, USA). To analyze samples in a 96-well format, we used a High Throughput Sampler unit according to the manufacturer's protocol.

For cell sorting experiments we used a BD Aria II cell sorter with five lasers (360 nm, 405 nm, 488 nm, 561 nm, 633 nm). The instrument was set up and calibrated following the UCSF Flow Cytometry & Cell Sorting core facility workflow. Briefly, calibration involved laser and detector calibration with Cytometer Setup and Tracking (CST) beads and drop delay time calibration with Accudrop beads according to the manufacturer's protocol. All cells were sorted using the 85 micron nozzle. Before sorting, target practice was performed to ensure proper sorting of cells into the collection tubes. Cells were trypsinized if applicable and pelleted at room temperature at 500 xg for 10 min and then resuspended in PBS supplemented with 0.5% FBS. Immediately before loading the sample onto the cell sorter, cells were pushed through a cell strainer into a FACS tube. For sorting, we gated on living, singlet cells with the desired fluorescence properties using the FACSDiva software.

3.2.8.2 Generation of Hsp90 Client Reporter Cell Lines

We screened for modulators of SHR activity in Hek293T and K562 cell lines using CRISPRi technology. The parental cell lines were lentivirally transduced with pHR-SFFV-dCas9-BFP-KRAB and selected via a Blue Fluorescent Protein (BFP) cassette (Gilbert et al., 2013; Gilbert et al., 2014). The SHR genes were cloned into the pMK1253 vector as Clover-tagged and untagged versions. A reporter cassette was introduced into the pXG207 backbone. The reporter cassette comprised mCherry cloned downstream of a minimal Alcohol Dehydrogenase (ADH) promoter equipped with two upstream activating Glucocorticoid Response Elements (GREs) (Freeman et al., 2000). Both plasmids were lentivirally transduced into the cell lines to ensure genomic insertion.

To select polyclonal cell lines, we treated cells over-night at 37 °C with 50 nM dexamethasone, aldosterone or progesterone for GR, MR and PR, respectively. Positives were selected using Fluorescence-Activated Cell Sorting (FACS) gating on living singlet cells with BFP^+ signal. For cell lines transduced with the Clover-tagged SHR, we additionally gated on cell populations with $FITC^+$ $dsRed^+$ during cell sorting, while for cell lines transduced with the untagged SHR, we selected only for $dsRed^+$ cells. To select monoclonals, single cells of an induced population were sorted into 96-well plates. Cells were expanded in hormone-free medium until 50% - 100% confluency and then replica-split into two 96-well plates. In one plate, cells were induced by addition of 10 nM of the respective hormone while cells in the other plate were treated with DMSO. The cultures were then incubated at 37 °C over-night. Subsequently, each well was analyzed by flow cytometry and the culture with the strongest activation compared to the untreated control was expanded and used for further experiments.

3.2.8.3 Generation of a single guide RNA Library

To screen for SHR modulators, we designed a pooled CRISPRi library targeting 357 genes of the proteostasis system. The design of the library was performed based on a previously published algorithm (Horlbeck et al., 2016). For each gene, the library contained five single guide RNAs (sgRNAs) targeting either the coding or the template strand and a total of 250 non-coding sgRNAs. The oligonucleotide library was synthesized by Agilent (provided by Martin Kampmann, UCSF, USA). The chaperone-focused sgRNA library was amplified by PCR in 6 PCR reactions of 50 µL. 0.5 µL of the template (used at a stock concentration of 0.05 pmol μL^{-1} were used and primers specific for the chaperone sublibrary (Table 9) were used at 0.25 µM each. The annealing temperature was set to 56 °C and the extension time was 15 s. The PCR product was confirmed by TBE-PAGE as a 84 bp amplicon.

The PCR product and the pSLQ1371 backbone were digested with 1 µL of BstXI and BlpI per 1 µg of PCR product or per 2 µg of backbone at 37 °C over-night. To purify the digested PCR product, the sample was run on a 20% TBE gel, the 33 bp band was excised and purified using the *'Crush and Soak'* protocol. The digested backbone was purified after agarose gel electrophoresis with a 0.8% agarose gel. For ligation, 10 ng of insert were mixed with 500 ng of backbone DNA, 1x T4 DNA Ligase buffer and 0.5 µL of T4 Ligase in a 10 µL reaction volume. The reaction was incubated at 16 °C over-night and then stored at 4 °C.

To ensure a homogeneous distribution of sgRNAs in the library, we aimed to achieve at least a 100-fold coverage of the library elements. Hence, we scaled our transformation to get at least 200,000 clones for the the approximately 2200 elements (including non-targeting control sequences) in the focused chaperone library. We did test-transformations with 0.5 µL of ligation mix with chemically competent *E. coli* DH5α cells to estimate ligation efficiency. To transform CRISPRi library ligations, we used electrocompetent *E. coli* MegaX cells, for which we assumed a 50-fold

increased transformation efficiency compared to *E. coli* DH5α cells. For the transformation, 75 µL of *E. coli* MegaX cells were mixed gently with 4 µL of the ligation reaction and incubated on ice for 30 minute. Subsequently, 75 µL of a 10% solution of sterile glycerol were added to the cells and the mix was transferred to pre-chilled 0.1 cm electroporation cuvettes. Electroporation took place at 2 kV, 200 Ω and 25 µF with an exponential decay pulse. After electroporation, 500 µL of SOC medium were added immediately and cells were recovered at 37 °C for 1.5 h while shaking. To confirm the transformation efficiency, 0.1% and 0.01% of the suspension were plated on ampicillin-containing LB plates and incubated at 37 °C over-night. The remaining transformation mix was used to inoculate 100 mL of pre-warmed LB medium supplemented with ampicillin. The culture was incubated at 37 °C over-night while shaking before the library was extracted using the Qiagen Plasmid Plus Midi Kit according to the manufacturer's protocol. The quality of the CRISPRi library was confirmed by next-generation sequencing (Section 3.2.8.5).

3.2.8.4 Client Activity-Based Cell Sorting

For pooled CRISPRi screens, a total of 20×10^6 cells of the target cell line were transduced to provide a 1000-fold coverage of the library elements (approximately 2200) assuming an infection rate of at least 10%. Lentivirus harvested 48 h and 72 h after transfection from one 15 cm dish was used to infect 20×10^6 cells.

For Hek293 cells, 20×10^6 cells were pelleted and resuspended in the filtered virus solution. To enhance infection, 0.8 µg mL^{-1} of polybrene were added and cells were distributed to 15 cm dishes with 5×10^6 cells per dish. Cells were then incubated at 37 °C for 48 h. One plate was trypsinized to determine the infection rate by determining the ratio of BFP$^+$ to BFP$^-$ cells by flow cytometry. Note that, BFP$^-$ cells were still positive for the pHR-SFFV-dCas9-BFP-KRAB construct. To select for cells carrying the sgRNA expressing plasmid, the cultures were supplemented with puromycine at a final concentration of 2 µg mL^{-1}. The rate of BFP$^+$ cells was determined in regular time periods until a positives rate of at least 80% was reached. The cultures were then recovered in media lacking puromycine for at least 48 h before cell sorting.

For K562 cells, virus from one 15 cm dish was concentrated to 500 µL and then diluted to a final volume of 12 mL with RPMI-1640 media. The virus solution was used to resuspend 20×10^6 K562 cells as described and the cells were supplemented with 8 µg mL^{-1} polybrene. The suspension was transferred to a 6-well plate and viral infection was carried out as described. Afterwards, cells were transferred to T175 flasks with 10×10^6 cells per flask. After 48 h infection rate was determined and positives selection was performed with 0.8 µg mL^{-1} puromycine as described.

The cells infected with the library were then treated with the respective hormone for 24 h before sorting. The total time between infection and sorting was usually between 8 d and 10 d to allow the gene knockdown to establish. To sort for SHR activity, populations with the highest 30% and lowest 30% mCherry reporter signal

were collected. Approximately 2×10^6 cells were collected from each population to ensure 1000-fold coverage of the library elements. Afterwards, cells were pelleted by centrifugation at approximately 200 xg and stored at -80 °C until sample preparation.

3.2.8.5 Sample Preparation for Next-Generation Sequencing

Cell pellets were thawed and genomic DNA (gDNA) was extracted using the NucleoSpin Blood Kit according to the manufacturer's protocol. For next-generation sequencing, the sgRNA encoding region was then PCR-amplified in each sample with barcoded indexing primers (Table S24). To this end, first, a test-PCR was done with 800 ng of gDNA as the template, 0.4 µM of the indexing and reverse primers and 10 µL of Q5 High-Fidelity 2x Master Mix in a 20 µL reaction volume. The thermocycling conditions are shown in Table 21. The success of the PCR was evaluated by analyzing 5 µL of the reaction on a 15% TBE gel. If the PCR was successful with the chosen indexing and reverse primers, the reaction was scaled up using the entire gDNA extracted from a population with 2 µg of gDNA as the template per 50 µL PCR reaction.

TABLE 21: PCR Conditions to Amplify sgRNA-Encoding Cassettes

Step	**Temperature**	**Time**
Initial Denaturation	98 °C	30 s
23 Cycles		
Denaturation	98 °C	30 s
Annealing	60 °C	15 s
Extension	72 °C	15 s
Final Extension	72 °C	10 min

The PCR products were then pooled and purified using SPRI bead purification. The beads were prepared by adding 1 mL of Sera-Mag beads into a tube, collecting the beads in a magnetic rack, aspirating the supernatant and resuspending the cells in 1 mL of TE buffer (10 mM Tris, 1 mM EDTA, pH 8.0). The suspension was then added to premixed 18% (w/v) PEG-8000, 1 M NaCl, 10 mM Tris and 1 mM EDTA in 50 mL H_2O. To select the 270 bp PCR product, the sample was first mixed with a SPRI bead volume of 0.65x of the sample volume. The sample was incubated at room temperature for 10 min before the beads were collected with a magnetic rack and the supernatant was aspirated. The supernatant was then mixed with a SPRI bead volume of 1x of the original sample volume and incubated at room temperature for 10 min. Subsequently, the beads were collected and the supernatant was discarded. The beads were washed twice with 80% ethanol and air-dried. The bound DNA fragment was eluted by addition of water.

Amplicons with different indices were pooled and subjected to next-generation sequencing together with the appropriate primers for forward or mirror amplicons (Table 9). Next-generation sequencing and demultiplexing based on the indices was

performed by the the UCSF Center for Advanced Technology (San Francisco, USA) on the HiSeq 4000 system.

3.2.8.6 Next-Generation Sequencing Data Analysis

To identify sgRNAs enriched in the populations with high or low reporter activity, we followed a previously published python-based analysis pipeline, named Model-based Analysis of Genome-wide CRSIPR-Cas9 knockout including Negative Controls (MAGeCK-iNC) (Kampmann et al., 2013; Kampmann et al., 2014; Tian et al., 2019). Briefly, sequencing reads were cropped, aligned to the used library and the read counts between the high and low mCherry populations were compared. To that end, log_2-fold changes of the reads between the two samples were calculated for all sgRNAs. Mann-Whitney U-test comparing the phenotypes of targeting sgRNAs *versus* non-targeting sgRNAs was used to calculate the statistical significance for each gene (Kampmann et al., 2013). The means of the top 3 scoring sgRNAs was used to calculate an average phenotype. Hit strength, defined as the product of the phenotype score and the $-log_{10}(P)$ value derived from Mann-Whitney U-testing was calculated. A 0.05 false discovery rate was set as the threshold to identify significant hits. Additionally, only sgRNAs with at least 100 counts were included in the analysis.

3.2.8.7 Individual Knockdown Analysis

For the knockdown of individual genes, sgRNA expression sequences were cloned into the pSLQ1371 or the pLG15 plasmid. The plasmid was digested with BstXI and BlpI at 37 °C for 12 h without AP treatment and purified via agarose gel electrophoresis. The insert was generated by annealing top and bottom oligonucleotides (Table S25). To this end, 1 µL each of the top and bottom oligo strand (100 µM stock concentration) were mixed with 25 µL of 2x annealing buffer (200 mM potassium acetate, 60 mM HEPES, 4 mM magnesium acetate, pH 7.4) in a 50 µL reaction volume. The sample was then heated at 95 °C for 5 min and then slowly cooled to 8 °C at a cooling rate of 0.1 °C s^{-1} in a thermocycler.

For the ligation, 20 ng of digested vector were mixed with 0.5 µL of a 1:20 dilution of the annealed oligonucleotides, 2.5 µL of 2x quick ligase buffer and 0.5 µL of T4 DNA ligase in a 5 µL reaction volume. Ligation occurred for 5 min - 30 min at room temperature. The entire reaction was then used for transformation into *E. coli* DH5α and positive clones were selected. Subsequently, the sgRNA encoding plasmid was transduced into the desired cell line by lentiviral infection. Infection rates were determined as the BFP^+ fraction two days post infection and positives were selected by addition of 1 µg mL^{-1} puromycin if necessary.

Results And Discussion

4.1 The Epistatic Network of Hsp90 Co-Chaperones in Yeast

The Hsp90 chaperone system has been extensively studied in yeast, since the yeast Hsp90 system faithfully recapitulates the human Hsp90 system and the maturation of heterologous clients can be studied in the absence of interfering endogenous mechanisms. We know that different clients require specific co-chaperones for their maturation (Sahasrabudhe et al., 2017). Despite significant research efforts, it is still largely unknown how co-chaperones co-operate during client maturation. Here we set out to study the genetic interactions of 11 yeast Hsp90 co-chaperones in the context of client maturation using the GR, MR and v-Src as model clients.

4.1.1 Generation of a Co-Chaperone Double Mutant Library

To determine epistatic relationships between Hsp90 co-chaperones we first generated a double mutant library of 11 known yeast Hsp90 co-chaperones (Sti1, Cdc37, Cns1, Tah1, Pih1, Cpr6, Cpr7, Sba1, Aha1, Hch1, Ppt1) (Table 2). For non-essential genes we used knockout strains in the BY4741 background obtained from Euroscarf. For the essential co-chaperones Cdc37 and Cns1 we made use of Decreased Abundance by mRNA Perturbation (DAmP) technology (Schuldiner et al., 2005). DAmP strains contain a resistance cassette in the 3' UTR, thus destabilizing the mRNA and decreasing mRNA half-life. DAmP strains are marked with asterisks throughout the thesis (e.g. *cns1**).

To generate a double mutant library, first the G418 resistance cassette (KanR; KanMX4) of a single KO/KD library was swapped to a Nourseothricin resistance cassette (NatR; NatMX) using the Knop toolbox (Janke et al., 2004). To switch the mating type, the resulting $NatR^+$ strains were mated with the Y8205 query strain and MATα mating type haploids were selected (Figure 13A). To that end, the strains were selected for Nourseothricin resistance and leucine prototrophy as in the diploid cells the *LEU2* gene is driven by the *STE3* promoter which is only transcribed in MATα yeast cells (Tong et al., 2001; Tong and Boone, 2006). The resulting haploid strains were then mated with all original single KO/KDs (Figure 13B). Hence, a matrix of 144 diploid strains was generated, including 12 negative controls that contain the KOs/KDs of the same gene with different markers (e.g. *sti1Δ::NatMX,*

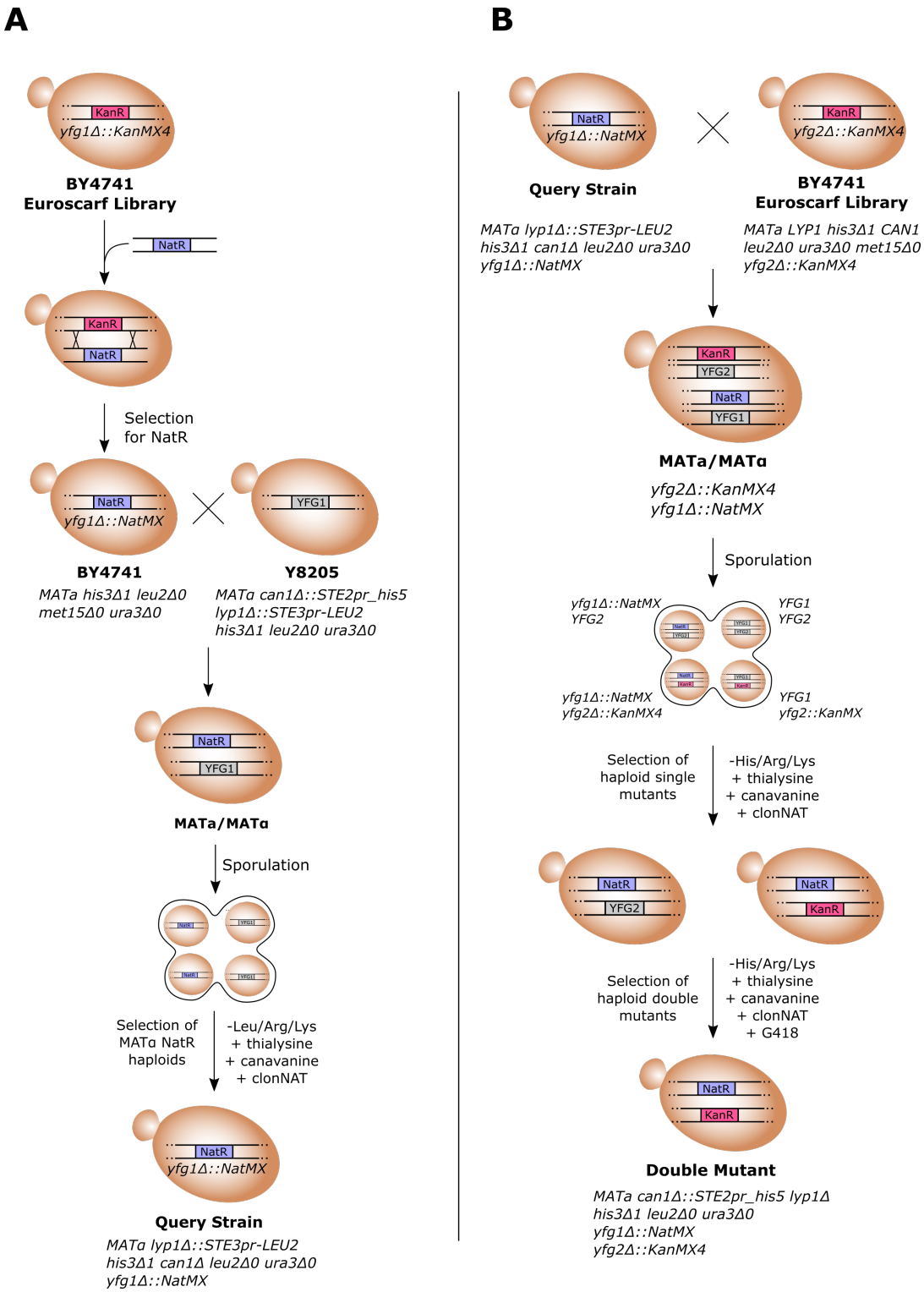

FIGURE 13 | **The Generation of a Co-Chaperone Double Mutant Library.**
A The query strain was generated by swapping the KanMX4 cassette in the single co-chaperone knockouts/knockdowns (KOs/KDs) to a NatMX cassette. To switch the mating type, the strains were mated with the Y8205 strain and MATα haploids carrying the NatMX cassette were selected for leucine prototrophy and Nourseothricin resistance.
B The strains generated in **(A)** were mated with the initial single KO/KD strains (MATa, KanMX4). After sporulation, haploid single mutants and subsequently double mutants were selected.
[KanR: G418 resistance; NatR: Nourseothricin resistance; YFG: Your favorite gene]

sti1Δ::KanMX4). After sporulation, we first selected for single mutants as a control and subsequently for double mutants (Figure 13B). Unexpectedly, several *sgt1**-containing strains were not viable even during single mutant selection with either Nourseothricin or G418. Hence, the lethal phenotype was not a consequence of synthetic lethality, but rather due to erratic distribution of genes during mating and subsequent sporulation. This is in line with the published role of Sgt1 in the assembly of the kinetochore complex (Kitagawa et al., 1999). Hence, *sgt1**-containing mutants were excluded from further analysis. In summary, a matrix of 110 double mutants remained, which includes inherent biological replicates in which the same genes were knocked out/down with different resistance markers (e.g. *sti1Δ::NatMX, cdc37*::KanMX4* and *sti1Δ::KanMX4, cdc37*::NatMX*) (Figure 14). Of note, apart from *sgt1**-containing mutants, all double mutants were viable during the selection, suggesting that no severe growth phenotypes resulted from potential negative genetic interactions between the Hsp90 co-chaperones.

WT	sti1Δ	cdc37*	cns1*	tah1Δ	pih1Δ	cpr6Δ	cpr7Δ	sba1Δ	aha1Δ	hch1Δ	ppt1Δ
sti1Δ		cdc37*/ sti1Δ	cns1*/ sti1Δ	tah1Δ/ sti1Δ	pih1Δ/ sti1Δ	cpr6Δ/ sti1Δ	cpr7Δ/ sti1Δ	sba1Δ/ sti1Δ	aha1Δ/ sti1Δ	hch1Δ/ sti1Δ	ppt1Δ/ sti1Δ
cdc37*	sti1Δ/ cdc37*		cns1*/ cdc37*	tah1Δ/ cdc37*	pih1Δ/ cdc37*	cpr6Δ/ cdc37*	cpr7Δ/ cdc37*	sba1Δ/ cdc37*	aha1Δ/ cdc37*	hch1Δ/ cdc37*	ppt1Δ/ cdc37*
cns1*	sti1Δ/ cns1*	cdc37*/ cns1*		tah1Δ/ cns1Δ	pih1Δ/ cns1*	cpr6Δ/ cns1*	cpr7Δ/ cns1*	sba1Δ/ cns1*	aha1Δ/ cns1*	hch1Δ/ cns1*	ppt1Δ/ cns1*
tah1Δ	sti1Δ/ tah1Δ	cdc37*/ tah1Δ	cns1*/ tah1Δ		pih1Δ/ tah1Δ	cpr6Δ/ tah1Δ	cpr7Δ/ tah1Δ	sba1Δ/ tah1Δ	aha1Δ/ tah1Δ	hch1Δ/ tah1Δ	ppt1Δ/ tah1Δ
pih1Δ	sti1Δ/ pih1Δ	cdc37*/ pih1Δ	cns1*/ pih1Δ	tah1Δ/ pih1Δ		cpr6Δ/ pih1Δ	cpr7Δ/ pih1Δ	sba1Δ/ pih1Δ	aha1Δ/ pih1Δ	hch1Δ/ pih1Δ	ppt1/ pih1Δ
cpr6Δ	sti1Δ/ cpr6Δ	cdc37*/ cpr6Δ	cns1*/ cpr6Δ	tah1Δ/ cpr6Δ	pih1Δ/ cpr6Δ		cpr7Δ/ cpr6Δ	sba1Δ/ cpr6Δ	aha1Δ/ cpr6Δ	hch1Δ/ cpr6Δ	ppt1Δ/ cpr6Δ
cpr7Δ	sti1Δ/ cpr7Δ	cdc37*/ cpr7Δ	cns1*/ cpr7Δ	tah1Δ/ cpr7Δ	pih1Δ/ cpr7Δ	cpr6Δ/ cpr7Δ		sba1Δ/ cpr7Δ	aha1Δ/ cpr7Δ	hch1Δ/ cpr7Δ	ppt1Δ/ cpr7Δ
sba1Δ	sti1Δ/ sba1Δ	cdc37*/ sba1Δ	cns1*/ sba1Δ	tah1Δ/ sba1Δ	pih1Δ/ sba1Δ	cpr6Δ/ sba1Δ	cpr7Δ/ sba1Δ		aha1Δ/ sba1Δ	hch1Δ/ sba1Δ	ppt1Δ/ sba1Δ
aha1Δ	sti1Δ/ aha1Δ	cdc37*/ aha1Δ	cns1*/ aha1Δ	tah1Δ/ aha1Δ	pih1Δ/ aha1Δ	cpr6Δ/ aha1Δ	cpr7Δ/ aha1Δ	sba1Δ/ aha1Δ		hch1Δ/ aha1Δ	ppt1Δ/ aha1Δ
hch1Δ	sti1Δ/ hch1Δ	cdc37*/ hch1Δ	cns1*/ hch1Δ	tah1Δ/ hch1Δ	pih1Δ/ hch1Δ	cpr6Δ/ hch1Δ	cpr7Δ/ hch1Δ	sba1Δ/ hch1Δ	aha1Δ/ hch1Δ		ppt1/Δ hch1Δ
ppt1Δ	sti1Δ/ ppt1Δ	cdc37*/ ppt1Δ	cns1*/ ppt1Δ	tah1Δ/ ppt1Δ	pih1Δ/ ppt1Δ	cpr6Δ/ ppt1Δ	cpr7Δ/ ppt1Δ	sba1Δ/ ppt1Δ	aha1Δ/ ppt1Δ	hch1Δ/ ppt1Δ	

FIGURE 14 | **The Matrix of Hsp90 Co-Chaperone Double Knockouts/Knockdowns.** Library of Hsp90 co-chaperone double KOs/KDs used during this study. Note that the matrix includes inherent biological replicates due to knockout of the same co-chaperones with different selection markers (e.g. *sti1Δ::NatMX, cdc37*::KanMX4*; *sti1Δ::KanMX4, cdc37*::NatMX*).

4.1.2 The Growth Phenotypes of Co-Chaperone Double Mutants

To validate the double mutants and to test whether genetic interactions between co-chaperones exist that affect viability, first all mutants were screened at 30 °C for fitness defects. To that end, we performed drop-dilution assays with 10-fold serial dilutions (Figure 15). To prevent experiment-to-experiment variation only strains grown on a single plate were compared. As a control, each plate contained the wild-type strain and the respective single KO/KD strain in addition to the double

KOs/KDs. To obtain a quantitative score for viability, a suitable dilution was chosen, spot density was quantified and normalized to the wild-type control that was grown on the same plate.

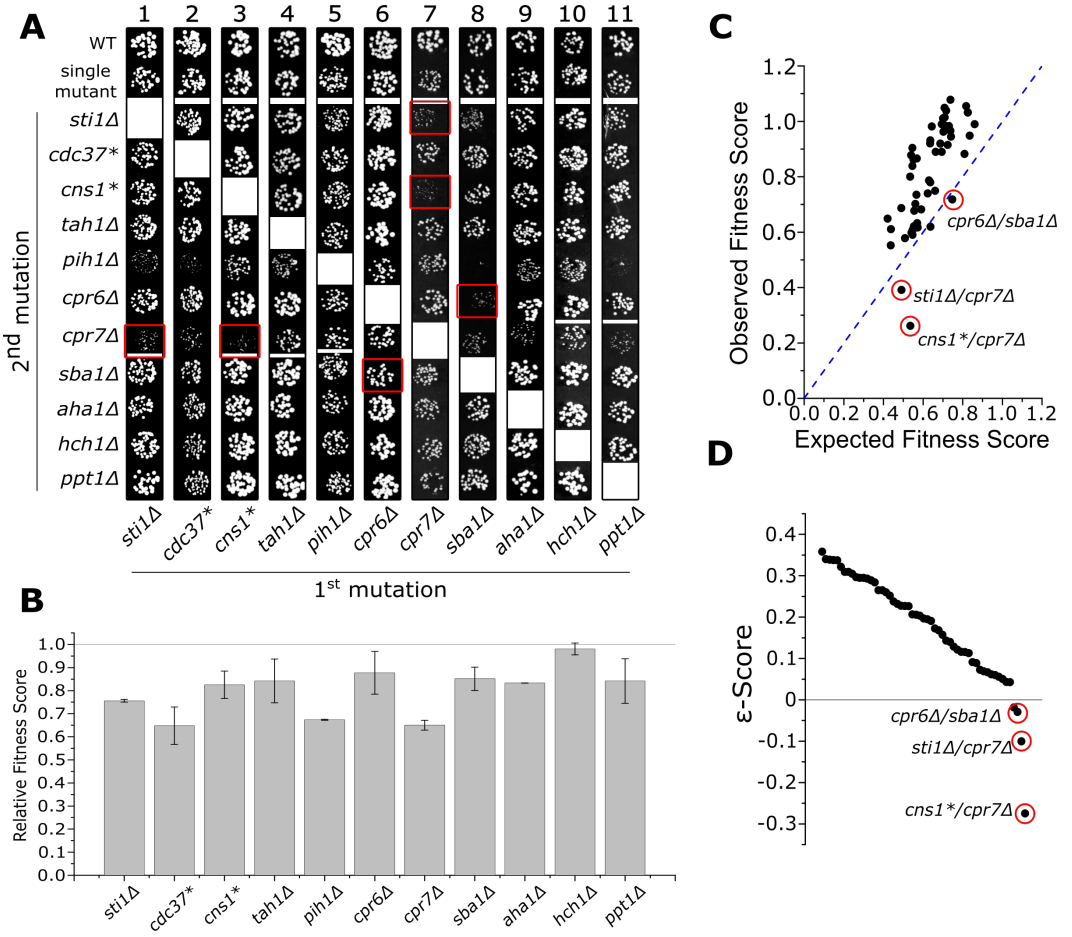

FIGURE 15 | **Genetic Interactions of Co-Chaperones Under Physiological Conditions.**
A Viability of co-chaperone double mutants at 30 °C. Five serial 10-fold dilutions were spotted, but only one representative dilution is depicted. The spots of each column (1-11) originate from the same plate. Synthetic sick mutants are highlighted in red boxes. Screening was performed in duplicates or triplicates with comparable results.
B Densitometric analysis of the single KO/KD viability. Fitness was quantified from a suitable dilution of the serial dilutions from **A**. Relative fitness scores were obtained by normalization to the wild-type control grown on the same plate. The bars indicate means ± SD from at least two biological replicates.
C Correlation of observed and expected fitness scores. The expected phenotype was calculated by multiplication of the relative fitness scores of the single mutants. Shown are the averages of the inherent biological replicates resulting from the KO/KD of the same genes with different resistance markers. Synthetic sick mutants are marked with red circles.
D The ϵ-scores were calculated from the fitness scores from **(B)** and **(C)** with $\epsilon = f_{ab} - f_a \times f_b$ with f_a and f_b representing single mutant fitness and f_{ab} denoting the fitness score of the double mutant. Synthetic sick mutants are marked with red circles.

Among the single mutant controls, a slight fitness decrease compared to the wild-type was evident in all strains (Figure 15A,B). A more pronounced negative growth phenotype was identified for the *pih*Δ and *cpr7*Δ strains, consistent with previous studies (Duina et al., 1996; Deutschbauer et al., 2005) (Figure 15A,B). Additionally,

we noticed decreased fitness in the *cdc37** mutant, which is consistent with the essential function of this co-chaperone for yeast viability. Of note, the depletion of the essential Cns1 protein in the *cns1** strain only led to a slight decrease of viability which was less pronounced as for Cdc37. Since Cns1 is expressed at only approximately 600 copies/cell under physiological conditions whereas Cdc37 expression is about 15-fold higher, Cdc37 function may be impaired to a greater degree by decreased cellular abundance (Ghaemmaghami et al., 2003).

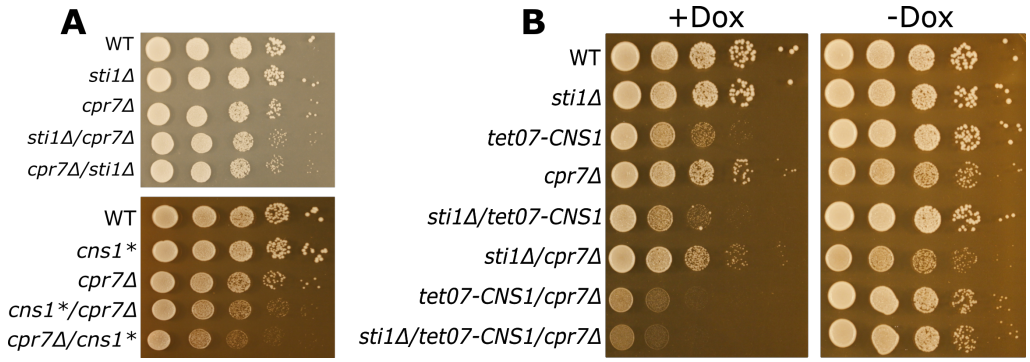

FIGURE 16 | **Sti1, Cpr7 and Cns1 Form a Tripartite Epistatic Module.**
A Validation of the genetic interaction of Cpr7 with Sti1 and Cns1 by drop-dilution spot assay. 10-fold dilution series were grown at 30 °C. To prevent false positive effects due to genetic instability of the slow-growing mutants, fresh cultures from original cryo-stocks were used. The results are representative of three biological replicates.
B Analysis of the genetic interaction between Cns1 and Sti1. The indicated yeast strains were analyzed by 10-fold dilution series spotted on agar with our without 10 µg mL^{-1} doxycycline (+/-Dox). The results are representatives of three biological replicates.

Different models have been developed to quantify genetic interactions that differ in their definition of the neutrality function, which describes the phenotype of genes that do not interact, i.e. the expected phenotype (Mani et al., 2008). The ϵ-score is used to display the difference between the observed phenotype and the expected phenotype (Elena and Lenski, 1997; Mani et al., 2008). In the multiplicative model that was used throughout this study, the ϵ-score is defined as $\epsilon = f_{ab} - f_a \times f_b$ in which f_a and f_b represent single mutant fitness and f_{ab} denotes the fitness score of the double mutant. In this model, the neutrality function is the term $f_a \times f_b$. Thus, the ϵ-score is a measure of epistatic relationships. A ϵ-score of 0 indicates that genes do not genetically interact and the observed effects are additive. Negative ϵ-scores suggest a negative genetic interaction (aggravating effect; synthetic sick/lethal) and often point towards parallel pathways that partially compensate for each other (Collins et al., 2007; Mani et al., 2008; Kampmann, 2018). By contrast, positive ϵ-scores imply a buffering genetic interaction, meaning that the resulting phenotype is less severe than expected from the single mutants. Positive genetic interactions may hint at genes that are involved in the same protein complex or pathway.

When we screened fitness at 30 °C, the majority of co-chaperones had positive

ϵ-scores suggesting that most co-chaperones are connected by buffering genetic interactions (Figure 15C,D). Since positive genetic interactions are often reminiscent of proteins involved in a shared complex, this illustrates that all co-chaperones loosely co-operate to modulate the essential Hsp90 machinery in non-redundant pathways. Only two mutant displayed strong synthetic sick phenotypes: *sti1*Δ/*cpr7*Δ with $\epsilon = -0.101$ and *cpr7*Δ/*cns1** with $\epsilon = -0.275$ (Figure 15C,D). This suggests that the growth phenotype observed in the *cpr7*Δ single mutant is further aggravated by the deletion of *STI1* and *CNS1*. To rule out aberrant phenotypes as a result of genetic instability that is common in slow-growing yeast strains, fresh mutants were obtained from the original cryo-stocks and the results were reproduced, confirming the validity of the observed genetic interactions (Figure 16A). To analyze this epistatic module in more detail, Cns1 was depleted using the tet-off system, which yields more stringent knockdown efficiency (Schopf et al., 2019). Viability in the *tet07-CNS1* strain was markedly reduced, in line with the essential function of Cns1 (Figure 16B). Importantly, knockout of *STI1* in the *tet07-CNS1* background further reduced viability, while viability remained unchanged in the *sti1*Δ mutant, confirming a negative genetic interaction between Cns1 and Sti1 (Figure 16B). Furthermore, knockout of Sti1 in the *cpr7*Δ/*tet07-CNS1* yielded a synthetic sick strain with very low viability (Figure 16B). Together, this indicates that Sti1, Cns1 and Cpr7 form a tripartite epistatic module and are likely involved in the same biological process and may act in parallel, partially compensatory pathways. This is in line with the notion that Cns1 and Cpr7 genetically interact and co-operate in maintaining the solubility of eEF2 in yeast and that over-expression of Cpr7 can rescue the loss of Cns1. (Tesic et al., 2003; Tenge et al., 2015; Schopf et al., 2019). Of note, a weak negative genetic interaction has been observed between *CPR6* and *SBA1* with $\epsilon = -0.03$. In summary, these results extend data from previous studies and define a tripartite genetic module of Cns1, Cpr7 and Sti1 that regulates viability (Costanzo et al., 2016; Rizzolo et al., 2017; Kuzmin et al., 2018; Rizzolo et al., 2018; Schopf et al., 2019). The data show buffering interactions between most co-chaperones and that the simultaneous loss of two co-chaperones generally did not lead to severe growth defects.

4.1.2.1 The Epistatic Co-Chaperone Network is not Rewired Under Heat Stress

At physiological conditions, the Hsp90 co-chaperones formed few negative genetic interactions and most co-chaperones loosely co-operated with positive epistasis. Since the Hsp90 machinery is involved in the protection against heat stress, this begs the question whether the co-chaperone network changes upon heat stress. Hence, yeast viability was tested by drop-dilution spot assays at mild heat-stress conditions at 37 °C (Figure 17A). Surprisingly, for most double KOs/KDs, viability remained unaffected by heat stress and no synthetic lethal phenotypes were evident (Figure 17B). Synthetic sick phenotypes that were evident at 30 °C exacerbate at 37 °C, especially regarding the *cpr6*Δ/*sba1*Δ mutant. In line with the results obtained at 30 °C, also

at elevated temperature most co-chaperones formed positive genetic interactions. Together, this implies that the co-chaperone network is robust against stress.

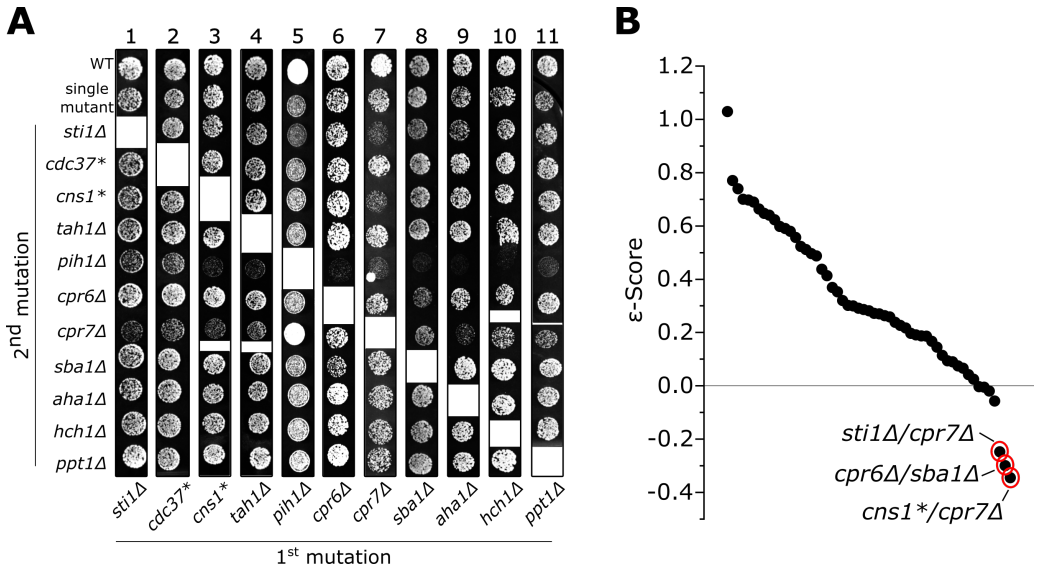

FIGURE 17 | **Genetic Interactions of Co-Chaperones Under Stress Conditions.**
A Viability of co-chaperone double mutants at 37 °C. A representative dilution of drop-dilution spot assay with five 10-fold serial dilutions is shown. The spots of each column (1-11) originate from the same plate.
B The ϵ-scores were calculated as in Figure 15.

While the distribution of positive and negative genetic interactions among co-chaperones was similar at 30 °C and 37 °C (Figure 15, Figure 17), it is not clear whether the co-operation of co-chaperones is altered by heat-stress. Hence, the correlation between the ϵ-scores obtained for viability at 30 °C and 37 °C was analyzed (Figure 18). The ϵ-scores obtained for 30 °C and 37 °C were strongly correlated with a Pearson R of 0.73, showing that the epistatic network between co-chaperones remained largely unchanged by heat stress. In summary, these results show that the Hsp90 machinery is robust against the loss of co-chaperones even under heat-stress and that the co-operative network between co-chaperones remains mostly unaltered under heat stress.

4.1.2.2 Genetic Interactions are not Masked by Hsp90 Upregulation

Only few negative genetic interactions were identified when double KO/KD viability was tested at 30 °C and under mild heat stress at 37 °C. We reasoned that induction of Hsp90 expression as part of an induced HSR could potentially mask negative genetic interactions or be responsible for the buffering genetic interactions that were evident for the majority of co-chaperones.

Hence, viability screening was first repeated at severe heat stress conditions at 42 °C to increase stress and overwhelm the capacity of potentially upregulated chaperone systems (Figure 19A). Expectedly, most strains including the wild-type grew poorly under these conditions. Among the single KOs/KDs, heat sensitivity was observed for the *sti1*Δ, *cdc37**, *cpr6*Δ and *aha1*Δ strain, matching previous studies

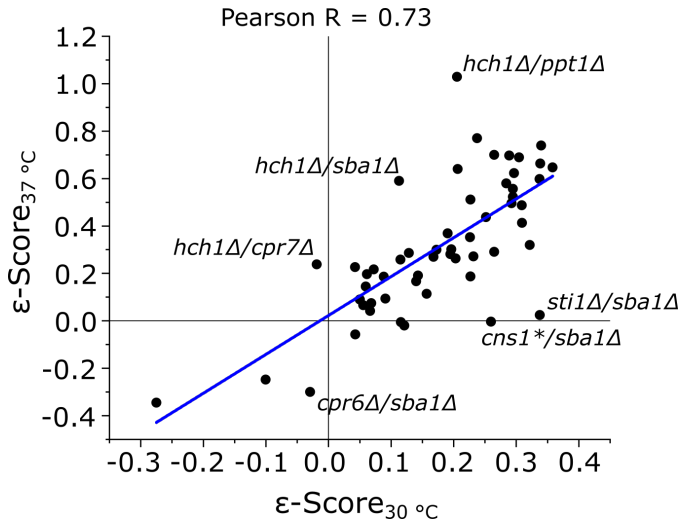

FIGURE 18 | **The Epistatic Network of Co-Chaperones Remains Unaltered by Heat Stress.** The ϵ-scores from Figures 15 and 17 were correlated and the Pearson Correlation Coefficient was calculated. Outliers are labeled.

(Reed, 1980; Panaretou et al., 2002; Sinha et al., 2008; Teng et al., 2011). Furthermore, the *ppt1*Δ strain displayed profound heat sensitivity, in contrast to previous findings (Chen et al., 1994). To confirm this finding, growth kinetics of the *ppt1*Δ strain were measured and compared to the wild-type (Figure 19B). In line with the spot assay data, the *ppt1*Δ strain grew considerably slower than the wild-type, suggesting that Ppt1 function is important for heat stress survival. Surprisingly, no negative genetic interactions were revealed at 42 °C that were not present at 30 °C and 37 °C (Figure 19). This suggests that individual co-chaperones play an important role in the survival of heat stress, yet negative genetic interactions were not masked by induction of a heat shock response due to co-chaperone deletion. To show this more directly, the Hsp90 levels were quantified in all double KOs/KDs, confirming that Hsp90 levels remained largely unaffected by the deletion or depletion of Hsp90 co-chaperones (Figure 19C). Together, these results provide evidence that upregulation of Hsp90 in response to co-chaperone KO/KD did not mask genetic interactions.

4.1.2.3 Synthetic Sick Double Mutants Have No General Cellular Defects

To test whether the defects in the synthetic sick double mutants were a result of a disrupted global protein homeostasis or due to more specific effects, the mutants were first analyzed concerning their ability to trigger a HSR after heat stress (Figure 20). To this end, the expression of Hsp26, whose expression is strongly upregulated upon heat shock was tested (Kurtz et al., 1986; Mühlhofer et al., 2019). In all mutants, a dramatic upregulation of Hsp26 upon heat stress at 42 °C was observed, suggesting that the co-chaperone double KOs/KDs can still induce a HSR (Figure 20). Additionally, global protein aggregation was analyzed by separating supernatant and pellet fractions, showing that aggregation was not increased in the single or double KOs/KDs compared to the wild-type (Figure 21A-C). As a control, proteome-wide

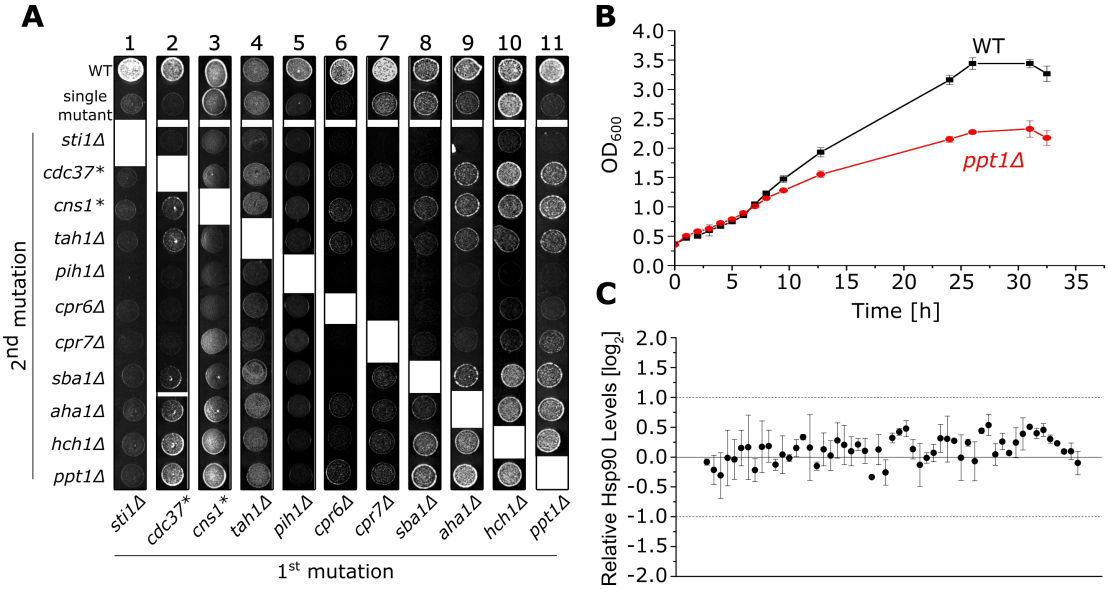

FIGURE 19 | **Genetic Interactions Between Co-Chaperones are not Masked by Hsp90 Up-regulation.**
A Viability of co-chaperone double mutants at 42 °C. Each strain was tested in five 10-fold serial dilutions and one representative dilution is shown. Spots within each column (1-11) originate from the same plate.
B Growth kinetics of the *ppt1*Δ strain at 42 °C. Data points represent means ± SD of three biological replicates.
C Hsp90 levels in double KO/KD strains. The Hsp90 levels of logarithmically growing yeast cultures were analyzed by Western Blot. Shown are the averages of the two replicates originating from KO/KD of the same genes with different selection markers normalized to the WT. Data points represent means ± SD.

aggregation was analyzed after heat shock of the wild-type at 42 ° or after treatment with the Hsp90 inhibitor radicicol. While aggregation increased upon heat stress, inhibition of Hsp90 led to a global reduction of aggregated species, indicating that on a macroscopic level Hsp90 inhibition poises proteins for degradation rather than aggregation (Figure 21D,E). This matches previous findings that found no increased aggregation in yeast strains expressing a defective Hsp90 mutant (Nathan et al., 1997). In summary, these results indicate that the synthetic sick co-chaperone double KOs/KDs mutants do not display general defects of the protein homeostasis system. Hence, it is more likely that specific pathways are disrupted in the synthetic double mutants.

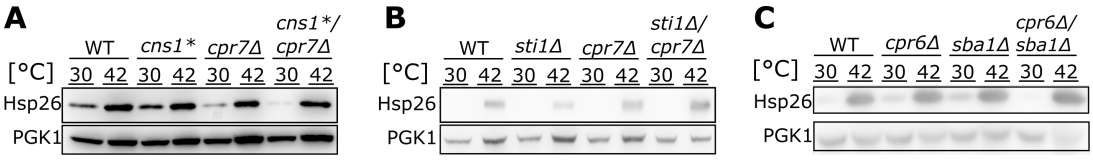

FIGURE 20 | **Synthetic Sick Double Mutants Have a Functional Heat Shock Response.**
A - **C** The induction of the HSR in synthetic sick double mutants. The shown strains were incubated at 30 °C for 1 h before either shifting to 42 °C for 4 h or continued growth at 30 °C for 4 h. Hsp26 levels were quantified as a reliable reporter of the HSR. PGK1 was used as a loading control.

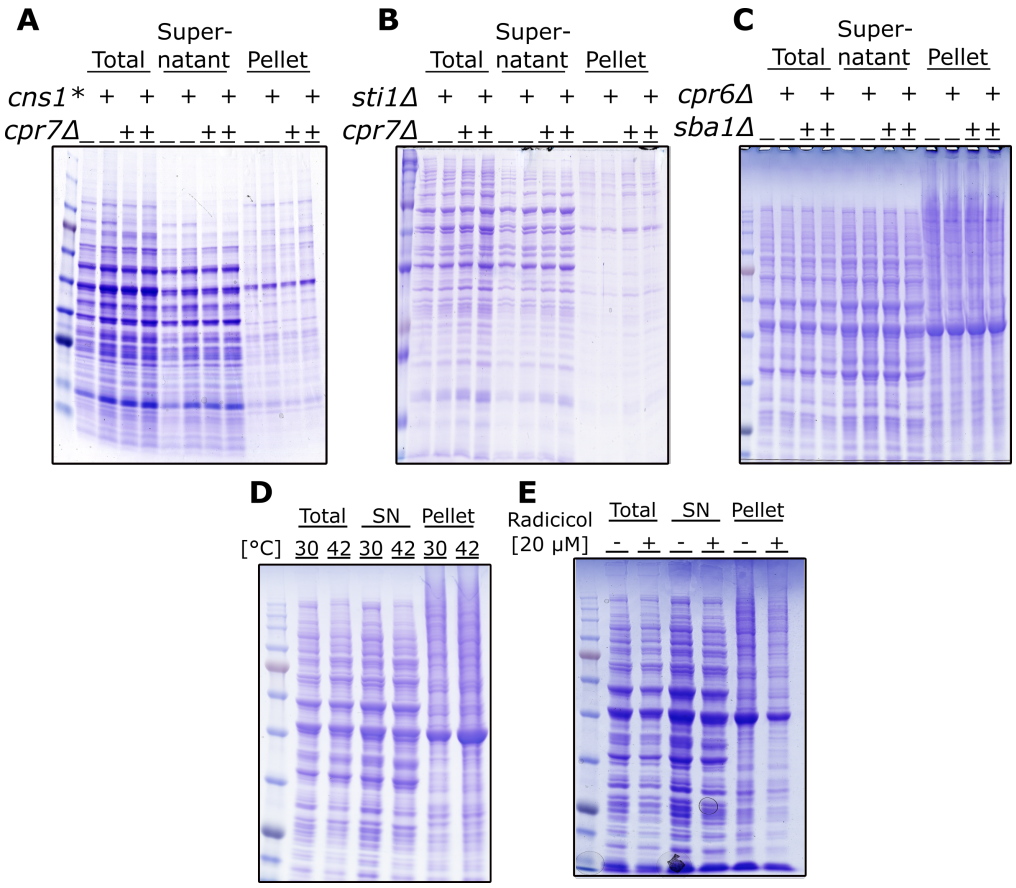

FIGURE 21 | **Global Aggregation is not Altered in Synthetic Sick Double Mutants.**
A - C Proteome-wide aggregation in synthetic sick double mutants. Supernatant and pellet fractions were separated in logarithmically growing yeast cells and analyzed by SDS-PAGE.
D Protein aggregation after heat-shock. After inoculation, cells were incubated at 30 °C for 1 h and then either shifted to 42 °C for 4 h or kept at 30 °C for 4 h before supernatant and pellet fractions were separated and analyzed by SDS-PAGE.
E Protein aggregation after treatment with the Hsp90 inhibitor radicicol. After inoculation, cells were treated with 20 µM radicicol or DMSO for 4 h before supernatant and pellet fractions were separated and analyzed by SDS-PAGE.

4.1.3 Client Maturation in Hsp90 Co-Chaperone Double Mutants

The analysis of the effects co-chaperone double KOs/KDs had on viability provided evidence that co-chaperones form a network mainly composed of buffering genetic interactions with few negative epistatic relationships that modulate Hsp90 function. Notably, the co-chaperone network was not rewired upon heat stress. Since the defects of synthetic sick double KOs/KDs seems to be due to disruption of specific pathways, this raises the question how Hsp90 co-chaperone networks are organized for the maturation of clients. To that end, we systematically tested the effect of simultaneous deletion/depletion of two co-chaperones on the maturation of stringent Hsp90 clients, namely the closely related clients GR and MR and the unrelated oncogenic kinase v-Src.

4.1.3.1 Maturation of v-Src in Hsp90 Co-Chaperone Double Mutants

Oncogenic v-Src is an established Hsp90 client that has been successfully used as a reporter of Hsp90 function in yeast for decades due to the robust lethal phenotype of active v-Src (Kornbluth et al., 1987; Nathan and Lindquist, 1995; Dey et al., 1996a; Dey et al., 1996b; Goeckeler et al., 2002; Lee et al., 2002; Panaretou et al., 2002; Vaughan et al., 2008; Sahasrabudhe et al., 2017). To investigate the effect of co-chaperone deletions on v-Src activity, v-Src was conditionally expressed under the GAL1 or GAL-S promoter and viability was measured by drop-dilution spot assays (Figure 22). First, the activity of v-Src in single co-chaperone KOs/KDs was analyzed, showing that loss of *STI1* or depletion of *CDC37* significantly increased survival compared to the wild-type (Figure 22). This indicates that besides the established kinase-specific co-chaperone Cdc37, also Sti1 plays a crucial role in the maturation of v-Src, confirming previous observations (Lee et al., 2004; Sahasrabudhe et al., 2017). Interestingly, slightly increased viability was evident for most co-chaperones, suggesting that v-Src maturation is strongly regulated by Sti1 and Cdc37, but the cohort of remaining co-chaperones add a secondary regulatory layer.

To reveal genetic relationships between co-chaperones in the context of v-Src maturation, next the viability of all Hsp90 co-chaperone double KOs/KDs was quantified and ϵ-scores were calculated (Figure 23). Due to the inverse relationship between viability and v-Src activity, ϵ-scores describing genetic interactions concerning v-Src maturation were defined as $\epsilon = f_a * f_b - f_{ab}$ with f_a and f_b representing single mutant fitness scores and f_{ab} denoting the viability of the respective double mutant. In more than 90% of the mutants the observed fitness was lower than expected from single mutant fitness (Figure 23). Accordingly, the ϵ-scores were positive for the majority of double KOs/KDs. This means that v-Src was more active in the double mutants than predicted from multiplicative combination of the phenotype in the respective single mutants. Hence, co-chaperones form a buffering epistatic network to maintain v-Src activity and co-chaperones tend to act in non-redundant pathways.

Deletion of *STI1* significantly increased viability in combination with all other co-chaperones (Figure 22). The effect of Cdc37 was much less dominant in most genetic backgrounds and a strong effect of the depletion of Cdc37 was mainly limited to strains lacking *STI1* and *CPR7*. The *cns1*/cpr7*Δ double mutant was remarkably resistant against v-Src toxicity. Yet the decreased protein biosynthesis capacity of the *cpr7*Δ strain, especially in combination with the *cns1** mutation (Schopf et al., 2019) suggests that this the effect is non-specific and reduced v-Src expression caused increased fitness in this mutant rather than disruption of v-Src maturation. Since viability was close to the uninduced control in the *sti1*Δ single KO and not discernible from the glucose control in the *sti1*Δ*/cdc37** double mutant, a potential negative genetic interaction between *STI1* and *CDC37* could be masked (Figure 24A). In *S. cerevisiae* tyrosine phosphorylation levels are low as it only expresses a single

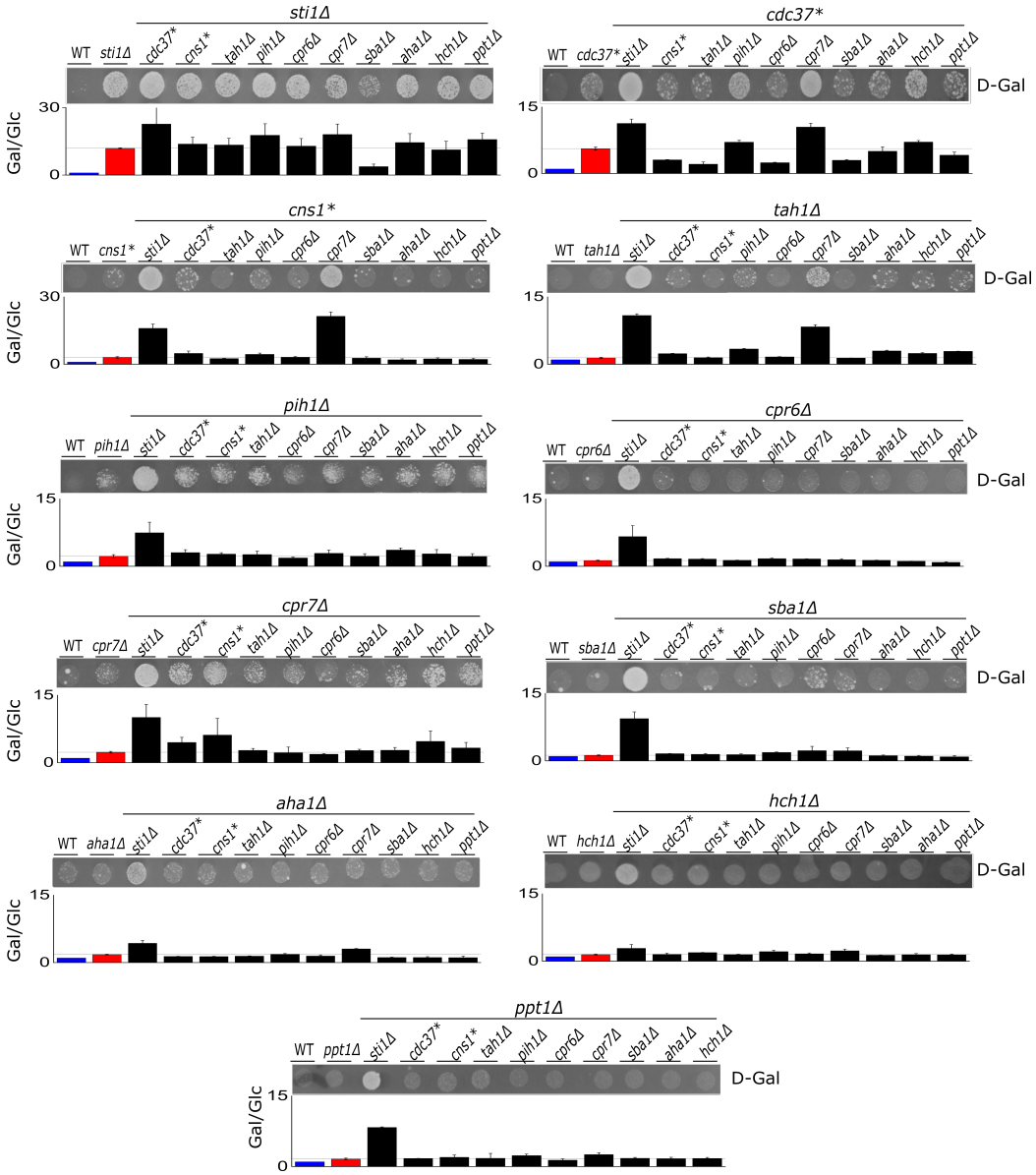

FIGURE 22 | **v-Src Maturation in Hsp90 Co-Chaperone Double Mutants.**
Maturation of v-Src at 30 °C in co-chaperone double mutants. The indicated yeast strains were spotted in serial dilutions on agar plates containing D-galactose to induce v-Src encoded on p416GAL-S and on plates containing D-glucose as a growth control. Spots of a representative dilution on D-galactose plates are shown and were used for densitometric quantification. The fitness scores from D-galactose plates were normalized to fitness scores obtained D-glucose containing plates. The bar charts show the growth of the wild-type (blue) and the normalized single (red) and double KOs/KDs (black). Note that the scale for the *sti1*Δ and *cns1** strains differ from the others. Screening was performed in duplicates or triplicates and means ± SD are shown.

tyrosine kinase endogenously. Thus, unspecific v-Src-mediated tyrosine phosphorylation can be exploited to quantify v-Src activity (Xu and Lindquist, 1993; Aligue et al., 1994). Hence, tyrosine phosphorylation by v-Src was measured as an orthogonal approach to test how *STI1* and *CDC37* genetically interact (Figure 24B). pTyr levels were reduced by about 80% in the *sti1*Δ strain and by about 50% in the *cdc37** mutant. Simultaneous deletion/depletion of Sti1 and Cdc37 reduced pTyr even further to almost undetectable levels. Hence, Sti1 and Cdc37 act in synergism to maintain v-Src maturation, indicating a negative genetic interaction.

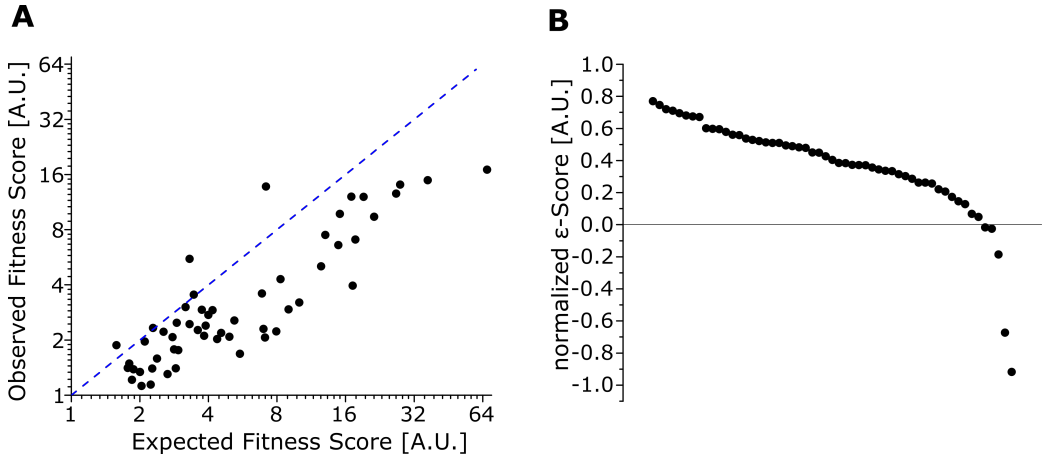

FIGURE 23 | **Genetic Interactions Underlying v-Src Maturation.**
A Correlation between the expected and observed fitness scores of v-Src expressing double mutants. The fitness scores from Figure 22 were used and averages of the inherent biological replicates originating from KO/KD of the same gene with different selection markers were plotted.
B The ϵ-scores were calculated from data in (**A**) according to $\epsilon = f_a * f_b - f_{ab}$ with f_a and f_b representing single mutant fitness scores and f_{ab} denoting the viability of the respective double mutant.

Surprisingly, we noticed that deletion of *SBA1* increased v-Src toxicity in the *sti1*Δ background (Figure 22, top panel). An alleviating genetic interaction implies a connection of the genes within a pathway and an antagonistic relationship (Bellay et al., 2011). This is in agreement with the opposing effect of Sti1 and Sba1 on the conformation of Hsp90 and the proposed roles of Sti1 acting early and Sba1 acting late in the Hsp90 cycle (Li et al., 2011; Biebl and Buchner, 2019).

In summary, screening for genetic interactions among Hsp90 co-chaperones in the context of client maturation revealed that Sti1 and Cdc37 play an important role and act synergistically in v-Src maturation. Additionally, a positive genetic interaction network consisting of the majority of co-chaperones underlies the maturation of v-Src, matching our findings for the organization of the Hsp90 co-chaperone network observed during growth fitness studies.

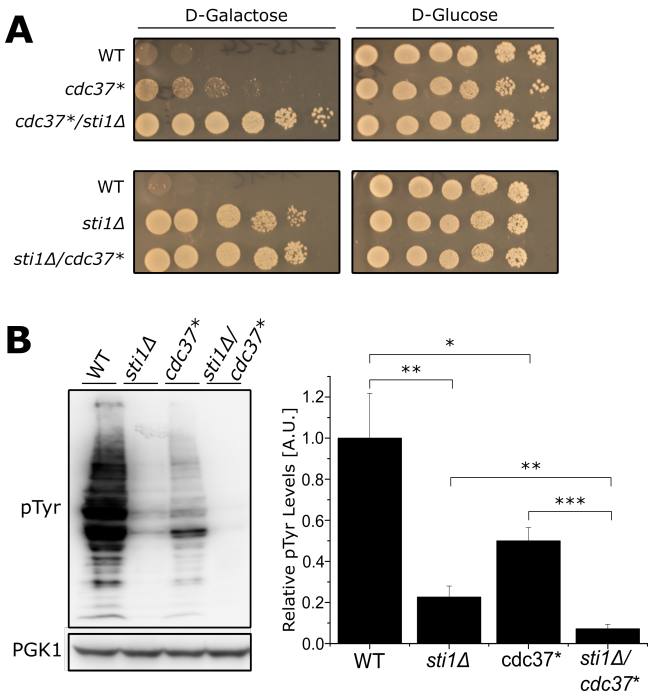

FIGURE 24 | **Sti1 and Cdc37 Form a Negative Genetic Interaction.**
A v-Src toxicity in the *sti1Δ/cdc37** mutant. Drop-dilution spot assays of the indicated strains conditionally expressing v-Src (p416GAL-S) at 30 °C are depicted. Expression was induced on D-galactose containing plates and repressed on D-glucose containing agar plates.
B v-Src activity in the *sti1Δ/cdc37** mutant. v-Src expression from p416GAL1 was induced by addition of D-galactose to logarithmically growing yeast cultures. Phosphotyrosine (pTyr) levels were quantified 4 h after induction by Western Blot. PGK1 was detected as a loading control. A representative Western Blot image of three biological replicates is shown. Bars represent means ± SD. Significance was evaluated by t-testing (n.s.≥0.05; * p≤0.05; ** p≤0.01; *** p≤0.001).

4.1.3.2 Maturation of SHRs in Hsp90 Co-Chaperone Double Mutants

Few synergistic relationships between co-chaperones, but a plethora of buffering genetic interactions were found to underly the maturation of v-Src and the maintenance of growth fitness. To examine whether this scenario also holds true for unrelated clients, the maturation of the GR and MR was analyzed in all single and double co-chaperone mutants. To that end, the GR or MR were heterologously expressed in yeast in the presence of a reporter plasmid driving the expression of the β-galactosidase in a SHR-dependent manner.

Among the single co-chaperone KOs/KDs, the activity of GR was strongly decreased in the *sti1Δ* and the *cpr6Δ* mutants and to a lesser degree in the *sba1Δ* mutant (Figure 25A,B). Matching previous observations, strong activation of the GR activity was observed when *AHA1* or *HCH1* were knocked out and slight activation in the absence of Ppt1 (Sahasrabudhe et al., 2017). The pattern was similar for MR activity consistent with the close evolutionary relationship of the receptors (Figure 25A,B). *sti1Δ* and *sba1Δ* showed decreased activity and *aha1Δ* and *hch1Δ* led to increased MR activity. For MR, loss of Cpr7, but not Cpr6 led to decrease receptor activity, highlighting the differences between Cpr6 and Cpr7, despite their close homology.

Surprisingly, knockdown of *CDC37* activated MR activity, while it did not affect GR activity. While the molecular mechanism for this effect is unclear, it stresses the previously published client-specificity of the co-chaperome (Sahasrabudhe et al., 2017). Interestingly, the overall effects of co-chaperone deletions or KDs affected MR activity to a smaller degree than GR, suggesting that GR is more stringently controlled by Hsp90 than MR.

When co-chaperone double KOs/KDs were tested, we found that approximately 80% of the double mutants had lower GR and MR activity than expected from the multiplicative combination of single KO/KD activities (Figure 25C,D), suggesting that many co-chaperones co-operate in a synergistic manner for SHR maturation. This finding is in contrast to our findings for v-Src activation, in which the activity of v-Src was generally higher than expected from the single mutant phenotypes. Surprisingly, this suggests that the co-chaperone network is organized in different ways for the maturation of SHRs versus kinases. Importantly, since single KOs/KDs not only led to the deactivation but could also activate the GR and MR, the definition of genetic interactions is more complex in the case for SHRs (Figure 25E-G). In case the loss of each co-chaperone under investigation leads to a deactivation, aggravating (negative) genetic interactions represent lower activities than expected, while higher activity than expected are classified as buffering (positive) genetic interactions (Figure 25E). If loss of each co-chaperone leads to increased activity, aggravating genetic interactions have higher activity than expected while positive genetic interactions have lower activity than expected (Figure 25F). Finally, if KO/KD of one co-chaperone has an activating function, while the other has a deactivating effect, mixed phenotypes are possible that can either be closer to the deactivating mutant or the activating mutant (Figure 25G). For GR, 3 aggravating genetic interactions were found, 28 buffering interactions and 24 masking interactions in which the deactivating gene was dominant in 14 mutants. For MR, 9 aggravating, 14 buffering and 32 masking interactions were evident, out of which 27 mutants showed a dominant phenotype of the deactivating mutation. Together, this suggests that co-chaperones form a complex co-operative network to promote the folding and maturation of SHRs.

Next, we sought to understand which co-chaperones form the most relevant genetic interactions for SHR maturation. For GR-expressing double KOs/KDs, deletion of Sti1, Cpr6 and to a smaller degree Sba1 entailed a dominant negative effect on activity, irrespective of the second KO/KD (Figure 25A). Furthermore, double mutants containing a deletion of one of these genes tended to have lower activity than expected (aggravating or deactivating masking interaction). This suggests that these co-chaperones play a central role in the maturation of GR and that they form a core in the co-chaperone network. For MR, loss of Sti1 had a dominant negative effect on activity, whereas the effect of the *sba1*Δ mutation had a much less prominent effect than observed for GR. Additionally, the mentioned negative effect of *cpr7*Δ was dominant in combination with other co-chaperones while the loss of Cpr6 did not

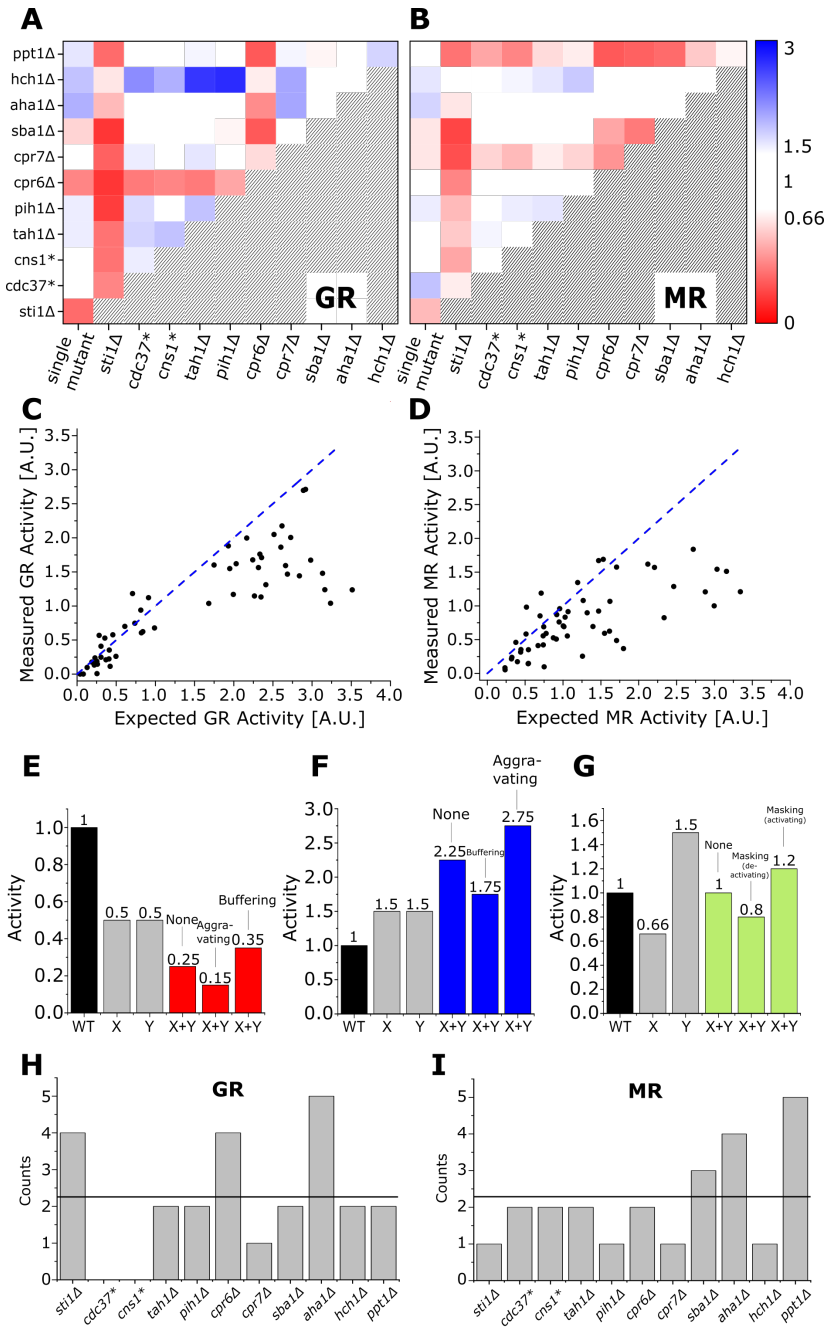

FIGURE 25 | **Genetic Interactions Underlying SHR Maturation.**
A + **B** Activities of (**A**) GR and (**B**) MR in co-chaperone double mutants. Reporter activity was measured at least in 4 replicates. The averages of the inherent replicates originating from KO/KD of the same genes with different resistance markers were normalized to WT activity and are shown as heat maps. The scale indicates fold-activity compared to WT.
C + **D** Correlation of expected and observed (**C**) GR and (**D**) MR activities. The expected activities were derived from the multiplied activities of the single mutants. Data points represent the double mutants from (**A**) and (**B**).
E - **G** Definition of genetic interactions. The definition of genetic interactions are shown for cases in which (**E**) both single KOs/KDs are deactivating, (**F**) both single KOs/KDs are activating and (**G**) one single KO/KD has a activating and the other has a deactivating effect on receptor activity.
H + **I** Distribution of individual KOs/KDs among strong genetic interaction partners. The occurrence of the individual KOs/KDs was assessed in the 6 double mutants with the highest positive and the 6 double mutants with strongest negative ϵ-score for (**H**) GR and (**I**) MR. The expected counts for non-enriched single mutations are indicated by horizontal lines ($\frac{24}{11} = 2.18$).

affect MR activity, also in the presence of other KOs/KDs. Surprisingly, the *ppt1*Δ mutant had wild-type like activity but led to a severe deactivation of MR in combination with other co-chaperone deletions, suggesting a strong co-operation of Ppt1 with co-chaperones in the maturation of MR.

By contrast, the loss of Hch1 generally had a dominant activating effect in combination with other co-chaperones for GR and, albeit to smaller degree, also for MR. Hch1 is a truncated homolog of Aha1 that is only present in yeast (Panaretou et al., 2002; Meyer et al., 2004). While Aha1 is a strong activator of the Hsp90 ATPase, Hch1 binds a similar region on Hsp90 but it less potent in ATPase activation (Panaretou et al., 2002; Meyer et al., 2004). Despite the high homology between Hch1 and Aha1 and the activating effect of the *aha1*Δ deletion, the activating effect of *aha1*Δ was less dominant than the loss of Hch1 in combination with other knockouts. This is also reflected in the positive genetic interaction scores that were on average higher for *aha1*Δ containing double KOs/KDs than for *hch1*Δ containing double mutants for both receptors, suggesting that the differences between Aha1 and Hch1 were not client-specific. Importantly, the *aha1*Δ/*hch1*Δ double mutant had the highest buffering ϵ-score for GR and the second highest score for MR. The activity in the *aha1*Δ/*hch1*Δ double mutant was even lower than in the *aha1*Δ or *hch1*Δ single mutant indicating that loss of the Aha1/Hch1 as a second deletion could suppress the activating effect of the first deletion. Hence, Aha1 and Hch1 form a tight positive genetic interaction, indicating that they are part of the same regulatory process.

To test, if co-chaperones that have a strong effect on client maturation form the tightest genetic interactions, the occurrence of single KOs/KDs within 10% of the highest positive ϵ-scores and 10% of the lowest negative ϵ-scores was analyzed (Figure 25H,I). Hence, 12 double mutants carrying 24 KOs or KDs were examined. For GR, among the 12 double mutants that formed the strongest genetic interactions, the *sti1*Δ, *cpr6*Δ and *aha1*Δ mutations were found 4, 4 and 8 times, respectively. All other deletions occurred up to 2 times, which is consistent with the expected frequency of non-enriched mutations (24 KOs/KDs combined from 11 single KOs/KDs). For MR, *sba1*Δ, *aha1*Δ and *ppt1*Δ counted 3, 4 and 5 times, respectively. These results suggest that co-chaperones that have the strongest effect on client maturation also tend to form the tightest genetic interactions. Additionally, it seems that marked differences within the genetic interactions between co-chaperones are present between the closely related receptors.

In summary, analysis of the genetic network underlying SHR maturation revealed that most double KOs/KDs had lower activity than expected from the single mutants. Additionally, the data show that some co-chaperones that strongly impact SHR activity also form strong genetic interactions with other co-chaperones. However, at the same time strongly impacting co-chaperones can also be part of looser epistatic relationships. This suggests that some co-chaperones rely more on co-operation with other co-chaperones than other members of the co-chaperome.

4.1.4 The Co-Chaperone Network Adapts to Different Clients

Analysis of v-Src, GR and MR maturation in Hsp90 co-chaperone double mutants hinted at differences of the co-chaperone organization. To obtain a clearer picture of the influence of double mutants on client activity, the ϵ-scores of double mutants were systematically compared (Figure 26A). For the effects of double KOs/KDs on GR and MR activity, a Pearson R of 0.61 was calculated, suggesting that double mutants affected GR and MR in similar ways. Nevertheless, despite the close homology of the SHRs, important client-specific differences in the co-chaperone requirement are obvious, in agreement with previous findings (Sahasrabudhe et al., 2017). Since the general stability of clients seems to dictate the Hsp90 dependence of clients (Taipale et al., 2012), the stability of GR and MR was compared. Since both receptors showed comparable degradation kinetics in cycloheximide chase experiments, the differences of the co-chaperone dependence are not a product of the overall stability (Figure 27). Importantly, correlation of the double mutant effects on GR and MR with the effects on v-Src yielded considerably lower Pearson coefficients of 0.38 and 0.35, respectively (Figure 26A). Furthermore, the weak correlation was mostly a result of the conserved adverse effect of the *STI1* deletion on client activity. Hence, these results show that double mutants had profoundly different effects on different clients, highlighting the client-specificity of co-chaperones.

To analyze how the co-chaperone networks are organized for the maturation of different clients, the ϵ-scores for double mutants in the context of GR, MR and v-Src maturation were normalized to the respective expected activities and correlated (Figure 26B). In this way a picture of how well the genetic interaction maps of co-chaperones correlate could be obtained. Surprisingly, even between the related GR and MR, the Pearson R was only 0.29 suggesting that the co-chaperones form substantially different networks for the maturation of clients. When the normalized ϵ-scores for GR and MR were correlated with the scores obtained for v-Src, no statistically significant correlation could be calculated, implying that the genetic interaction maps were entirely different for the maturation of SHRs and kinases. In summary, these results provide evidence for a plastic genetic interaction network among co-chaperones that rewires to adapt to the maturation necessities of clients in a client-specific manner.

4.1.5 Analysis of Specific Epistatic Modules Affecting Client Activity

Comparing the co-chaperone requirements of GR, MR and v-Src revealed marked differences in the organization of the co-chaperone network between clients. Additionally, specific epistatic modules were identified that have a strong positive or negative effect on client activation and form tight genetic interactions with other co-chaperones. To get mechanistic insight, how these epistatic modules affect client maturation, we set out to investigate them in more detail.

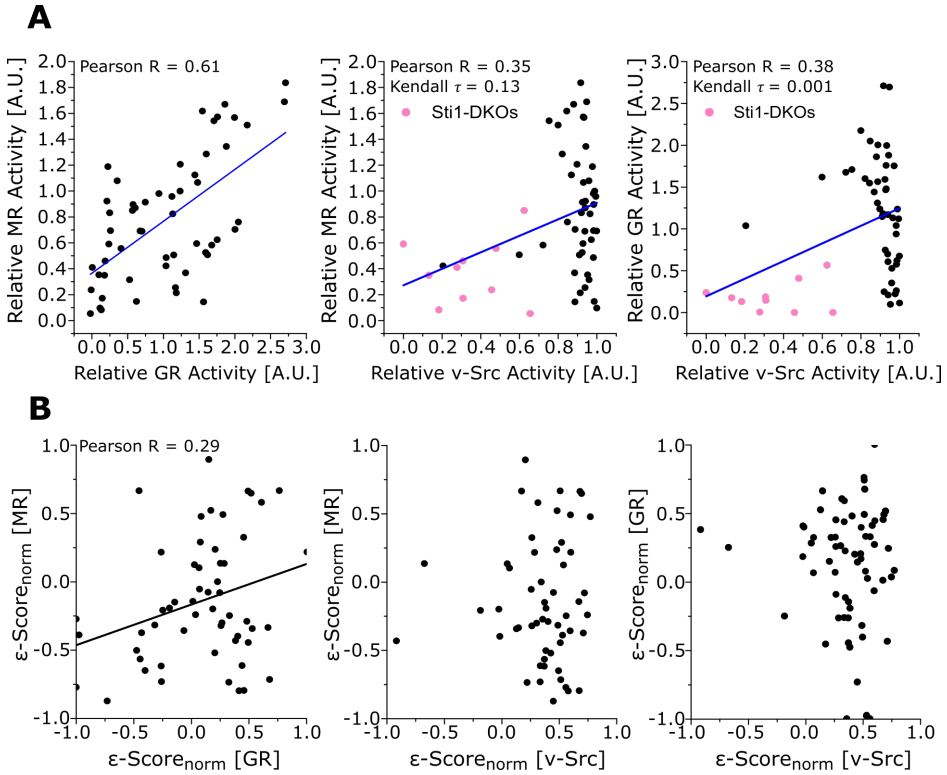

FIGURE 26 | **Co-Chaperones Form Client-Specific Epistatic Networks.**
A Correlation of the relative client activity in co-chaperone double mutants. The activity of GR, MR and v-Src in co-chaperone double KOs/KDs was normalized to the WT and correlated. Each data point represents the average of the two inherent replicates resulting from KO/KD of the same genes with different selection markers. Mutations containing the *sti1*Δ mutation are marked in pink. Pearson Correlation Coefficients and Kendall Coefficients were calculated.
B Correlation of the ϵ-scores of co-chaperone double mutants. The normalized ϵ-scores (ϵ-score divided by the neutrality function) of each double mutant obtained for v-Src, GR and MR maturation were correlated. Each data point represents the average of the two inherent replicates resulting from KO/KD of the same genes with different selection markers. Pearson Correlation Coefficients were calculated.

4.1.5.1 Epistatic Modules Affecting Viability

Analysis of yeast viability in co-chaperone double KOs/KDs revealed strong genetic interactions of *CPR7* with *STI1* and *CNS1*. This could indicate that these co-chaperones are involved in the same cellular process. To better understand how Sti1 and Cpr7 co-operate, protein biosynthesis rates were probed by S^{35}-methionine incorporation in proteins during logarithmic growth (Figure 28A). In agreement with previous results, loss of Cpr7 led to reduced S^{35}-methionine incorporation (Schopf et al., 2019). By contrast, deletion of *STI1* alone had no impact on protein biosynthesis, whereas S^{35}-methionine levels in proteins were significantly reduced in the *sti1*Δ/*cpr7*Δ double mutant. This is in line with the synergistic (negative) genetic interaction observed on the level of growth (Figure 15) and suggests that the epistatic relationship between Sti1 and Cpr7 is due to their joint role in maintaining protein biosynthesis. Since for Cns1 and Cpr7 a role in the maturation of eEF2 has been

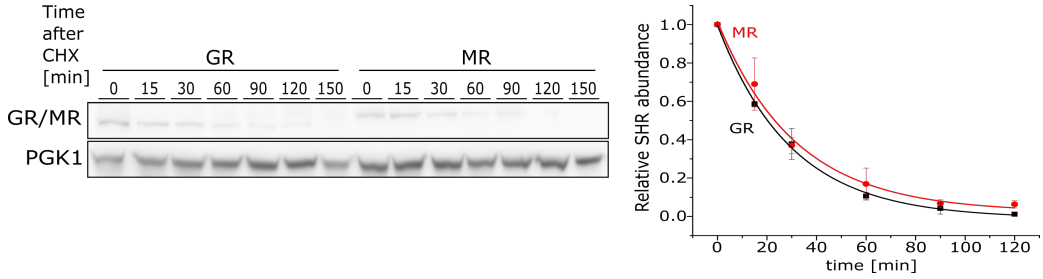

FIGURE 27 | **The Stability of GR and MR is Similar *in vivo*.**
Stability of GR and MR *in vivo*. Logarithmically growing yeast cells expressing HA-tagged GR or MR from p413GPD were treated with cycloheximide and the abundance of GR and MR was analyzed by Western Blot at the indicated time points.

shown (Schopf et al., 2019), the effect of Sti1 in the *sti1*Δ/*cpr7*Δ mutant on the maturation of eEF2 was tested (Figure 28B). In line with the effects on *de novo* protein biosynthesis, solubility of eEF2 was not affected by loss of Sti1, but loss of Cpr7 increased aggregation considerably (Figure 28B). Importantly, aggregation was further increased in the *sti1*Δ/*cpr7*Δ double mutant (Figure 28B). Knockdown of *CNS1* using DAmP had only a minor impact on eEF2 solubility, in line with the lacking effect on viability (Figure 15, Figure 28C). Yet, knockout of *STI1* in the *cns1** background decreased eEF2 solubility, showing that Sti1 and Cns1 genetically interact to keep eEF2 soluble (Figure 15C). In summary, these results define a tripartite epistatic module between Sti1, Cpr7 and Cns1 and revealed a novel function of Sti1 in the maturation of eEF2 in addition to the known modulators Cpr7 and Cns1.

4.1.5.2 Epistatic Modules Regulating v-Src Activity

For v-Src maturation, a striking role of Sti1 became evident. Depletion of Cdc37 in the *sti1*Δ background completely rescued growth to the level of the uninduced control. To further explore the negative genetic interaction between Sti1 and Cdc37 for v-Src maturation, we first tested the dependence of v-Src on Hsp90 *in vivo*. Inhibition of Hsp90 with radicicol did not lead to the degradation of v-Src (Figure 29A). Since lacking degradation suggests that Hsp90 affects v-Src conformation, solubility of v-Src was tested. Even in the wild-type strain, inhibition of Hsp90 considerably reduced v-Src solubility (Figure 29A). Of note, inhibition of Hsp90 in the *sti1*Δ and *cdc37** strains also did not lead to v-Src degradation in cycloheximide chase experiments (Figure 29B). Since native v-Src seems to be resistant to degradation and requires Hsp90 to retain a soluble form, the expression kinetics of v-Src were tested in the *sti1*Δ, *cdc37** and *sti1*Δ/*cdc37** strains. Compared to the wild-type, the accumulation of v-Src was slower in the *cdc37** and *sti1*Δ strains and even slower in the *sti1*Δ/*cdc37** mutant. Interestingly, steady-state levels of v-Src were only slightly different between mutants. This suggests, that Sti1 and Cdc37 play a pivotal role in accelerating *de novo* v-Src maturation. In summary, these results show that Sti1 and Cdc37 are important for *de novo* maturation of v-Src and that mature v-Src relies on the Hsp90 system to remain soluble.

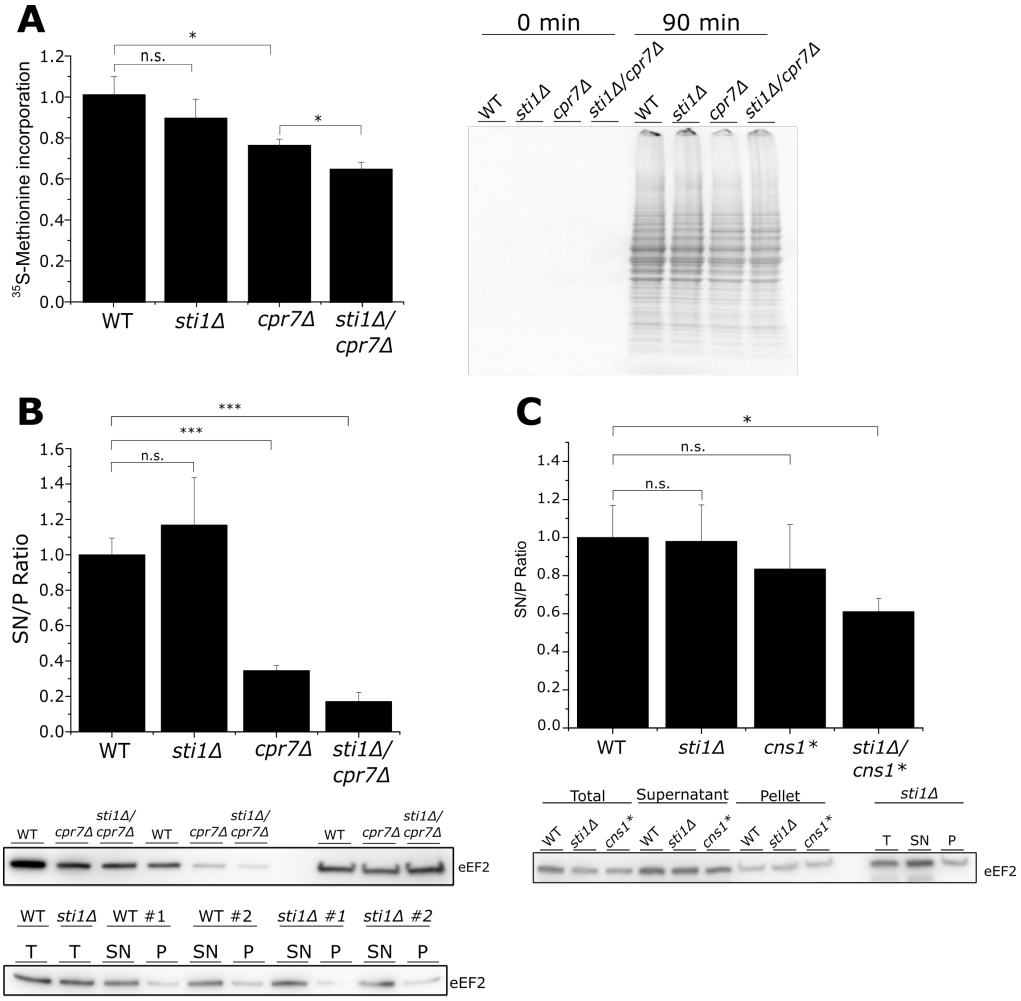

FIGURE 28 | **Sti1, Cpr7 and Cns1 Form an Epistatic Module for eEF2 Maturation.**
A *De novo* protein biosynthesis in the *sti1*Δ/*cpr7*Δ mutant. S^{35}-methionine incorporation was quantified in logarithmically growing cells in SD-Met medium supplemented with a mix of cold and hot L-methionine. Bars represent means ± SD of three biological replicates. A representative autoradiogram is depicted. Statistical significance was tested using t-testing (n.s.≥0.05; * p≤0.05; ** p≤0.01; *** p≤0.001).
B,C Solubility of eEF2 in the *sti1*Δ/*cpr7*Δ and *sti1*Δ/*cns1** mutants. Log-phase growing yeast cultures were harvested to separate supernatant and pellet fractions. eEF2 was quantified using Western Blot. Analysis was performed in biological triplicates and representative Western Blot images are shown. Bars indicate means ± SD. Statistical significance was tested using t-testing (n.s.≥0.05; * p≤0.05; ** p≤0.01; *** p≤0.001).

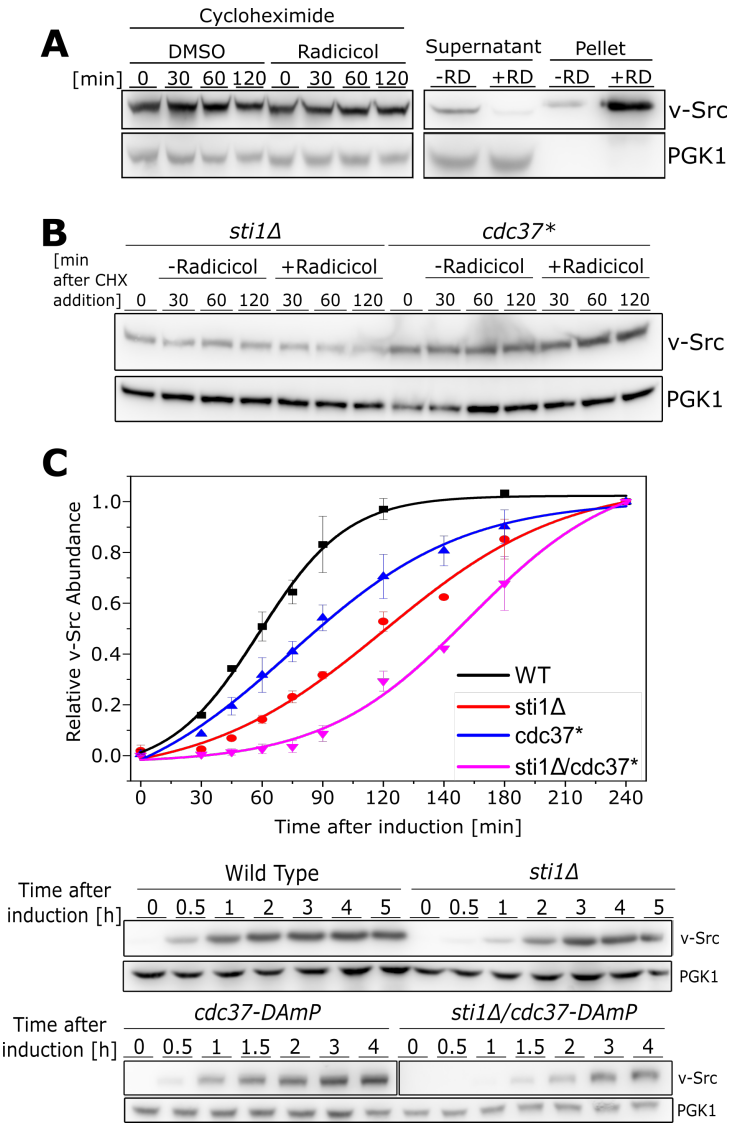

FIGURE 29 | **Sti1 and Cdc37 Affect v-Src Solubility.**
A Stability of v-Src after Hsp90 inhibition. In log-phase growing yeast cells, HA-v-Src expression from p413GAL1 was allowed for 3 h in the presence or absence of radicicol. (**Left**) Cycloheximide was added and v-Src levels were analyzed at the indicated time points using Western Blot. (**Right**) Cells were lysed, supernatant and pellet fractions were separated and analyzed by Western Blot.
B Degradation kinetics of v-Src in the absence of Sti1 and Cdc37. Log-phase growing cells carrying the *sti1*Δ or *cdc37** mutation were induced to express v-Src for 3 h from p413GAL1 and were treated with DMSO or 25 µM radicicol. After 3 h, cycloheximide (CHX) or DMSO were added and HA-v-Src levels were quantified after the indicated time points using Western Blot.
C Folding kinetics of v-Src. Expression of HA-tagged v-Src (p413GAL1) was induced in the indicated log-phase growing yeast mutants. v-Src levels were quantified at the indicated time points by Western Blot. Steady state levels of each strain were normalized to 1. Representative Western Blot images of biological triplicates are shown.

To test, whether Sti1 and Cdc37 also affect solubility of mature v-Src, soluble and pellet fractions of yeast cultures expressing v-Src were separated (Figure 30A). Similar to Hsp90 inhibition with radicicol (Figure 29A), deletion of *STI1* and depletion of Cdc37 reduced the amount of soluble v-Src (Figure 30A). In the *sti1*Δ/*cdc37** double mutant, v-Src almost exclusively fractionated into the pellet fraction. This confirms that not only inhibition of Hsp90, but also loss of Sti1 and Cdc37 markedly reduced the solubility of v-Src. This raised the question, whether Sti1 and Cdc37 fulfill different functions in the v-Src maturation process.

To probe functional overlap between Sti1 and Cdc37, the aggregation of v-Src was followed in the *sti1*Δ and *cdc37** strains ectopically expressing Sti1 or Cdc37 (Figure 30B). As expected, loss of Sti1 or depletion of Cdc37 could be rescued by overexpression of Sti1 and Cdc37 from plasmids, respectively. Surprisingly, Sti1 or Cdc37 overexpression could also rescue the loss/depletion of each other regarding v-Src solubility. In line with the negative genetic interaction between Sti1 and Cdc37, this suggests that Sti1 and Cdc37 have partially overlapping functions and act in parallel pathways. To test whether the overlapping function also holds true in the context of v-Src activity, pTyr levels were quantified in the *sti1*Δ background (Figure 30C). Overexpression of Cdc37 partially rescued v-Src function, matching the finding that overexpression of Cdc37 could increase v-Src solubility in the *sti1*Δ strain. As mentioned, Sti1 harbors three TPR domains and acts as an adapter protein between the Hsp70 and Hsp90 system (Johnson et al., 1998; Wegele et al., 2006; Röhl et al., 2015b). TPR1 preferentially binds Hsp70, TPR2A binds Hsp90 and TPR2B is suggested to bind both Hsp90 and Hsp70 with relatively weak affinity (Schmid et al., 2012). The mutations N39A and N435A in TPR1 and TPR2B, respectively, abrogate Hsp70 binding, whereas mutation of R341 in the TPR2A domain inhibits Hsp90 binding (Flom et al., 2006; Röhl et al., 2015b). Surprisingly, the Hsp90 binding-deficient Sti1^{R341A} mutant could still rescue v-Src activity in the *sti1*Δ mutant, suggesting that the binding of Sti1 to Hsp90 is not essential for kinase maturation (Figure 30C). By contrast, abrogation of Hsp70 binding in the Sti1$^{N39A/N435A}$ mutant rendered Sti1 incapable of rescuing v-Src activity. Hence, binding of Sti1 to Hsp70, but not to Hsp90 is required to assure v-Src maturation. This finding is in line with a model, in which v-Src is trapped on Hsp70 and binding of Sti1 to Hsp70 promotes client release.

In summary, the key epistatic module Sti1-Cdc37 affects *de novo* v-Src maturation as well as maintaining solubility of mature v-Src. Besides the well-studied kinase-specific recruiter protein Cdc37, Sti1 is pivotal to keep v-Src active. For that function, association of Sti1 with Hsp70 seems to be paramount, while the effect of Sti1 on Hsp90 is less relevant. Importantly, Sti1 and Cdc37 have synergistic, overlapping functions and can partially replace each other.

4.1.5.3 Epistatic Modules Regulating SHR Activity

For v-Src function, deletion of co-chaperones either had no effect or led to decreased activity. By contrast, deletion of Aha1 or Hch1 led to the activation of GR and MR.

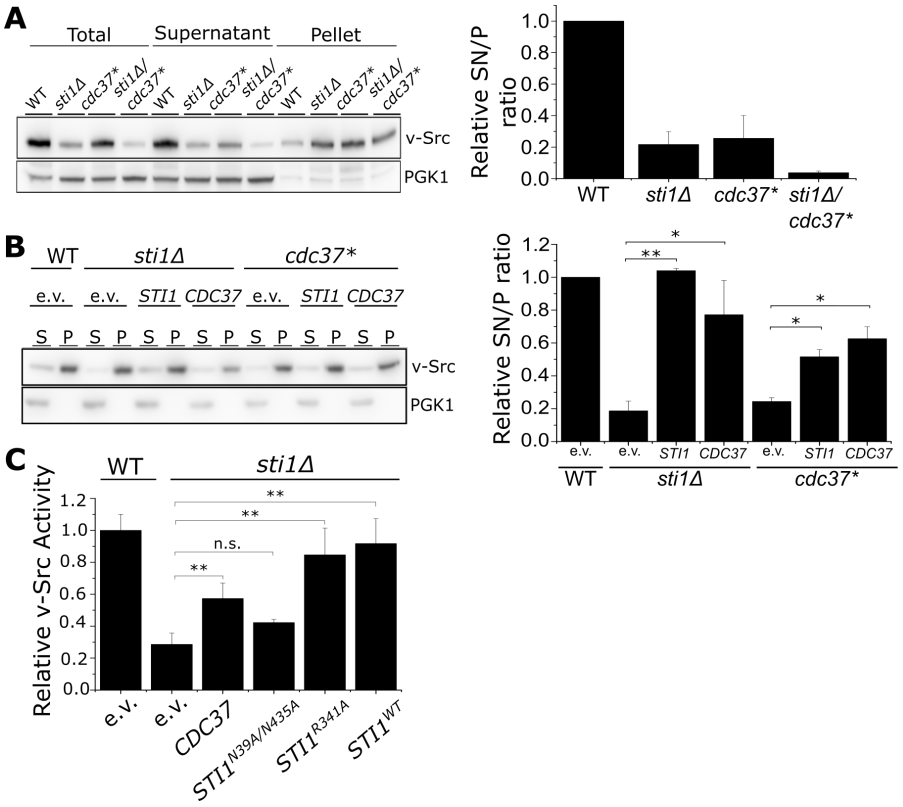

FIGURE 30 | **Sti1 and Cdc37 Have Overlapping Functions.**
A Solubility of v-Src in the *sti1Δ/cdc37** mutant. HA-tagged v-Src was expressed from p413GAL1 for 4 h in logarithmically growing cells after induction by the addition of 2% of D-galactose. Bars represent means ± SD of three biological replicates. A representative Western Blot is depicted. Statistical significance was tested using t-testing (n.s.≥0.05; * p≤0.05; ** p≤0.01; *** p≤0.001).
B Overlapping functions of Sti1 and Cdc37. Sti1 and Cdc37 were constitutively expressed from p415GPD plasmids in log-phase yeast cultures lacking *STI1* or with depleted Cdc37. Expression of HA-tagged v-Src from p413GAL1 was analyzed by Western Blot after separation of supernatant (S) and pellet (P) fractions. Analysis was performed in biological duplicates and a representative Western Blot image is shown. Bars indicate means ± SD. Statistical significance was tested using t-testing (n.s.≥0.05; * p≤0.05; ** p≤0.01; *** p≤0.001).
C Rescue of v-Src activity in *sti1Δ* by Sti1 mutants. v-Src expression from p416GAL1 was induced in log-phase yeast cells expressing the indicated co-chaperones from p415GPD plasmids. Phosphotyrosin levels were quantified 4 h after induction. Bars indicate means ± SD. Statistical significance was tested using t-testing (n.s.≥0.05; * p≤0.05; ** p≤0.01; *** p≤0.001).

Strikingly, while both co-chaperones increased activity when knocked out individually, the *aha1*Δ*/hch1*Δ double mutant had even lower activity than the individual KOs. To understand the epistatic relationship between Aha1 and Hch1 in more detail, first the effect of overexpressed Aha1 and Hch1 in wild-type yeast was tested (Figure 31A). Overexpression of Aha1 and Hch1 led to a marked decrease of GR activity, suggesting that Aha1 and Hch1 are dose-dependent, negative regulators of GR activity. This effect was Hsp90-dependent, since overexpression of the Hsp90 binding mutants Aha1^{D53K} or the Hch1^{D53K} had no impact on GR activity. Of note, the expression levels of Aha1 or Hch1 were not affected by the mutation (Figure 31A). To test the generality of the negative regulatory effect, Aha1 and Hch1 were expressed in wild-type yeast conditionally expressing c-Src or v-Src (Figure 31B). While neither Aha1 nor Hch1 overexpression had an effect on viability in c-Src expressing strains, both could rescue the lethal phenotype of v-Src expression, confirming that the negative effect of overexpressed Aha1 and Hch1 on client activation is not client-specific. Notably, the deactivating effect of Aha1 and Hch1 were also evident in yeast strains lacking *AHA1*, showing that the effect does not rely on the combined action of Aha1 and Hch1 (Figure 31C). To discern whether the KO of Aha1 and Hch1 affected GR activity due to increased abundance of GR or due to conformational alterations, the *in vivo* stability of GR was tested in the *aha1*Δ, *hch1*Δ and *aha1*Δ*/hch1*Δ mutants by cycloheximide chase (Figure 31D). While degradation was slower in the *aha1*Δ and *hch1*Δ it was not further decreased in the *aha1*Δ*/hch1*Δ double mutant, matching results from the presented GR activity data. In conclusion, these results indicate that Aha1 and Hch1 act as negative regulators of Hsp90 client activity and that the absence of Aha1 or Hch1 stabilizes GR *in vivo*.

To understand the roles of Aha1 and Hch1 as negative regulators on a mechanistic level, the competition of Aha1, Hch1 and the GR-LBD for Hsp90 binding was tested by aUC (Figure 32). GR-LBD bound to the partially closed Hsp90 conformation induced by ATP-γS as previously shown (Figure 32A) (Lorenz et al., 2014). Addition of Aha1 and Hch1 led to the dissociation of the GR-LBD from Hsp90, which is consistent with the overlapping binding sites of Aha1, Hch1 and GR-LBD (Lorenz et al., 2014). Notably, we observed a shift from approx. 6.3 S of the GR-LBD*:Hsp82 complex to about 7 S when Hch1 was added, but not when Aha1 was added, suggesting that the formation of a GR-LBD*:Hsp82:Hch1 complex is possible, while the GR-LBD*:Hsp82:Aha1 does not exist. Furthermore, Aha1 displaced GR-LBD* more efficiently from Hsp90 than Hch1, whereas loss or overexpression of Hch1 had a stronger effect than Aha1 *in vivo*. Labeled Aha1* was able to form a ternary Aha1*:Hsp82:Hch1 complex despite the overlapping binding sites, indicating different binding modes (Figure 32B). This suggests that Aha1 and Hch1 have at least partially distinct functions, despite significant sequence homology.

In summary, Aha1 and Hch1 serve as negative regulators of GR activity by regulating dwell time of GR on Hsp90. In combination, *in vitro* and *in vivo* data suggest

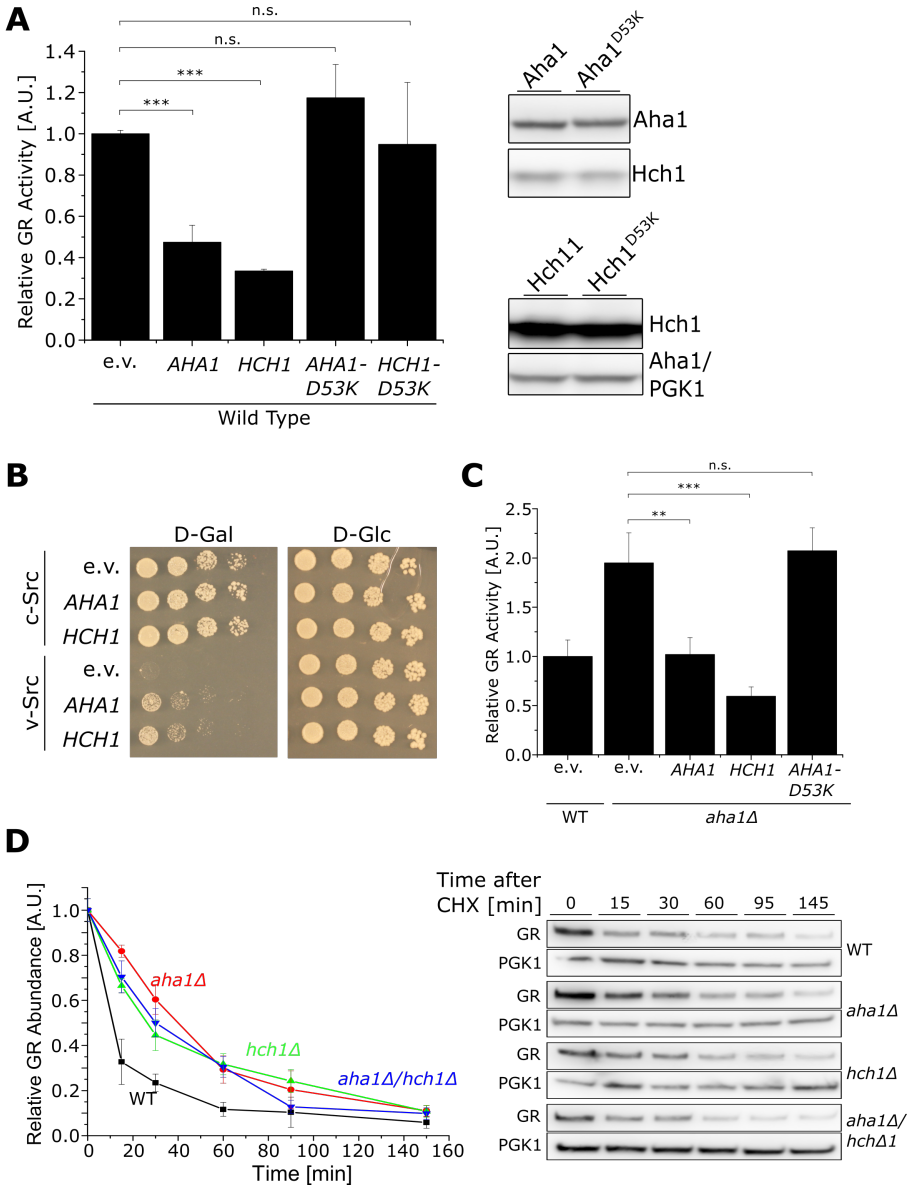

FIGURE 31 | **Aha1 and Hch1 are Negative Regulators of SHR and v-Src Activity.**
A The effect of Aha1 and Hch1 overexpression on GR. GR activity was measured in wild-type yeast strains overexpressing the indicated proteins from p415GPD. Expression levels of the mutants were confirmed in triplicates by Western Blot. A representative replicate is shown. Note that Aha1 runs at the same molecular weight as the PGK1 loading control. Bars represent means ± SD of at least four biological replicates. Statistical significance was tested using t-testing (n.s.≥0.05; * p≤0.05; ** p≤0.01; *** p≤0.001).
B The effect of Aha1 and Hch1 overexpression on v-Src. v-Src or the non-toxic c-Src were conditionally expressed from a p413GAL1 plasmid and *AHA1* and *HCH1* were cloned in p425-GAL1 vectors. Cells were incubated at 30 °C on D-galactose or D-glucose containing plates for 3 days.
C Rescue of Aha1 by Hch1. GR activity was measured in the *aha1*Δ strain expressing the indicated co-chaperones from p415GPD plasmids. Bars indicate means ± SD of at least 4 biological replicates. Statistical significance was tested using t-testing (n.s.≥0.05; * p≤0.05; ** p≤0.01; *** p≤0.001).
D Cycloheximide chase of GR in the absence of Aha1 and Hch1. HA-tagged GR was constitutively expressed from p413GPD in the indicated co-chaperone KO strains. Cycloheximide (CHX) was added to logarithmically growing cultures and GR levels were detected at the indicated time points by Western-Blot. Data points show means ± SD of three biological replicates. A representative Western Blot image is shown.

that the loss of Aha1 and Hch1 increases the dwell time of GR on Hsp90, thus increasing the activity and decreasing degradation. Yet, loss of both Aha1 and Hch1 does not further increase activity, probably since increased the dwell time does not further promote maturation. Consistently, overexpression of Aha1 and Hch1 has a negative effect client activity that seems to be client-unspecific. Despite similar effects on GR activity *in vivo*, Aha1 and Hch1 bind Hsp90 in different ways and seem to have at least in part different functions.

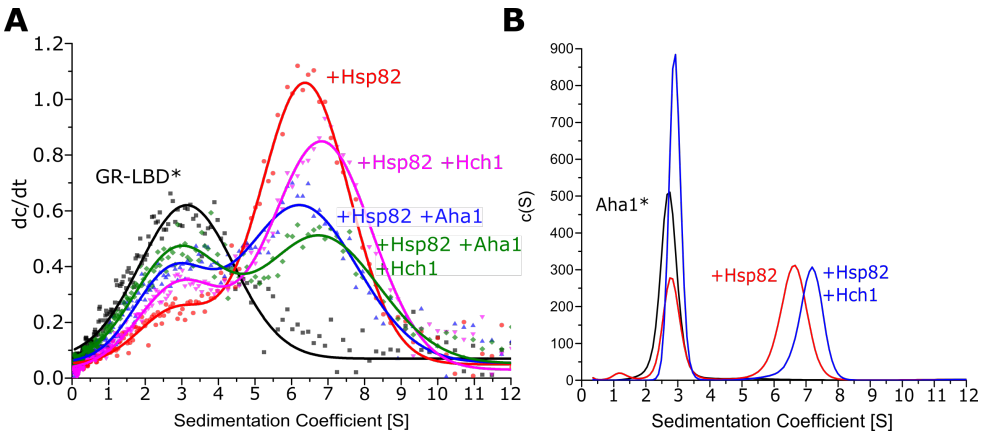

FIGURE 32 | **Aha1 and Hch1 Compete with GR-LBD for Hsp90 Binding.**
A aUC experiment showing the competition between Aha1, Hch1 and GR-LBD for Hsp90 binding. Atto-488 labeled GR-LBD (GR-LBD*; 500 nM) was analyzed with yeast Hsp90 (Hsp82; 4 µM monomer concentration) in the presence or absence of Aha1 and Hch1 (6 µM each). Experiments were performed in the presence of 2 mM ATP-γS.
B aUC analysis of the simultaneous binding of Aha1 and Hch1 to Hsp90. Atto488- labeled Aha1 (Aha1*; 500 nM) was tested in the presence of yeast Hsp90 (Hsp82, 4 µM monomer concentration) and Hch1 (6 µM).

4.1.6 The Epistatic Network of Hsp90 Co-Chaperones in Yeast - Summary and Discussion

Hsp90 function is modulated by co-chaperones for client recruitment, conformational control and ATPase activity. Surprisingly little is known about the function of co-chaperones for client maturation, especially in the cellular environment. Whether co-chaperones act independently or function in a coordinated network for client maturation has previously not been studied. In this thesis, a comprehensive library of 110 Hsp90 co-chaperone double KOs/KDs was generated to examine the epistasis between co-chaperones affecting viability and the maturation of the Hsp90 clients GR, MR and v-Src.

4.1.6.1 Epistasis of Co-Chaperones Affecting Viability

None of the co-chaperone double mutants showed a synthetic lethal phenotype at physiological temperature or under heat stress. Synthetic sickness was limited to the *cpr7*Δ/*sti1*Δ and *cpr7*Δ/*cns1** double mutants under physiological conditions and

additionally to the *cpr6*Δ/*sba1*Δ double mutant under heat stress. This is in line with results from large-scale screening efforts that did not find synthetic lethality within Hsp90 co-chaperones and few negative genetic interactions (Costanzo et al., 2016; Rizzolo et al., 2017; Kuzmin et al., 2018; Rizzolo et al., 2018). This work showed that most combinations of two co-chaperones can be lost without severe growth phenotypes. Hence, most co-chaperones do not depend on the presence of other co-chaperones for their function and the Hsp90 co-chaperome is robust against perturbation. The majority of co-chaperones was connected by positive genetic interactions, consistent with a model in which most co-chaperones fine-tune Hsp90 function. The organization of the genetic interaction network found at physiological temperature remained largely unaltered when cells were shifted to heat-stress conditions. However, the coordination between the co-chaperones became tighter as evident from generally increased genetic interaction scores. This could be a result of the increased dependence on Hsp90 that cells encounter when unfolded proteins accumulate under stress.

Follow-up analysis of the negative genetic interactions that were evident at physiological temperature revealed a novel role of Sti1 as part of a previously published epistatic module between Cns1 and Cpr7 that regulates protein biosynthesis by maintaining eEF2 function (Tenge et al., 2015; Schopf et al., 2019). Loss of Cpr7 or depletion of Cns1 both individually decrease the solubility of eEF2 and *de novo* protein biosynthesis (Schopf et al., 2019). As a result depletion of Cns1 and loss of Cpr7 both entail a growth defect (Duina et al., 1996; Schopf et al., 2019). By contrast, our analysis showed that deletion of Sti1 alone had no effect on eEF2 aggregation or protein biosynthesis and fitness was not reduced in the *sti1*Δ strain. Hence, Cns1 and Cpr7 together are able to buffer the loss of Sti1. Yet, deletion of *STI1* in the *cpr7*Δ or *cns1** background further reduced eEF2 solubility. Notably, a genetic interaction between Cns1 and Sti1 on the level of viability was only observed when the levels of Cns1 were drastically reduced using the tet-off system instead of the DAmP mutation as compared to the more stringent knockdown reached by the Tet-off system (Schopf et al., 2019). Cns1 is expressed at approximately 600 copies per cell and is thus probably fit to fulfill its function to a sufficient degree in the DAmP strain, in which the abundance is reduced by approximately 50% (data not shown). These data strongly support the hypothesis of Sti1, Cpr7 and Cns1 forming a tripartite epistatic module to maintain eEF2 solubility.

At 37 °C additionally a genetic interaction between Cpr6 and Sba1 became obvious. In the co-chaperone-assisted Hsp90 cycle, Sti1 is thought to interact first and keep Hsp90 in an open conformation, whereas Sba1 acts late and stabilizes a closed Hsp90 conformation. Cpr6 has been found to compete with Sti1 binding and thus promotes progression in the Hsp90 cycle towards the closed conformation (Richter et al., 2004; Li et al., 2011). Hence, Sba1 and Cpr6 both push Hsp90 towards the closed conformation, providing a molecular explanation for the observed genetic interaction between Cpr6 and Sba1.

4.1.6.2 Epistasis Affecting Client Maturation

When the activity of GR, MR and v-Src was screened in co-chaperone double mutants we found fundamentally different organizations of the genetic networks of co-chaperone (Figure 34). While activity of v-Src was higher in most double mutants than expected from the single mutants, SHR activity in the double mutants was generally lower than expected from the single mutant phenotypes. Yet, even in the closely related GR and MR, markedly different genetic interaction maps were evident. However, in all cases co-chaperones that had strong effects on client activity also tended to form tighter genetic interactions. Early findings by the Lindquist lab suggested that perturbation of the Hsp40/70-Hsp90 system had opposing effects on v-Src and SHRs, which is in line with the findings presented in this study (Kimura et al., 1995). The exact role of Hsp90 in the maturation of kinases and SHRs is not entirely understood, yet differences in the maturation process may be reflected in the distinct co-chaperone network organization. Kinase maturation involves a state, in which the N- and C-lobes of the kinase are ripped apart and threaded through the Hsp90 dimer orifice (Figure 33 A) (Verba et al., 2016). By contrast, binding of GR-LBD was mapped to the outside of the dimerized Hsp90 interface (Figure 33 B) (Lorenz et al., 2014). While nucleotide exchange has been proposed as the main reason for Hsp90 involvement for kinase maturation, Hsp90 seems to prevent the unfolding of a loop that locks the hormone in place in GR (Eckl et al., 2013; Suren et al., 2018). In conclusion, the conformational processing of kinases and SHRs by Hsp90 is quite different, consistent with the different co-chaperone requirements and co-chaperone organization shown in this study.

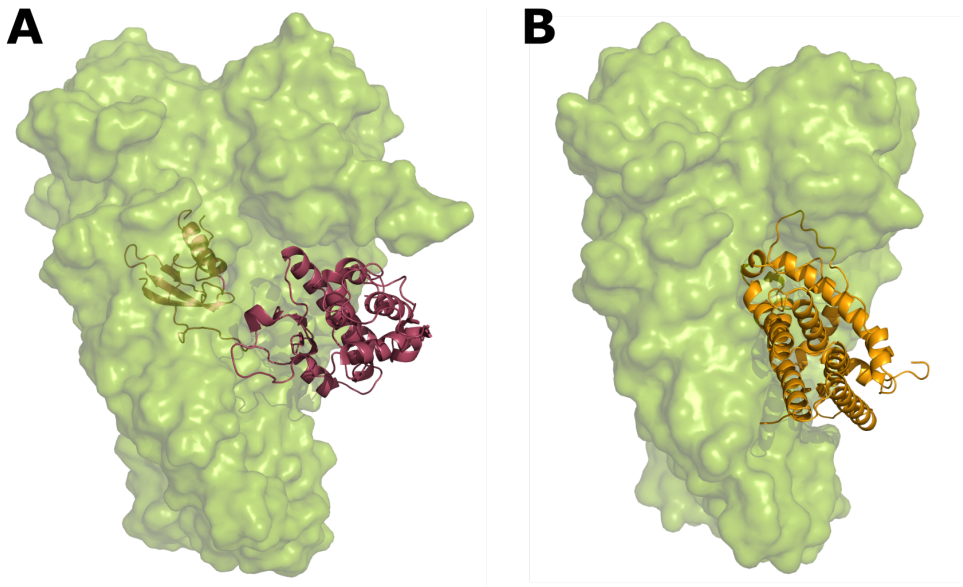

FIGURE 33 | **Cdk4 and GR-LBD Bind Hsp90 in Different Ways.**
The **(A)** cryo-EM structure of Cdk4 bound to Hsp90β (PDB: 5FWL) and the model of **(B)** GR-LBD docked onto yeast Hsp90 (Lorenz et al., 2014) are shown.

Epistatic Modules Affecting v-Src Maturation

Most co-chaperones had a weak effect on v-Src maturation, and only a few affected v-Src activity profoundly, suggesting that the majority of co-chaperones fine-tune the function of centrally acting factors. Additionally, most co-chaperones formed positive genetic interactions, suggesting that co-chaperones are not working independently. A surprisingly central role of Sti1 for v-Src activity became evident (Figure 34). Additionally, Sti1 formed a negative genetic interaction with the classical kinase co-chaperone Cdc37. We found evidence of overlapping functions between Sti1 and Cdc37, since one could partially rescue the loss of the other. Sti1 is pivotal for the transfer of clients from Hsp70 to Hsp90 by physically linking both chaperone systems (Chen and Smith, 1998; Johnson et al., 1998; Schmid et al., 2012; Röhl et al., 2015a). By contrast, Cdc37 has been proposed as a kinase-specific recruiter of kinases (Kimura et al., 1997; Grammatikakis et al., 1999; Citri et al., 2006; Keramisanou et al., 2016). The results of this thesis indicate that Sti1 can functionally replace Cdc37 at least for some kinases. Notably, in this context, the function of Sti1 seems to rely on the ability to associate with Hsp70 and not on the modulation of Hsp90. Since findings for GR, luciferase and p53 indicate that these clients are inactive when bound to Hsp70 (Kirschke et al., 2014; Morán Luengo et al., 2018; Boysen et al., 2019; Dahiya et al., 2019), we propose that release of kinases from Hsp70 is a decisive step during kinase maturation. The unfolding effect of Hsp70 on clients (Kirschke et al., 2014; Boysen et al., 2019; Dahiya et al., 2019) and the mild unfolding pressue exerted by Cdc37 on kinases (Keramisanou et al., 2016) support partially overlapping effects of Cdc37 and Sti1:Hsp70. Importantly, these functions of Cdc37 and Sti1:Hsp70 seem to be conserved in evolution, since they were observed in yeast, mammalian and mixed systems (Kirschke et al., 2014; Keramisanou et al., 2016; Morán Luengo et al., 2018; Boysen et al., 2019; Dahiya et al., 2019). Nevertheless, distinct functions of Sti1 and Cdc37 are evident, since Cdc37, but not Sti1 is essential in yeast. Additionally, both co-chaperones could only partially rescue the loss of the other. Sti1 and Cdc37 are distinct in their abundance, structure and their interaction with Hsp90. While Sti1 exclusively binds the open Hsp90 conformation and is a strong non-competitive inhibitor of ATPase, Cdc37 was found bound to closed Hsp90 and only partially inhibits ATPase (Prodromou et al., 1999; Siligardi et al., 2002; Richter et al., 2003; Verba et al., 2016). Furthermore, Cdc37 binds the NTD and MD of Hsp90 (Eckl et al., 2015; Verba et al., 2016), whereas Sti1 is primarily bound by the C-terminal MEEVD motif forming additional contacts in the CTD and MD (Roe et al., 2004; Schmid et al., 2012; Verba et al., 2016).

Together, the data are consistent with a model, in which two partially parallel pathways for the recruitment of kinases to Hsp90 exist (Figure 35): In the canonical Cdc37-directed pathway, Cdc37 binds a client, stabilizes its partially unfolded structure and promotes recruitment to Hsp90. The presented results additionally propose a pathway in which kinases are bound by Hsp70, also stabilizing a partially unfolded conformation. Recruitment to Hsp90 then requires the bridging function

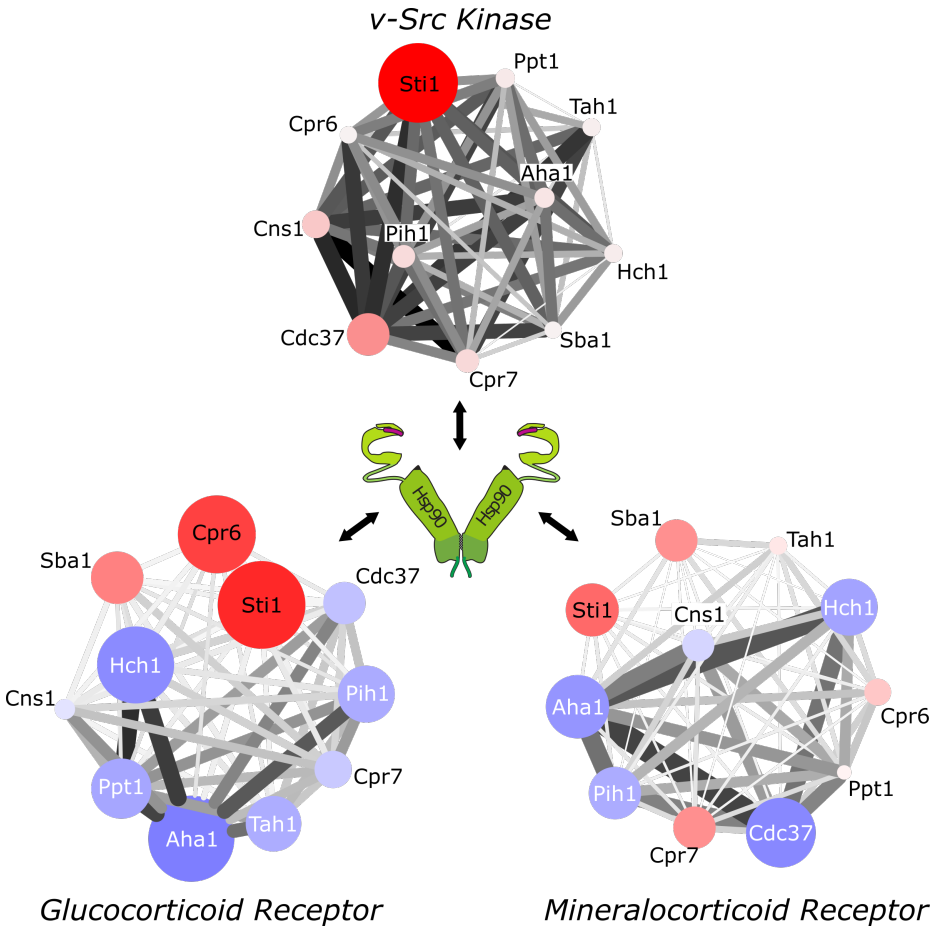

FIGURE 34 | **Co-Chaperones Form Plastic Genetic Networks Adapted to Client Activation.**
Schematic representation of client-specific co-chaperone networks. The deactivating (red) or activating (blue) effects of co-chaperones on client activity were visualized using Cytoscape 3.6.1. The amplitude of the effect is visualized by circle size and color saturation. Genetic interactions between co-chaperones are shown as edges and the strength of the genetic interaction is represented by saturation and edge thickness. Note that for simplicity, positive and negative genetic interactions are not distinguished.

of Sti1. In both pathways, Cdc37 may additionally bind these Hsp90:kinase complex and promote folding, consistent with the published ternary complex between Hsp90, Cdk4 and Cdc37 (Verba et al., 2016). The existence of parallel pathways may be beneficial to increase the spectrum of kinase conformations that can be bound and funneled to the Hsp90 machinery.

Besides the strong negative genetic interaction between Sti1 and Cdc37, a positive genetic interaction between Sti1 and Sba1 was found. This finding matches the antagonistic behavior of Sti1 and Sba1 on Hsp90 conformation and is compatible with a deterministic model, in which a Sti1:Hsp90:kinase complex is formed first which transitions to a Sba1:Hsp90:kinase complex later in the cycle (Li et al., 2011).

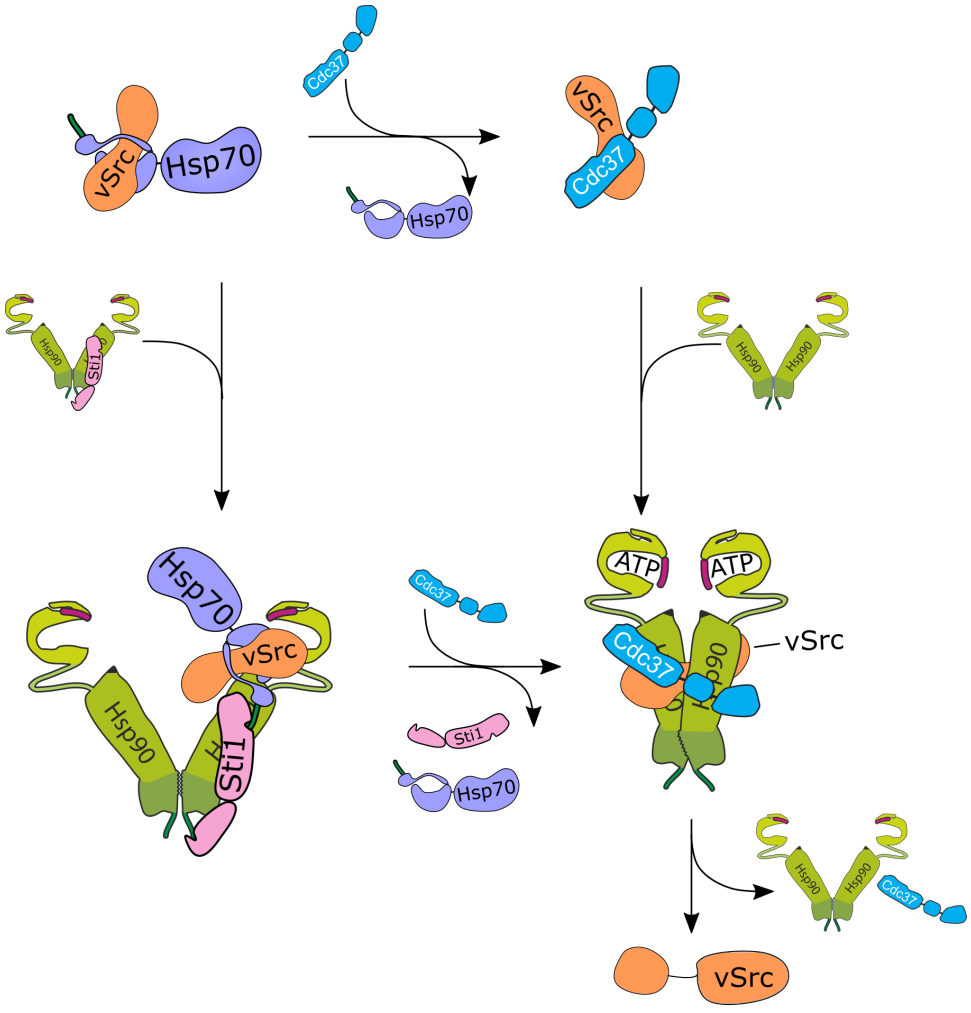

FIGURE 35 | **Sti1 and Cdc37 Have Overlapping Functions for Kinase Mautration.** Schematic model showing two partially overlapping pathways for kinase recruitment to Hsp90. Kinase may be bound and stabilized by Cdc37 and then recruited to Hsp90. In an alternative pathway, a partially unfolded kinase conformation is stabilized by Hsp70. Client transfer from Hsp70 to Hsp90 requires the function of Sti1. In both pathways the Hsp90:kinase complex may contain Cdc37.

Epistatic Modules Affecting SHR Maturation

Sti1 also played a pivotal role in the maturation of the GR and MR (Figure 34). Interestingly, while Sti1 was part of the highest scoring genetic interactors for GR, it formed less prevalent genetic interactions for MR maturation. This highlights a different co-operation between co-chaperones even for co-chaperones that have strong effects on the activity of both receptors. Loss of Aha1 and Hch1 led to activation in both SHRs and the *aha1*Δ mutation was enriched in double mutants forming the highest positive genetic interactions for GR and MR, suggesting a central role of Aha1. Strikingly, the *aha1*Δ*/hch1*Δ double mutant showed a suppressing genetic interaction phenotype (loss of a second co-chaperone reduces the effect of the deletion of the first co-chaperone). Our analysis revealed that Aha1 and Hch1 compete with GR binding to Hsp90 and thus function as dwell time regulators. Hence, overexpression of Aha1 and Hch1 *in vivo* reduced the activity of GR and v-Src, whereas knockout of Aha1 or Hch1 increased GR stability *in vivo*. This is in line with the overlapping binding site of Aha1 and the proposed client binding site (Bohen and Yamamoto, 1993; Nathan and Lindquist, 1995; Meyer et al., 2004; Genest et al., 2013; Lorenz et al., 2014; Verba et al., 2016). Notably, Hch1 has been lost during evolution and it has been posited that Yes kinase-mediated phosphorylation of Tyr627 in human Hsp90 phenocopies Hch1, proposing a dynamic regulatory mechanism (Zuehlke et al., 2017). Depletion of Aha1 has been found to stabilize the mutant Δ508 cystic fibrosis transmembrane conductance regulator (CFTR) protein associated with cystic fibrosis and it was hypothesized that reduction of Aha1 levels increased time on Hsp90 to allow the Δ508 CFTR to bypass a kinetic block in folding (Qu et al., 1997; Wang et al., 2006). Another study found that release of the androgen receptor (AR) by phosphorylation of Hsp90 increased nuclear translocation and activity (Dagar et al., 2019). On the other hand, hyperacetylation of Hsp90 by treatment with histone deacetylase inhibitors led to the dissociation of AR and subsequent degradation, thus reducing AR activity (Gibbs et al., 2009). Hence, it seems that the dwell time of clients on Hsp90 has to be tightly regulated to ensure that clients are only released when they have reached a specific point in the folding pathway.

4.1.6.3 Conclusion

Investigation of the epistatic network formed by Hsp90 co-chaperones revealed a robust system that is resistant against loss of components under physiological and heat stress conditions. Analysis of genetic interactions underlying client maturation uncovered client-specific reorganization of the co-chaperone network. Genetic networks include central strongly regulating components, but the majority of co-chaperones adds a subordinate layer of modulation. In this context, we found Sti1-Cns1-Cpr7 as a tripartite module regulating eEF2 solubility, Sti1-Cdc37 as a module for v-Src maturation and Aha1-Hch1 as dwell time regulators of SHRs. Hence,

the picture emerging from this study is that of highly dynamic and adaptable co-chaperome that rewires for client-specific requirements with central epistatic modules composed of few co-chaperones embedded in a looser network for fine-tuning by the remaining co-chaperones. This work introduces a concept of co-chaperones that do not function in static relationships for client maturation but form different dependencies that are specifically adapted to each client. Due to the general mechanistic conservation of Hsp90 and its regulation by co-chaperones it is reasonable to assume that in higher eukaryotes the co-chaperome is similarly coordinated. Yet, differences between the co-chaperomes and Hsp90 itself make further research essential to proof similarities and unveil distinctions between the yeast and human system.

4.2 Screening For Novel Hsp90 Co-Factors in Mammalian Cells

The Hsp90 co-chaperome expanded during evolution from bacteria to man, in which more than 25 co-chaperones are known. The role of co-chaperones in the maturation of different clients is ill understood and mostly limited to anecdotal knowledge of a subset of co-chaperones. New co-chaperones are still discovered, suggesting that only a part of the Hsp90 modulators is known so far. Additionally, several co-chaperones have merely been categorized as Hsp90 co-chaperone candidates based on high-throughput studies and not been validated in depth. In this thesis we sought to establish a screening system to reliably identify regulators that affect Hsp90-mediated maturation and to investigate the function of known modulators in mammalian cells. The project has been conducted in collaboration with the laboratory of Prof. Dr. Martin Kampmann at the Institute of Neurodegenerative Diseases (IND) at the University of California, San Francisco (UCSF). The cooperation included two research visits at the IND for three months and one month, respectively.

4.2.1 CRISPR Interference-Based Functional Genomics

4.2.1.1 CRISPR Interference Technology

Genetic screens are a powerful tool for uncovering the components of biological processes and assigning their function. Screening setups have been developed in yeast, which are made possible by the easily accessible genetic manipulations in yeast. Screening in mammalian cells has long been limited to RNA interference technology, which tends to produce unspecific off-target effects (Kampmann et al., 2013; Kampmann et al., 2015; Kampmann, 2018). Development of CRISPR enabled the specific manipulation of genomic loci by inducing double strand breaks, but often induced a toxic DNA damage response (Mojica et al., 2000; Jinek et al., 2012; Cong et al., 2013; Jinek et al., 2013; Mali et al., 2013; Wang et al., 2016). To overcome the problem of unspecific off-targeting of RNA interference and the toxicity of CRISPR nuclease (CRISPRn), a screening approach based on CRISPRi has been pioneered in the Weissman lab (Figure 36) (Gilbert et al., 2013; Qi et al., 2013a). CRISPRi relies on the transcriptional repression by a nuclease-dead Cas9 (dCas9) molecule fused to the transcriptional repressor Krüppel-Associated Box (KRAB) (Gilbert et al., 2013). dCas9 is directed to the promoter region by specific sgRNAs and inhibits transcription both by physically blocking the RNA polymerase and by transcriptional repression via the KRAB module. Knockdown efficiency usually ranges between 90%-99%, making CRISRPi a highly efficient and specific method for downregulating protein expression (Gilbert et al., 2014).

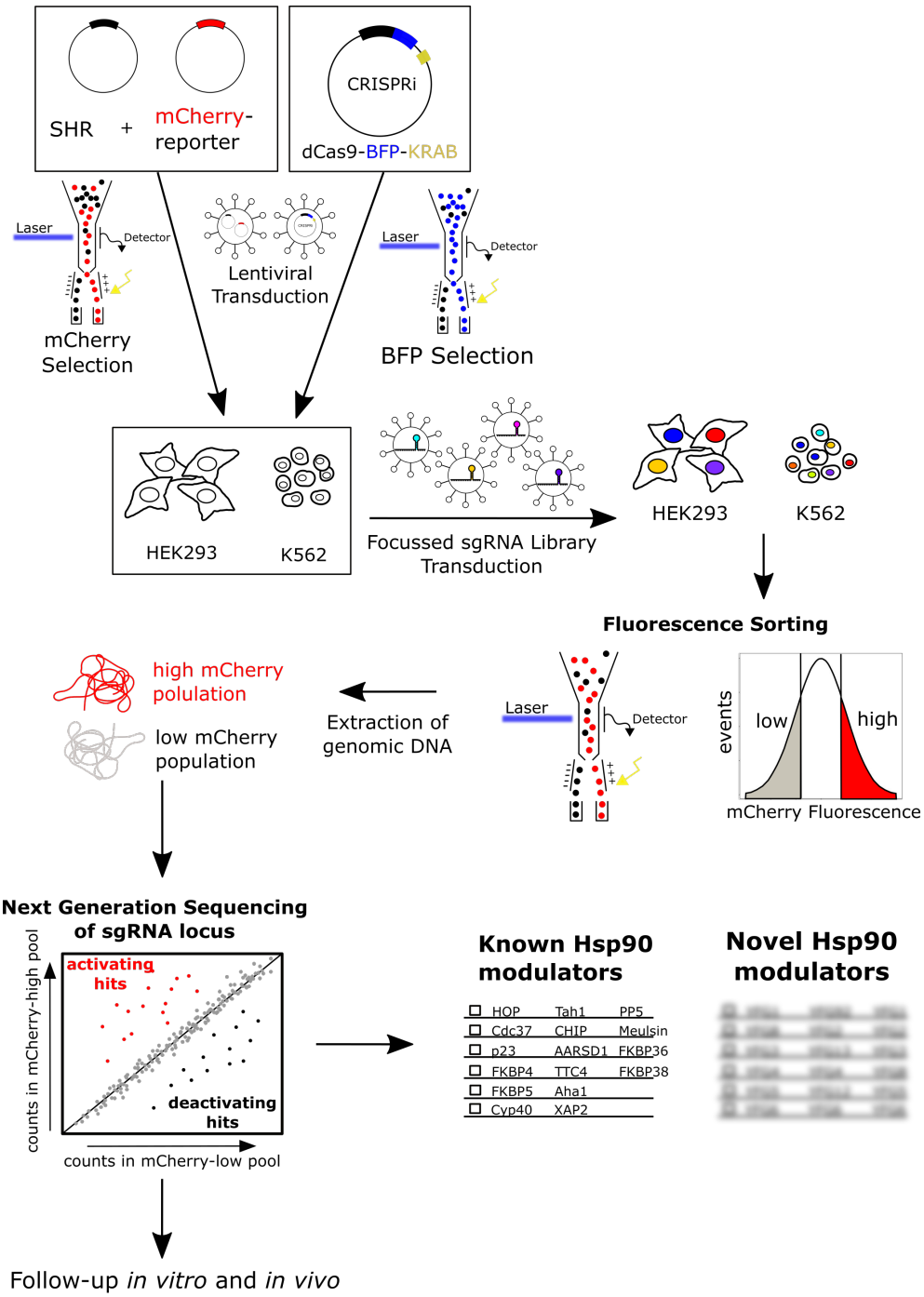

FIGURE 36 | **CRISPRi Screening Workflow to Identify Hsp90 Modulators.**
A SHR-expressing cassette and a SHR reporter construct driving mCherry expression was lentivirally transduced in cell lines expressing the dCas9-BFP-KRAB fusion protein. The resulting screening cell lines were infected with lentivirus encoding the pool of sgRNAs present in the screening library in a ratio to ensure the infection of the screening cell line with a single sgRNA per cell. The knockdown was allowed to establish itself for 8-10 days. After hormone treatment for 24 h, populations with high and low reporter activity were selected by FACS. Genomic DNA was extracted, the sgRNA-encoding loci were amplified by PCR and subjected to next-generation sequencing. A Python-based analysis pipeline developed by the Kampmann laboratory (UCSF) was used to extract hits.

4.2.1.2 Using CRISPRi for Functional Genomics

In this work, a functional genomics screening setup using CRISPRi was developed to identify new modulators of the Hsp90 network and to analyze known modulators. For this purpose, the effects of gene knockdowns on the activity of SHRs were used as an indicator of Hsp90 function. An overview of the screening workflow is shown in Figure 36. Hek293 cells and K562 cell lines constitutively expressing the fusion protein dCas9-BFP-KRAB were infected with lentivirus carrying an SHR-expressing cassette and a reporter plasmid driving mCherry expression in a SHR-dependent manner. A focused sgRNA library was constructed, comprising sgRNAs targeting 357 genes involved in protein homeostasis together with non-targeted control sgRNAs. The library was lentivirally transduced in a ratio that ensured that only a single sgRNA-expressing plasmid was transduced and was selected to achieve a rate of at least 80% positive cells. Taking into account the half-life of the proteins, the knockdown was allowed to establish itself for 8-10 days prior to screening. After treatment with hormone, the populations with 30% of the highest and 30% of the lowest mCherry activities were separated by FACS. In the mCherry^{low} population, the enrichment of cells carrying sgRNAs targeting genes important for SHR activity is expected, while the mCherry^{high} fraction is enriched in cells carrying sgRNAs targeting genes that suppress SHR activity. Genomic DNA was extracted in each population and the sgRNA-encoding loci were amplified by PCR. Next-generation sequencing was then performed to count the occurrance of sgRNAs in both populations. A Python-based analysis pipeline developed by the Kampmann lab was used to extract a statistically significant accumulation or decrease of sgRNAs in the populations. This was achieved by a Mann-Whitney U-test of the targeted sgRNAs and the non-targeted sgRNA controls.

4.2.2 Development of a CRISPRi Screening Setup

Successful screening for Hsp90 modulators that affect client maturation is dependent on three factors: (1) A readout system that connects Hsp90 function with reporter activity and lacks background activation is required. (2) A screening library with a homogeneous distribution of sgRNA-encoding plasmids is required to prevent bias for certain sgRNAs. Additionally, to increase the chance of identifying Hsp90 regulators, a screening library which is enriched in protein homeostasis factors is desirable. (3) A stable and homogeneous cell population, in which the screen is performed is advantageous to reduce noise.

4.2.2.1 Generation of a Steroid Hormone Receptor Reporter System

Pooled functional genomics screens are based on using FACS to separate populations with increased and decreased reporter activity (Figure 36). Hence, we first sought to generate a fluorescence-based reporter system for SHR activity. To that end, the lentiviral pXG207 plasmid (Kampmann Lab, UCSF) carrying mCherry as a

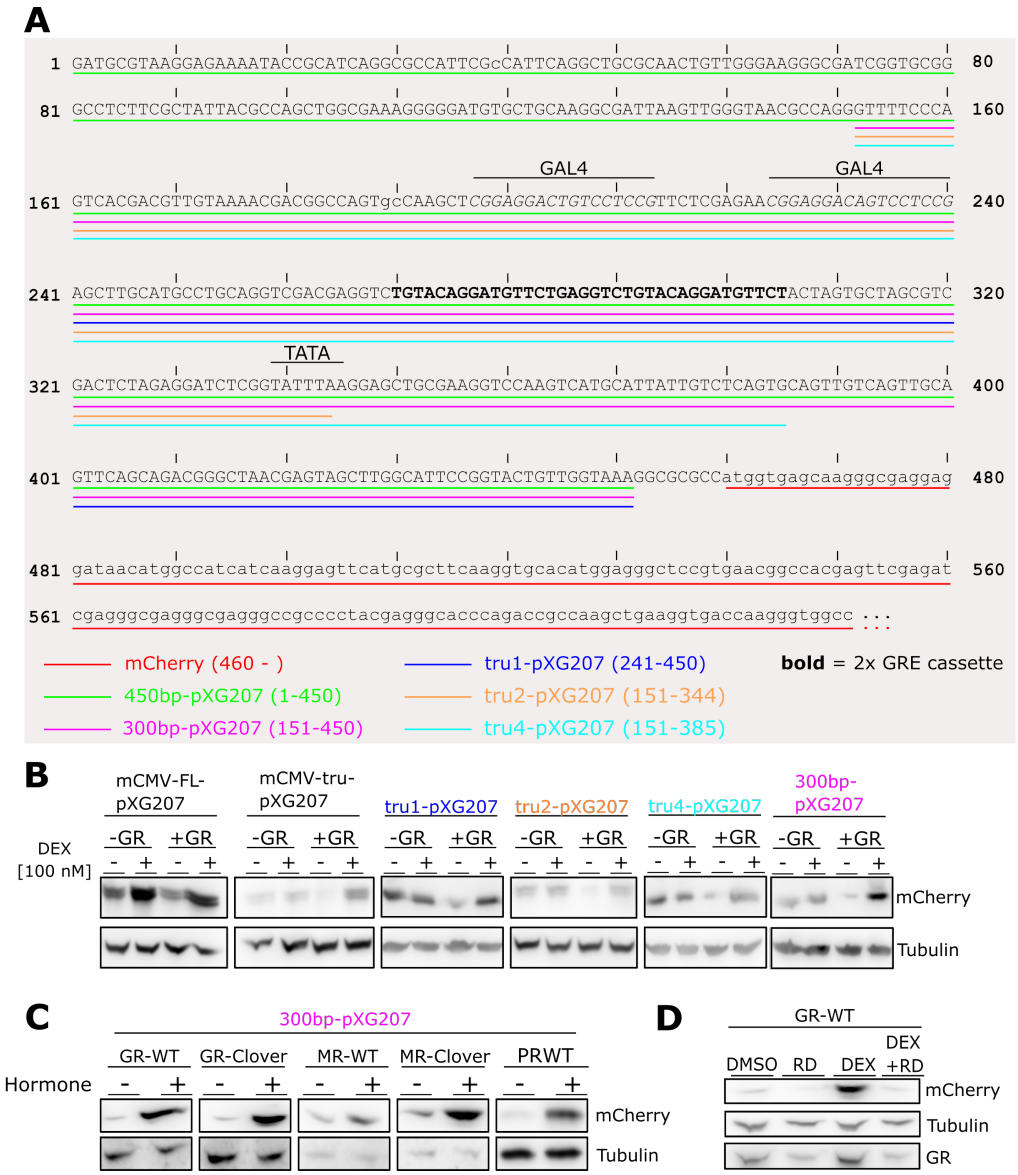

FIGURE 37 | **Generation of a SHR Reporter System for Mammalian Cells.**
A Annotated promoter region of reporter constructs. The shown segments of the pDLO-2xGAL4-2xGRE plasmid were cloned into the pXG207 reporter plasmid between the EcoRI and AscI restriction sites.
B Reporter expression upon GR activation. HeLa cells were transiently co-transfected with 250 ng of the pMK1253 plasmid encoding GR and 500 ng of the indicated reporter constructs in the pXG207 backbone. GR was induced by addition of 100 nM dexamethasone (DEX) 48 h after transfection and mCherry levels were quantified by Western Blot 24 h after induction.
C Reporter activation by different SHRs. HeLa cells were transiently transfected with 350 ng of the pMK1253 plasmid encoding the indicated SHR constructs and 500 ng of the 300bp-pXG207 reporter construct. After 48 h, receptors were induced with 100 nM dexamethasone, 10 nM aldosterone or 100 nM progesterone for GR, MR and PR, respectively. mCherry levels were quantified 24 h after induction.
D Hsp90 dependence of reporter expression. 500 ng of the pMK1253 plasmid encoding GR and 500 ng of the 300bp-pXG207 reporter were co-transfected using a reverse transfection protocol. Cells were treated with 50 µg mL^{-1} of radicicol (RD) or DMSO 15 h after transfection. To induce GR, 100 nM dexamethasone were added 8 h after radicicol treatment. mCherry levels were quantified 24 h after induction using Western Blot.

reporter was used as a framework to test a variety of different promoter constructs cloned upstream of the mCherry coding sequence (Figure 37A). To ensure low background activity, minimal promoters lacking upstream activating sequences (UAS) were used. First, different promoters were tested in the presence or absence of dexamethasone in HeLa cells either expressing only endogenous GR or constitutively expressing GR from the strong EF1a promoter (Figure 37A,B). A setup containing the minimal human cytomegalovirus immediate early promoter (mCMV) fused to three repeats of the glucocorticoid response element (GRE) derived from the pUCΔSS-26X plasmid (Sahasrabudhe et al., 2017) yielded strong activation, but suffered from background transcription in the absence of hormone (Figure 37B). Deletion of the CAAT box (mCMV-tru-pXG207) reduced the background but led to considerably reduced activation upon hormone addition (Figure 37B). We then switched to a system based on the *D. melanogaster* minimal ADH (mADH) promoter derived from the pDLO-2xGAL4-2xGRE plasmid (kind gift from Brian Freeman, University of Illinois) (Figure 37A). Different constructs containing the mADH segment together with only the GREs (tru1-pXG207), or the GAL4 and GRE elements with different lengths of spacers between the TATA box and the translated region were tested (Figure 37A,B). The best signal to noise ratio after was observed in a construct encompassing a 300 bp fragment (300bp-pXG207) from the pDLO-2xGAL4-2xGRE harboring all upstream activating sequences (Figure 37A,B). Of note, transfer of a 450 bp segment into the pXG207 vector (450bp-pXG207) did not further increase hormone responsiveness or affect background activation (data not shown). To test whether the screening for the activation of the MR and progesterone receptor (PR) was also feasible with the 300bp-pXG207 reporter system, mCherry expression was tested in HeLa cells expressing the GR, MR or PR either as the wild-type protein or fused to the Clover2 tag (Figure 37C). Importantly, the GREs present in the 300bp-pXG207 reporter were also sufficient to strongly upregulate MR and PR activity. This is in line with observations from SHR screening in yeast, in which the GRE-based reporter was used to quantify GR, MR, PR and AR activity (this study, Sahasrabudhe et al., 2017). Since mCherry expression was intended as a readout for Hsp90 activity, the response of the mCherry expression to Hsp90 inhibition was tested (Figure 37D). Importantly, treatment with radicicol decreased reporter expression to background levels. Concomitantly, GR levels were decreased upon radicicol treatment. In summary, the results show that a reporter construct containing GREs upstream of the minimal ADH promoter allows strong reporter upregulation upon activation of different SHRs. Additionally, reporter expression induced by SHR activation was found to be suitable to read out Hsp90 activity.

4.2.2.2 Construction of Screening Library

Screening for novel factors can be performed in an unbiased manner using the entire genome or in a focused screen by using a biased library enriched in factors that are involved in the biological process of interest. While unbiased screening has the

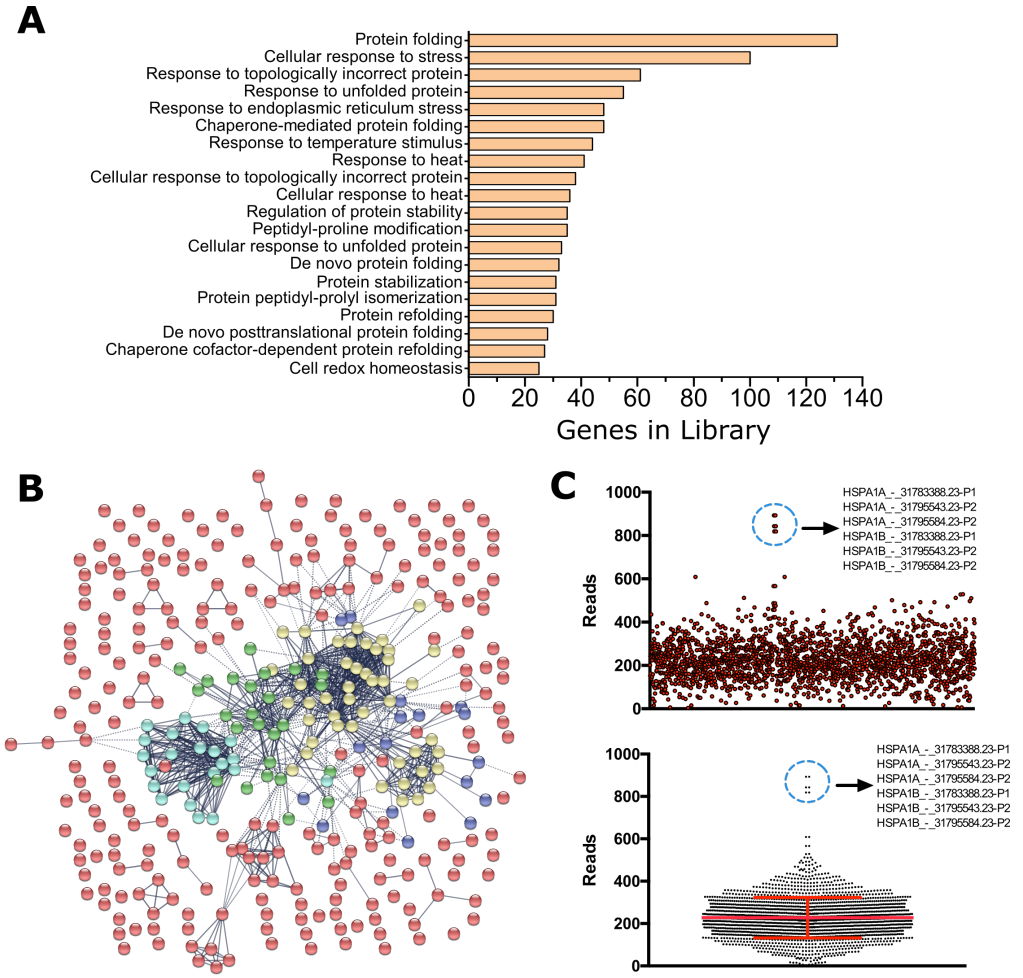

FIGURE 38 | **Generation of a Screening Library.**
A GO term enrichment of library elements. The highest ranking GO annotations of the library elements were determined using the ShinyGo tool. The number of genes in the library annotated for each GO term is depicted.
B Interactome map of screening library elements. The STRING-DB (v.11.0) tool was used to map interactions (from experiments and databases) with a high confidence (0.700) and extract clusters using k-means clustering with 5 clusters (green: Hsp90-associated; yellow: Hsp70-associated; cyan: TRiC/CCT & prefoldin; blue: ER maintenance; red: unassociated).
C Homogeneity of the screening library. Deep sequencing was used to determine how homogeneous the sgRNAs were distributed in the library. Note that the indicated HSPA1A and HSPA1B targeting sgRNAs are identical and thus produce twice the number of reads. The 95% intervals are shown (right).

potential to identify uncharacterized genes, important drawbacks are the increased technical effort and the high background of functionally unrelated pathways and consequently the risk of missing hits that induce smaller effects, but are mechanistically relevant. To identify Hsp90 modulators with a high probability, a sgRNA library targeting 357 genes involved in proteostasis was used for screening (Figure 38A). The library was cloned as a sub-library from a previously published screening library (Horlbeck et al., 2016) and contained 5 sgRNAs for each gene targeting either the (+)-strand or (-)-strand as well as a total of 250 non-targeting sgRNAs. Gene ontology (GO) term enrichment showed that most genes of the library were associated with protein folding, stabilization and the cellular stress response (Figure 38A). These included proteins associated with the TRiC/CCT (mammalian Hsp60) complex and prefoldin system, the ER proteostasis system, Hsp90-associated factors, Hsp70-associated factors as well as a plethora of factors for which no association has been published (Figure 38B).

To prevent bias during screening due to the heterogeneous distribution of sgRNAs that might occur in the cloning process, the library was tested for homogeneity by next-generation sequencing (Figure 38C). Next-generation sequencing revealed a tight distribution of sgRNAs in the library, confirming that the library was suitable for screening. Notably three sgRNAs targeting HSPA1A (Hsp70-1a) and HSPA1B (Hsp70-1b) had the same sequence due to the high homology between the targeted genes. Hence, the genes occurred with approximately twice the read count as anticipated. In summary, a compact sgRNA library biased for proteostasis factors was generated that showed a homogeneous distribution of sgRNAs suitable for screening.

4.2.2.3 Generation and Characterization of Stable Screening Cell Lines

Besides a potent reporter system with little background expression and a suitable screening library, the homogeneity of the cell population in which the screen is performed is a determining factor affecting noise in the screen. To this end, stable cell lines were generated by lentiviral transduction. Cells constitutively expressing the dCas9-BFP-KRAB construct (Gilbert et al., 2013; Gilbert et al., 2014) were infected with lentivirus carrying the 300bp-pXG207 reporter and the pMK1253 backbone encoding the SHR. SHRs were either encoded as wild-type or with a C-terminal Clover tag (denoted as SHR-WT and SHR-Cl throughout this thesis). For selection, cells were treated with hormone and positives were selected by FACS: We gated on BFP^+ cells for SHR-WT expressing cells and on the BFP^+ $FITC^+$ population for cell lines expressing Clover2-tagged SHRs (Figure 39A). From this population, the cells with the highest mCherry expression were selected. Unfortunately, the resulting polyclonal populations, especially the Hek293 cell lines, did not support reporter activation and lost a reporter response within about two weeks (data not shown). This was likely caused by silencing of the reporter locus, since SHR expression was not

affected (data not shown). To obtain a potentially more stable population, monoclonals displaying a strong activation of the reporter after hormone treatment were selected and expanded (Figure 39B). In Hek293 cell lines expressing the GR-WT and PR-WT, reporter activation by addition of hormone was more than 250-fold and 150-fold, respectively, and about 15-fold for GR-Clover (Figure 39B). mCherry expression in the selected monoclonal GR-WT expressing K562 cell line was increased by about 30-fold by hormone addition (Figure 39B). Notably, K562 and Hek293 cell lines expressing the MR-WT displayed only weak activation by aldosterone and a large fraction of the population remained inactivated (Figure 39B). The inducible behavior of cell lines expressing GR and PR remained comparable over the course of several passages. The reporter activation in MR expressing monoclonals tended to decrease, hinting towards silencing of the reporter locus as one of the reasons for the observed weak induction.

To detect subtle effects of Hsp90 modulators in the screen, we reasoned that SHR activation by hormone should be close to saturation, but not entirely saturated to increase the sensitivity and dynamic range. Additionally, excess hormone treatment may be toxic for cells. For that purpose either the duration of hormone treatment or the hormone concentration could be controlled. First, the kinetics of reporter activation upon treatment was tested by supplementing cells with hormone for different durations and quantifying the activated fraction (Figure 39C). Reporter activation kinetics were surprisingly slow and started to reach saturation after more than 17 h. Since it is technically challenging to exactly control the duration of hormone treatment for screening, next the dose-response of all monoclonal cell lines used for screening was tested (Figure 39D). The EC_{50} value for K562-GRWT and K562-MRWT were approximately 0.3 nM and for Hek293-GRClover, Hek293-GRWT and Hek293-PRWT the EC_{50} value was about 0.5 nM, 0.5 nM and 0.8 nM, respectively. Of note, the EC_{50} value for Hek293-MRWT was found to be around 0.01 nM, yet the strong background activation and unusual dose-response curve may affect the accuracy of this result. In the other cell lines, saturation was reached with hormone concentrations between 1 nM and 10 nM. Together, these results showed that except for MR expressing constructs, reporter expression in monoclonal cell lines was inducible to high expression levels by treatment with 1-10 nM hormone for longer than 20 h.

4.2.3 Screening for Modulators of Steroid Hormone Receptor Activity

Screening for Hsp90 modulators was performed in all selected monoclonal K562 (K562-GRWT, K562-MRWT) and Hek293 (Hek293-GRWT, Hek293-GRCl, Hek293-MRWT, Hek293-PRWT) cell lines. To this end, the cell lines were infected with lentiviruses harboring the proteostasis factor-biased library and selected until at least 80% of the population were BFP+. Knockdown was allowed to establish for 8-10 days and cells were then treated with hormone for 24 h before FACS was done to separate populations with high or low mCherry levels (Figure 36).

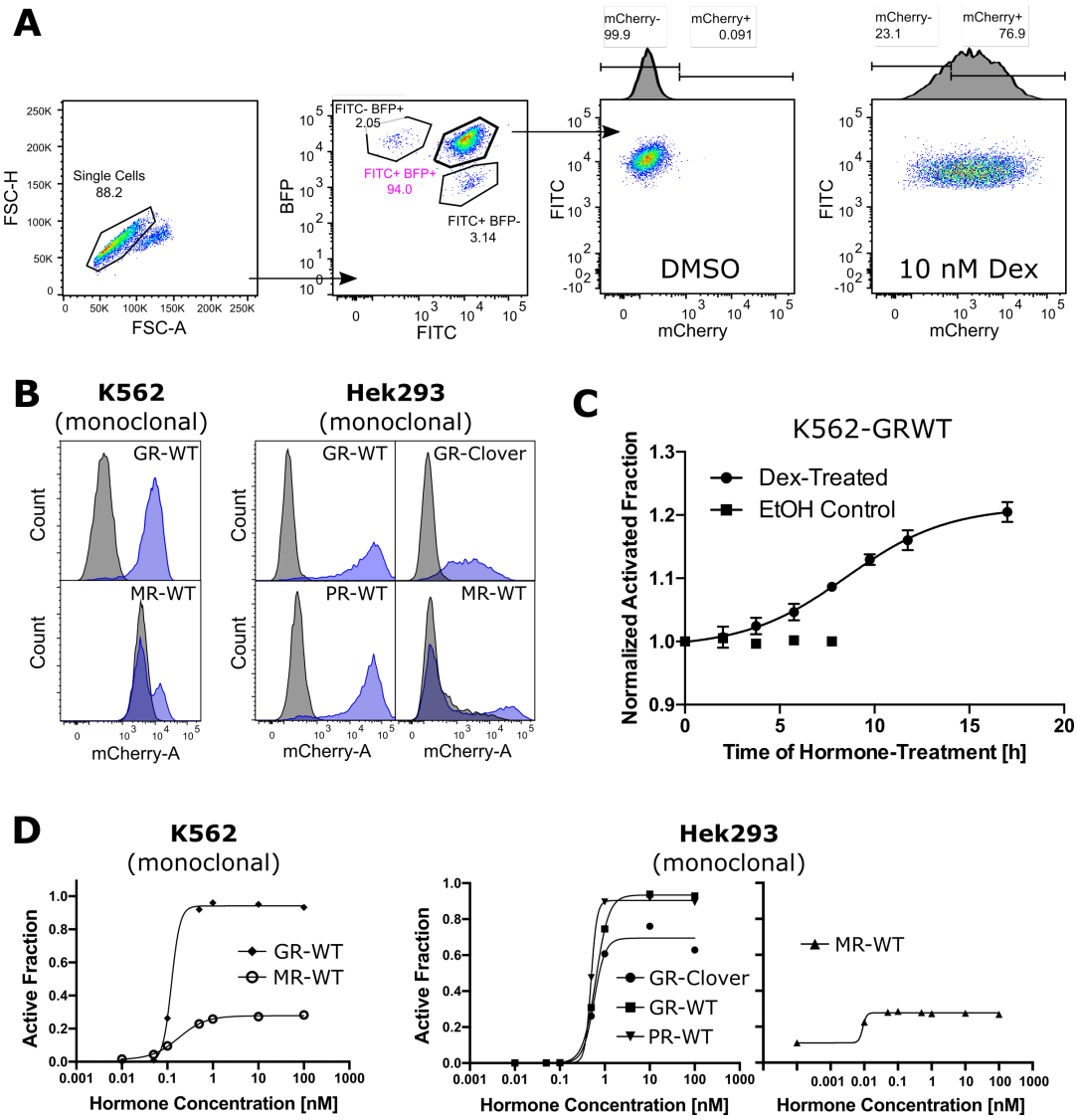

FIGURE 39 | **Selection and Characterization of Screening Cell Lines.**
A Gating strategy to select positive cell lines. The representative gating strategy to select cells containing the dCas9-BFP-KRAB cassette, the GR-Clover-expressing plasmid and the 300bp-pXG207 reporter construct is shown. [FSC: Forward Scatter; FITC: Fluorescein-isothiocyanate; BFP: Blue fluorescent protein; Dex: Dexamethasone]
B Response of monoclonal reporter cell lines to hormone treatment. Stably transfected, monoclonal K562 and Hek293 cell lines expressing the dCas9-BFP-KRAB fusion protein, the respective SHR and carrying the reporter construct were treated with hormone (blue) or ethanol as control (grey) for 24 h. The mCherry fluorescence was measured by flow cytometry. GR, MR and PR were treated with 10 nM dexamethasone, 100 nM (Hek293) or 10 nM (K562) aldosterone, or 10 nM progesterone, respectively.
C Time-dependence of the mCherry response. A polyclonal K562 cell line carrying the GR expressing plasmid together with the CRISPRi machinery and the reporter plasmid was treated with 10 nM dexamethasone for the indicated time points and the mCherry$^+$ fraction was determined by flow cytometry. The data represent the means $\pm$ SD of biological triplicates.
D Dose-response of screening cell lines. The cell lines from (**B**) were treated with the indicated concentrations of hormone (dexamethasone, aldosterone and progesterone for GR, MR and PR, respectively) for 24 h and the mCherry$^+$ fraction was determined by flow cytometry. Data represent the means $\pm$ SD of biological triplicates.

4.2.3.1 Validation of the CRISPRi Screening Setup

To test how reproducible screening in the monoclonal cell lines was, four cell lines (Hek293-GRWT, Hek293-PRWT, Hek293-GRCl, K562-GRWT) were independently infected and screened in duplicates (Figure 40). The hit strength defined as the product of the $-log_{10}(P) \times \epsilon$ was calculated: Log_2-fold differences of the sgRNA counts between the high and low mCherry populations were determined and P was derived from significance testing using the Mann-Whitney U-test of the targeting sgRNAs against all non-targeting sgRNAs; ϵ describes the phenotype defined as the log_2 difference of the sgRNA counts between the mCherry^{high} and mCherry^{low} population (Section 3.2.8.6). Hence, negative ϵ values indicate reduced activity upon knockdown of the target gene, while positive values suggest that the query gene knockdown leads to increased SHR activity.

The hit strength between replicates was correlated with a Pearson R score between 0.5 and 0.57 for replicate measurements of the Hek293-GRWT, Hek293-PRWT and K562-GRWT cell lines and 0.4 for replicates of the Hek293-GRClover cell line (Figure 40A). Importantly, non-targeting controls showed no correlation, confirming the specificity of the CRISPRi screening setup (Figure 40B). The counts of replicate measurements were then combined and significant hits were extracted using the MAGeCK-iNC analysis pipeline (Tian et al., 2019) allowing a false discovery rate of 0.05 (Figure 40C,D). With approximately 50 hits, the highest number of significant hits were obtained for GR-WT in the Hek293 and K562 cell lines, suggesting that approximately 15% of the genes targeted by the screening library affected regulated GR activity (Figure 40D). In Hek293 cells expressing MR-WT and PR-WT about 30 to 35 significant hits were identified, while GR-Clover expressing Hek293 cells and MR-WT expressing K562 cells yielded about 25 hits. Notably, except for the K562-MRWT setup, the majority of hits were positive SHR regulators, entailing reduced SHR activity when knocked down. Hence, most regulatory mechanisms seem to have evolved to increase SHR activity rather than limit activity.

To understand how much different parts of the cellular proteostasis system affect SHR activity, hits were categorized into 5 categories: (1) Genes linked to the Hsp90 system, (2) the Hsp40/70 system, (3) the TRiC/CCT system, (4) general cytosolic quality control pathways and (5) genes involved in DNA replication, gene transcription and translation (Figure 40D). The knockdown of genes involved in replication, transcription and protein translation caused significant effects on reporter activity in all cell lines, but were generally considered to not directly affect SHR maturation. Additionally, several members of this category have been shown to be essential for viability and thus may be found as false-positive hits in genetic screens (Hart et al., 2014). Other essential genes include parts of the TRiC/CCT system and the proteasome (Hart et al., 2014). Interestingly, the TRiC/CCT system played a less prevalent role in Hek293 cells with 0% to 8% of the hits found in that category than in K562 cells in which about 15% of the hit genes belonged to the TRiC/CCT system. Since SHRs are not known to interact with chaperonins this suggests that the hits

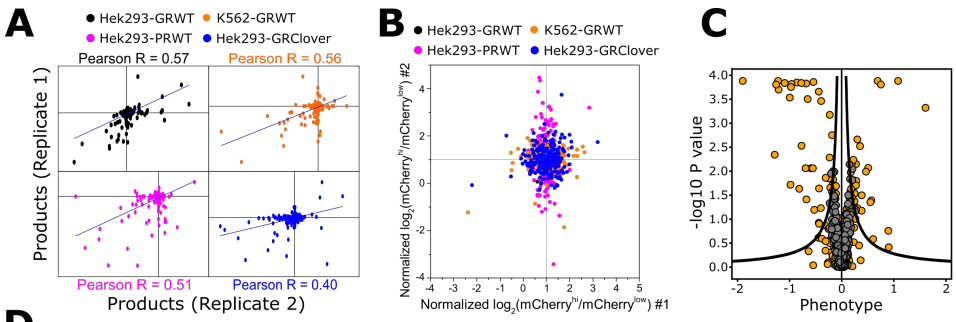

D

Negative SHR Regulators

Hek293-GRCL		Hek293-GRWT		Hek293-MRWT		Hek293-PRWT		K562-GRWT		K562-MRWT	
Gene	Product	Gene	Product	Gene	Product	Gene	Product	Gene	Product	Gene	Product
PRPF6	1,59	PPIL1	3,88	PPIL1	2,46	OGT	2,64	FKBP5	3,27	CTR9	6,30
OGT	1,20	OGT	3,73	OGT	2,45	HSPH1	1,56	MCMBP	1,93	PFDN2	5,82
VCP	1,18	NUDC	2,58	NTC	1,66	PPIA	0,54	TXN	1,14	RPAP3	2,14
PPWD1	1,01	TTC27	2,26	VCP	1,00	CDC37	0,52	PPIL1	0,99	DNAJC24	1,97
PDIA6	0,69	CALR	0,84	OPA1	0,67			SUGT1	0,92	CABIN1	1,04
DCP1A	0,52	DNAJC8	0,74	CCT6A	0,64			PPP5C	0,89	HSP90AB1	0,99
		PRPF6	0,52	TXN	0,60			DNAJC24	0,81	PSMD4	0,59
		SUGT1	0,43	PDIA6	0,51			CNOT10	0,58	NTC	0,49
		FKBP1B	0,42					VCP	0,45	FKBP1A	0,45
		TMTC3	0,37					DCP1A	0,36	UXT	0,44
		HSPH1	0,34					PPIH	0,30	CDC16	0,34
		PPWD1	0,34							VBP1	0,32
		NTC	0,31							PDIA6	0,32
		EMC2	0,30								

Positive SHR Regulators

Hek293-GRCL		Hek293-GRWT		Hek293-MRWT		Hek293-PRWT		K562-GRWT		K562-MRWT	
Gene	Product	Gene	Product	Gene	Product	Gene	Product	Gene	Product	Gene	Product
DNAJC19	-0,41	TTC4	-0,33	HSPA5	-0,50	CCT8	-0,53	HSP90B1	-0,31	PRDX4	-0,37
PDCD11	-0,45	ADRM1	-0,33	DNAJC17	-0,51	ASNA1	-0,55	ASNA1	-0,32	CCT2	-0,39
TTC1	-0,51	CNOT10	-0,37	KLC1	-0,59	HSPA9	-0,55	PDRG1	-0,32	PHB2	-0,53
HSPA9	-0,53	AHSA1	-0,44	AFG3L2	-0,59	HSPD1	-0,58	TMX2	-0,33	TCP1	-0,55
PHB	-0,56	DNAJC2	-0,45	PDRG1	-0,65	PSMD2	-0,65	UXT	-0,34	CCT7	-0,60
DNAJA1	-0,56	HSPE1	-0,45	CCT8	-0,73	HSPA4	-0,66	CCT5	-0,35	DNAJA2	-0,60
NTC	-0,58	HSP90AA1	-0,46	HSF1	-0,74	GTF3C3	-0,67	MLF2	-0,44	PDCD11	-0,72
LONP1	-0,66	ZFC3H1	-0,48	IRS4	-0,79	PSMC1	-0,70	GTF3C3	-0,47	NUDCD3	-0,88
PSMG3	-0,68	PSMG3	-0,65	PSMC1	-0,88	UXT	-0,73	PRPF6	-0,55	CCT6A	-1,01
PFDN2	-0,70	HSPA9	-0,66	CTR9	-1,03	TTC4	-0,73	CBL	-0,56	PSMC1	-1,18
PHB2	-0,74	TTC1	-0,71	TMX2	-1,32	HSF1	-0,81	PSMC1	-0,66	PSMD2	-2,40
CNOT10	-0,88	HSF1	-0,72	PDCD11	-1,37	TTC27	-0,85	HSPA5	-0,68	VCP	-4,37
PSMG4	-1,12	NUDCD3	-0,76	DNAJA1	-1,44	NKTR	-0,86	PSMG3	-0,68		
DNAJC2	-1,18	PDRG1	-0,82	UXT	-1,59	NUDCD3	-1,00	PFDN2	-0,70		
CTR9	-1,25	STUB1	-0,85	LONP1	-1,74	HSPA5	-1,06	PSMD4	-0,79		
PTGES3	-1,43	DNAJC19	-1,06	PSMD4	-2,25	PSMD4	-1,18	DNAJC19	-0,81		
PSMD4	-2,13	HSPD1	-1,07	GTF3C3	-2,25	RPAP3	-1,21	HSF2	-1,00		
NUDCD3	-2,52	PPID	-1,11	TTC4	-2,38	PDCD11	-1,22	NUDCD3	-1,07		
		PSMC1	-1,57	PSMG4	-2,96	CLPB	-1,28	DNAJA1	-1,14		
		DNAJA1	-1,61	STIP1	-3,85	SUGT1	-1,37	HSCB	-1,26		
		UXT	-2,05	PTGES3	-4,55	PTGES3	-1,40	LONP1	-1,30		
		XAB2	-2,08	RPAP3	-6,02	CCT6B	-1,54	TCP1	-1,40		
		STIP1	-2,18			DNAJA3	-1,82	HSPA9	-1,45		
		PFDN2	-2,37			HSP90AA1	-1,87	CCT3	-1,52		
		PHB2	-2,47			DNAJC19	-1,94	DNAJA2	-1,53		
		PHB	-2,59			PDRG1	-2,20	PSMG4	-1,53		
		HSP90AB1	-2,64			AFG3L2	-2,28	CCT4	-1,56		
		RPAP3	-2,89			PSMG4	-2,53	STIP1	-1,67		
		PDCD11	-2,94			LONP1	-2,81	PHB2	-1,76		
		CTR9	-3,18			TTC1	-2,82	NUDC	-1,99		
		PSMG4	-3,80			HSP90AB1	-3,28	PHB	-2,02		
		PSMD4	-4,45			PFDN2	-4,31	CCT7	-2,33		
		PTGES3	-4,77					TTC4	-2,35		
		FKBP5	-7,38					CCT2	-2,36		
								CCT6A	-2,38		
								CTR9	-2,46		
								AFG3L2	-2,51		
								PTGES3	-3,22		
								TTC27	-3,41		
								PDCD11	-4,48		

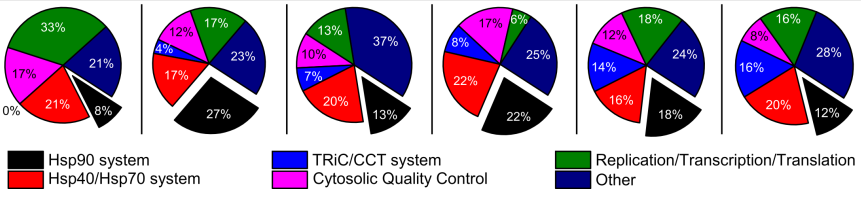

FIGURE 40 | **CRISPRi Screening for SHR Modulators in Monoclonal Cell Lines.**
A Replicate correlations of independent screens. The hit strength as defined in the main text of independently performed screens were correlated.
B Replicate correlation of non-targeting sgRNAs. The $\log_2$-fold enrichment of sgRNA counts in the mCherry^{high} vs mCherry^{low} populations of two replicates is shown.
C Representative volcano plot of a SHR modulator in the Hek293-GRWT cell line. The phenotype is defined as the $\log_2$-fold enrichment of sgRNA counts in mCherry^{high} vs mCherry^{low} samples. Orange dots represent targeted genes, grey dots indicate non-targeting sgRNAs. The lines indicate the threshold conforming to a 5% false discovery rate.
D Significant hits obtained from CRISPRi screening. The hit strength of activating and de-activating hits obtained from screening for SHR modulators are shown for the indicated cell lines. The percentages of hits belonging to the indicated categories are shown as pie charts.

are mostly a product of cellular defects. Hence, this indicates that the K562 cell line is generally more dependent on the TRiC/CCT system than the Hek293 celll line. Between 10% and 17% of the genes were part of the general cytosolic quality control machinery, mostly composed of the proteasome and HSR regulators. While several components of the proteasome are essential for viability, proteasomal degradation has also been proposed as a regulatory mechanism of SHRs and could thus directly impact SHR activity (Whitesell and Cook, 1996; Connell et al., 2001). In all screens, about 20% of the significant hits were part of the Hsp40/Hsp70 system, suggesting that the Hsp40/Hsp70 system is important for SHR regulation across different cell lines and SHRs. Importantly, also knockdown of components of the Hsp90 system affected SHR maturation in all screens, representing between 8% and 27% of the identified hits. Hence, between 30% and 45% of the identified hits belonged to the Hsp40/Hsp70 and Hsp90 system matching the known folding pathway of SHRs encompassing chaperoning by Hsp70 and Hsp90 (Pratt and Toft, 1997; Kirschke et al., 2014; Lorenz et al., 2014). In addition, about 20% to 40% of the hits could not be assigned to the mentioned categories, providing the prospect of containing specific SHR modulators that have not previously been associated with SHR chaperoning. In summary, these results show that SHR-dependent reporter activation is affected by general cellular machineries, but also by different chaperone systems that have previously been associated with SHR maturation. Importantly, this shows the general suitability of the screening setup to identify specific regulators of SHRs.

4.2.3.2 Comparing the Regulation of Different SHRs in Hek293 Cells

Marked differences in the regulation of different SHRs have been found in yeast (this study, Sahasrabudhe et al., 2017). Hence, we asked whether differences of the regulators of SHRs are also found in the mammalian system. To that end, the hit strength of all screening library elements determined in the Hek293-GRWT, Hek293-MRWT and Hek293-PRWT screening constructs was correlated (Figure 41A). Pearson Correlation Coefficients between 0.52 and 0.68 were found which are similar to the Pearson R values determined for screening replicates (Figure 40A,B), indicating that the hit strength of the targeted genes was highly correlated between GR, MR and PR in Hek293 cells.

Since few common genes with a high hit strength may skew the correlation, next the significant hits obtained for screening with GR-WT, MR-WT and PR-WT in Hek293 cells were compared (Figure 41B). For GR-WT 21 specific hits were found and 9 hits were unique each for PR-WT and MR-WT. By contrast, 5 common genes were identified as hits between GR and MR as well as MR and PR and 11 common hits between GR and PR. Only 11 query genes were found as significant hits for all three receptors. Yet, a caveat concerning the overlap of hits between the receptors lies in the limited reproducibility of replicates as discussed (Figure 40). As a consequence, differences within the hits between screens is expected. On the other hand, common hits found for more receptors are thus less likely to be false-positive.

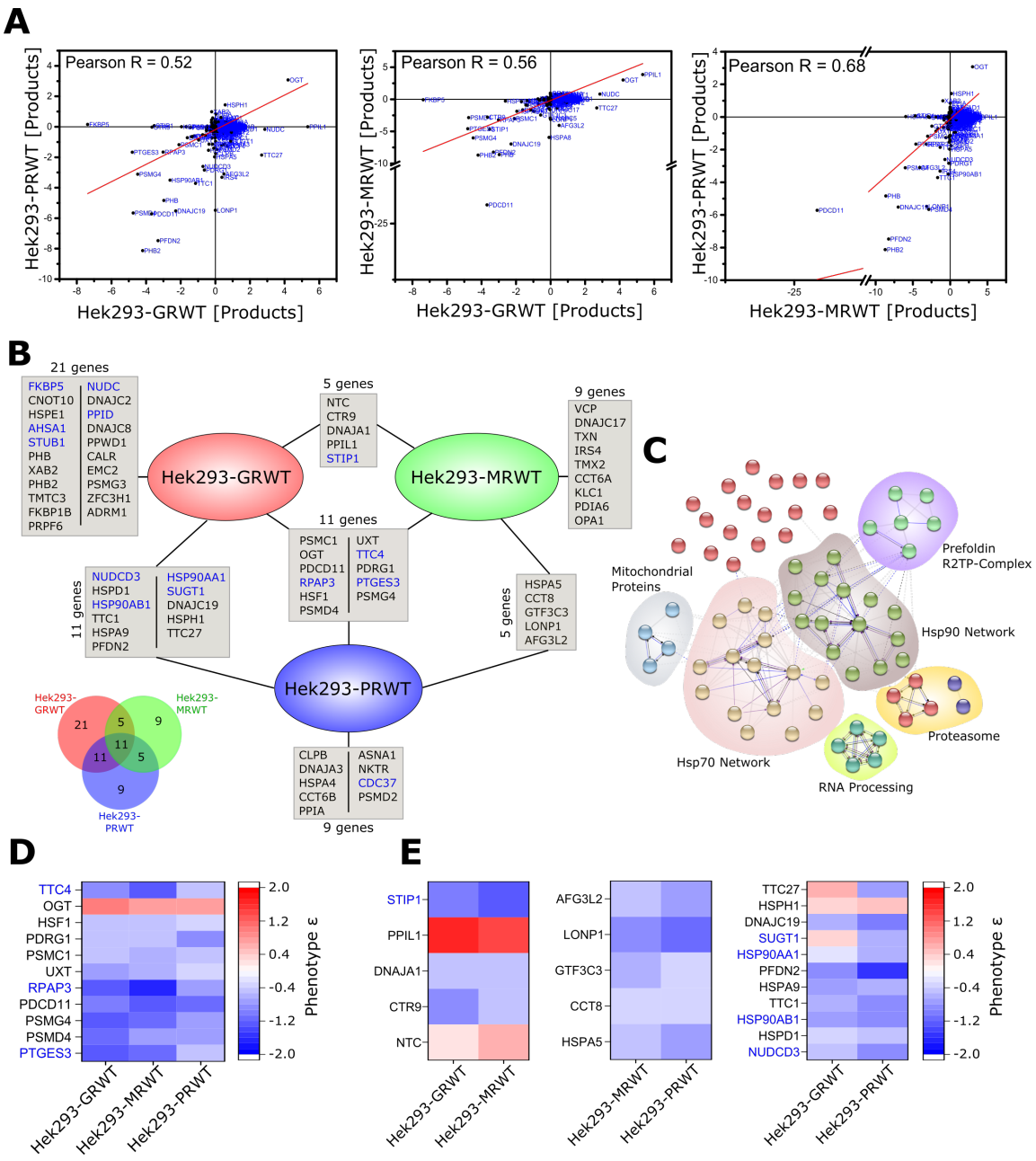

FIGURE 41 | **Regulators of SHRs in the Hek293 Cell Line.**
A Correlation of the CRSIPRi screening hit strengths for GR, MR and PR in Hek293 cells. The hit strength of all elements of the CRISPRi library obtained for screening in the Hek293-GRWT, Hek293-MRWT and Hek293-PRWT were correlated.
B Significant screening hits obtained for GR, MR and PR in Hek293 cells. The shared and individual significant hits are depicted. Known or suspected Hsp90 co-chaperones are marked in blue. A Venn diagram is shown in the bottom left corner.
C Protein association network of Hek293 hit genes. The hits obtained for GR, MR and PR were clustered using the STRING algorithm (v. 11.0). The assignment of proteins to protein networks is indicated. Unconnected, red dots represent proteins for which no high confidence association with the networks is known.
D, **E** Phenotypes of hit gene knockdowns in Hek293 cells. The phenotype ϵ ($\log_2$-fold difference of sgRNA reads in mCherry$^{hi/low}$ populations) of the significant hits obtained from CRISPRi screening were used to compare the effect of hit gene knockdown on SHR activity. Negative phenotypes indicate reduced SHR activity after gene depletion. Known or suspected Hsp90 co-chaperones are marked in blue.

Looking at the combined list of hits obtained for either one of the three receptors, we found mitochondrial genes, RNA processing genes, parts of the proteasome and the R2TP-Prefoldin (R2TP/PFDN) complex (Figure 41C). Additionally, hits belonging to the Hsp70 and Hsp90 network were identified. Several well-studied Hsp90 co-chaperones were found as hits in addition to the cytosolic Hsp90α and Hsp90β isoforms: FKBP51 (FKBP5), Aha1 (AHSA1), CHIP (STUB1), Cyp40 (PPID), Sti1 (STIP1), Sgt1 (SUGT1), Cdc37, Tah1 (RPAP3), p23 (PTGES3) and Cns1 (TTC4) (Figure 41B). Notably, besides well studied Hsp90 co-chaperones, the ill-studied NudC and NudCD3 proteins that have been associated with Hsp90 in few studies were identified as regulators of GR, and GR and PR, respectively. Yet, most co-chaperones have only been found for one or two of the tested SHRs, suggesting that many co-chaperones may affect SHRs in a client-specific way. Interestingly, from the established and *bona fide* Hsp90 co-chaperones (Table 2), PP5, Pih1 and, surprisingly, FKBP52 were not found as significant hits for either of the receptors, which may either indicate that they only weakly affect SHR activity or that the knockdown from the five sgRNAs in the library was not sufficient to show an effect.

Within the group of regulators that significantly affected all three receptors, 11 genes were found including three known Hsp90 co-chaperones: The well-known p23 (PTGES3), which is known to affect SHRs, Cns1 (TTC4), for which regulation of translation elongation has been shown in yeast (Schopf et al., 2019) and Tah1 (RPAP3). Mammalian RPAP3 is more complex than yeast Tah1 and forms additional contacts with a prefoldin (PFDN) module that includes ubiquitously expressed transcript protein (UXT) as well as p53 and DNA damage regulated 1 (PDRG1), which were both also found as hits for all receptors in Hek293 cells (Figure 41B) (Boulon et al., 2010; Cloutier et al., 2017; Houry et al., 2018). The R2TP/PFDN complex regulates several different clients mainly involved in gene expression and genome stability (Houry et al., 2018). Hence, these results suggest that the effect of R2TP/PFDN on reporter activation during the screen may be indirect. Yet, for UXT association with the androgen receptor has been proposed and PDRG1 has been shown to interact with Hsp90 in a high-throughput screen, suggesting that parts of the R2TP/PFDN complex may also directly influence SHR activation (Markus et al., 2002; Skarra et al., 2011). Additional shared hits include parts of the proteasome, HSF1 and O-GlcNAc transferase (OGT). For OGT, the association with Hsp90 has previously been proposed, yet the molecular details are poorly understood (Zhang et al., 2012). In conclusion, besides well-established Hsp90 co-chaperones we also found parts of the R2TP/PFDN complex and OGT that may affect SHR activity in an Hsp90-dependent mode.

The phenotypes of hits that were found for GR, MR and PR were analyzed to elucidate whether knockdown had the same effect on different receptors (Figure 41D. All hits that were identified for all three receptors were either activators or suppressors across all receptors and only the strength of the phenotype varied. Interestingly, OGT was the only gene which increased SHR activity when it was depleted,

suggesting it may limit SHR activity, while all other common hits promoted SHR activity. Surprisingly, FKBP51, which had been suggested as a negative regulator of GR function increased GR activity in our screen when it was depleted (Pratt and Toft, 2003). Knockdown of the Hsp90 co-chaperones Cns1 (TTC4), Tah1 (RPAP3) and p23 (PTGES3) led to strong deactivation of SHRs indicating that they are important promoters of SHR activity. Notably, knockdown of UXT and PDRG1 which are associated with Tah1 (RPAP3) induced less severe phenotypes, suggesting they may play a more subtle role.

Next, the common hits identified for two receptors each were analyzed (Figure 41E). Again, most hits were positive SHR regulators except for the peptidyl prolyl-*cis/trans* isomerase PPIL1, NineTeen Complex (NTC) and the Hsp110-class NEF HSPH1. Notably, knockdown of tetratricopeptide repeat protein 27 (TTC27) and Sgt1 (SUGT1) caused opposing phenotypes for GR and PR.

In summary, screening for modulators of GR, MR and PR in the Hek293 cell line produced several known components of the Hsp70 and Hsp90 system as significant hits, including well studied Hsp90 co-chaperones but also less understood co-chaperone candidates, in particular NudC and NudCD3. Additional, OGT, UXT and PDRG1 were identified as potential regulators of SHRs that have previously not been associated with Hsp90-dependent client maturation. There were differences in the hits obtained for different receptors including differences in the known Hsp90 co-chaperones found as hits, which may in part be caused by the limited reproducibiltiy of screens and requires further analysis. Most hits that were identified for different receptors had a either an activating or a deactivating effect on all receptors and only few displayed opposing phenotypes for different receptors. This suggests that GR, MR and PR underlie similar regulatory mechanisms but subtle differences have evolved to adapt to the individual requirements of each receptor.

4.2.3.3 Comparing the Regulation of GR in Hek293 and K562 Cell lines

The regulation of different SHRs in Hek293 cells seemed to be similar. Hence, we asked, how well the regulation of SHRs is conserved between cell lines. To this end, the regulation of GR-WT in the Hek293 and K562 cell lines was compared, since both screens were performed in duplicates and yielded many significant hits (Figure 42).

Surprisingly, the hit strength values obtained for GR modulator screening in Hek293 and K562 showed little correlation with a Pearson R of 0.24, suggesting that GR is distinctly regulated in Hek293 and K562 cells (Figure 42A). To test, whether the differences between the regulation of GR may be caused by the different expression of the screened genes, the protein levels of library elements obtained from a previously published proteomics study were correlated (Figure 42B) (Geiger et al., 2012). The protein levels of the library genes in Hek293 and K562 cells were highly correlated with a Pearson R of 0.88, suggesting that the low correlation of the the hit strengths between K562 and Hek293 were not due to differences in the protein levels of the targeted genes (Figure 42B). Comparisons of the protein levels in the K562

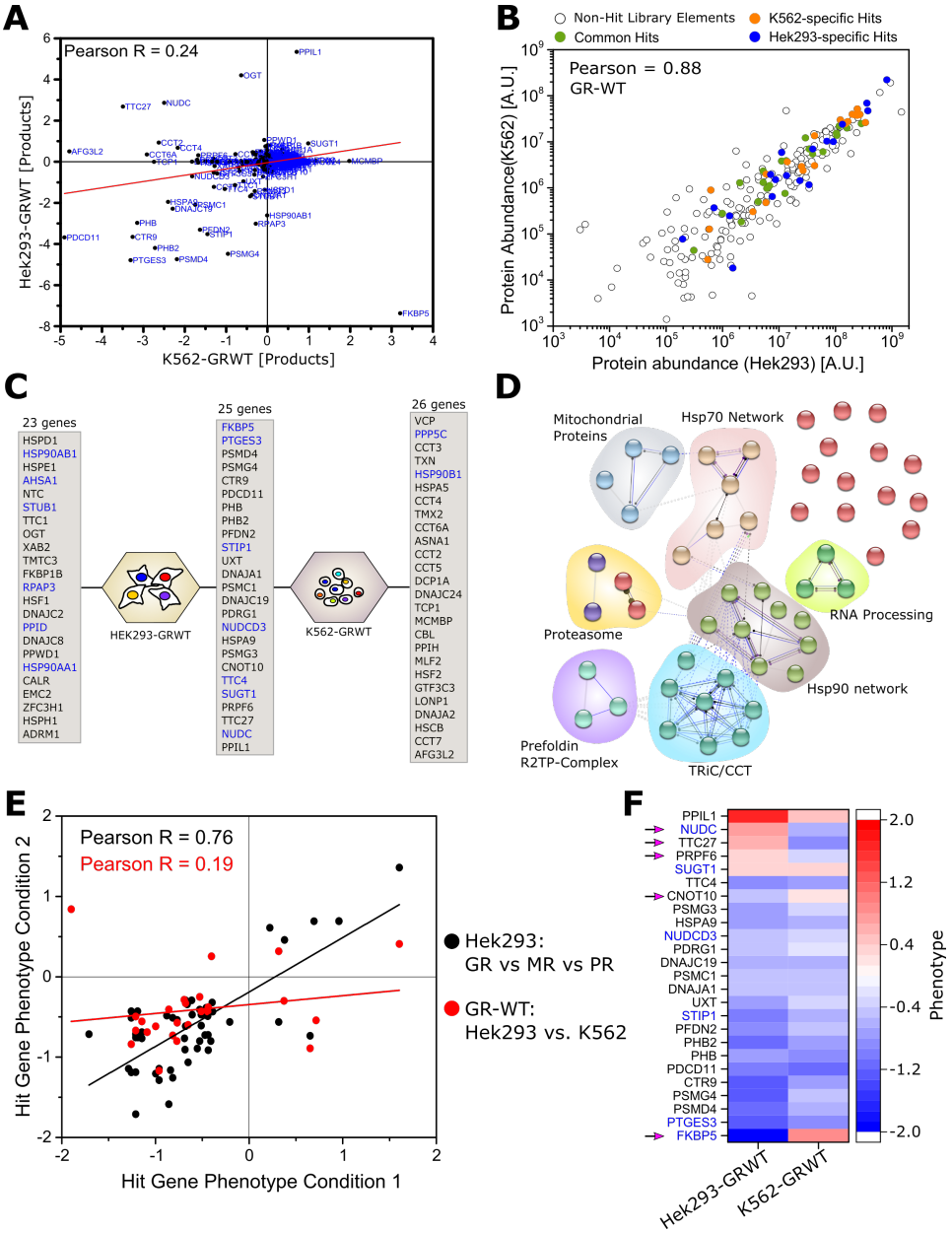

FIGURE 42 | **Regulation of GR in K562 and Hek293 Cell Lines.**
A Correlation of hit strengths for GR in Hek293 and K562 cells. The hit strength, as defined in the main text, of CRISPRi library elements obtained for GR-WT in Hek293 and K562 cells were correlated and the Pearson Correlation Coefficient was calculated.
B Proteomics of library elements in Hek293 and K562 levels. Proteomics data for CRISPRi library genes expressed in K562 and Hek293 cell lines were used (Geiger et al., 2012). K562-specific hits, Hek293-specific hits and common hits obtained for GR-WT as shown in **C** are marked in green, orange and blue, respectively.
C Significant screening hits obtained for GR Hek293 and K562 cells. Known or suspected Hsp90 co-chaperones are marked in blue.
D Protein association network of K562 hit genes. The hits obtained for GR obtained in the K562 cell line were clustered using the STRING algorithm (v. 11.0). Unconnected, red dots represent proteins for which no high confidence association with the shown networks is known.
E Phenotype correlations of screens in Hek293 and K562. The phenotypes of GR vs. MR vs. PR in Hek293 cells (black; Figure 41D,E) and the phenotypes of GR in K562 vs. Hek293 cells (red) were correlated.
F Phenotypes of GR in K562 vs. Hek293 cells. The phenotypes of significant hits were compared. Negative phenotypes indicate reduced SHR activity after protein depletion. Known or suspected Hsp90 co-chaperones are marked in blue and hits causing opposing phenotypes in Hek293 and K562 are marked with arrows.

vs. Jurkat cell line and that of the Hek293 vs. HeLa cell line were correlated with a Pearson R of 0.88 and 0.91, respectively, showing that the correlation of protein levels between Hek293 and K562 cells is similar (data not shown).

To investigate these differences in more detail, the protein levels of significant hits obtained for Hek293 and K562 cell lines were analyzed (Figure 42B,C). Importantly, there was no bias in the protein levels between K562 or Hek293 cells for K562- and Hek293-specific hits (Figure 42B), confirming that differences in the expression levels of the targeted genes in one cell line cannot be the reason for the observed differences in the activation of the SHR.

For Hek293 and K562 cells, 23 and 26 cell line-specific hits were obtained, respectively, and 25 hits were found in both screens (Figure 42C). In addition to the hit categories also found in Hek293 cells, parts of the TRiC/CCT chaperonin complex were found as hits in the K562 cell line. Since the TRiC/CCT complex has been shown to be essential for viability as mentioned and likely not directly regulating SHRs, this suggests that K562 cells are more sensitive to disruption of the TRiC/CCT system than Hek293 cells (Figure 42C,D). Among the hits that affected GR in both cell lines, 7 Hsp90 co-chaperones were identified: FKBP51 (FKBP5), p23 (PTGES3), Hop (STIP1), NudCD3, Cns1 (TTC4), Sgt1 (SUGT1) and NudC. Hence, p23 and Cns1 were not only found as regulators for GR, MR and PR in Hek293 cells but also seem to affect GR activity in K562 cells, suggesting that their regulatory function is conserved between different cell lines. Additionally, PDRG1 and UXT were also found as regulators in K562 and Hek293 cells. The well known Hsp70-Hsp90 adapter co-chaperone Hop was important for GR regulation in both cell lines. The largely unstudied Hsp90 co-chaperone candidates NudC and NudCD3 affected GR in both cell lines, indicating that they may function as previously undetected regulators of SHRs. Notably, PP5 (PP5C) was the only K562-specific Hsp90 co-chaperone that was found in the screen. OGT, which acted as a negative regulator of GR, MR and PR in Hek293 cells did not significantly affect GR in K562 cells, indicating it may be a cell line-specific regulator.

Since the hit categories were largely overlapping between Hek293 and K562 cells and many overlapping genes were found, it was tested next how the knockdown of shared hit genes impacted GR activity in Hek293 and K562 cells. First, the phenotypes of hits for GR, MR and PR in Hek293 cells (Figure 41) were correlated as a reference and compared to the correlation of the hit phenotypes obtained for GR in Hek293 *versus* K562 cells (Figure 42E). While the effect of hit gene knockdown were very similar for GR, MR and PR in Hek293 cells with an overall Pearson R of 0.76, the effects of knockdowns on GR when compared between Hek293 and K562 cells varied significantly more with a Pearson R of 0.24 (Figure 42E).

Next, the phenotypes for GR in Hek293 and K562 were compared for each common hit gene, which revealed that for many genes, the severity of the phenotype was different and most importantly, for several genes, opposing effects on GR activity were observed (Figure 42F). These include the Hsp90 co-chaperones NudC and

FKBP51. While the role of NudC in the context of Hsp90 client maturation is entirely unknown, FKBP51 has been implicated in SHR maturation, but seems to play a different role in Hek293 and K562 cells. The NudC homolog NudCD3 on the other hand promoted GR activity both in Hek293 and K562 cell lines, suggesting that NudC and NudCD3 have different functions. Additionally, opposing phenotypes were caused by knockdown of TTC27, which also showed opposing phenotypes for GR and PR in Hek293 cells, Pre-mRNA-processing factor 6 (PRPF6) and CCR4-NOT transcription complex subunit 10 (CNOT10).

In summary, comparison of the regulation of GR in the Hek293 and K562 cell lines revealed substantial differences. While there was some overlap in the identified hits, many hits affected GR activity distinctly in Hek293 and K562 cell lines, including NudC, FKBP51 and TTC27. This is in contrast to the shown comparison between GR, MR and PR in the Hek293 cell line, in which common hits had similar effects on SHR activity. OGT, which was a negative regulator for all receptors in Hek293 cells did not significantly affect GR in the K562 cell line. Together this suggests that SHRs are distinctly regulated between cell lines. Despite the differences, p23, Cns1, PDRG1 and UXT, which were hits for all receptors in Hek293 cells also affected GR in K562 cells, indicating a cell line-independent function that is important for different receptors.

4.2.4 Individual Knockdowns of Steroid Hormone Receptor Modulators

Screening for GR modulators in different cell lines revealed distinct regulation by some co-factors, whereas different receptors in the same cell line seemed to be regulated in similar ways. To confirm these findings, a subset of known Hsp90 co-chaperones, co-chaperone candidates and previously unknown regulators of SHRs was validated by knocking down the respective genes individually (Table 22). For each gene, at least two sgRNAs were tested individually and compared to two non-targeting controls in the Hek293-GRCl, Hek293-GRWT, Hek293-MRWT, Hek293-PRWT and K562-GRWT cell line. Due to technical problems, the analysis of individual KDs (IKDs) in the K562-MRWT cell lines was omitted. Cells were infected with the respective sgRNA-expressing plasmids individually leading to infection rates between 30 % and 90 % as determined by the ratio of the BFP^+ versus BFP^- populations (data not shown). The SHR activity was tested 7 days post infection for Hek293 cells and 11 days post infection for K562 cells, which is similar to the time periods between library infection and screening. Notably, SHR activity in K562 cells was also tested 6 days after infection, yet at that time no difference between the non-targeting controls and the cells infected with targeting sgRNA plasmids was observed, suggesting that the knockdown was not sufficiently established after 6 days (data not shown).

TABLE 22: Individual Knockdown of SHR Modulators

Protein (Gene)	**Behavior in CRISPRi Screen**	**Known Function**
FKBP52 (FKBP4)	Not identified as a hit in the screens.	Supposedly functions as a positive modulator of GR, PR and AR, but not ER and PR (Storer et al., 2011).
FKBP51 (FKBP5)	Identified as a positive and negative regulator in Hek293 and K562 cells, respectively.	Supposedly functions as a negative modulator of SHR activity (Storer et al., 2011).
p23 (PTGES3)	Identified as a positive regulator in all screens.	Known Hsp90 co-chaperone and important for SHR maturation (Felts and Toft, 2003).
NudC (NUDC)	Identified as a negative regulator and positive regulator for GR in Hek293 and K562 cells, respectively.	Function unknown. Supposedly interacts with Hsp90 (Taipale et al., 2014; Zheng et al., 2011.
NudCD3 (NUDCD3)	Identified as a positive regulator of GR in Hek293 and K562 cells and for PR in Hek293 cells.	Function unknown. Homolog of NudC (Taipale et al., 2014.
OGT (OGT)	Identified as the only significant negative regulator of GR, MR and PR in Hek293 cells.	Supposedly interacts and is stabilized by Hsp90 (Zhang et al., 2012).
Hop (STIP1)	Identified as a positive regulator of GR and MR in Hek293 and GR in K562 cells.	Well-studied Hsp90 co-chaperone. Adapter to the Hsp70 system (Wegele et al., 2006).

First, the agreement of phenotypes derived from screening and the SHR activities measured in the individual knockdown strains was tested (Figure 43A). For all constructs based on the Hek293 cell line, a high correlation between screen phenotypes and SHR activities of the IKDs was evident with Pearson Correlation Coefficients between 0.79 and 0.91. For K562-GRWT, a weak correlation with R = 0.27 was observed, yet this was mainly the result of the small number of seven genes under analysis and a single sgRNA that resulted in increased activity in the screen but had only a weak phenotype in the IKD analysis (Figure 43A). Notably, the correlation between the phenotypes produced by sgRNA #1 and sgRNA #2 was very high with a Pearson Correlation Coefficient of 0.99, confirming the specificity of the sgRNAs

(Figure 43B). Together, these results suggest that the potential to predict phenotypes of gene knockdowns and thus gene function from the CRISPRi screens alone is high, especially in Hek293 cells.

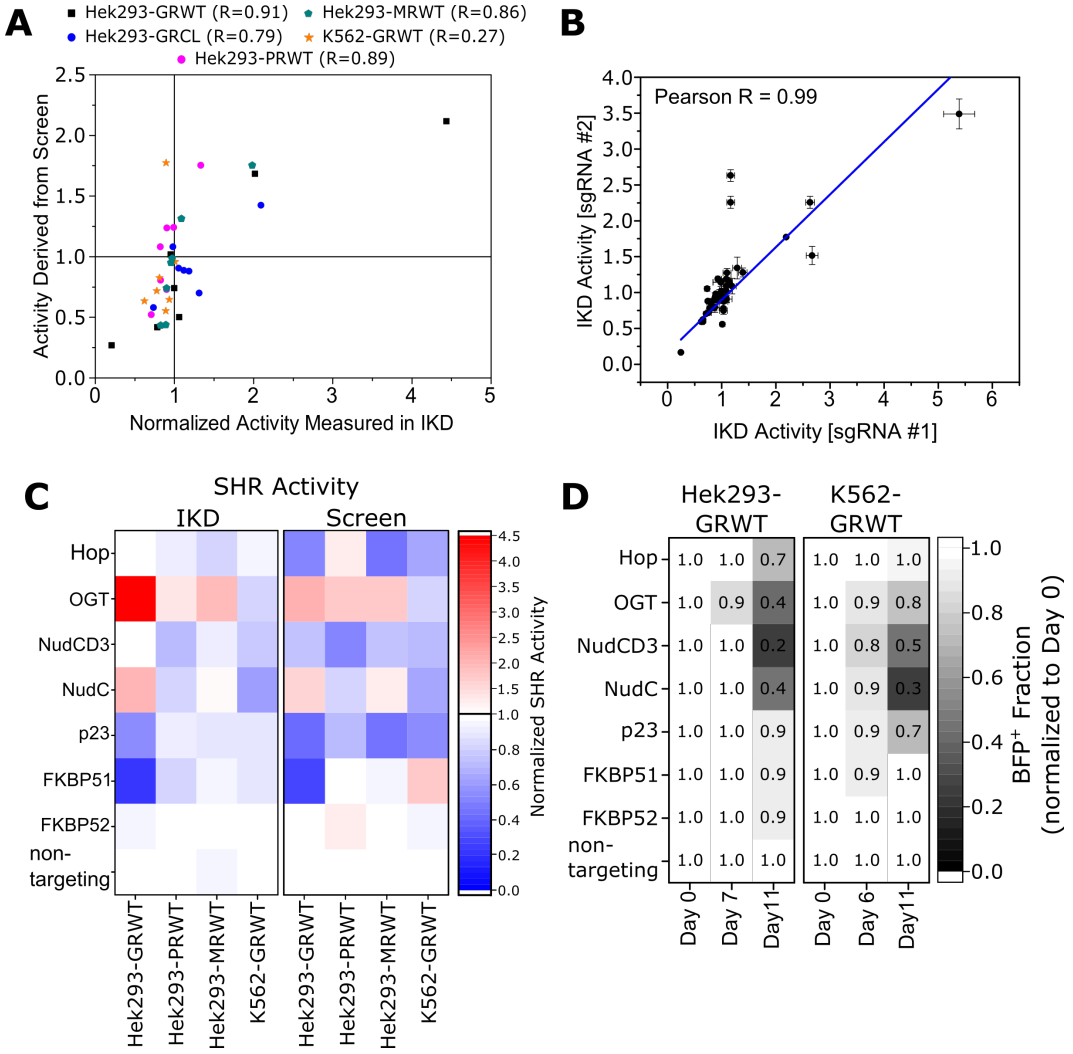

FIGURE 43 | **Individual Knockdown of CRISPRi Hits.**
A Correlation of SHR activities derived from screening and individual knockdowns (IKDs). The activities of SHRs in the indicated cell lines were determined after individual knockdown by the lentiviral transduction of sgRNA-expressing plasmids (X-axis) and from the phenotype ϵ values from screening (Y-axis). SHR activity in IKD cell lines was measured 7 days (for Hek293) or 11 days (for K562) after infection after 24 h treatment with 10 nM of dexamethasone, aldosterone or progesterone, for GR, MR and PR, respectively. Activity was read out by quantifying the mCherry levels, which were then normalized to mCherry signals from a cell line transduced with a non-targeting sgRNA-expressing plasmid. Pearson Correlation Coefficients are depicted.
B Correlation between sgRNAs targeting the same gene. The SHR activities measured in two cell lines in which a target gene was knocked down with different sgRNAs (sgRNA #1 and sgRNA #2) were correlated and the Pearson Correlation Coefficient was calculated.
C The effect of IKDs of hit genes on SHR activity. The SHR activities measured after knockdown with sgRNA #1 and #2 were averaged and are shown. The activities derived from phenotypes in the screen are shown on the right as a reference.
D The effect of IKDs of hit genes on cell viability. The fraction of BFP^+ cells, which carry the sgRNA-expressing plasmid was determined at the indicated time points after infection.

Next, the SHR activity in IKD strains of the different cell lines were compared (Figure 43C). As a reference, the phenotypes derived from screening are depicted, even if the gene was not identified as a statistically significant hit in the screen (Figure 43C). In line with the correlation shown in Figure 43A, the overall pattern of SHR activities was similar between the data derived from the screen and measurements in IKDs (Figure 43C). Due to the more controlled condition of individual knockdowns, the strength of the effect on SHR activity from IKDs is assumed to be more accurate than the phenotypes obtained from screening. Overall, the modulation of SHR activity was strongest for GR in Hek293 cells, with loss of OGT leading to an approximate 4.5-fold activation and loss of FKBP51 reducing activity by about 80 %. The phenotypes of IKDs in the other cell lines were more moderate suggesting that GR is subject to tighter regulation by the factors under investigation than the other receptors. Note that the comparison of the effects on Hek293-GRWT to the effects on GR in the K562 cell line is not possible, since GR activities in Hek293 and K562 cell lines were measured after different times post infection, since the knockdowns needed more time to establish in the K562 than the Hek293 cell lines.

While FKBP52 (FKBP4) knockdown did not affect SHR activity, knockdown of FKBP51 (FKBP5) led to a strong loss of function for GR in the Hek293 cell line and a more subtle loss of function for Hek293-PRWT and K562-GRWT. This is in contrast to the phenotype found in the screen, in which FKBP51 loss had a positive effect on GR activity in the K562 cell line (Figure 43C) and opposes the published inhibiting effect of FKBP51 on GR, MR and PR activity (Storer et al., 2011). By contrast, loss of p23 consistently led to a reduced SHR activity across all receptors and both cell lines. Knockdown of NudC yielded remarkably similar activities in the IKDs and the screen, with an activating effect on GR in Hek293, but a deactivating effect in K562 cells. This also confirms the hypothesis that NudC may be a novel regulator of SHR activity. Depletion of the NudC homolog NudCD3 either had no effect or a slightly deactivating effect for all receptors in both the IKDs and the screen. OGT was the only significant negative regulator of all SHRs in Hek293, but was not a significant hit in the K562 cell line. IKD analysis confirmed that OGT knockdown led to activation of SHRs in Hek293 cells. However, in both the screen and the IKDs, knockdown of OGT reduced GR activity sightly in the K562 cell line, suggesting that OGT has different regulatory functions in Hek293 and K562 cells. Notably, the well-studied Hsp90 co-chaperone Hop which strongly affected SHRs activity in yeast (Section 4.1) had only a small effect on receptor activity but generally acted as a positive modulator, in line with its known role in transferring SHRs from Hsp70 to Hsp90 (Smith et al., 1993; Johnson et al., 1998; Wegele et al., 2006; Röhl et al., 2015b). In summary, these results show that the hits obtained from screening could almost entirely be validated by individually knocking down suspected SHR regulators. In addition, these results support the potential role of OGT, NudC and NudCD3 in the regulation of SHRs.

When IKD strains were selected with puromycine to obtain a homogeneous BFP^+ fraction, some strains displayed a sick phenotype. To systematically test, whether the knockdown of the genes under investigation affected viability, the BFP^+ fraction was determined directly after infection (day 0) and at about 1 week and 11 days after infection in Hek293-GRWT and K562-GRWT cell lines in the absence of selective agents (Figure 43D). While the viability of IKD strains was largely unaffected at day 6 and day 7 for Hek293 and K562 cells, respectively, viability was strongly reduced after 11 days in cells depleted of NudC and NudCD3 in both cell lines. Loss of OGT had a strong negative effect on viability in Hek293 cells but had only a minor effect in K562 cells, in line with the finding that OGT was a significant hit in Hek293 cells, but not in K562 cells. Together, this shows that NudC and NudCD3 are important to maintain viability irrespective of the cell line, whereas OGT tends to be more important for viability in Hek293 cells than in the K562 cell line.

In summary, knockdown of screening hits individually showed a high correlation of the phenotypes observed in the screen and the IKDs. Hence, the phenotypes obtained from CRISPRi screening faithfully predicts the phenotype when target genes are knocked down individually, especially in the Hek293 cell line. The relevance of NudC, NudCD3 and OGT on SHR receptor activity could be validated and it could be shown that knockdown has a negative effect on viability.

4.2.5 Screening For Novel Hsp90 Co-Factors in Mammalian Cells - Summary and Discussion

The Hsp90 co-chaperone expanded from yeast to man and comprehensive knowledge of the role of the human co-chaperome in the maturation of Hsp90 clients is lacking. In cooperation with the Kampmann Lab at the UCSF, we set out to develop a screening platform to identify novel factors that modulate the activity of SHRs and to analyze the effect of known Hsp90 co-chaperones on the maturation of SHRs as one of the best studied classes of stringent Hsp90 clients.

4.2.5.1 Development of a CRISPRi Reporter System

CRISPRi-based functional genomics was used as a powerful screening tool which allows the efficient knockdown of target genes with minimal unspecific off-targeting (Gilbert et al., 2013; Qi et al., 2013a; Gilbert et al., 2014). For pooled functional genomics screens, a fluorescent-based reporter system that faithfully translates SHR activity into reporter expression is required. A reporter construct containing tandem GREs upstream of a minimal *D. melanogaster* ADH promoter was found to efficiently upregulate reporter expression with little background activation. We found that the reporter setup is robust against background activation as only little reporter activation could be observed by endogenous GR, even though GR is expressed in Hek293, HeLa and K562 cells (Thul et al., 2017). By contrast, co-expression of SHRs led to a strong activation of reporter activity.

To expand the screening platform for the screening of other clients, additional client-specific readout systems may be feasible. While v-Src activity in mammalian cells can be reliably detected by unspecific tyrosine phosphorylation similar to the yeast system (data not shown), this setup is not suitable for pooled screening. Adaption of a split-GFP system may be feasible to read out v-Src activity in pooled screens. Split-GFP systems contain GFP segments fused to known dimerization molecules (Ghosh et al., 2000; Havranek and Harbury, 2003; Mishra and Bolon, 2014; Romei and Boxer, 2019). Introduction of kinase recognition sites into the dimerization sites may prevent association due to the introduction of negative charges. In this case, a pooled functional genomics screen could be performed in which knockdown of kinase-specific factors causes a reduction of GFP fluorescence.

E3 ubiquitin ligases are a large emerging class of Hsp90 clients comprising a plethora of members regulating many cellular pathways (Taipale et al., 2012). Yet, at the same time almost no information about the co-factor dependence of Hsp90-dependent E3 ubiquitin ligase maturation is available to date. Since several Hsp90 clients are degraded upon disruption of the Hsp90 system including the E3 ubiquitin ligase UHRF1 (Kundrat and Regan, 2010; Theodoraki and Caplan, 2012; Ding et al., 2016; Savitski et al., 2018) GFP-tagging E3 ubiquitin ligases may provide a suitable means of studying the Hsp90 co-chaperone dependence of E3 ubiquitin ligases. A complementary approach to investigate E3 ubiquitin ligases exploits the recently established role of C-terminal degron sequences for substrate degradation (Koren et al., 2018). Degrons are short sequences specifically recognized by E3 ubiquitin ligases (Lucas and Ciulli, 2017), which can be attached to GFP to track the activity of E3 ubiquitin ligases (Koren et al., 2018). In contrast to GFP-tagging of E3 ubiquitin ligases, this approach allows to read out client activity and not only client stability.

4.2.5.2 Generation of a CRISPRi Screening Library

To identify previously unknown co-factors that modulate SHR activity in a Hsp90-dependent manner, a proteostasis-biased sgRNA library targeting 357 genes involved in the protein homeostasis network was generated in this work. The library showed a homogeneous distribution of sgRNAs suggesting that homogeneity of the CRISPRi library should not be bottlenecking the screening process. While a focused library limits the extent to which novel factors can be found, for this study a library biased for proteostasis-factors was chosen for several reasons: Firstly, screening with a compact library reduces the technical effort of a screen, since the number of cells required for screening to assure sufficient coverage of library elements scales with the number of library elements. Since the aim of this work was to screen for modulators of different receptors in different cell lines to draw conclusions about cell and receptor-specific SHR regulation, a compact library was preferred. Secondly, small but important effects of genes may be masked by strong indirect effects of other genes to a higher degree in genome-wide screens compared to screens with small libraries. As an example, genes participating in the transcription or translation of proteins may

impact reporter expression significantly while regulation of SHR function by Hsp90 co-chaperones may be much more subtle. Thirdly, the chance of discovering Hsp90-associated regulators of SHRs is higher in a compact library containing genes that have already been associated with proteostasis.

4.2.5.3 Generation of Screening Cell Lines

To efficiently screen for regulators of different SHRs, monoclonal cell lines were selected, which displayed significant upregulation of the reporter after hormone addition. In particular, GRWT in the Hek293 cell line was highly responsive to hormone reaching about 150-fold activation of mCherry expression. In polyclonal Hek293 cell lines, we observed weaker activation and significant silencing of the reporter locus within few passages. Silencing could also have occurred at the SHR expression cassette. However, in the Hek293-GRCl cell line, cells lacking activation by hormone still expressed the Clover2-tagged GR, suggesting that the reporter locus was silenced. While silencing was less problematic in monoclonal cell lines, partial loss of activation was still observed. Promoter silencing has been described as problematic for biotechnological processes in particular for the CMV promoter (Osterlehner et al., 2011; Zúñiga et al., 2019). Since lentiviral transduction leads to the random integration of DNA into the genome, variability between clones is expected. To minimize the risk of unfavorable pleiotropic effects and to reduce variability between clones, integration into genomic safe harbors using for example adenoviral transduction or transcription activator-like effector nucleases (TALEN) approaches have been developed (Papapetrou and Schambach, 2016). Another approach to ensure stable transgene expression compatible with lentiviral transduction employed in this study is the use of chromatin insulator sequences, flanking DNA sequences that protect a transgene from silencing (Christian et al., 2010; Matzat and Lei, 2014; Pérez-González and Caro, 2019).

4.2.5.4 Screening for SHR Modulators

The monoclonal cell lines were then used to screen for SHR modulators using the compact proteostasis factor-based CRISPRi library. To evaluate the reproducibility of screening results, four cell lines were screened in biological duplicates, showing moderate correlation of the screening hits with Pearson Correlation Coefficients between 0.4 and 0.57. Previously published replicate correlations between independent viability-based CRISPRi screens were usually found to be between 0.7 and 0.9, depending in part on the size of the library and the experimental setup (Liu et al., 2017; Jost et al., 2020; Momen-Roknabadi et al., 2020). Due to lacking negative selection in reporter activation-based CRISPRi screens compared to viability-based screens, additional noise is expected between replicates, which has been confirmed in previous reporter-activity CRISPR/CRISRPi screens (Parnas et al., 2015; Adamson et al., 2016).

The number of significant hits obtained for each cell line differed, ranging from 24 to 51 hits, which correlated with the fold activation observed when the hormone responsiveness of each monoclonal cell line was tested. Hence, the highest number of hits was observed for GR in Hek293 and K562 cells and PR in the Hek293 cell line. Significant overlap between the significant hits obtained for GR, MR and PR in the Hek293 cell line was evident, suggesting that these receptors underlie similar regulation in Hek293. By contrast, when GR regulation was compared between Hek293 and K562 cell lines was compared, hit strength was poorly correlated suggesting different regulatory mechanisms. The analysis of previously published proteomic data could not explain the differences between K562 and Hek293 cells. However, combined omics approaches attested substantial differences in HeLa cell lines obtained from different laboratories (Frattini et al., 2015; Liu et al., 2019). Additionally, there is an abundance of studies that found differences between cancer cell lines regarding genetics, transcriptomics and the susceptibility to therapy (Gerlinger et al., 2014; Ben-David et al., 2018). A study by the Chiosis lab furthermore found that a rewiring of the chaperone systems occurs between different cancer cell lines (Rodina et al., 2016). Together these studies provide evidence for substantial differences between cell types, which may be reflected in the distinct regulation of SHRs. Hence, it may be interesting to test the regulation of SHRs in additional cell lines including different cancer cell lines. In particular, the plasticity of complexes containing (co-)chaperones which affect SHRs distinctly in different cell lines could be tested by co-IP to test whether the different regulatory role is reflected in the formed complexes.

4.2.5.5 Promising SHR Regulator Candidates

Screening yielded several potential regulators of SHR activity in Hek293 and K562 cells. A subset of potential novel SHR modulators and known regulators were validated by IKD of the respective genes. Notably, a high correlation of the phenotypes observed in the screen and the phenotype produced by IKD was evident with Pearson R values of approximately 0.8 - 0.9, confirming the validity of the screening system established in this work and matching literature values (Gilbert et al., 2014; Potting et al., 2018).

The most promising hits based on their occurrence in the screen, the validation by individual knocking down the gene and previously published studies are summarized in Figure 44. Among the Hsp90 co-chaperones, with the exception of p23 (PTGES3) only members that were found repeatedly and usually have not been associated with SHR maturation specifically are shown. Tah1 (RPAP3), PDRG1 and UXT are part of an Hsp90-associated module with Tah1 (RPAP3) as a *bona fide* Hsp90 co-chaperone and PDRG1 and UXT as part of the prefoldin complex, which are known to bind Hsp90 and androgen receptor, respectively, making them interesting candidates for further analysis (Markus et al., 2002; Skarra et al., 2011). Cns1 (TTC4)

maintains protein biosynthesis in yeast and may have a similar function in mammals, suggesting that this co-chaperone may have indirect effects on reporter expression, which has to be cleared in future studies (Schopf et al., 2019). Even though p23 (PTGES3) is well known for its function in the Hsp90 cycle and facilitating the maturation of SHRs, its function in the mammalian cellular context on SHR maturation has not been studied intensively (Dittmar et al., 1997; Bohen, 1998; Fang et al., 1998; Pratt and Dittmar, 1998; Freeman et al., 2000; Pratt and Toft, 2003; McLaughlin et al., 2006; Picard, 2006; Sahasrabudhe et al., 2017). Since it was found as a strong positive regulator in all screens presented in this work, the paramount role of p23 in SHR maturation *in vivo* could be confirmed. Interestingly, Hop played a less prominent role for SHR maturation, while Sti1 had a strong effect on GR and MR activity in yeast (Section 4.1), suggesting that maybe additional factors are present in mammalian cells that modulate SHR transfer from Hsp70 to Hsp90. NudC played a particularly interesting role in the screen, since it presented as a negative regulator for GR in Hek293 cells but as a positive regulator in K562 cells. Since it has been found to associate with Hsp90 and been suspected as an Hsp90 co-chaperone, the presented data suggest an Hsp90-dependent regulation of SHRs by NudC (Zheng et al., 2011; Taipale et al., 2014). While OGT has been studied as a client of Hsp90 it may also modify Hsp90 post-translationally (Zhang et al., 2012). It was a strong negative regulator of all SHRs in Hek293 and found as a positive regulator in K562, making it an interesting target for further research. Lastly, TTC27 displayed opposing phenotypes in Hek293 and K562 cells. While it has not been associated with Hsp90 and SHRs yet, the presence of a TPR domain suggests it may associated with Hsp90 and thus function as an Hsp90-dependent regulator.

Gene	Hek293			K562	Known Function	Validation by IKD	References
	GR	MR	PR	GR			
RPAP3	↓	↓	↓	-	Known Hsp90 co-chaperone	n.d.	Schopf et al. 2017
PDRG1	↓	↓	↓	↓	Interacts with Hsp90	n.d.	Skarra et al. 2011
UXT	↓	↓	↓	↓	Interacts with AR	n.d.	Markus et al. 2002
TTC4	↓	↓	↓	↓	Known Hsp90 co-chaperone	n.d.	Schopf et al. 2017
PTGES3	↓	↓	↓	↓	Known Hsp90 co-chaperone	yes	Schopf et al. 2017
NUDC	↑	-	-	↓	Suspected Hsp90 co-chaperone	yes	Taipale et al. 2014
NUDCD3	↓	-	↓	↓	Suspected Hsp90 co-chaperone	yes	Taipale et al. 2014
OGT	↑	↑	↑		Hsp90 client; May regulate Hsp90	yes	Zhang et al. 2012
TTC27	↑	-	↓	↓	Contains TPR domain	n.d.	

FIGURE 44 | **High-Confidence Screening Hits.**
High-confidence hits obtained from SHR modulator screening in Hek293 and K562 cell line are shown. The effects of gene knockdowns are indicated by arrows and color (blue = reduced activity, red = increased activity). [n.d. = not tested]

4.2.5.6 Conclusion

In this study, a versatile activity-based screening-platform for functional genomics has been developed to analyze the key players that affect the maturation of Hsp90 clients. The validity of the system was shown by screening for SHR modulators in the context of two different cell lines, identifying known SHR modulators as well as

potential, novel SHR regulators such as UXT, PDRG1, NudC and OGT suitable for future analysis. Using individual sgRNAs, we showed that the majority of hits could be validated, confirming that the screening framework produces high-confidence phenotypes. Genome-wide screening for modulators of SHRs may be possible in the future to identify novel co-factors that affect Hsp90 client maturation in an unbiased manner. Unbiased, genome-wide functional screening may be most favorable with Hek293-GRWT for several reasons: GR in the monoclonal Hek293 cell line could be activated more than 250-fold by hormone addition; Hek293-GRWT produced many hits in the screen and displayed a substantial regulation by several factors; All tested hit genes could be validated by individual knockdown of the genes; GR is the best-studied SHR as an Hsp90 client. Comparing the screening results for the different cell lines suggested marked differences in the maturation of GR in different cell lines. Since SHRs dysregulation has been implicated in mental illness, lymphoma, leukemia, breast cancer, prostate cancer, ovarian cancer, lung cancer and many more, testing the requirements of SHR maturation in different cell lines will be interesting to unravel potential Achilles heels for therapy (Miller and Langdon, 1997; Ahmad and Kumar, 2011; Criado-Marrero et al., 2018). In particular, testing type 1 and type 2 cancer cell lines, in which the epi-chaperome is distinctly organized will be interesting to understand how this rewiring affects Hsp90 client maturation (Rodina et al., 2016.

4.3 The Hsp90 Co-Chaperone NudC

In the course of this work, we performed functional genomics screening for SHR modulators using CRISPRi technology (Section 4.2). The results indicated that NudC may function as an Hsp90-dependent regulator of SHRs. Furthermore, NudC has been found in a high-throughput interactome study as a potential interactor of Hsp90, but also the Hsp70 system (Taipale et al., 2014). Few studies have investigated NudC regarding its interaction with Hsp90, but how NudC affects the Hsp90 system and client maturation is entirely unknown (Zhu et al., 2010; Zheng et al., 2011). Here, we set out to characterize the role of NudC in client maturation and how it interacts with Hsp70 and Hsp90. NMR experiments were performed by Dr. Florent Delhommel (Prof. Dr. Michael Sattler's lab, TU Munich, Germany) or by Dr. Ofrah Faust (Prof. Dr. Rina Rosenzweig's lab, Weizmann Institute of Science, Israel) as indicated in the respective sections. Single molecule FRET measurements were performed together with Ganesh Agam (Prof. Dr. Don Lamb's lab, LMU, Germany).

First, to evaluate the role of NudC for the maturation of Hsp90 clients *in vivo*, the effects of NudC on GR for individual co-chaperone knockdowns as presented in section 4.2) were revisited. Importantly, NudC knockdown significantly decreased GR activity in the K562-GRWT cell line, while it increased GR activity in the Hek293-GRWT cell line, proving that NudC affects GR maturation *in vivo* (Figure 45A). Despite the different effects on GR activity, knockdown of NudC strongly reduced viability by about 60% to 80% after 12 days in the Hek293 and the K562 cell lines stressing the importance of NudC for cellular viability (Figure 45B). Together, these results indicate that NudC affects GR activity and viability in *in vivo* and prompted us to investigate the molecular mechanism of NudC function in more detail.

4.3.1 The Interaction of NudC with Hsp40, Hsp70 and Hsp90

4.3.1.1 NudC interacts with the Hsp40/Hsp70 and Hsp90 systems *in vivo*

To test directly whether NudC interacts with Hsp70 and Hsp90, the interactome of NudC was validated in the cellular context by pulldown analysis in cooperation with Moritz Mühlhofer (Prof. Dr. Johannes Buchner's lab, TU Munich, Germany) (Figure 46). Hek293 cells were transiently transfected with NudC-GFP or GFP alone and subjected to GFP-pulldown followed by mass spectrometry. Significant interactions were found between NudC and DNAJA1 and DNAJB1 as well as the Hsp70s HSPA1B and HSPA4L. Additionally, Hsp90β (HSP90AB1) and Sgt1 (SUGT) were identified as interaction partners. Gene ontology enrichment analysis of the hits obtained from NudC pulldown indicated a significant enrichment in the 'protein folding' category (FDR < 0.00074). In summary, pulldown analysis confirmed that NudC interacts with the Hsp70 and Hsp90 systems *in vivo* and may be part of the cellular protein folding machinery.

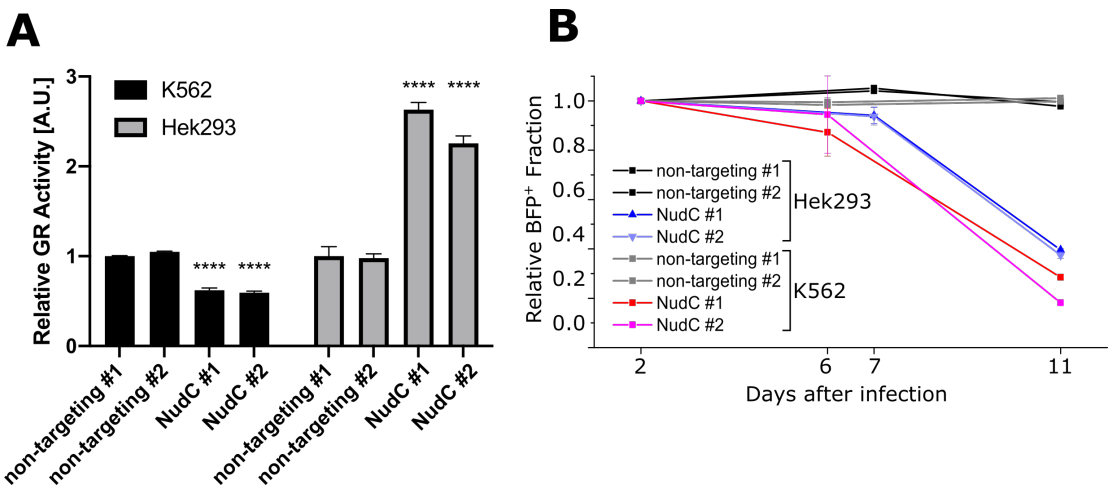

FIGURE 45 | **The Effect of NudC on Client Maturation *In Vivo*.**
A *In vivo* GR activity in the Hek293 and K562 cell lines. NudC was knocked down using CRISPRi with two different sgRNAs and GR activity was measured 24 h after induction with hormone using flow cytometry. Data extracted from Figure 43. Shown are the means ± SD of three replicates. Significance was evaluated by t-testing (n.s.≥0.05; * p≤0.05; ** p≤0.01; *** p≤0.001, *** p≤0.0001)
B Effect of NudC depletion on viability. The viability data from Figure 43 was extracted to highlight the effect of NudC depletion on viabiltiy. Shown is the fraction of BFP^+ cells, representing the cells carrying the sgRNA-expressing plasmid. Shown are the means ± SD of three replicates.

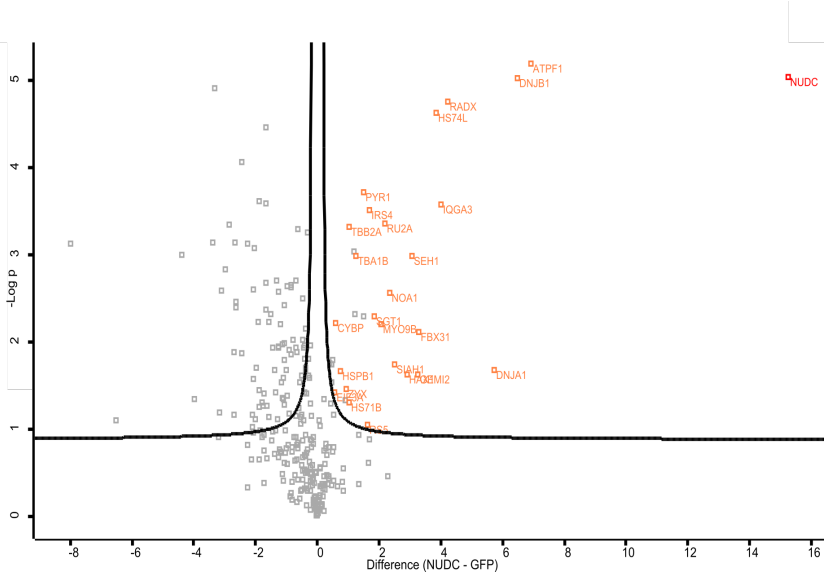

FIGURE 46 | **The Interactome of NudC.**
In vivo pulldown of NudC. NudC-GFP or GFP alone were transiently transfected into Hek293 cells. Cells were harvested and NudC was pulled down using GFP-binding beads. After on-bead tryptic digestion, the samples were subjected to LC-MS/MS. LC-MS/MS was performed by Moritz Mühlhofer (TU Munich). Genes enriched in the NudC-GFP sample over the GFP control are marked in orange.

4.3.1.2 The Domain Architecture of NudC

In a previously published study using a combined approach of NMR, crystallography and structure prediction NudC was separated into an N-terminally unstructured region (residues 1-50), followed by a coiled-coil-containing region (residues 50-141) mediating dimerization, a CS domain (residues 158-274) that shares homology with p23 and a C-terminal stretch potentially structured as two short α-helices (residues 275-331) (Figure 47) (Zheng et al., 2011). To analyze the structure of NudC in more detail, truncation constructs of NudC were analyzed by NMR (Figure 47). For that purpose, the truncation mutants NudC$^{1-96}$, NudC$^{1-141}$, NudC$^{158-274}$ and NudC$^{158-331}$ were generated to assign backbone chemical shifts. Chemical shifts were then used to predict secondary structure elements using Talos-N (Shen and Bax, 2013).

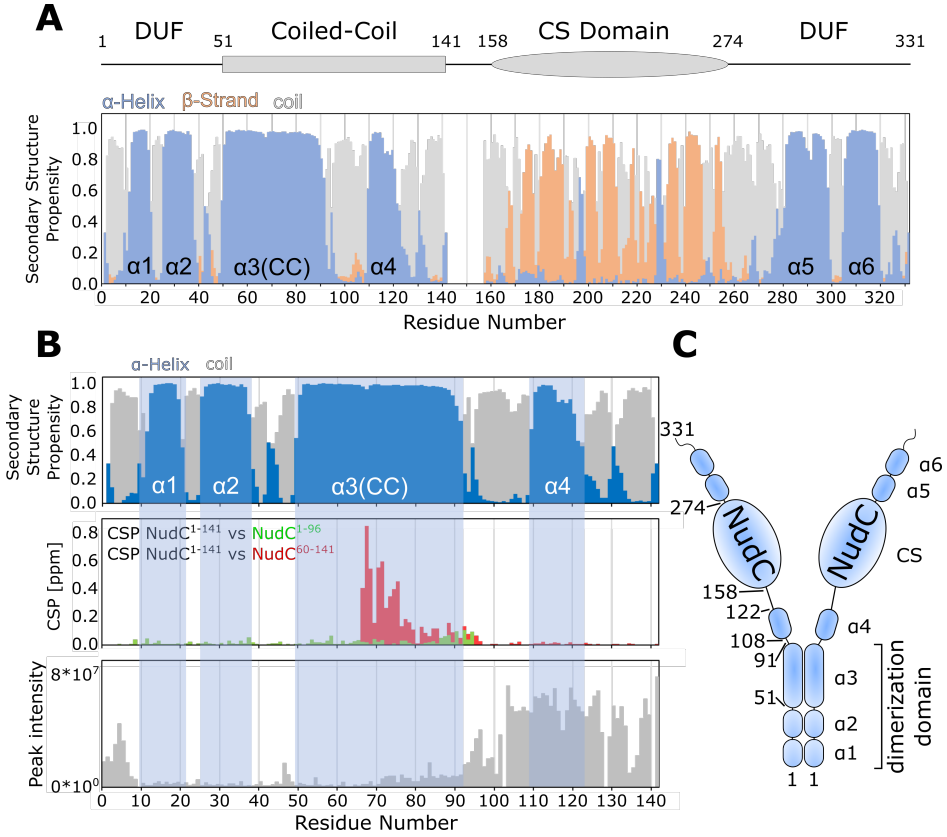

FIGURE 47 | **The Domain Architecture of NudC.**
A Secondary structure propensity of NudC. The domain architecture derived from a previous study (Zheng et al., 2011) is shown on the top. The Talos-N secondary structure prediction based on the backbone chemical shifts is shown on the bottom (Data acquired by Florent Delhommel, TU Munich). [DUF = Domain of unknown function].
B Elucidation of the dimerization domain. The chemical shift perturbations between the dimerization-competent NudC$^{1-141}$ truncation and the dimerization-competent NudC$^{1-96}$ or the dimerization-impaired NudC$^{60-141}$ truncations are shown in the middle. The peak intensities in the NudC$^{1-141}$ mutation are shown in the bottom (Data acquired by Florent Delhomme,l TU Munich).
C Schematic representation of the NudC domain architecture.

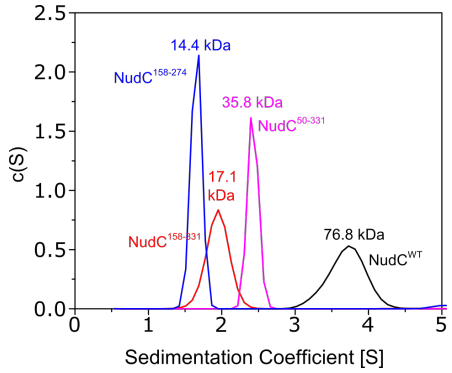

FIGURE 48 | **Dimerization of NudC.**
The role of the N-terminal helices in NudC dimerization. The indicated NudC constructs (15 µM monomer concentration) were analyzed by absorption aUC.

Secondary structure prediction suggested two short helical regions in the N-terminal domain of unknown function (DUF), between residues 1 and 50 (Figure 47A,C). A longer helix was found between residues 51 and approximately 91, presumably forming the coiled-coil domain. Additionally a short helix, designated as α4 was predicted between residues 108 and 122. The CS domain between residues 158 and 274 is composed mainly of β-sheets consistent with the crystal structure of the NudC CS domain (Zheng et al., 2011). In the C-terminal stretch two α-helices were predicted (α5 and α6), confirming previous findings (Zheng et al., 2011). Since the previously suggested dimerization region contained two helices (α3 and α4), the dimerization of NudC was investigated in more detail. To that end, the chemical shift perturbations (CSPs) between the NudC$^{1-96}$ and NudC$^{60-141}$ mutants and the NudC$^{1-141}$ construct were analyzed (Figure 47B). While NudC$^{1-96}$ and NudC$^{1-141}$ mutant are capable of dimerization based on the T_1/T_2 ratios, the NudC$^{60-141}$ mutant is dimerization-deficient (data not shown). Importantly, the α3 region displayed significant CSPs, whereas no CSPs were found in the α4 region, suggesting that the α3, but not the α4 helix is involved in NudC dimerization (Figure 47B). When peak intensity was analyzed, similar intensities were observed for the α1, α2 and α3 helices, but α4 had much higher peak intensity (Figure 47B). This suggests that α1, α2 and α3 rotate as one unit in solution producing the same relaxation time. Consequently, dimerization seems to be mediated not only by the α3 helix but also by the α1 and α2 helices, implicating that the dimerization region is longer than previously found (Figure 47C) (Zheng et al., 2011). Of note, helix α4 is independent of the dimerization region.

To confirm these findings, NudC^{WT} and NudC$^{50-331}$ were analyzed by absorption aUC, showing that NudC^{WT} forms dimers of about 80 kDa, whereas NudC$^{50-331}$ sedimentation suggested a molecular mass of about 35 kDa, consistent with the mass of a monomeric species (Figure 48). This suggests that the helices α1 and α2 are involved in NudC dimerization supporting the NMR findings.

To confirm the secondary structure predictions based on backbone chemical shifts, NudC was also analyzed by CD spectroscopy (Figure 49). With a local minimum at

about 220 nm and a global minimum at approximately 207 nm, CD spectroscopy indicated a substantial α-helical content in NudC (Figure 49). Secondary structure prediction using the DiochroWeb tool (Whitmore and Wallace, 2008) suggested a α-helical content of 28% along with 19% β-sheet and 53% random coil content, matching the Talos-N predictions obtained from NMR experiments.

In summary, NMR and aUC analysis revealed the presence of three N-terminal helices mediating dimerization and a fourth helix that functions independently in the N-terminal region of NudC. The β-sheet-rich CS domain is followed by two two α-helices in the C-terminal region. The schematic domain architecture of NudC is summarized in Figure 47C.

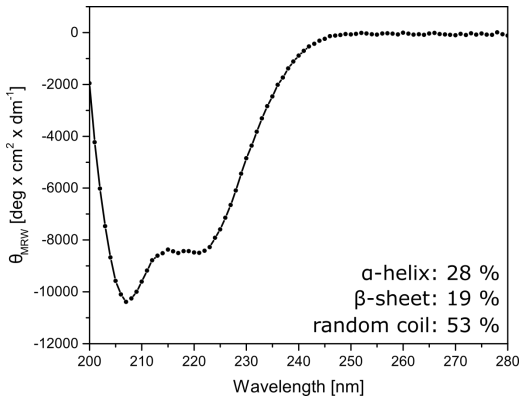

FIGURE 49 | **The Secondary Structure Composition of NudC.**
The secondary structure of NudC determined by circular dichroism (CD) spectroscopy. NudC was measured by Far-UV CD spectroscopy at a concentration of 0.3 mg mL^{-1}. The spectrum is representative of five averaged traces. The mean residue ellipticity was calculated and fed into the DichroWeb tool using the K2D algorithm to predict the secondary structure composition.

4.3.1.3 NudC Interacts with Hsp90

Next, we sought to analyze the binding of NudC to Hsp90 in more detail. To that end, NudC was specifically labeled with the Atto488 fluorescent dye on Cys188 (NudC*) and analyzed by aUC (Figure 50, 51). AUC measurement confirmed the homodimeric nature of NudC forming a monomer peak at about 2.5 S corresponding to approximately 45 kDa and a dimer peak at about 3.6 S representing approximately 84 kDa (Figure 50). Dimerization was very efficient with more than 50% of the dimer population formed at a concentration of 50 nM.

To test, whether NudC binds Hsp90, the sedimentation of NudC* was analyzed in combination with Hsp90α in the presence of different nucleotides (Figure 51A). NudC* bound to Hsp90α in all nucleotide states, suggesting that binding is not restricted to a specific Hsp90 conformation (Figure 51A). Binding was also possible to Hsp90β with comparable results (data not shown). The binding affinity of NudC* to Hsp90α was determined to be about 650 nM, indicating a tight binding similar to other known Hsp90 co-chaperones (Figure 51B) (Wandinger et al., 2006; Onuoha et al., 2008; Koulov et al., 2010).

To assess the stoichiometry of NudC binding to Hsp90, binding was analyzed by SEC-MALS (Figure 51C). Despite the high affinity of the Hsp90-NudC interaction, complex formation in SEC-MALS was only possible under mild crosslinking conditions. The size of the NudC dimer was determined as 85 kDa, similar to the molecular weight obtained by aUC. The Hsp90α dimer eluted earlier with a calculated size of 180 kDa matching the anticipated Hsp90 dimer size. The molecular weight of the Hsp90:NudC complex was found to be about 270 kDa hinting at a 1:1 binding stoichiometry. In contrast to earlier findings, no effect of NudC on the Hsp90 ATPase activity was found (Figure 51D) (Zhu et al., 2010).

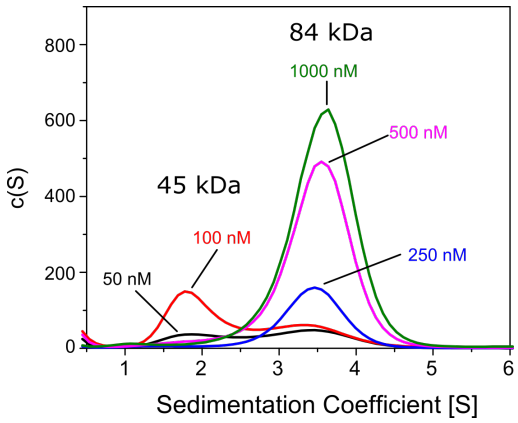

FIGURE 50 | **NudC Preferentially Forms Dimers.**
AUC experiment examining NudC dimerization. Atto488-labeled NudC (NudC*) was used at the indicated concentrations and analyzed by aUC.

To explore the interaction site between NudC and Hsp90, different NudC truncation mutants were tested regarding their ability to displace NudC* from Hsp90α (Figure 51E). Addition of excess NudC^{WT} displaced approximately 60% of NudC* from Hsp90 (Figure 51E). By contrast, addition of the NudC$^{1-141}$ truncation mutant comprising the α1, α2 and α3 helices involved in dimerization as well as the independent α4 helix, did not displace NudC* from Hsp90. However, the isolated CS domain (NudC$^{158-274}$) displaced NudC* from Hsp90, indicating that the CS domain of NudC interacts with Hsp90. The C-terminal tail of NudC harboring the α5 and α6 helices slightly increased the binding of the CS domain, suggesting that the C-terminal helices play a minor role in the interaction with Hsp90. Dimerization of NudC increased the ability to displace NudC* from Hsp90, confirming the finding that NudC binds Hsp90 as a dimer. Together, these results show that NudC binds Hsp90 mainly via its CS domain.

Next, we sought to study the interaction site of NudC on Hsp90. Using domain constructs of Hsp90, aUC showed that NudC binds the Hsp90^{NTD-MD} and the Hsp90^{MD-CTD}, suggesting a binding site in the Hsp90 MD (Figure 52). Using full-length, deuterated Hsp90 with $^{13}CH_3$ labeling of Ile and Met residues, the interaction between NudC and Hsp90 was probed by NMR (Figure 53). Addition of NudC to Hsp90 induced CSPs predominantly in the Hsp90 MD with few CSPs found also in the CTD, while no Ile/Met was affected in the NTD (Figure 53A-C). CSPs occurred

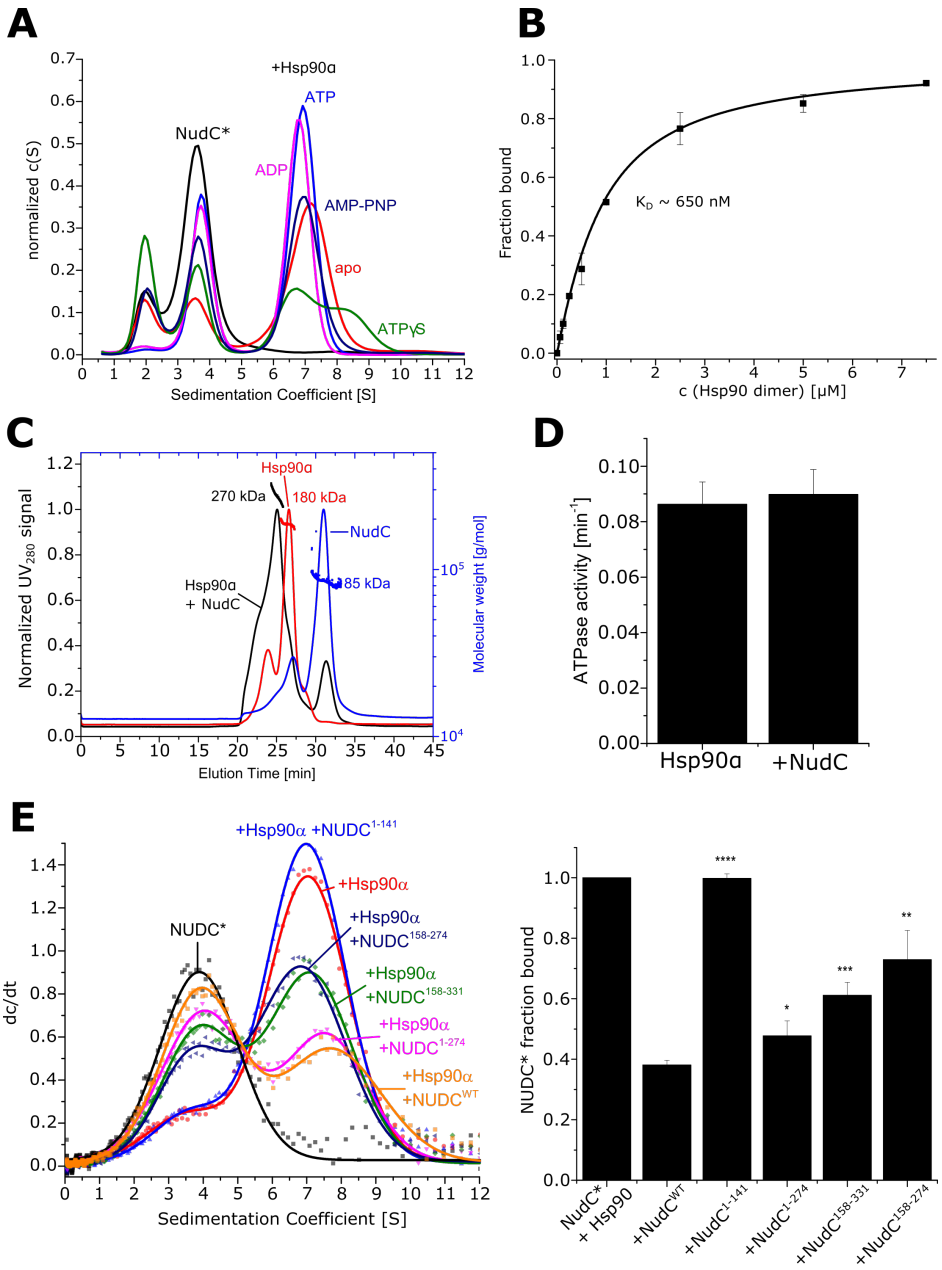

FIGURE 51 | **NudC Binds Hsp90 With High Affinity.**
A Nucleotide-dependence of Hsp90 binding. The binding of NudC* (500 nM) to Hsp90α (2 µM dimer concentration) in the presence of the indicated nucleotides (2 mM) was analyzed by aUC.
B Binding affinity analysis. The binding affinity of NudC* (500 nM) with the indicated Hsp90α concentrations in the absence of nucleotides was analyzed by aUC. Data points were fitted using a quadratic fit model.
C Stoichiometry of NudC binding. The binding of NudC to Hsp90α was analyzed by size exclusion chromatography coupled to multi-angle light scattering (SEC-MALS). NudC and Hsp90 were used at a concentration of 35 µM and crosslinked with 0.025% glutardialdehyde for 5 min at 37 °C.
D NudC effect on the Hsp90 ATPase. The effect of NudC (6 µM) on the ATPase activity of Hsp90α (1.5 µM dimer concentration) was tested with a regenerative ATPase assay. Data is representative of three replicates.
E Mapping of the Hsp90 binding site on NudC. The Hsp90-binding site on NudC was analyzed by aUC. NudC* (500 nM) was bound to Hsp90α (2 µM dimer concentration). The indicated unlabeled NudC fragments were added in molar excess (10 µM). The bar chart depicts the fraction of bound NudC*. Data are representative of three biological replicates.

in two clusters, one located on the β1-β2 interface and the α2 helix of the Hsp90 MD, and a second cluster at the MD/CTD interface (Figure 53C). The CSPs located at the MD/CTD surface may either be caused by weak contacts or by structural changes in the Hsp90 dimer conformation.

For a more comprehensive analysis of the interaction, NudC$^{155-274}$ was added to the ^{15}N-labeled Hsp90 MD (Figure 53D). Importantly, the induced CSPs confirmed the involvement of the β1-β2 loop and the α2 helix and additionally revealed that the β5-α2 loop is involved forming a continuous binding surface (Figure 53E). Additional, smaller CSPs were observed at the MD/CTD surface, matching data from $^{13}CH_3$-IM Hsp90 experiments. To confirm the central role of the continuous surface at the N-terminal region of the Hsp90 MD, the Hsp90$\beta^{322-328GS}$ mutant was generated in which the β5-α2 loop was exchanged by a GS linker and binding was analyzed by aUC (Figure 54). While Hsp90β readily bound to NudC*, Hsp90$\beta^{322-328GS}$ did not associated with NudC, supporting the role of these Hsp90 residues in the binding of NudC (Figure 54). Together, these findings indicate that the primary NudC binding site is located at the N-terminal region of the Hsp90 MD.

In conclusion, *in vitro* analysis of the Hsp90:NudC interaction revealed that NudC preferentially forms stable dimers and binds Hsp90 at high affinity via its CS domain. The binding site on Hsp90 was located to the N-terminal region of the MD on a surface that is solvent-exposed in the open and closed state, explaining the nucleotide-independent binding of NudC to Hsp90.

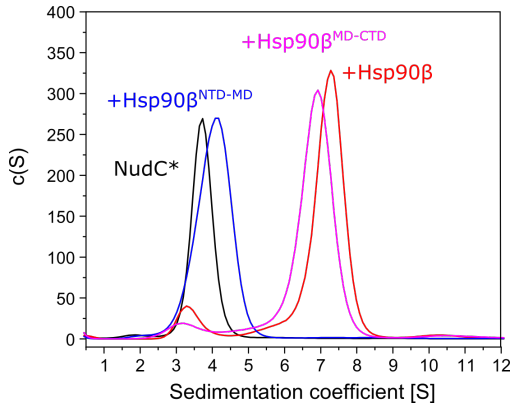

FIGURE 52 | **NudC Interacts With the Hsp90 MD.**
Binding of NudC to Hsp90 domain constructs. The binding of the Hsp90β^{NTD-MD} and Hsp90β^{MD-CTD} (2 µM dimer concentration) to labeled NudC (500 nM) was monitored by aUC in the absence of nucleotides.

4.3.1.4 NudC Interacts with Hsp40

As mass spectrometric analysis of NudC pulldowns indicated that NudC associates also with the Hsp40/Hsp70 system, next, the binding of NudC to Hsp40 and Hsp70 was analyzed (Figure 55). Surprisingly, NudC did not associate with Hsp70 in the presence or absence of ATP (Figure 55A). However, NudC efficiently bound to Hsp40. Notably, oligomerization of the NudC:Hsp40 complex was possible if Hsp40

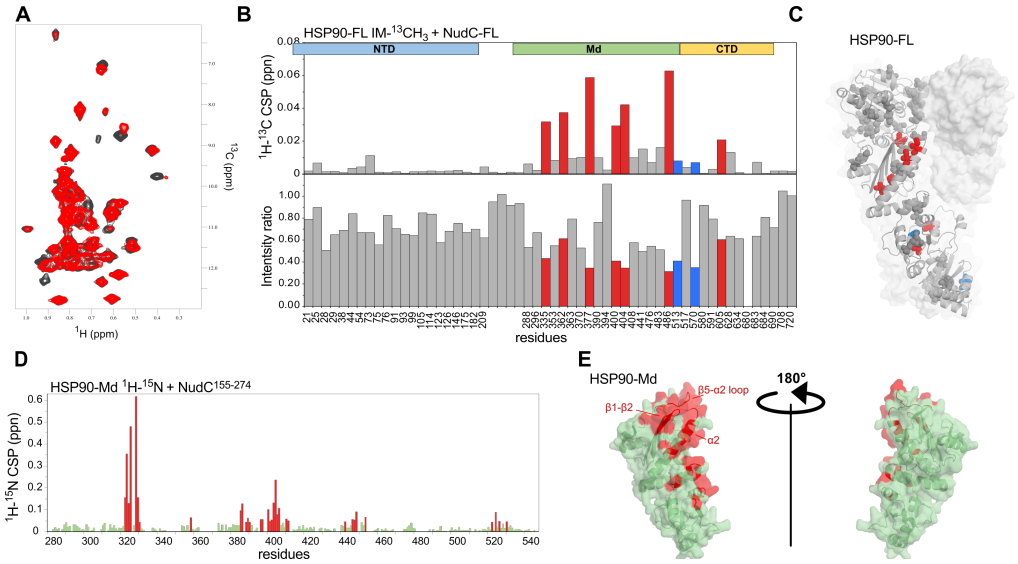

FIGURE 53 | **The NudC Binding Site on Hsp90.**
A Isoleucine and methionine $^{13}CH_3$-labeled Hsp90β was analyzed in the absence and presence of unlabeled NudC by ^{1}H-^{13}C methyl-TROSY (**A**). (Data acquired and analyzed by Florent Delhommel, TU Munich)
B Chemical shift perturbations (CSPs) and intensity changes of $^{13}CH_3$ IM-labeled Hsp90β resonances after addition of unlabeled NudC. In the top and bottom panels the CSPs and the intensity changes for Ile/Met residues along the Hsp90 sequence are shown. Red bars indicate significant CSPs (>0.02) and blue bars indicate significant intensity changes (<0.45) without significant CSPs. (Data acquired and analyzed by Florent Delhommel, TU Munich)
C Mapping of CSPs on Hsp90. The significant CSPs from (**B**) were mapped on the human Hsp90 structure (PDB: 5FWK). Color coding as in (**B**). (Data acquired and analyzed by Florent Delhommel, TU Munich).
D CSPs of Hsp90-MD ^{1}H-^{15}N resonances after the addition of NudC$^{155-274}$. The CSPs along the Hsp90 MD sequence are shown. (Data acquired and analyzed by Florent Delhommel, TU Munich)
E Mapping of CSPs on the Hsp90-MD. The CSPs from (**D**) were mapped on the human Hsp90 MD structure (PDB: 5FKW). (Data acquired and analyzed by Florent Delhommel, TU Munich)

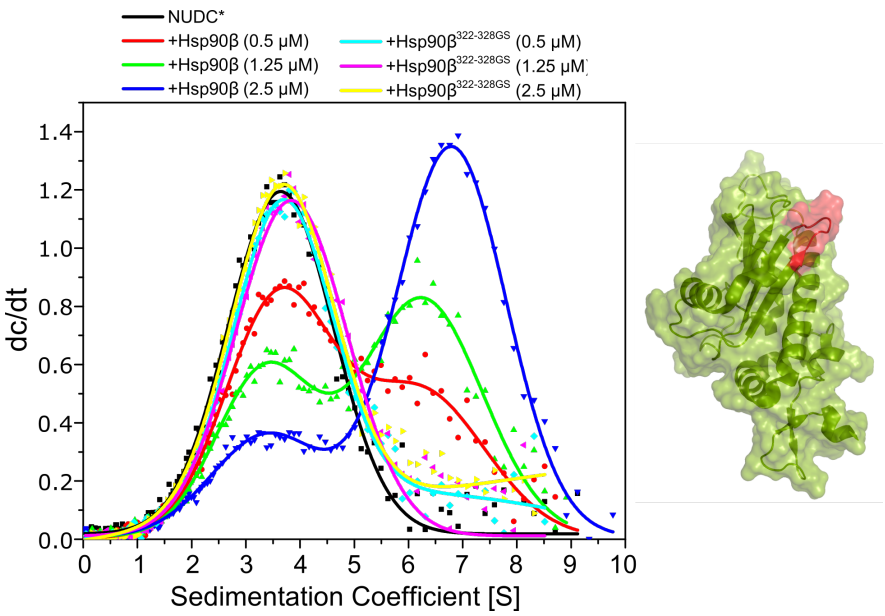

FIGURE 54 | **The Role of the β5-α2 Loop of Hsp90 in NudC Binding.**
Binding of NudC to the Hsp90$\beta^{322-328GS}$ mutant. The binding of NudC* (500 nM) to Hsp90β^{WT} or Hsp90$\beta^{322-328GS}$ at the indicated concentrations was tested by aUC in the absence of nucleotides. The mapping of the mutated β5-α2 loop (red) on human Hsp90 (PDB: 5FWL) is depicted on the right.

was added in excess (Figure 55A). Hence, each monomer of the NudC dimer seems to interact with a single monomer of a Hsp40 dimer, making oligomer formation with an Hsp40$_n$:NudC$_n$ stoichiometry possible. The binding affinity of Hsp40 to NudC was estimated to be approximately 500 nM, since at that concentration about 50% of Hsp40 were bound to NudC. In the presence of Hsp40, formation of a trimeric NudC:Hsp40:Hsp70 was possible, suggesting that Hsp40 does not bind to NudC via the J-domain, which is the main binding site between Hsp40 and Hsp70 (Figure 55B). Importantly, the binding of NudC to Hsp40 could also be confirmed using HPLC and *in vitro* pulldown with His$_6$-tagged NudC (Figure 55C and data not shown). Additionally, the interaction of NudC with Hsp40 was conserved between yeast and humans, since NudC also readily bound human DNAJB1 (Figure 55D). Together, these results provide evidence that NudC associates with the Hsp40/Hsp70 system by interacting with Hsp40 and that the interaction with Hsp40 occurs independent of the Hsp40 J-domain.

To better understand which part of NudC mediates the interaction with Hsp40, the competition of NudC truncations with NudC* bound to Hsp40 was analyzed by aUC (Figure 55E). While NudC$^{1-141}$ and NudC$^{1-274}$ readily displaced labeled NudC* from Hsp40 similar to NudC^{WT}, neither the NudC$^{158-274}$ nor the NudC$^{158-331}$ mutant were able to displace NudC* (Figure 55E). Interestingly, deletion of the α1 and α2 helices from NudC in the NudC$^{50-331}$ mutant did not affect binding to Hsp40, suggesting that the region between residues 51-141 mediate Hsp40 binding.

To obtain detailed information about the binding mechanism of NudC to Hsp40, ^{15}N-NudC was subjected to NMR analysis together with human DNAJB1 (Figure

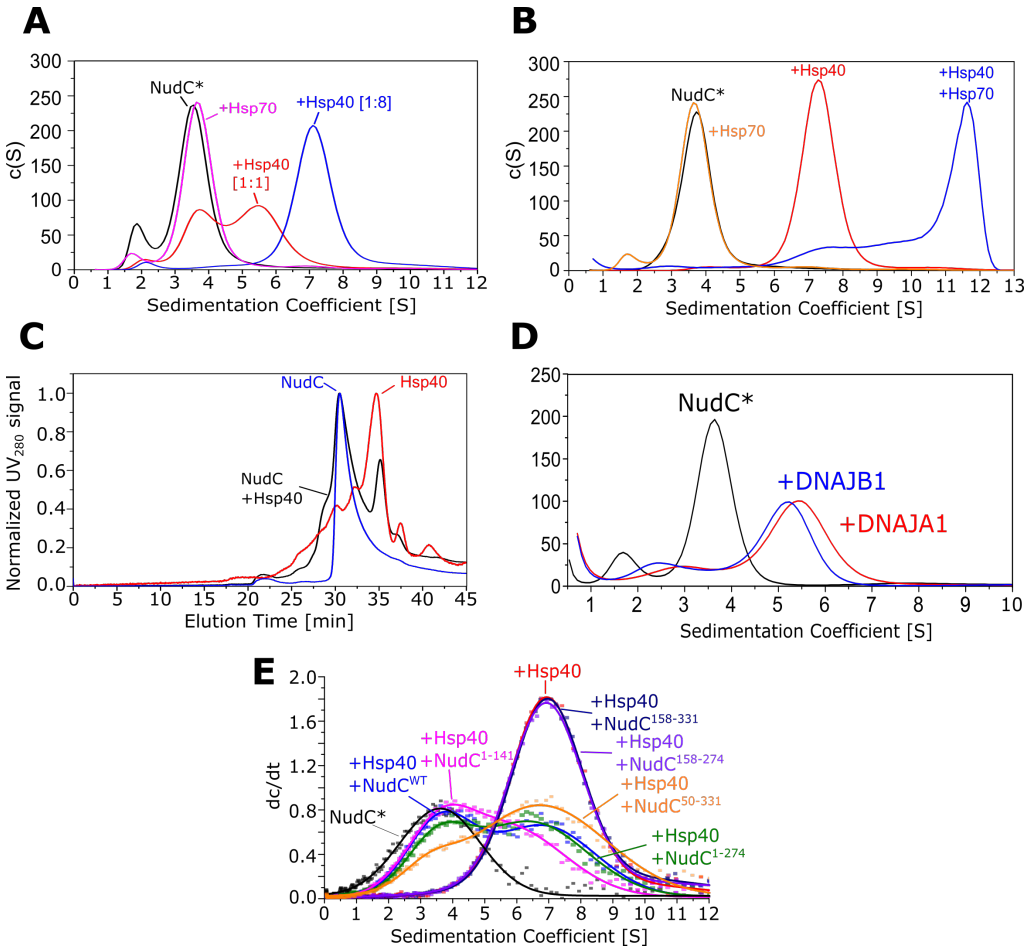

FIGURE 55 | **The Interaction Between NudC and Hsp40.**
A AUC analysis of the NudC:Hsp40 interaction. NudC* (500 nM) was analyzed by aUC in the presence of Ydj1 (Hsp40) in the indicated ratios. Hsp70 was used at a concentration of 3 µM in the presence of 2 mM ATP.
B Formation of a trimeric NudC:Hsp40:Hsp70 complex. NudC* (500 nM) was measured in the presence of 4 µM Ydj1 (Hsp40), 3 µM Hsp70 and 2 mM ATP by aUC.
C HPLC analysis of the NudC:Hsp40 interaction. The binding of NudC to Hsp40 was analyzed by HPLC. NudC and Ydj1 were used at a concentration of 35 µM.
D NudC binding to the human Hsp40 homolog DNAJA1 and DNAJB1. The binding of NudC* (500 nM) to DNAJB1 (4 µM) and Hsp90 (2 µM dimer concentration) was analyzed by aUC in the presence of 2 mM ATP.
E Mapping of the Hsp40-interacting domain in NudC. NudC* (500 nM) was bound to Hsp90 (2 µM dimer concentration) and displacement of NudC* by excess amount of the shown NudC fragments (10 µM) was monitored by aUC.

56A). Analysis of the peak intensity showed that addition of DNAJB1 to ^{15}N-NudC did not affect helices α1-α3 involved in NudC dimerization, showing that the binding motif for Hsp40 lies outside of the dimerization domain. By contrast, the peak intensity of the α4 helix and flanking residues was strongly affected by DNAJB1 addition, indicating that the NudC residues 101-128 mediate Hsp40 binding. Testing the conservation of this NudC region among homologs using the ConSurf tool revealed several strongly conserved residues, including several hydrophobic residues (Figure 56B). Introduction of the I104A and L107A mutations into NudC entirely abolished Hsp40 binding, confirming the proposed Hsp40 binding site in NudC (Figure 56B). Together, these results show that NudC binds Hsp40s via helix α4 and the flanking regions and the interaction is governed by hydrophobic residues.

Interestingly, the residues 101-109 from NudC display significant similarity with the Hsp70 IEEVD motif (Figure 56B). While the IEEVD motif of Hsp70 primarily interacts with TPR-domain-containing proteins, secondary contacts of Hsp70 with Hsp40 via the IEEVD binding independent of the Hsp40 J-domain have been reported (Freeman et al., 1995; Aron et al., 2005; Li et al., 2006; Yu et al., 2015b; Jiang et al., 2019; Rosenzweig et al., 2019). This prompted us to investigate where NudC interacts with Hsp40. To this end, ^{13}C-Ile labeled DNAJB1 was analyzed by NMR in the presence of NudC (Figure 56C). CSPs occurred mainly in the G/F linker and the CTD-I region confirming that NudC interacts independently of the J-domain with Hsp40 (Figure 56C). Interestingly, the NudC binding site on DNAJB1 overlaps with the binding of a C-terminal IEEVD-containing peptide of Hsp70 (Figure 4D, 56C) (Suzuki et al., 2010). Since the CTD-I and CTD-II regions are also involved in client binding, NudC may modulate both Hsp70 and client interactions with Hsp40. In conclusion, these data suggest that NudC binds the same region on Hsp40 as the C-terminal Hsp70 IEEVD motif, hinting at a potential competition of NudC with Hsp70 for Hsp40 binding.

In summary, analysis of the interaction between NudC and Hsp40/Hsp70 system revealed that NudC binds Hsp40 but does not form a direct interaction with Hsp70. The binding between Hsp40 and NudC occurs via helix α4 of NudC and the CTD-I region of Hsp40 overlapping with the binding site of the Hsp70-IEEVD motif.

4.3.2 The Role of NudC in Client Transfer Complexes between Hsp70 and Hsp90

In vitro and *in vivo* analysis of the NudC interactome revealed that NudC interacts stably with Hsp90 and the Hsp40/Hsp70 system. Thus, we sought to test whether NudC is also present in mixed complexes of Hsp40/Hsp70 and Hsp90.

First, the ability of NudC to bridge the Hsp40/Hsp70 system to the Hsp90 machinery was probed by aUC (Figure 57). As presented above, NudC readily interacted with Hsp40 and was found in NudC:Hsp40:Hsp70 complexes (Figure 57A). Intriguingly, also a NudC*:Hsp40:Hsp90 complex could be formed, confirming the separate interaction surfaces of Hsp40 and Hsp90 on NudC and implicating a link

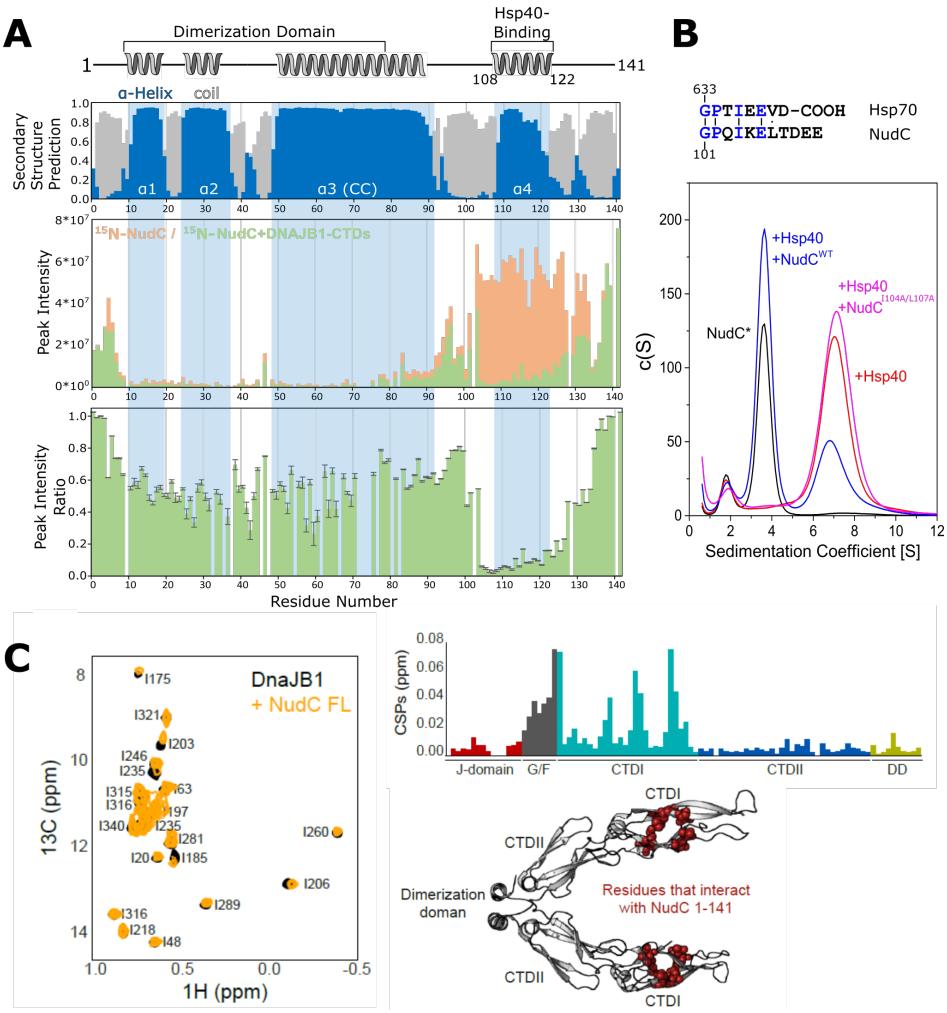

FIGURE 56 | **Structural Analysis of the Interaction Between NudC and Hsp40.**
A NMR analysis of the Hsp40-binding site in NudC. ^{15}N NudC was analyzed alone and in the presence of DNAJB1^{CTD-DD}, which lacks the J-domain and G/F linker. The Talos-N secondary structure prediction from Figure 47 is shown in the top panel, the peak intensities and peak intensity ratios are shown in the bottom panels. (Data acquired and analyzed by Florent Delhommel, TU Munich).
B Mutagenesis of Hsp40-binding residues in NudC. NudC* (500 nM) was bound to Ydj1 (Hsp40, 4 µM) and NudC^{WT} or NudC$^{I104A/L107A}$ was added in excess (10 µM). The sedimentation coefficient distribution obtained by aUC is shown.
C NMR analysis of the NudC-interacting site in Hsp40. ^{13}C-Ile labeled DNAJB1 was measured alone or in the presence of NudC^{WT}. The ^{1}H-^{13}C HMQC spectrum is shown. The CSPs were plotted against the DNAJB1 residues. The interacting residues (red) are shown as spheres in the structure of DNAJB1 (PDB: 3AGY). (Data acquired and analyzed by Ofrah Faust, Weizmann Institute of Science).

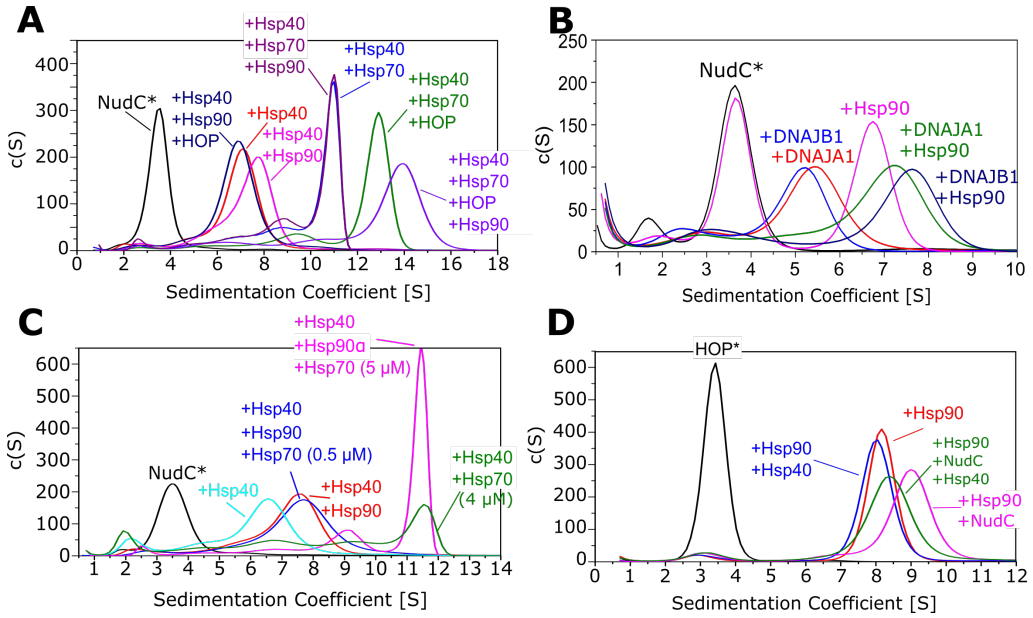

FIGURE 57 | **NudC is Present in Hop-Bridged Hsp70:Hsp90 Complexes.**
A Binding of NudC to the Hsp70:Hop:Hsp90 complex. The sedimentation coefficient distribution of complexes containing NudC* (500 nM), Ydj1 (Hsp40; 4 μM), Hsp70 (3 μM), HOP (6 μM) and Hsp90α (2 μM dimer concentration) acquired by aUC in the presence of 2 mM ATP is shown.
B Formation of a trimeric NudC:Hsp90:DNAJA1/DNAJB1 complex. The formation of a trimeric complex between NudC* (500 nM), Hsp90 (2 μM dimer concentration) and DNAJA1/DNAJB1 (4 μM) was followed by aUC in the presence of 2 mM ATP.
C NudC binds either Hsp40/Hsp70 or Hsp90 in the absence of Hop. The ability of NudC* to replace Hop in the context of bridging Hsp40/Hsp70 to Hsp90 was tested by aUC. The concentrations were used as in (**A**) or as indicated and measurements were performed in the presence of 2 mM ATP.
D The competition between Hop and NudC for Hsp90 binding. Labeled Hop (Hop*; 500 nM) was analyzed by aUC in the presence of Hsp90 (2 μM dimer concentration), Ydj1 (Hsp40, 4 μM) and NudC (6 μM). The experiment was performed in the presence of 2 mM ATP.

between Hsp40 and Hsp90 mediated by NudC (Figure 57A). The human Hsp40 homologs DNAJA1 and DNAJB1 were also able to form a ternary complex of NudC*, Hsp90 and DNAJA1/B1, suggesting that this interaction is conserved in evolution and independent of the JDP class (Figure 57B).

Since a screening study by the Lindquist lab suggested NudC may function as a bridge between the Hsp70 and Hsp90 system (Taipale et al., 2014), we tested if NudC alone can bridge the two chaperone systems (Figure 57A,C). Importantly, formation of the quaternary NudC*:Hsp40:Hsp70:Hsp90 complex was not possible and resulted in either the NudC*:Hsp40:Hsp70 or the NudC*:Hsp40:Hsp90 complex depending on the molar ratio between Hsp70 and Hsp90 (Figure 57A,C). Yet, addition of Hop resulted in a stable high-molecular weight complex containing NudC*, Hsp40, Hsp70, Hsp90 and Hop. Hence, NudC is part of a client transfer complex between Hsp70 and Hsp90 bridged by Hop.

While Hop binds to the C-terminal MEEVD motif of Hsp90 it also forms secondary contacts with the Hsp90 MD, potentially overlapping with the binding site of NudC. No complex between NudC*:Hsp40:Hsp90 and Hop could be formed (Figure 57A), suggesting competition between NudC* and Hop. To test this hypothesis directly, labeled Hop (Hop*) was bound to Hsp90 leading to a significant shift to approximately 8 S (Figure 57D). Addition of NudC further shifted the complex to 9 S suggesting that the ternary Hop*:Hsp90:NudC complex is possible. Notably, addition of Hsp40 to Hop*:Hsp90:NudC released NudC inducing a reduction of the observed sedimentation coefficient to about 8.4 S. Hence, Hop and NudC:Hsp40 compete for Hsp90 binding.

In summary, NudC directly links Hsp40 to Hsp90 and is part of a complex between Hsp40/Hsp70 and Hsp90 that is bridged via Hop.

4.3.3 The Effect of NudC on the Client Transfer to Hsp90

Since NudC both links Hsp40 to Hsp90 and is part of Hop-bridged Hsp70-Hsp90 complexes, we hypothesized that NudC may affect client transfer from Hsp40/Hsp70 to Hsp90. To test this notion, the GR-LBD was studied as a Hsp90 model client that binds Hsp40/Hsp70 and is known to be transferred to Hsp90 via Hop (Johnson et al., 1998; Pratt et al., 2006; Lorenz et al., 2014; Kirschke et al., 2014). GR-LBD was found to bind to the NudC*:Hsp40 complex as well as the NudC*:Hsp40:Hsp90 complex, while GR-LBD* did not bind NudC directly (Figure 58A,C). This suggests that NudC and GR-LBD interact differently with Hsp40 or that the two monomers of Hsp40 bind NudC and GR-LBD simultaneously. Hence, NudC could recruit client-bound Hsp40 directly to Hsp90, bypassing the Hsp70 system.

To test, whether NudC also affected client bound to Hsp40/Hsp70, GR-LBD* was mixed with Hsp40 and Hsp70 resulting in a high-molecular complex sedimenting at about 16.3 S likely containing several Hsp40 and Hsp70 molecules (Figure 58B). Notably, the binding of GR-LBD* to Hsp40/Hsp70 was inefficient in line with the low affinity of folded client for Hsp40/Hsp70. Surprisingly, addition of NudC to the

complex shifted the sedimentation coefficient to about 7.5 S matching the sedimentation coefficient found for the GR-LBD:Hsp40:NudC complex (Figure 58B). Importantly, this suggests that NudC disrupts the GR-LBD*:Hsp40:Hsp70 complex and releases Hsp70 from this complex, which is in line with the overlapping binding site of NudC and Hsp70-EEVD on Hsp40. To test this hypothesis further, the $NudC^{1-141}$ mutant was added to the GR-LBD*:Hsp40:Hsp70 complex, since it is considerably smaller, but still contains the Hsp40-binding motif (Figure 58D). In line with the previous results, the $NudC^{1-141}$ mutant disrupted the GR-LBD*:Hsp40:Hsp70 complex and formed a species at approximately 6.3 S (Figure 58D). To confirm that Hsp70 is not part of the emerging GR-LBD*:Hsp40:NudC complex and as Hsp70 cannot be labeled efficiently, labeled Hop was mixed with Hsp40, Hsp70 and GR-LBD forming a species at about 14.5 S. The complex was disrupted by the addition of NudC forming a species sedimenting at 8.4 S, matching the S value of a Hop*:Hsp40:Hsp70:NudC complex lacking the GR-LBD (Figure 58E). This indicates that GR-LBD is not bound to Hsp70 when the GR-LBD:Hsp40:Hsp70 is disrupted by NudC. Together, these results show that NudC is capable of recruiting Hsp40-bound client to Hsp90 directly and disrupt Hsp40:Hsp70:client complexes by dissociating Hsp70 from the complex.

Finally, the fate of GR-LBD that was released from Hsp40:Hsp70 by NudC was analyzed in the presence of Hsp90 (Figure 58F,G). GR-LBD* in the presence of Hsp40, Hsp70 and Hsp90 sedimented at about 12.3 S and addition of NudC shifted the complex to about 8.1 S matching the S value found for the GR-LBD*:Hsp40:Hsp90:NudC complex, suggesting that NudC relieves the client of Hsp70 and facilitates the transfer of client to Hsp90. To understand the binding of the GR-LBD* to Hop-bound Hsp90, we first formed a GR-LBD*:Hsp90:Hop species. Addition of NudC and Hsp40 released Hop and produced a complex that matched the sedimentation coefficient of GR-LBD*:Hsp40:Hps90:NudC (Figure 58G). To understand the competition between NudC:Hsp40 and Hop better, the Hop^{TPR2A} fragment was bound to GR-LBD*:Hsp90 (Figure 58H). Notably, addition of Hsp40 and NudC shifted the complex to a higher S-value indicating that the competition between NudC:Hsp40 and Hop lies in the secondary contacts Hop^{WT} forms with the MD of Hsp90, which confirms the mapping of the NudC binding site on Hsp90 (Figure 53).

In summary, analysis of the fate of the model client GR-LBD in client-transfer complexes revealed that NudC may promote the transfer of the GR-LBD to Hsp90 in two ways: (1) NudC may bind client-bound Hsp40 and transfer it to Hsp90, bypassing Hsp70. Alternatively, NudC may disrupt Hsp40:Hsp70:client complexes by competing with Hsp70 for Hsp40 binding and forming a NudC:Hsp40:client complex. This notion is in line with the overlapping binding sites of Hsp70-IEEVD and NudC in the Hsp40 CTD-I. (2) The Hsp40:Hsp70:client complex may be recruited to Hsp90 via Hop and NudC then facilitates the release of Hsp70 and promote transfer to Hsp90. In both cases, release of Hsp70 by NudC presumably brings the client into a conformation that is closer to the native conformation which is preferentially bound by Hsp90.

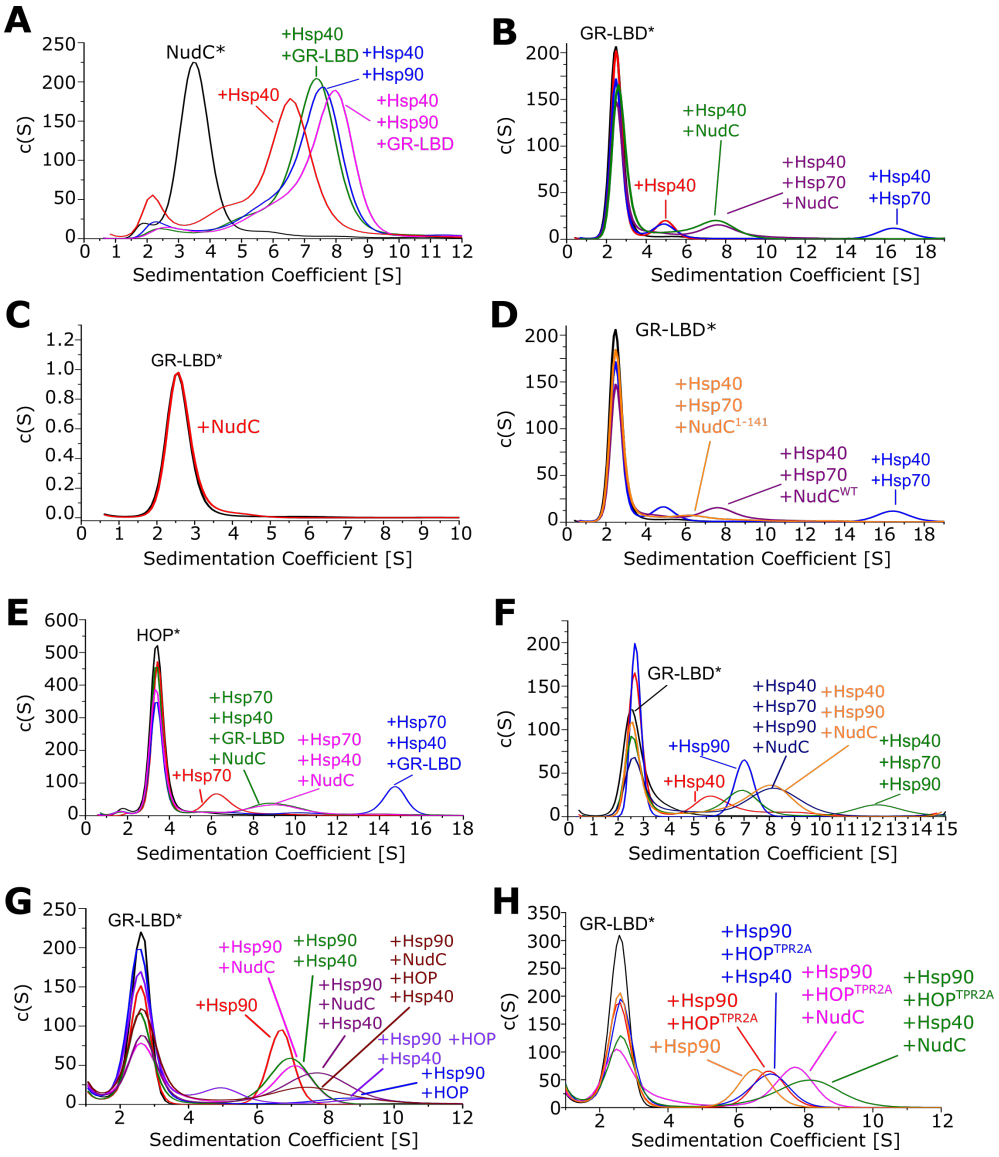

FIGURE 58 | **NudC Disrupts the Formation of Hsp70:Hsp40:Client Complexes.**
A - **G** Fate of the GR-LBD in NudC-containing complexes of the Hsp40/Hsp70 and Hsp90 systems. The formation of complexes of GR-LBD with different chaperone complexes was analyzed by aUC. Shown are the sedimentation velocity distributions. Labeled proteins (marked with asterisks) were used at a concentration of 500 nM. Unlabeled species were used at the following concentrations: Ydj1 (Hsp40, 4 µM), Hsp90α (2 µM dimer concentration), Hsp70 (3 µM), NudC (6 µM), GR-LBD (3 µM), Hop (6 µM). All experiments were performed in the presence of 2 mM ATP.

4.3.3.1 The Consequences of NudC for Client Function

Since NudC seems to either directly link Hsp40:client complexes to Hsp90 or release Hsp40 associated to client from Hsp40:Hsp70:client complexes, this begged the question how this affects client maturation. To study the effect of NudC on client activation, an *in vitro* hormone binding assay was employed in which the rebinding of dexamethasone fluorescein (F-Dex) to apo GR-LBD is monitored by fluorescence anisotropy (Figure 59A). Previous work suggested that binding of Hsp40 and Hsp70 partially unfolds the GR-LBD releasing bound hormone, while release of GR-LBD from Hsp40/Hsp70 promotes hormone rebinding (Kirschke et al., 2014).

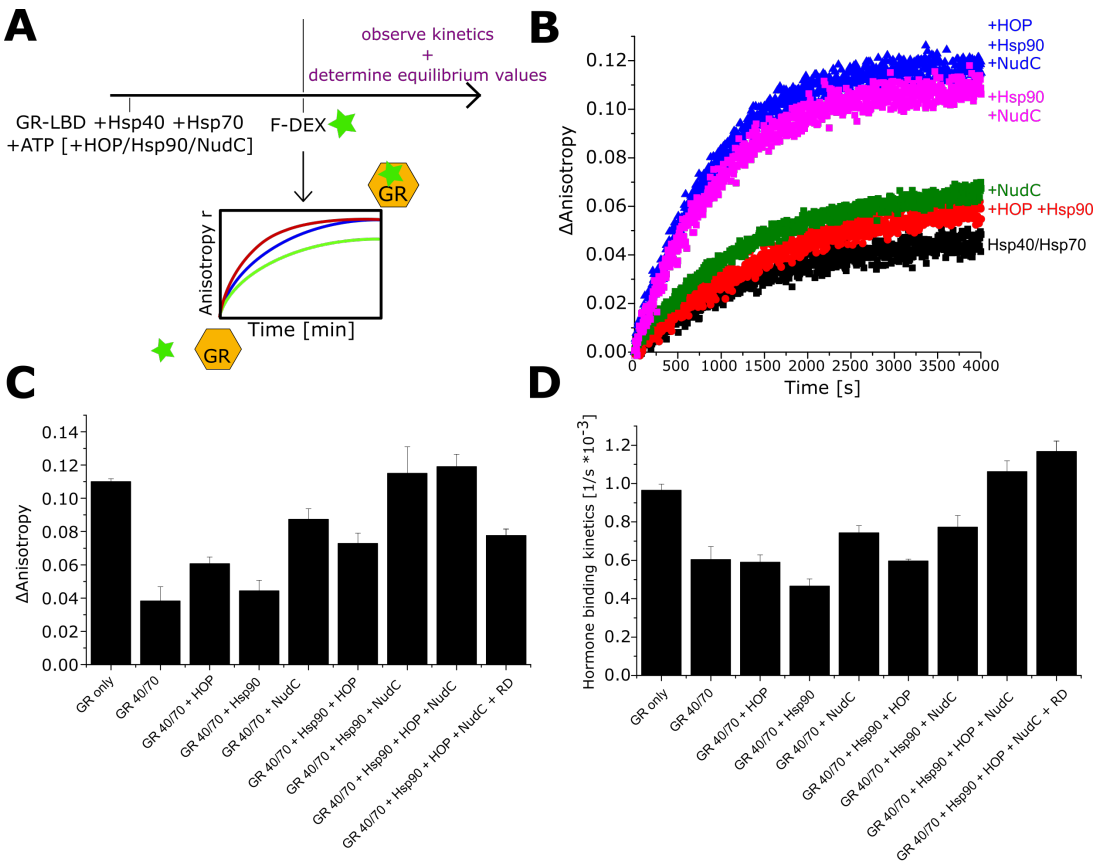

FIGURE 59 | **NudC Promotes GR Maturation *In Vitro*.**
A Hormone-binding to the GR-LBD analyzed by fluorescence anisotropy. A schematic representation of the assay workflow is shown. Apo-GR-LBD is incubated with Hsp40, Hsp70, ATP and co-chaperones for 1 h at room temperature before F-Dex is added to initiate the reaction. Subsequently, the binding kinetics and equilibrium are measured.
B Representative traces showing hormone binding to the GR-LBD. The fluorescence anisotropy values were plotted against the time after addition of F-Dex. The shown data are representatives of three independent replicates.
C Quantification of hormone binding equilibrium values. Equilibrium binding of F-Dex to GR-LBD as shown in (**B**) was analyzed in biological triplicates. Bars represent means and SD. [RD: Radicicol]
D Quantification of the hormone binding kinetics. The hormone binding kinetics of F-Dex to GR-LBD from (**B**) were quantified in biological triplicates. Bars represent means and SD.

First, the effect of co-chaperones on the equilibrium fluorescence anisotropy values was analyzed (Figure 59B,C). For that purpose, all samples except for the control

sample only containing GR-LBD were incubated with Hsp40, Hsp70 and a combination of co-chaperones in the presence of ATP (Figure 59B,C). Incubation of GR-LBD with Hsp40 and Hsp70 markedly reduced the steady state binding of F-Dex, consistent with the unfolding effect of the Hsp40/Hsp70 system. Addition of Hsp90 and Hop or the combination of both moderately increased hormone binding, confirming previous studies (Kirschke et al., 2014). This suggests that Hop alone leads to a moderate release of GR-LBD from Hsp70 and transfer to Hsp90 is inefficient in the absence of Hop in line with the proposed mechanism of GR-LBD maturation (Lorenz et al., 2014; Kirschke et al., 2014). Importantly, addition of NudC alone significantly increased hormone binding to the GR-LBD suggesting that the GR-LBD is released from Hsp40/Hsp70. In addition, NudC in the combination with Hsp90 or Hop and Hsp90 increased equilibrium hormone binding to a value similar to that of the control sample that was not incubated with Hsp40/Hsp70. Addition of the Hsp90 inhibitor radicicol decreased F-Dex binding efficiency to a level of the sample in which only NudC was added. In summary, these results indicate that NudC significantly increases the hormone binding ability of the GR-LBD bound to Hsp40/Hsp70 and even more in the presence of Hsp90 and Hop. This matches the proposed role of NudC as a transfer facilitator that promotes the release of clients from client:Hsp40:Hsp70 complexes.

Since NudC together with Hsp90 increased F-Dex equilibrium binding of GR-LBD bound to Hsp40/Hsp70 to values similar to the unincubated control, no further increase could be observed when Hop was added. This prompted us to gain deeper insight into the interplay of NudC and Hop for GR-LBD maturation. To this end, the hormone binding kinetics of F-Dex to GR-LBD were analyzed (Figure 59D). Treatment of the GR-LBD with Hsp40 and Hsp70 in the presence of ATP reduced the hormone binding kinetics. Unexpectedly, while addition of Hop and Hsp90 increased equilibrium hormone binding (Figure 59C), it did not affect the hormone binding kinetics (Figure 59D). By contrast, addition of NudC increased hormone binding velocity. Intriguingly, addition of Hsp90, Hop and NudC revealed a synergistic increase of the hormone binding kinetics between NudC and Hop. Supplementing radicicol in addition to Hsp90, Hop and NudC did not decrease hormone binding kinetics suggesting that NudC accelerates client transfer independent of the Hsp90 chaperone function. Together, these data strongly support a model in which NudC acts as a client transfer accelerator from the Hsp40/Hsp70 system.

The surprising adverse effect of NudC depletion on viability in two cell lines (Figure 45) raised the question of the generality of the observed NudC effects on client activation. To test this notion, the p53-DBD, which is also dependent on the Hsp40/Hsp70 and Hsp90 system was analyzed (Blagosklonny et al., 1996; Sepehrnia et al., 1996; Rudiger et al., 2002; Müller et al., 2004; Hagn et al., 2011; Alexandrova et al., 2015). Similar to the GR-LBD, the p53-DBD is unfolded when bound to Hsp40/Hsp70 in the presence of ATP and refolds upon release (Boysen et al.,

2019; Dahiya et al., 2019). A previously published p53-DBD construct was used carrying two fluorescent dyes that allow FRET in the folded state but do not display FRET when unfolded by Hsp40/Hsp70 (Dahiya et al., 2019). This construct was then analyzed using single-molecule FRET technology in collaboration with Ganesh Agam at the Don Lamb lab (LMU, Germany). First, the p53-DBD* was unfolded by Hsp40/Hsp70 and then the refolding after addition of different chaperones or co-chaperones was analyzed and equilibrium values were gathered. Incubation of the p53-DBD* with Hsp40 and Hsp70 in the presence of ATP at 37 °C for 1 h led to a loss of FRET signal, confirming that p53-DBD was unfolded under these conditions (Figure 60A). Addition of NudC or Hsp90 individually significantly increased the fraction of p53-DBD in its folded state, while addition of Hsp90 and NudC together did not further increase the high-FRET efficiency fraction beyond the level of the sample only treated with NudC (Figure 60B). As a consequence, NudC seems to act before Hsp90 on the folding of p53-DBD and the effect of Hsp90 seems to be rate-limiting. Additionally, addition of NudC increased conformational dynamics in the p53-DBD as evident from the FRET-lifetime analysis (Figure 60C.) In agreement with the synergism of Hop and NudC found for GR-LBD maturation, addition of NudC to Hop:Hsp90 and addition of Hop to NudC:Hsp90 further increased the high-FRET fraction, indicating that NudC and Hop co-operate to allow client transition from Hsp70 to Hsp90. Investigating the dynamics of p53-DBD refolding indicated that p53-DBD maturation was significantly accelerated when NudC was present compared to Hsp90 alone. In the presence of NudC alone or in combination with Hsp90, saturation of was reached after about 30 min. When Hop was supplemented in addition to NudC and Hsp90, the increase of high-FRET species plateaued after about 5 min, confirming the cooperation of NudC and Hop in p53-DBD maturation.

In summary, these results showed that NudC functions as a transfer accelerator that promotes the transfer of clients from Hsp40/Hsp70 to Hsp90 in co-operation with Hop. The data indicate that the effect of NudC is functionally important since it facilitates the maturation to a functional state in unrelated Hsp90 clients.

4.3.4 The Hsp90 Co-Chaperone NudC - Summary and Discussion

For many Hsp90 clients, the canonical maturation process involves the interaction with Hsp40 stabilizing partially unfolded stretches of a client and recruiting the client to Hsp70 (Fan et al., 2003). Binding of Hsp70 exerts an unfolding pressure on substrates that is released by transfer to Hsp90 via the adapter protein Hop linking Hsp70 to Hsp90 by interacting with the C-terminal EEVD motifs of both chaperones (Morán Luengo et al., 2018; Boysen et al., 2019; Dahiya and Buchner, 2019; Morán Luengo et al., 2019). Yet, how the process of client handover between Hsp70 and Hsp90 is regulated and whether additional factors are involved is largely unknown. Protein-protein interaction screening by the Lindquist lab had revealed that the interactome of NudC was similar to Hop, suggesting they may be involved in the same pathway (Taipale et al., 2014). Previous works had associated NudC with

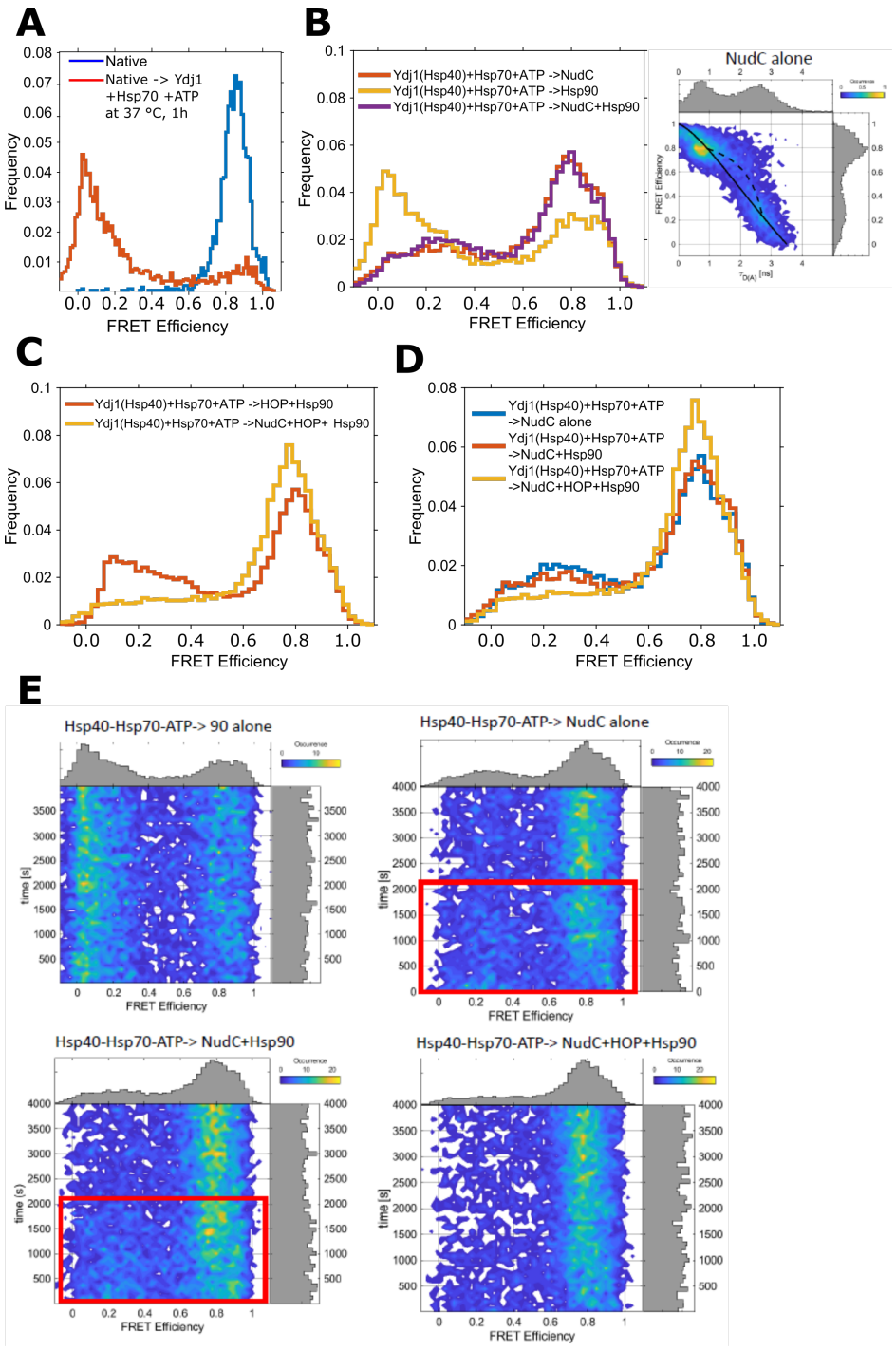

FIGURE 60 | **NudC Promotes p53 Folding *In Vitro*.**
Single-pair FRET (SpFRET) analysis of p53-DBD^{C182C229} carrying fluorescent, FRET-compatible labels ligated to C182 and C229.
A Unfolding of the p53-DBD by Hsp40 and Hsp70. The SpFRET histogram of p53-DBD before and after treatment with Hsp40, Hsp70 and ATP at 37 °C for 1 h.
B The NudC effect on p53-DBD refolding. The SpFRET histograms of the p53-DBD analyzed in the presence of NudC, Hsp90 or both are shown as indicated. A 2D histogram plotting FRET efficiency vs donor lifetime in the presence of the acceptor is depicted in the right panel. The solid line describes the ideal relationship for static molecules, while the dashed line indicates the observed dynamics.
C + **D** The synergism between NudC and Hop for p53-DBD refolding. The SpFRET histograms of the p53-DBD analyzed in the presence of the indicated combinations of Hop, Hsp90 and NudC are shown.
E The effect of NudC on the p53-DBD refolding kinetics. Time-resolved plots of the SpFRET histograms from (**B** - **D**) are shown. The contour plot colors indicate the occurrence. Red bars indicate the first 2000 seconds of measurement.

cytokinesis, nuclear migration and platelet production among other pathways (Fu et al., 2016). These functions have been linked to the stabilizing effect of NudC on Plk1, Lis1, PAF-AH, Mp1 and cofilin 1 (Fu et al., 2016). Some, but not all of these clients have also been associated with Hsp90, suggesting NudC may affect these clients in an Hsp90-independent way similar to p23 which shares a common CS domain with NudC and has Hsp90-independent chaperone functions (Bose et al., 1996; Freeman et al., 1996; Echeverría et al., 2011). In line with this notion, NudC has been found to reduce the aggregation of citrate synthase incubated at 45 °C in PBS in the absence of Hsp90 (data not shown and Zheng et al., 2011). However, it has not been studied if and how NudC affects client maturation in an Hsp90-dependent way. In the course of this work, CRISPRi-based screening for modulators of SHRs identified NudC as a potent regulator of GR function. In this part of this thesis, the interaction of NudC with the Hsp70-Hsp90 network and the mechanistic details of how NudC affects client maturation were investigated with a variety of different techniques to better understand the function of NudC.

4.3.4.1 The Interaction of NudC with Hsp40, Hsp70 and Hsp90

Previous studies dissected NudC into an N-terminal region encompassing two helices and a coiled coil domain for dimerization, followed by the a CS domain sharing homology with p23 and Sgt1 and proposed two helices in the C-terminal region of NudC (Zheng et al., 2011). Studying the domain architecture of NudC we found four N-terminal α-helices and confirmed the two C-terminal α-helices in addition to the β-sheet rich CS domain. NudC forms dimers with high affinity (K_D approx. 100 nM - 250 nM) mediated by interactions between the three N-terminal α-helices, α1 to α3, extending the previously suggested dimerization interface and revealing the previously unknown function of α1 and α2 (Zheng et al., 2011). While the function of the C-terminal helices was not studied in detail, preliminary results indicate they may loosely fold onto the NudC-CS domain and are able to directly bind GR (unpublished results from Florent Delhommel, TU Munich). The interaction between the C-terminal helices and GR seems to be transient, since not stable complexes could be detected in aUC experiments (data not shown). Yet, this finding is in agreement with a direct interaction we found for the p23-tail with GR (data not shown) and may contribute to the Hsp40/Hsp70/Hsp90-independent chaperone activity of NudC.

The presented results provided evidence that NudC and Hsp90 interact tightly with a dissociation constant below 1 µM, matching the binding constant of other Hsp90 co-chaperones (Wandinger et al., 2006; Onuoha et al., 2008; Koulov et al., 2010). The interaction of NudC with Hsp90 is mediated by the CS domain interacting with the Hsp90 MD independent of the Hsp90 dimer conformation. While the interaction of the NudC dimer to Hsp90 was more efficient, binding of the isolated CS domain was still possible. The binding site for NudC on Hsp90 that we mapped with NMR overlaps significantly with the interaction surface Hsp90 forms with p23

and is accessible in the closed and open Hsp90 state in line with the nucleotide-independent binding mode of NudC (Ali et al., 2006). Similar to the crystal structure of yeast Hsp90 with p23 (Ali et al., 2006), both CS domains of NudC may interact with the opposing surfaces formed by the Hsp90 dimer, in line with the 2:2 stoichiometry we found for the NudC:Hsp90 interaction. Despite the higher abundance of Hsp90 over NudC levels in the cell, a 2:2 interaction stoichiometry is physiologically relevant due to the dimeric nature of NudC. Between the dimerization domain and the CS domain, NudC carries long linkers and the short helix α4, providing sufficient flexibility to allow the interaction of the CS domains with the opposing Hsp90 surfaces. Two binding sites may increase the efficiency of client loading onto Hsp90 due to avidity effects: With one binding site tethered to Hsp90, the second monomer could potentially undergo dynamic rearrangements required for client transfer from Hsp40 to Hsp90. Notably, the binding site of NudC on Hsp90 overlaps with the known interaction surfaces of other Hsp90 co-chaperones, suggesting that the binding of NudC is also affected by Hsp90 co-chaperones, which presumably adds a layer of regulation that was not investigated in the course of this study (Lotz et al., 2003; Ali et al., 2006; Retzlaff et al., 2010; Schmid et al., 2012; Verba et al., 2016).

We found that NudC binds Hsp40 with high affinity (K_D approx. 500 nM), while it does not bind Hsp70. Hsp40s usually also occur as homodimers, indicating that NudC and Hsp40 could interact in a similar 2:2 fashion as NudC and Hsp90. Yet, the stoichiometry between NudC and Hsp40 is not entirely clear. Since addition of excess Hsp40 to NudC led to the formation of higher-order structures suggests that in the Hsp40:NudC complex one monomer of NudC and Ydj1 remains unbound to be able to bind additional Hsp40 and NudC dimers. The interaction with Hsp40 is mediated by the NudC α4 helix between the dimerization region and the CS domain forming contacts with the CTD-I region of Hsp40 (Figure 61A). Intriguingly, the CTD-I and CTD-II regions are also the binding site for substrates as well as the Hsp70 C-terminal EEVD motif (Figure 61B,C) (Suh et al., 1999; Lee et al., 2002; Li et al., 2003; Li and Sha, 2005; Yu et al., 2015a; Yu et al., 2015b). Notably, the accessibility of CTD-I and CTD-II is Hsp40-specific: In some Hsp40s both are accessible, in others only one CTD is accessible and in others additional binding sites in the zink-finger domain may be possible (Jiang et al., 2019). Additionally, a single polypeptide-chain can form contacts with more than one CTD (Jiang et al., 2019). Hence, Hsp70-EEVD and NudC compete with clients for Hsp40 binding suggesting a complex regulatory network. While there may be slight regulatory differences between Hsp40 classes, the presented data obtained with yeast Ydj1, human DNAJA1 and DNAJB1 combined suggest that the general mechanism regarding the function of NudC seems to be conserved.

4.3.4.2 NudC Facilitates the Transfer of Clients to Hsp90

While chaperones generally promote substrate folding they also keep clients in a near-native but inactive state (Mashaghi et al., 2016). Our results show that NudC

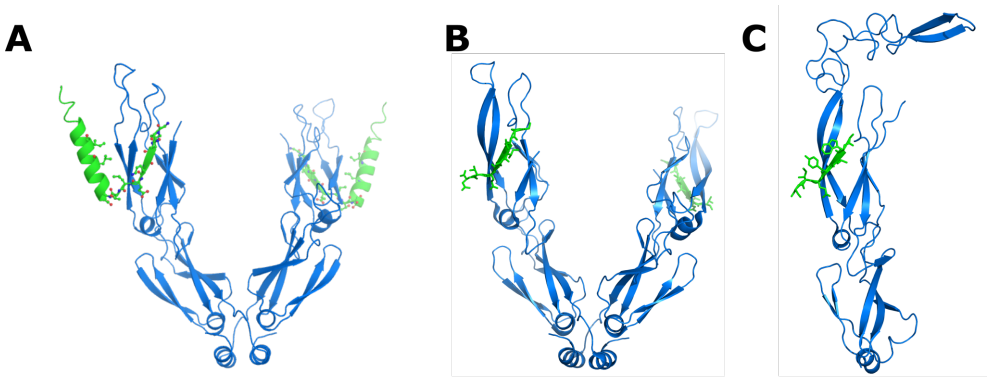

FIGURE 61 | **Crystal Structures of Hsp40 Bound to Peptides.**
A-C The crystal structures of **A** DNAJB1 bound to the NudC 100-141 fragment (data obtained by Florent Delhommel, TU Munich), **B** DNAJB1 bound to the Hsp70-GPTIEEVD motif (PDB: 3AGY) and **C** Ydj1 bound to the substrate peptide GWLYEIS (PDB: 1NLT) are shown.

is a potent promoter of the transfer of clients from Hsp70 to Hsp90. NudC is part of complexes between Hsp40:Hsp70 and Hsp90 that are connected by Hop. In agreement with the overlapping binding sites of NudC and Hsp70-IEEVD on Hsp40, our results show that addition of NudC to Hsp40:Hsp70:client complexes promotes the disassembly of these high molecular weight complexes by facilitating Hsp70 release yielding a NudC:Hsp40:client that readily binds Hsp90. Hence, in this regard NudC functions as an Hsp40 co-chaperone. NudC was found to increase the release of GR from Hsp40:Hsp70 and increase the binding efficiency and kinetics for hormone. Notably, the function of NudC is not client-specific since a similar effect of NudC was found for the structurally and functionally unrelated p53 bound to Hsp40:Hsp70. The effect of NudC on GR and p53 release and maturation in the presence of Hsp90 showed synergism with the adapter co-chaperone Hop. Hence, we propose that NudC is a facilitator of client transfer from Hsp40:Hsp70 to Hsp90 by disrupting Hsp40:Hsp70:client complexes.

Together, based on our findings, we propose a model in which Hop binds Hsp90 and recruits the Hsp40:Hsp70:client complex as previously proposed (Figure 62) (Lorenz et al., 2014; Kirschke et al., 2014). Nudc binds Hsp40 yielding a short-lived complex in which the association of Hsp70 is destabilized. Hsp40:NudC:client additionally destabilizes Hop binding to Hsp90. Hence, Hop and Hsp70 dissociate from the complex leaving a Hsp90:NudC:Hsp40:client complex. Release of Hsp70 from the client allows the client to fold into a more native conformation that is preferentially bound by Hsp90. Release of NudC and Hsp40 yields a partially closed Hsp90:client complex (closed-1 state). Binding of PPIases and p23 promotes transition to the ATPase-competent closed-2 state. ATP hydrolysis and opening of Hsp90 leads to the release of the folded client and completes the chaperone cycle. Notably, our data are also compatible with a non-mutually exclusive pathway in which dissociation of Hsp70 from Hsp40:Hsp70:client complexes via NudC proceeds the direct recruitment of NudC:Hsp40 to Hsp90. Additionally, in some cases, depending on

the conformation of the substrate, Hsp70 action may not be required, thus funneling to Hsp90 via Hsp40:NudC bypassing Hsp70 may increase the efficiency of refolding/cycling of clients. Yet, since we observed synergistic behavior between NudC and Hop for the activation of GR-LBD and p53-DBD *in vitro*, we suggest that the direct recruitment via NudC:Hsp40:client plays a less prevalent role than the disruption of Hsp40:Hsp70:client complexes by NudC.

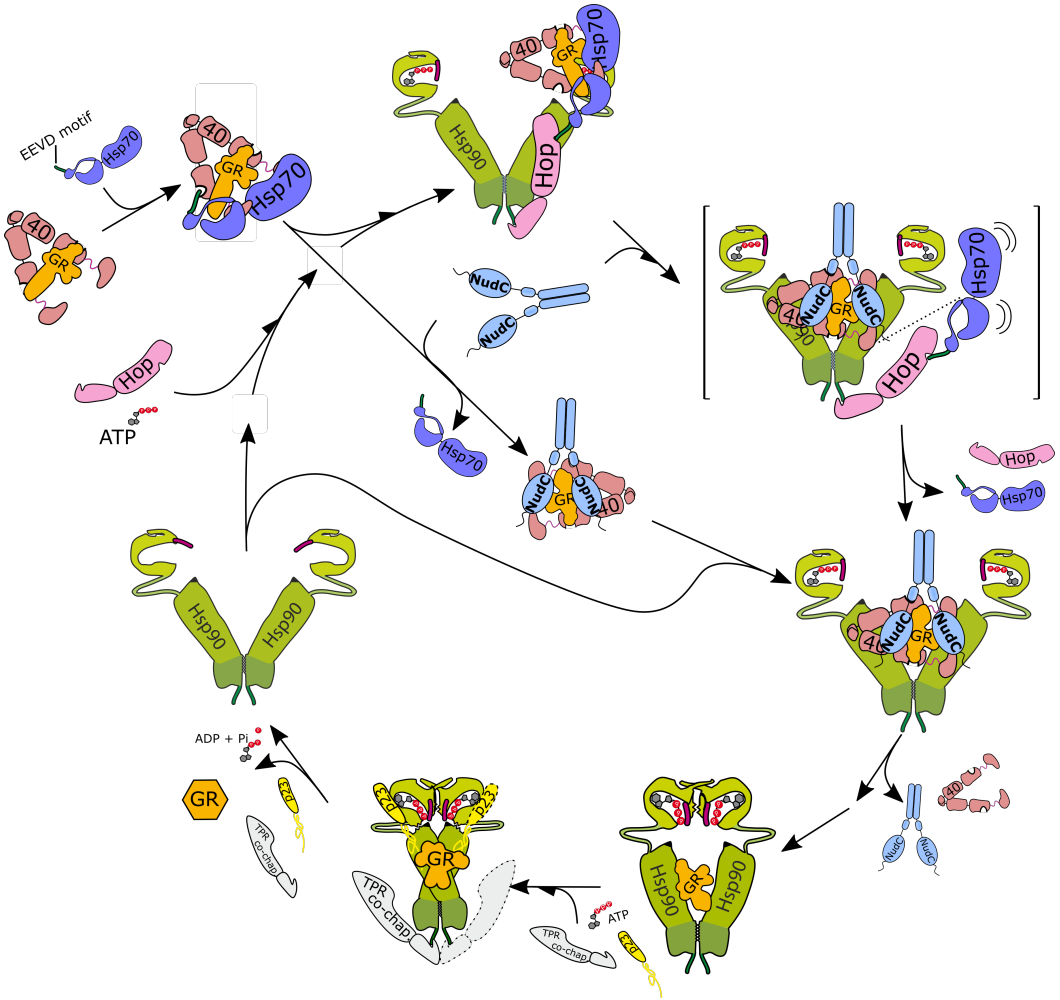

FIGURE 62 | **Schematic Model of the NudC Function.**
A schematic model of the effect of NudC on client maturation by Hsp90 is shown based on the previously published model for GR maturation (Lorenz et al., 2014). Hsp40 recruits Hsp70 to the client forming a Hsp40:Hsp70:client complex. Hop binds Hsp90 and recruits the Hsp40:Hsp70:client complex. Binding of NudC to Hsp40 destabilizes this complex and leads to the dissociation of Hsp70, thus reducing the unfolding pressure of Hsp70 and bringing the client into a more native conformation that is bound by Hsp90. Binding of Hsp40:NudC:client complexes to Hsp90 via NudC releases Hop. The transition of Hsp90 to the closed-1 and closed-2 states promotes ATP hydrolysis of Hsp90 and completes the cycle. The EEVD motifs of Hsp70 and Hsp90 are represented as green tails. For clarity, the domain architecture of NudC is simplified and helix α1-α3 are summarized as one domain and helices α5 and α6 are not shown. [40 = Hsp40]

The release of clients from Hsp70 could also lead to productive folding in the absence of Hsp90. Due to the approximate 15-fold excess of Hsp90 over NudC in the cellular environment, the abundance of unbound NudC will be low (Finka and

Goloubinoff, 2013). The binding motifs for Hsp40 and Hsp70 are very frequent in a substrate and a single substrate may be coated by several Hsp70s (Rüdiger et al., 1997). The release of Hsp40:Hsp70 complexes from the substrate by free NudC may be beneficial to increase the binding fidelity of Hsp40:Hsp70 to the thermodynamically most instable regions (Sekhar et al., 2018). As the substrate samples different conformations, Hsp40:Hsp70 binding sites may become buried and new binding sites are revealed. In this model, NudC can promote the dynamics of Hsp70 on the substrate in analogy to the model of p23 increasing the dynamics of transcription complexes on DNA (Echtenkamp et al., 2016).

4.3.4.3 NudC Affects Client Activity and Viability *In Vivo*

Notably the effect of NudC on client activity could also be shown in human cells. Surprisingly, knockdown of NudC decreased GR activity in K562 cell lines while it increased activity in Hek293 cells. Yet, viability was seriously reduced in both cell lines when NudC was lost. These results illustrate marked differences between cell lines that have also been obvious when CRISPRi was used to screen for SHR modulators in this thesis (Section 4.2). This suggests that the timing of client transfer from Hsp70 to Hsp90 is precisely regulated in the cell to maintain optimized client activity for a certain type of cell, highlighting the importance of NudC as a modulator of client transfer kinetics and efficiency. The opposite consequence of NudC depletion in different cell lines may be a product of chaperome differences observed between cell lines (Rodina et al., 2016). Interestingly, the ratio of the predominant cytosolic Hsp70 isoforms (HspA1A, HspA1B) to Hsp90 (Hsp90α, Hsp90β) is dramatically shifted towards Hsp70 in Hek293 cells compared to K562 cells (Hsp70/Hsp90: 1.24 and 0.16 in Hek293 and K562, respectively) (Geiger et al., 2012). Accordingly, the combined level of DNAJA1 and DNAJB1 were about 4x higher in Hek293 compared to K562 cells. By contrast the ratio of NudC to Hop levels is similar in both cell lines (NudC/Hop: 0.65 and 0.77 for Hek293 and K562, respectively) (Geiger et al., 2012). This could mean that binding of clients to Hsp70 is especially important in Hek293 cells and release from Hsp70 is not beneficial for cellular survival. Hence, NudC acts as a negative regulator of client activity in Hek293 cells, limiting client activating to a rate adapted to cell line requirements. Previous studies have shown the importance of the cycle timing of Hsp90 (Zierer et al., 2016) and that the maturation of clients depends on the dwell time of clients on Hsp90 (this work, Section 4.1) (Wang et al., 2006). Our findings extend this concept and suggest that also the time clients are bound to Hsp70 and the time required for the transfer to Hsp90 are important for client activity and cellular viability.

Our results indicate that loss of NudC induces cell death. While this corroborates the importance of NudC, if this observation is a result of misregulation of individual clients or a general effect due to impaired client maturation remains to be investigated. To that end it will be interesting to evaluate the response to NudC

up- or down regulation in different cancer cell lines which are known to have distinctly organized chaperomes (Rodina et al., 2016). Due to the regulation of a variety of cancer-associated proteins by Hsp90, many studies have investigated the dependence of tumor cells on Hsp90, generally suggesting that tumor cells are more susceptible to inhibition than non-transformed cells (Whitesell et al., 1998; Kamal et al., 2003; Chiosis et al., 2006; Pick et al., 2007; Workman et al., 2007; Calderwood and Gong, 2016; Vartholomaiou et al., 2016). Since the unwanted induction of a HSR by Hsp90 inhibition has emerged as a problematic side-effect in therapy, new concepts to target co-chaperones have been proposed as a prospective therapeutic option (Brandt and Blagg, 2009; Yu et al., 2010; Li et al., 2016; Stiegler et al., 2017). Interestingly, gedunin has been found as a small molecule inducing the dissociation of p23 from Hsp90, which led to the selective destabilization of SHRs in mammalian cells (Patwardhan et al., 2013). Due to the similarities in the interaction of p23 and NudC regarding Hsp90 binding and our finding that NudC strongly regulates GR activity *in vitro* and *in vivo*, it could be interesting to test the effect of gedunin on NudC function in the future.

4.3.4.4 Conclusion

CRISPRi screening for SHR modulators had revealed that NudC is a potential Hsp90-dependent regulator of SHR activity. Here, we showed that NudC is a promoter of client processing by facilitating the transfer of clients from the Hsp40:Hsp70 system to Hsp90, working in synergism with the adapter co-chaperone Hop. NudC associates with Hsp90 via its CS domain. Additionally, NudC forms contacts with the Hsp70 system via interaction with Hsp40, mediated by a NudC helix binding to the CTD-I region of Hsp40 and competing with the Hsp70-EEVD motif for binding to Hsp40. Binding of NudC to Hsp40:Hsp70:client complexes leads to the displacement of Hsp70 and formation of a NudC:Hsp40:client complex that can associate with Hsp90 and promote client transfer. In line with this model, NudC promotes the release of GR and p53 from the Hsp70 trap and their folding and maturation. Importantly, the modulation of client activity could also be shown in mammalian tissue culture. Our knockdown data indicate that NudC promotes different outcomes on client activity in two cell lines. Yet, depletion of NudC reduces viability in either case, highlighting the importance of NudC *in vivo*. Together, we propose that NudC is a novel *bona fide* co-chaperone for Hsp90 and Hsp40 playing a pivotal role for client maturation. These results extend our understanding of the complex steps required for client transfer from Hsp70 to Hsp90 and to the best of our knowledge NudC is the first identified accelerator of client transfer. While we showed synergism between NudC and Hop, the integration of NudC into the spectrum of co-chaperones will be a task for the future to understand synergistic and antagonistic relationships between co-chaperones fine-tuning the client transfer process. Additionally, future studies will be necessary to shed light on the physiological implications of NudC in the heterogeneous chaperone complexes found in different cell lines.

Conclusion and Outlook

In this work, the interplay of Hsp90 with its co-chaperones in the context of client maturation has been investigated in yeast and mammalian cells. Analysis of the organization of the yeast co-chaperome revealed the existence of plastic genetic networks that adapt to client maturation. Within these networks, strongly interacting genetic modules are embedded in a network of loosely connected interactors. Specific modules affecting the maturation of SHRs, kinases and eEF2 could be defined. These findings expand our knowledge of the Hsp90 co-chaperone landscape and shift the perception of a static machinery to a flexible system that reorganizes to meet the specific requirements of each client. Thorough knowledge of the dependencies between co-chaperones is crucial to understand the results of perturbing specific parts of the Hsp90 system, e.g. by inhibitors. In the future, it will be interesting to expand the analysis to mammalian cells, in which additional co-chaperones are present. While the general organization of the Hsp90 machinery is conserved from yeast to man, additional core genetic modules may be formed by co-chaperones that are only present in mammals. Furthermore, genetic interactions between co-chaperones and Hsp90 mutants that favor or disfavor specific Hsp90 conformations will be interesting to better understand how the effect of Hsp90 co-chaperones depends on Hsp90 states for client maturation.

Within this thesis, a CRISPRi-based screening platform has been developed for mammalian cells to identify novel Hsp90 co-chaperones. The system is based on reading out the effect of CRISPRi-mediated gene knockdowns on the activity of SHRs as a class of stringent Hsp90 clients. Using a compact proteostasis factor-biased library, the system was validated by screening for modulators of SHR activity in different cell lines, identifying known Hsp90 co-factors as well as novel Hsp90 co-chaperone candidates. We studied NudC as one of these candidates extensively, establishing it as an Hsp90 co-chaperone. These results confirm the developed functional genomics platform as suitable means to study and identify Hsp90 regulators. Validation of additional candidate genes *in vitro* and *in vivo* will be required to define their role in client activation. Additionally, the screening revealed substantial overlap of the modulators affecting SHR activity within one cell line, but indicated significant differences between cell lines. Extension of the screening platform to additional cell lines will be important to understand the cell line specific regulation

of SHRs, which are dysregulated in different diseases. Furthermore, the CRISPRi-based screening system can be expanded to different clients by adapting the readout system, providing the opportunity to find client-specific regulators, which will be crucial to understand the client-adapted regulation of Hsp90 that has become evident from our studies in yeast.

Identified as a high-confidence hit during CRISPRi screening, NudC was analyzed in depth *in vitro* and *in vivo* in the course of this thesis, establishing NudC as a co-chaperone of Hsp40 and Hsp90. We found that NudC interacts with Hsp40 and Hsp90 but does not bind to Hsp70 or clients. By dissociating Hsp70 from Hsp40:client complexes, NudC functions as an accelerator of client transfer from Hsp70 to Hsp90. In two non-mutually-exclusive models NudC can free client:Hsp40 complexes of Hsp70 either before or after recruitment of the Hsp40:Hsp70:client complex to Hsp90 via Hop. Either way NudC frees clients from the Hsp70 trap and increases the kinetics of client transfer to Hsp90, increasing client activity *in vitro* and *in vivo*. The significance of NudC in the cellular environment further became evident by the lethality of NudC knockdown in two different cell lines. Together, these results identify NudC as the first known accelerator of client transfer and a co-chaperone of Hsp40 and Hsp90. Apart from Hop, it is currently unknown how NudC co-operates with other co-chaperones for client maturation and this will be subject to further studies. Additionally, investigating the transient direct interaction of NudC with clients in analogy to p23 will be interesting to understand an Hsp90-independent function of NudC.

Taken together, this work extends our understanding of the Hsp90 co-chaperome in yeast as well as mammalian cells. Studying epistasis of Hsp90 co-chaperones in yeast revealed plastic genetic networks adapted to client maturation. For mammalian cells, a powerful CRISPRi-based functional genomics screening platform was established, with which several Hsp90 modulator candidates were identified. In depth analysis of one of these hits defined the function of a new Hsp40 and Hsp90 co-chaperone, which functions as an accelerator of client transformation.

Supplementary Information

S1 CRISPRi Screening Library

The genes targeted by the focused chaperone CRISPRi library are shown in Table S23. Each gene was targeted by 5 sgRNAs, targeting either the sense- or antisense-strand.

TABLE S23: Genes Targeted by the Focused Chaperone CRISPRi Screening Library

Gene Name			
AARSD1	DNAJC25	IFT88	SGTA
ADRM1	DNAJC27	IRS4	SGTB
AFG3L2	DNAJC28	ITGB1BP2	SH3TC1
AGR2	DNAJC3	KLC1	SH3TC2
AGR3	DNAJC30	KLC2	SIL1
AHSA1	DNAJC4	KLC3	SPAG1
AHSA2	DNAJC5	KLC4	SRP68
AIP	DNAJC5B	LEPREL1	SRP72
AIPL1	DNAJC5G	LONP1	ST13
ANAPC5	DNAJC6	LONRF1	STIP1
ANAPC7	DNAJC7	LONRF3	STUB1
APPBP2	DNAJC8	LRP2BP	SUGT1
ASNA1	DNAJC9	LRRC6	TANC1
ASPH	DYX1C1	MCMBP	TCP1
ATAD3A	EDEM1	MKKS	TMTC1
ATAD3B	EDEM2	MLF1	TMTC2
ATAD3C	EDEM3	MLF2	TMTC3
ATF4	EIF2AK3	MZB1	TMTC4
ATF6	EMC2	NASP	TMX1
BAG1	ERLEC1	NCF2	TMX2
BAG2	ERN1	NKTR	TMX3
BAG3	ERO1L	NLN	TMX4
BAG4	ERO1LB	NOXA1	TOMM34

BAG5	ERP27	NUDC	TOMM70A
BAG6	ERP29	NUDCD1	TOR1A
BBS10	ERP44	NUDCD2	TOR1B
BBS4	FAXC	NUDCD3	TOR2A
BCS1L	FICD	ODF1	TOR3A
CABIN1	FKBP10	OGT	TOR4A
CACYBP	FKBP11	OPA1	TRAP1
CALR	FKBP14	P4HA1	TTC1
CANX	FKBP15	P4HA2	TTC12
CBL	FKBP1A	P4HA3	TTC13
CCT2	FKBP1B	P4HB	TTC14
CCT3	FKBP2	PDCD11	TTC16
CCT4	FKBP3	PDIA2	TTC17
CCT5	FKBP4	PDIA3	TTC18
CCT6A	FKBP5	PDIA4	TTC19
CCT6B	FKBP6	PDIA5	TTC21A
CCT7	FKBP7	PDIA6	TTC21B
CCT8	FKBP8	PDILT	TTC22
CCT8L2	FKBP9	PDRG1	TTC23
CDC16	FKBPL	PEX5	TTC24
CDC23	GAK	PEX5L	TTC25
CDC27	GPSM1	PFDN1	TTC26
CDC37	GPSM2	PFDN2	TTC27
CDC37L1	GRPEL1	PFDN4	TTC28
CHORDC1	GRPEL2	PFDN5	TTC29
CLGN	GTF3C3	PFDN6	TTC3
CLPB	HSCB	PHB	TTC30A
CLPX	HSF1	PHB2	TTC30B
CLU	HSF2	PHGDH	TTC32
CNOT10	HSF4	PIN1	TTC33
CRNKL1	HSF5	PLOD1	TTC36
CRYAA	HSFX1	PLOD2	TTC37
CRYAB	HSFY1	PLOD3	TTC39A
CTR9	HSP90AA1	PPIA	TTC39B
DCP1A	HSP90AB1	PPIB	TTC4
DCP1B	HSP90B1	PPIC	TTC5
DNAJA1	HSPA12A	PPID	TTC6
DNAJA2	HSPA12B	PPIE	TTC7A
DNAJA3	HSPA13	PPIF	TTC7B
DNAJA4	HSPA14	PPIG	TTC8
DNAJB1	HSPA1A	PPIH	TTC9
DNAJB11	HSPA1B	PPIL1	TTC9B

DNAJB12	HSPA1L	PPIL2	TTC9C
DNAJB13	HSPA2	PPIL3	TUSC3
DNAJB14	HSPA4	PPIL4	TXN
DNAJB2	HSPA4L	PPIL6	TXNDC11
DNAJB4	HSPA5	PPP5C	TXNDC12
DNAJB5	HSPA6	PPWD1	TXNDC16
DNAJB6	HSPA8	PRDX4	TXNDC5
DNAJB7	HSPA9	PRPF6	TXNRD1
DNAJB8	HSPB1	PSMC1	TXNRD3
DNAJB9	HSPB11	PSMD2	UNC45A
DNAJC1	HSPB2	PSMD4	UNC45B
DNAJC10	HSPB3	PSMG1	USP19
DNAJC11	HSPB6	PSMG2	UTY
DNAJC12	HSPB7	PSMG3	UXT
DNAJC13	HSPB8	PSMG4	VBP1
DNAJC14	HSPB9	PTGDS	VCP
DNAJC15	HSPBP1	PTGES3	WDTC1
DNAJC16	HSPD1	PTPLAD1	XAB2
DNAJC17	HSPE1	QSOX1	XBP1
DNAJC18	HSPH1	QSOX2	ZC3H7B
DNAJC19	HYOU1	RAPSN	ZFC3H1
DNAJC2	IFIT1	RPAP3	ZMYND12
DNAJC21	IFIT2	SACS	
DNAJC22	IFIT3	SEC63	
DNAJC24	IFIT5	SERPINH1	

S2 Indexing for Next-Generation Sequencing

Indexing primers were used to amplify genomic loci of different samples for next-generation sequencing during CRISPRi screening. The indices were used for demultiplexing after next-generation sequencing. The indices of Table S24 replace XXXXXX in the following oligonucleotide framework:

Forward primers: aatgatacggcgaccaccgagatcggaagagcacacgtctgaactccagtcacXXX-XXXgcacaaaaggaaactcaccct

Mirror primers: aatgatacggcgaccaccgagatctacacgatcggaagagcacacgtctgaactccagt-cacXXXXXXcgactcggtgccacttttc

Forward primers were used together with the oMK677-HS4K-CRISPR-rev primer and mirror primers were used together with the oMK732-HS4Kmirror-CIRSPR-rev primer.

oMK677: caagcagaagacggcatacgagatcgactcggtgccacttttc

oMK732: caagcagaagacggcatacgagatgcacaaaaggaaactcaccct

TABLE S24: Indexing Primers used for Next-Generation Sequencing for CRISPRi Screening

Primer-Name	**Index**
oMK731-HS4Kmirror-CRISPR-i1	ATCACG
oSEQ2-mirror-i2	CGATGT
oSEQ3-mirror-i3	TTAGGC
oMK752-HS4Kmirror-CRISPR-i4	TGACCA
oSEQ5-mirror-i5	ACAGTG
oMK729-HS4Kmirror-CRISPR-i6	GCCAAT
oSEQ7-mirror-i7	CAGATC
oMK766-HS4Kmirror-CRISPR-i8	ACTTGA
oMK730-HS4Kmirror-CRISPR-i10	TAGCTT
oMK754-HS4Kmirror-CRISPR-i11	GGCTAC
oSEQ12-mirror-i12	CTTGTA
oMK750-HS4Kmirror-CRISPR-13	AGTCAA
oSEQ14-mirror-i14	AGTTCC
oSEQ19-mirror-i19	GTGAAA
oSEQ20-mirror-i20	GTGGCC
oSEQ21-mirror-i21	GTTTCG
oSEQ23-mirror-i23	GAGTGG
oSEQ25-mirror-i25	ACTGAT
oSEQ27-mirror-i27	ATTCCT
oMK677-HS4K-CRISPR-rev	2^{nd} Primer (Forward)
oMK732-HS4Kmirror-CRISPR-rev	2^{nd} Primer (Mirror)

S3 Knockdown of Individual Genes in Mammalian Cells

TABLE S25: Oligonucleotides for the Individual Knockdown of Genes by CRISPRi

sgRNA ID	Sequence
FKBP4-1	Top: TTGGCTGACTGCGGACCGCGAGGGTTTAAGAGC Bottom: TTAGCTCTTAAACCCTCGCGGTCCGCAGTCAGCCAACAAG
FKBP4-2	Top: TTGGGGCGCGGCGGCACTGACTGGTTTAAGAGC Bottom: TTAGCTCTTAAACCAGTCAGTGCCGCCGCGCCCCAACAAG
FKBP5-1	Top: TTGGGGACACCGCCGCCCGAGACGTTTAAGAGC Bottom: TTAGCTCTTAAACGTCTCGGGCGGCGGTGTCCCCAACAAG
FKBP5-2	Top: TTGGCGCGGGCGCTGCCAGTCTCGTTTAAGAGC Bottom: TTAGCTCTTAAACGAGACTGGCAGCGCCCGCGCCAACAAG
PTGES3-1	Top: TTGGGTGCAAACGAGGGGTGGTGGTTTAAGAGC Bottom: TTAGCTCTTAAACCACCACCCCTCGTTTGCACCCAACAAG
PTGES3-2	Top: TTGGGGAGTCGACTTCTCTCCGGGTTTAAGAGC Bottom: TTAGCTCTTAAACCCGGAGAGAAGTCGACTCCCCAACAAG
NudC-1	Top: TTGGGCGGACGACTAGAGTCGTTGTTTAAGAGC Bottom: TTAGCTCTTAAACAACGACTCTAGTCGTCCGCCCAACAAG
NudC-2	Top: TTGGGCAGGAGCGTAGAGAGCGCGTTTAAGAGC Bottom: TTAGCTCTTAAACGCGCTCTCTACGCTCCTGCCCAACAAG

NudCD3-1	Top: TTGGCCTAGGGCGGGAGGCGACAGTTTAAGAGC Bottom: TTAGCTCTTAAACTGTCGCCTCCCGCCCTAGGCCAACAAG
NudCD3-2	Top: TTGGGTGTGTGTGAAGCGTACCTGTTTAAGAGC Bottom: TTAGCTCTTAAACAGGTACGCTTCACACACACCCAACAAG
OGT-1	Top: TTGGCTCTGGAGGGCTTGAGCGGGTTTAAGAGC Bottom: TTAGCTCTTAAACCCGCTCAAGCCCTCCAGAGCCAACAAG
OGT-2	Top: TTGGGCCGTAGCAATGCTCTGGAGTTTAAGAGC Bottom: TTAGCTCTTAAACTCCAGAGCATTGCTACGGCCCAACAAG
STIp1-1	Top: TTGGCGGTGGCCAGGCCGCGGTAGTTTAAGAGC Bottom: TTAGCTCTTAAACTACCGCGGCCTGGCCACCGCCAACAAG
STIp2-2	Top: TTGGCCCTGAAGGCGTCCCGAGGGTTTAAGAGC Bottom: TTAGCTCTTAAACCCTCGGGACGCCTTCAGGGCCAACAAG

Publications

Sahasrabudhe, P.*, Rohrberg, J.*, **Biebl, M. M.**, Rutz, D. A., and Buchner, J. (2017). The Plasticity of the Hsp90 Co-chaperone System. *Molecular cell* 67, 947–961

Schopf, F. H.*, **Biebl, M. M.***, and Buchner, J. (2017). The HSP90 chaperone machinery. *Nature reviews. Molecular cell biology* 18, 345–360

Schopf, F. H., Huber, E. M., Dodt, C., Lopez, A., **Biebl, M. M.**, Rutz, D. A., Mühlhofer, M., Richter, G., Madl, T., Sattler, M., Groll, M., and Buchner, J. (2019). The Co-chaperone Cns1 and the Recruiter Protein Hgh1 Link Hsp90 to Translation Elongation via Chaperoning Elongation Factor 2. *Molecular cell* 74, 73–87.e8

Biebl, M. M., Riedl, M., and Buchner, J. (2020). Hsp90 co-chaperones form plastic genetic networks adapted to client maturation. *Cell reports* 32, 108063

* denote shared first-authorships

Bibliography

Adamson, B. et al. (2016). A Multiplexed Single-Cell CRISPR Screening Platform Enables Systematic Dissection of the Unfolded Protein Response. *Cell* 167, 1867–1882.e21.

Ahmad, N. and Kumar, R. (2011). Steroid hormone receptors in cancer development: a target for cancer therapeutics. *Cancer letters* 300, 1–9.

Alderson, T. R., Kim, J. H., and Markley, J. L. (2016). Dynamical Structures of Hsp70 and Hsp70-Hsp40 Complexes. *Structure* 24, 1014–1030.

Alexandrova, E. M., Yallowitz, A. R., Li, D, Xu, S, Schulz, R, Proia, D. A., Lozano, G, Dobbelstein, M, and Moll, U. M. (2015). Improving survival by exploiting tumour dependence on stabilized mutant p53 for treatment. *Nature* 523, 352–356.

Ali, J. A., Jackson, A. P., Howells, A. J., and Maxwell, A (1993). The 43-kilodalton N-terminal fragment of the DNA gyrase B protein hydrolyzes ATP and binds coumarin drugs. *Biochemistry* 32, 2717–2724.

Ali, M. M. U., Roe, S. M., Vaughan, C. K., Meyer, P., Panaretou, B., Piper, P. W., Prodromou, C., and Pearl, L. H. (2006). Crystal structure of an Hsp90-nucleotide-p23/Sba1 closed chaperone complex. *Nature* 440, 1013–1017.

Aligue, R, Akhavan-Niak, H, and Russell, P (1994). A role for Hsp90 in cell cycle control: Wee1 tyrosine kinase activity requires interaction with Hsp90. *The EMBO journal* 13, 6099–6106.

Ammirante, M, Rosati, A, Gentilella, A, Festa, M, Petrella, A, Marzullo, L, Pascale, M, Belisario, M. A., Leone, A, and Turco, M. C. (2008). The activity of hsp90 alpha promoter is regulated by NF-kappa B transcription factors. *Oncogene* 27, 1175–1178.

Armstrong, H., Wolmarans, A., Mercier, R., Mai, B., and LaPointe, P. (2012). The co-chaperone Hch1 regulates Hsp90 function differently than its homologue Aha1 and confers sensitivity to yeast to the Hsp90 inhibitor NVP-AUY922. *PloS one* 7, e49322.

Aron, R., Lopez, N., Walter, W., Craig, E. A., and Johnson, J. (2005). In vivo bipartite interaction between the Hsp40 Sis1 and Hsp70 in Saccharomyces cerevisiae. *Genetics* 169, 1873–1882.

Backe, S. J., Sager, R. A., Woodford, M. R., Makedon, A. M., and Mollapour, M. (2020). Post-translational modifications of Hsp90 and translating the chaperone code. *The Journal of biological chemistry*.

Baker, J. D., Ozsan, I., Rodriguez Ospina, S., Gulick, D., and Blair, L. J. (2018). Hsp90 Heterocomplexes Regulate Steroid Hormone Receptors: From Stress Response to Psychiatric Disease. *International journal of molecular sciences* 20.

Balchin, D., Hayer-Hartl, M., and Hartl, F. U. (2016). In vivo aspects of protein folding and quality control. *Science* 353, aac4354.

Balchin, D., Hayer-Hartl, M., and Hartl, F. U. (2020). Recent advances in understanding catalysis of protein folding by molecular chaperones. *FEBS letters*.

Baldwin, R. L. and Rose, G. D. (2013). Molten globules, entropy-driven conformational change and protein folding. *Current opinion in structural biology* 23, 4–10.

Bali, P. et al. (2005). Inhibition of histone deacetylase 6 acetylates and disrupts the chaperone function of heat shock protein 90: a novel basis for antileukemia activity of histone deacetylase inhibitors. *The Journal of biological chemistry* 280, 26729–26734.

Bardwell, J. C. and Craig, E. A. (1988). Ancient heat shock gene is dispensable. *Journal of bacteriology* 170, 2977–2983.

Barends, T. R. M. et al. (2013). Combining crystallography and EPR: crystal and solution structures of the multidomain cochaperone DnaJ. *Acta crystallographica. Section D, Biological crystallography* 69, 1540–1552.

Behnke, J., Mann, M. J., Scruggs, F.-L., Feige, M. J., and Hendershot, L. M. (2016). Members of the Hsp70 Family Recognize Distinct Types of Sequences to Execute ER Quality Control. *Molecular cell* 63, 739–752.

Bellay, J. et al. (2011). Putting genetic interactions in context through a global modular decomposition. *Genome research* 21, 1375–1387.

Ben-David, U. et al. (2018). Genetic and transcriptional evolution alters cancer cell line drug response. *Nature* 560, 325–330.

Bergerat, A, Massy, B de, Gadelle, D, Varoutas, P. C., Nicolas, A, and Forterre, P (1997). An atypical topoisomerase II from Archaea with implications for meiotic recombination. *Nature* 386, 414–417.

Bertelsen, E. B., Chang, L., Gestwicki, J. E., and Zuiderweg, E. R. P. (2009). Solution conformation of wild-type E. coli Hsp70 (DnaK) chaperone complexed with ADP and substrate. *Proceedings of the National Academy of Sciences of the United States of America* 106, 8471–8476.

Biebl, M. M. and Buchner, J. (2019). Structure, Function, and Regulation of the Hsp90 Machinery. *Cold Spring Harbor perspectives in biology* 11.

Biswas, C., Ostrovsky, O., Makarewich, C. A., Wanderling, S., Gidalevitz, T., and Argon, Y. (2007). The peptide-binding activity of GRP94 is regulated by calcium. *The Biochemical journal* 405, 233–241.

Blagosklonny, M. V., Toretsky, J, Bohen, S, and Neckers, L (1996). Mutant conformation of p53 translated in vitro or in vivo requires functional HSP90. *Proceedings of the National Academy of Sciences of the United States of America* 93, 8379–8383.

Boczek, E. E., Reefschläger, L. G., Dehling, M., Struller, T. J., Häusler, E., Seidl, A., Kaila, V. R. I., and Buchner, J. (2015). Conformational processing of oncogenic v-Src kinase by the molecular chaperone Hsp90. *Proceedings of the National Academy of Sciences of the United States of America* 112, E3189–E3198.

Bohen, S. P. (1998). Genetic and biochemical analysis of p23 and ansamycin antibiotics in the function of Hsp90-dependent signaling proteins. *Molecular and cellular biology* 18, 3330–3339.

Bohen, S. P. and Yamamoto, K. R. (1993). Isolation of Hsp90 mutants by screening for decreased steroid receptor function. *Proceedings of the National Academy of Sciences of the United States of America* 90, 11424–11428.

Bohush, A., Bieganowski, P., and Filipek, A. (2019). Hsp90 and Its Co-Chaperones in Neurodegenerative Diseases. *International journal of molecular sciences* 20.

Boorstein, W. R., Ziegelhoffer, T, and Craig, E. A. (1994). Molecular evolution of the HSP70 multigene family. *Journal of molecular evolution* 38, 1–17.

Borkovich, K. A., Farrelly, F. W., Finkelstein, D. B., Taulien, J, and Lindquist, S (1989). hsp82 is an essential protein that is required in higher concentrations for growth of cells at higher temperatures. *Molecular and cellular biology* 9, 3919–3930.

Bose, S, Weikl, T, Bügl, H, and Buchner, J (1996). Chaperone function of Hsp90-associated proteins. *Science* 274, 1715–1717.

Boulon, S. et al. (2010). HSP90 and its R2TP/Prefoldin-like cochaperone are involved in the cytoplasmic assembly of RNA polymerase II. *Molecular cell* 39, 912–924.

Boysen, M., Kityk, R., and Mayer, M. P. (2019). Hsp70- and Hsp90-Mediated Regulation of the Conformation of p53 DNA Binding Domain and p53 Cancer Variants. *Molecular cell* 74, 831–843.e4.

Bracher, A. and Verghese, J. (2015a). GrpE, Hsp110/Grp170, HspBP1/Sil1 and BAG domain proteins: nucleotide exchange factors for Hsp70 molecular chaperones. *Sub-cellular biochemistry* 78, 1–33.

Bracher, A. and Verghese, J. (2015b). The nucleotide exchange factors of Hsp70 molecular chaperones. *Frontiers in molecular biosciences* 2, 10.

Brandt, G. E. L. and Blagg, B. S. J. (2009). Alternate strategies of Hsp90 modulation for the treatment of cancer and other diseases. *Current topics in medicinal chemistry* 9, 1447–1461.

Brockwell, D. J. and Radford, S. E. (2007). Intermediates: ubiquitous species on folding energy landscapes? *Current opinion in structural biology* 17, 30–37.

Brugge, J. S. and Erikson, R. L. (1977). Identification of a transformation-specific antigen induced by an avian sarcoma virus. *Nature* 269, 346–348.

Brugge, J. S., Erikson, E, and Erikson, R. L. (1981). The specific interaction of the Rous sarcoma virus transforming protein, pp60src, with two cellular proteins. *Cell* 25, 363–372.

Bryngelson, J. D., Onuchic, J. N., Socci, N. D., and Wolynes, P. G. (1995). Funnels, pathways, and the energy landscape of protein folding: a synthesis. *Proteins* 21, 167–195.

Buchner, J (1996). Supervising the fold: functional principles of molecular chaperones. *FASEB journal* 10, 10–19.

Calderwood, S. K. and Gong, J. (2016). Heat Shock Proteins Promote Cancer: It's a Protection Racket. *Trends in biochemical sciences* 41, 311–323.

Catlett, M. G. and Kaplan, K. B. (2006). Sgt1p is a unique co-chaperone that acts as a client adaptor to link Hsp90 to Skp1p. *The Journal of biological chemistry* 281, 33739–33748.

Chang, H. C. and Lindquist, S (1994). Conservation of Hsp90 macromolecular complexes in Saccharomyces cerevisiae. *The Journal of biological chemistry* 269, 24983–24988.

Cheetham, M. E. and Caplan, A. J. (1998). Structure, function and evolution of DnaJ: conservation and adaptation of chaperone function. *Cell stress & chaperones* 3, 28–36.

Chen, B., Zhong, D., and Monteiro, A. (2006). Comparative genomics and evolution of the HSP90 family of genes across all kingdoms of organisms. *BMC genomics* 7, 156.

Chen, M. X. and Cohen, P. T. (1997). Activation of protein phosphatase 5 by limited proteolysis or the binding of polyunsaturated fatty acids to the TPR domain. *FEBS letters* 400, 136–140.

Chen, M. X., McPartlin, A. E., Brown, L, Chen, Y. H., Barker, H. M., and Cohen, P. T. (1994). A novel human protein serine/threonine phosphatase, which possesses four tetratricopeptide repeat motifs and localizes to the nucleus. *The EMBO journal* 13, 4278–4290.

Chen, S and Smith, D. F. (1998). Hop as an adaptor in the heat shock protein 70 (Hsp70) and hsp90 chaperone machinery. *The Journal of biological chemistry* 273, 35194–35200.

Chiosis, G, Rodina, A, and Moulick, K (2006). Emerging Hsp90 inhibitors: from discovery to clinic. *Anti-cancer agents in medicinal chemistry* 6, 1–8.

Chiti, F. and Dobson, C. M. (2006). Protein misfolding, functional amyloid, and human disease. *Annual review of biochemistry* 75, 333–366.

Christian, M., Cermak, T., Doyle, E. L., Schmidt, C., Zhang, F., Hummel, A., Bogdanove, A. J., and Voytas, D. F. (2010). Targeting DNA double-strand breaks with TAL effector nucleases. *Genetics* 186, 757–761.

Citri, A. et al. (2006). Hsp90 recognizes a common surface on client kinases. *The Journal of biological chemistry* 281, 14361–14369.

Clayton, A., Turkes, A., Navabi, H., Mason, M. D., and Tabi, Z. (2005). Induction of heat shock proteins in B-cell exosomes. *Journal of cell science* 118, 3631–3638.

Clerico, E. M., Tilitsky, J. M., Meng, W., and Gierasch, L. M. (2015). How hsp70 molecular machines interact with their substrates to mediate diverse physiological functions. *Journal of molecular biology* 427, 1575–1588.

Clos, J, Westwood, J. T., Becker, P. B., Wilson, S, Lambert, K, and Wu, C (1990). Molecular cloning and expression of a hexameric Drosophila heat shock factor subject to negative regulation. *Cell* 63, 1085–1097.

Cloutier, P., Poitras, C., Durand, M., Hekmat, O., Fiola-Masson, E., Bouchard, A., Faubert, D., Chabot, B., and Coulombe, B. (2017). R2TP/Prefoldin-like component RUVBL1/RUVBL2 directly interacts with ZNHIT2 to regulate assembly of U5 small nuclear ribonucleoprotein. *Nature communications* 8, 15615.

Collins, S. R. et al. (2007). Functional dissection of protein complexes involved in yeast chromosome biology using a genetic interaction map. *Nature* 446, 806–810.

Cong, L. et al. (2013). Multiplex genome engineering using CRISPR/Cas systems. *Science* 339, 819–823.

Connell, P, Ballinger, C. A., Jiang, J, Wu, Y, Thompson, L. J., Höhfeld, J, and Patterson, C (2001). The co-chaperone CHIP regulates protein triage decisions mediated by heat-shock proteins. *Nature cell biology* 3, 93–96.

Costanzo, M. et al. (2016). A global genetic interaction network maps a wiring diagram of cellular function. *Science* 353.

Cotto, J. J., Kline, M, and Morimoto, R. I. (1996). Activation of heat shock factor 1 DNA binding precedes stress-induced serine phosphorylation. Evidence for a multistep pathway of regulation. *The Journal of biological chemistry* 271, 3355–3358.

Cox, J. and Mann, M. (2008). MaxQuant enables high peptide identification rates, individualized p.p.b.-range mass accuracies and proteome-wide protein quantification. *Nature biotechnology* 26, 1367–1372.

Cox, J., Hein, M. Y., Luber, C. A., Paron, I., Nagaraj, N., and Mann, M. (2014). Accurate proteome-wide label-free quantification by delayed normalization and maximal peptide ratio extraction, termed MaxLFQ. *Molecular & cellular proteomics* 13, 2513–2526.

Cox, M. B. and Johnson, J. L. (2018). Evidence for Hsp90 Co-chaperones in Regulating Hsp90 Function and Promoting Client Protein Folding. *Methods in molecular biology* 1709, 397–422.

Craig, E. A., Huang, P, Aron, R, and Andrew, A (2006). The diverse roles of J-proteins, the obligate Hsp70 co-chaperone. *Reviews of physiology, biochemistry and pharmacology* 156, 1–21.

Craig, E. A. and Marszalek, J. (2017). How Do J-Proteins Get Hsp70 to Do So Many Different Things? *Trends in biochemical sciences* 42, 355–368.

Criado-Marrero, M., Rein, T., Binder, E. B., Porter, J. T., Koren, J., and Blair, L. J. (2018). Hsp90 and FKBP51: complex regulators of psychiatric diseases. *Philosophical transactions of the Royal Society of London. Series B, Biological sciences* 373.

Cunningham, C. N., Krukenberg, K. A., and Agard, D. A. (2008). Intra- and intermonomer interactions are required to synergistically facilitate ATP hydrolysis in Hsp90. *The Journal of biological chemistry* 283, 21170–21178.

Cyr, D. M. (2008). Swapping nucleotides, tuning Hsp70. *Cell* 133, 945–947.

Dagar, M., Singh, J. P., Dagar, G., Tyagi, R. K., and Bagchi, G. (2019). Phosphorylation of HSP90 by protein kinase A is essential for the nuclear translocation of androgen receptor. *The Journal of biological chemistry* 294, 8699–8710.

Dahiya, V. and Buchner, J. (2019). Functional principles and regulation of molecular chaperones. *Advances in protein chemistry and structural biology* 114, 1–60.

Dahiya, V., Agam, G., Lawatscheck, J., Rutz, D. A., Lamb, D. C., and Buchner, J. (2019). Coordinated Conformational Processing of the Tumor Suppressor Protein p53 by the Hsp70 and Hsp90 Chaperone Machineries. *Molecular cell* 74, 816–830.e7.

Das, A. K., Cohen, P. W., and Barford, D (1998). The structure of the tetratricopeptide repeats of protein phosphatase 5: implications for TPR-mediated protein-protein interactions. *The EMBO journal* 17, 1192–1199.

Daugaard, M., Rohde, M., and Jäättelä, M. (2007). The heat shock protein 70 family: Highly homologous proteins with overlapping and distinct functions. *FEBS letters* 581, 3702–3710.

Deuerling, E., Gamerdinger, M., and Kreft, S. G. (2019). Chaperone Interactions at the Ribosome. *Cold Spring Harbor perspectives in biology* 11.

Deutschbauer, A. M., Jaramillo, D. F., Proctor, M., Kumm, J., Hillenmeyer, M. E., Davis, R. W., Nislow, C., and Giaever, G. (2005). Mechanisms of haploinsufficiency revealed by genome-wide profiling in yeast. *Genetics* 169, 1915–1925.

Dey, B, Lightbody, J. J., and Boschelli, F (1996a). CDC37 is required for p60v-src activity in yeast. *Molecular biology of the cell* 7, 1405–1417.

Dey, B, Caplan, A. J., and Boschelli, F (1996b). The Ydj1 molecular chaperone facilitates formation of active p60v-src in yeast. *Molecular biology of the cell* 7, 91–100.

Dill, K. A. and Chan, H. S. (1997). From Levinthal to pathways to funnels. *Nature structural biology* 4, 10–19.

Ding, G., Chen, P., Zhang, H., Huang, X., Zang, Y., Li, J., Li, J., and Wong, J. (2016). Regulation of Ubiquitin-like with Plant Homeodomain and RING Finger Domain 1 (UHRF1) Protein Stability by Heat Shock Protein 90 Chaperone Machinery. *The Journal of biological chemistry* 291, 20125–20135.

Dittmar, K. D. and Pratt, W. B. (1997). Folding of the glucocorticoid receptor by the reconstituted Hsp90-based chaperone machinery. The initial hsp90.p60.hsp70-dependent step is sufficient for creating the steroid binding conformation. *The Journal of biological chemistry* 272, 13047–13054.

Dittmar, K. D., Demady, D. R., Stancato, L. F., Krishna, P, and Pratt, W. B. (1997). Folding of the glucocorticoid receptor by the heat shock protein (hsp) 90-based chaperone machinery. The role of p23 is to stabilize receptor.hsp90 heterocomplexes formed by hsp90.p60.hsp70. *The Journal of biological chemistry* 272, 21213–21220.

Dobson, C. M. (2004). Principles of protein folding, misfolding and aggregation. *Seminars in cell & developmental biology* 15, 3–16.

Dollins, D. E., Warren, J. J., Immormino, R. M., and Gewirth, D. T. (2007). Structures of GRP94-nucleotide complexes reveal mechanistic differences between the hsp90 chaperones. *Molecular cell* 28, 41–56.

Duina, A. A., Marsh, J. A., and Gaber, R. F. (1996). Identification of two CyP-40-like cyclophilins in Saccharomyces cerevisiae, one of which is required for normal growth. *Yeast* 12, 943–952.

Duina, A. A., Marsh, J. A., Kurtz, R. B., Chang, H. C., Lindquist, S, and Gaber, R. F. (1998). The peptidyl-prolyl isomerase domain of the CyP-40 cyclophilin homolog Cpr7 is not required to support growth or glucocorticoid receptor activity in Saccharomyces cerevisiae. *The Journal of biological chemistry* 273, 10819–10822.

Dunker, A. K., Brown, C. J., Lawson, J. D., Iakoucheva, L. M., and Obradović, Z. (2002). Intrinsic disorder and protein function. *Biochemistry* 41, 6573–6582.

Ebong, I.-o., Morgner, N., Zhou, M., Saraiva, M. A., Daturpalli, S., Jackson, S. E., and Robinson, C. V. (2011). Heterogeneity and dynamics in the assembly of the heat shock protein 90 chaperone complexes. *Proceedings of the National Academy of Sciences of the United States of America* 108, 17939–17944.

Echeverría, P. C., Bernthaler, A., Dupuis, P., Mayer, B., and Picard, D. (2011). An interaction network predicted from public data as a discovery tool: application to the Hsp90 molecular chaperone machine. *PloS one* 6, e26044.

Echeverría, P. C., Briand, P.-A., and Picard, D. (2016). A Remodeled Hsp90 Molecular Chaperone Ensemble with the Novel Cochaperone Aarsd1 Is Required for Muscle Differentiation. *Molecular and cellular biology* 36, 1310–1321.

Echtenkamp, F. J., Zelin, E., Oxelmark, E., Woo, J. I., Andrews, B. J., Garabedian, M., and Freeman, B. C. (2011). Global functional map of the p23 molecular chaperone reveals an extensive cellular network. *Molecular cell* 43, 229–241.

Echtenkamp, F. J., Gvozdenov, Z., Adkins, N. L., Zhang, Y., Lynch-Day, M., Watanabe, S., Peterson, C. L., and Freeman, B. C. (2016). Hsp90 and p23 Molecular Chaperones Control Chromatin Architecture by Maintaining the Functional Pool of the RSC Chromatin Remodeler. *Molecular cell* 64, 888–899.

Eckl, J. M., Rutz, D. A., Haslbeck, V., Zierer, B. K., Reinstein, J., and Richter, K. (2013). Cdc37 (cell division cycle 37) restricts Hsp90 (heat shock protein 90) motility by interaction with N-terminal and middle domain binding sites. *The Journal of biological chemistry* 288, 16032–16042.

Eckl, J. M., Scherr, M. J., Freiburger, L., Daake, M. A., Sattler, M., and Richter, K. (2015). Hsp90·Cdc37 Complexes with Protein Kinases Form Cooperatively with Multiple Distinct Interaction Sites. *The Journal of biological chemistry* 290, 30843–30854.

Eckl, J. M., Daake, M., Schwartz, S., and Richter, K. (2016). Nucleotide-Free sB-Raf is Preferentially Bound by Hsp90 and Cdc37 In Vitro. *Journal of molecular biology* 428, 4185–4196.

Ehrlich, E. S., Wang, T., Luo, K., Xiao, Z., Niewiadomska, A. M., Martinez, T., Xu, W., Neckers, L., and Yu, X.-F. (2009). Regulation of Hsp90 client proteins by a

Cullin5-RING E3 ubiquitin ligase. *Proceedings of the National Academy of Sciences of the United States of America* 106, 20330–20335.

Elble, R (1992). A simple and efficient procedure for transformation of yeasts. *BioTechniques* 13, 18–20.

Elena, S. F. and Lenski, R. E. (1997). Test of synergistic interactions among deleterious mutations in bacteria. *Nature* 390, 395–398.

Ellis, R. J. (1990). The molecular chaperone concept. In: *Seminars in cell biology*. Vol. 1. 1, 1–9.

Ellis, R. J. and Minton, A. P. (2006). Protein aggregation in crowded environments. *Biological chemistry* 387, 485–497.

Elnatan, D., Betegon, M., Liu, Y., Ramelot, T., Kennedy, M. A., and Agard, D. A. (2017). Symmetry broken and rebroken during the ATP hydrolysis cycle of the mitochondrial Hsp90 TRAP1. *eLife* 6.

Esposito, A. M. and Kinzy, T. G. (2014). In vivo [35S]-methionine incorporation. *Methods in enzymology* 536, 55–64.

Falsone, S. F., Leptihn, S., Osterauer, A., Haslbeck, M., and Buchner, J. (2004). Oncogenic mutations reduce the stability of SRC kinase. *Journal of molecular biology* 344, 281–291.

Fan, C.-Y., Lee, S., and Cyr, D. M. (2003). Mechanisms for regulation of Hsp70 function by Hsp40. *Cell stress & chaperones* 8, 309–316.

Fan, C.-Y., Ren, H.-Y., Lee, P., Caplan, A. J., and Cyr, D. M. (2005). The type I Hsp40 zinc finger-like region is required for Hsp70 to capture non-native polypeptides from Ydj1. *The Journal of biological chemistry* 280, 695–702.

Fang, Y, Fliss, A. E., Robins, D. M., and Caplan, A. J. (1996). Hsp90 regulates androgen receptor hormone binding affinity in vivo. *The Journal of biological chemistry* 271, 28697–28702.

Fang, Y, Fliss, A. E., Rao, J, and Caplan, A. J. (1998). SBA1 encodes a yeast hsp90 cochaperone that is homologous to vertebrate p23 proteins. *Molecular and cellular biology* 18, 3727–3734.

Felts, S. J. and Toft, D. O. (2003). p23, a simple protein with complex activities. *Cell stress & chaperones* 8, 108–113.

Ferrari, L. and Rüdiger, S. G. D. (2019). Hsp90 Chaperone in Disease. In: *Heat Shock Protein 90 in Human Diseases and Disorders*. Ed. by A. A. A. Asea and P. Kaur. Cham: Springer International Publishing, 473–491.

Finka, A. and Goloubinoff, P. (2013). Proteomic data from human cell cultures refine mechanisms of chaperone-mediated protein homeostasis. *Cell stress & chaperones* 18, 591–605.

Flaherty, K. M., DeLuca-Flaherty, C, and McKay, D. B. (1990). Three-dimensional structure of the ATPase fragment of a 70K heat-shock cognate protein. *Nature* 346, 623–628.

Flom, G., Weekes, J., Williams, J. J., and Johnson, J. L. (2006). Effect of mutation of the tetratricopeptide repeat and asparatate-proline 2 domains of Sti1 on Hsp90 signaling and interaction in Saccharomyces cerevisiae. *Genetics* 172, 41–51.

Flynn, G. C., Chappell, T. G., and Rothman, J. E. (1989). Peptide binding and release by proteins implicated as catalysts of protein assembly. *Science (New York, N.Y.)* 245, 385–390.

Frattini, A., Fabbri, M., Valli, R., De Paoli, E., Montalbano, G., Gribaldo, L., Pasquali, F., and Maserati, E. (2015). High variability of genomic instability and gene expression profiling in different HeLa clones. *Scientific reports* 5, 15377.

Freeman, B. C., Myers, M. P., Schumacher, R, and Morimoto, R. I. (1995). Identification of a regulatory motif in Hsp70 that affects ATPase activity, substrate binding and interaction with HDJ-1. *The EMBO journal* 14, 2281–2292.

Freeman, B. C., Toft, D. O., and Morimoto, R. I. (1996). Molecular chaperone machines: chaperone activities of the cyclophilin Cyp-40 and the steroid aporeceptor-associated protein p23. *Science* 274, 1718–1720.

Freeman, B. C., Felts, S. J., Toft, D. O., and Yamamoto, K. R. (2000). The p23 molecular chaperones act at a late step in intracellular receptor action to differentially affect ligand efficacies. *Genes & development* 14, 422–434.

Fu, Q., Wang, W., Zhou, T., and Yang, Y. (2016). Emerging roles of NudC family: from molecular regulation to clinical implications. *Science China. Life sciences* 59, 455–462.

García-Cardeña, G, Fan, R, Shah, V, Sorrentino, R, Cirino, G, Papapetropoulos, A, and Sessa, W. C. (1998). Dynamic activation of endothelial nitric oxide synthase by Hsp90. *Nature* 392, 821–824.

Gasch, A. P., Spellman, P. T., Kao, C. M., Carmel-Harel, O, Eisen, M. B., Storz, G, Botstein, D, and Brown, P. O. (2000). Genomic expression programs in the response of yeast cells to environmental changes. *Molecular biology of the cell* 11, 4241–4257.

Gassler, C. S., Wiederkehr, T, Brehmer, D, Bukau, B, and Mayer, M. P. (2001). Bag-1M accelerates nucleotide release for human Hsc70 and Hsp70 and can act concentration dependent as positive and negative cofactor. *The Journal of biological chemistry* 276, 32538–32544.

Geiger, T., Wehner, A., Schaab, C., Cox, J., and Mann, M. (2012). Comparative proteomic analysis of eleven common cell lines reveals ubiquitous but varying expression of most proteins. *Molecular & cellular proteomics* 11, M111.014050.

Genest, O., Reidy, M., Street, T. O., Hoskins, J. R., Camberg, J. L., Agard, D. A., Masison, D. C., and Wickner, S. (2013). Uncovering a region of heat shock protein 90 important for client binding in E. coli and chaperone function in yeast. *Molecular cell* 49, 464–473.

Genest, O., Hoskins, J. R., Kravats, A. N., Doyle, S. M., and Wickner, S. (2015). Hsp70 and Hsp90 of E. coli Directly Interact for Collaboration in Protein Remodeling. *Journal of molecular biology* 427, 3877–3889.

Gerlinger, M., McGranahan, N., Dewhurst, S. M., Burrell, R. A., Tomlinson, I., and Swanton, C. (2014). Cancer: evolution within a lifetime. *Annual review of genetics* 48, 215–236.

Gething, M. J. and Sambrook, J (1992). Protein folding in the cell. *Nature* 355, 33–45.

Ghaemmaghami, S., Huh, W.-K., Bower, K., Howson, R. W., Belle, A., Dephoure, N., O'Shea, E. K., and Weissman, J. S. (2003). Global analysis of protein expression in yeast. *Nature* 425, 737–741.

Ghosh, I., Hamilton, A. D., and Regan, L. (2000). Antiparallel leucine zipper-directed protein reassembly: application to the green fluorescent protein. *Journal of the American Chemical Society* 122.23, 5658–5659.

Ghosh, K. and Dill, K. (2010). Cellular proteomes have broad distributions of protein stability. *Biophysical journal* 99, 3996–4002.

Gibbs, A., Schwartzman, J., Deng, V., and Alumkal, J. (2009). Sulforaphane destabilizes the androgen receptor in prostate cancer cells by inactivating histone deacetylase 6. *Proceedings of the National Academy of Sciences of the United States of America* 106, 16663–16668.

Gietz, R. D. and Schiestl, R. H. (2007). High-efficiency yeast transformation using the LiAc/SS carrier DNA/PEG method. *Nature protocols* 2, 31–34.

Gilbert, L. A. et al. (2013). CRISPR-mediated modular RNA-guided regulation of transcription in eukaryotes. *Cell* 154, 442–451.

Gilbert, L. A. et al. (2014). Genome-Scale CRISPR-Mediated Control of Gene Repression and Activation. *Cell* 159, 647–661.

Girstmair, H. et al. (2019). The Hsp90 isoforms from S. cerevisiae differ in structure, function and client range. *Nature communications* 10, 3626.

Goeckeler, J. L., Stephens, A., Lee, P., Caplan, A. J., and Brodsky, J. L. (2002). Overexpression of yeast Hsp110 homolog Sse1p suppresses ydj1-151 thermosensitivity and restores Hsp90-dependent activity. *Molecular biology of the cell* 13, 2760–2770.

Gowda, N. K. C., Kaimal, J. M., Kityk, R., Daniel, C., Liebau, J., Öhman, M., Mayer, M. P., and Andréasson, C. (2018). Nucleotide exchange factors Fes1 and HspBP1 mimic substrate to release misfolded proteins from Hsp70. *Nature structural & molecular biology* 25, 83–89.

Grammatikakis, N, Lin, J. H., Grammatikakis, A, Tsichlis, P. N., and Cochran, B. H. (1999). p50(cdc37) acting in concert with Hsp90 is required for Raf-1 function. *Molecular and cellular biology* 19, 1661–1672.

Greene, M. K., Maskos, K, and Landry, S. J. (1998). Role of the J-domain in the cooperation of Hsp40 with Hsp70. *Proceedings of the National Academy of Sciences of the United States of America* 95, 6108–6113.

Guo, Y., Guettouche, T., Fenna, M., Boellmann, F., Pratt, W. B., Toft, D. O., Smith, D. F., and Voellmy, R. (2001). Evidence for a mechanism of repression of heat shock factor 1 transcriptional activity by a multichaperone complex. *Journal of Biological Chemistry* 276.49, 45791–45799.

Gupta, A., Bansal, A., and Hashimoto-Torii, K. (2020). HSP70 and HSP90 in neurodegenerative diseases. *Neuroscience letters* 716, 134678.

Gvozdenov, Z., Bendix, L. D., Kolhe, J., and Freeman, B. C. (2019). The Hsp90 Molecular Chaperone Regulates the Transcription Factor Network Controlling Chromatin Accessibility. *Journal of molecular biology* 431, 4993–5003.

Ha, J. H., Hellman, U, Johnson, E. R., Li, L, McKay, D. B., Sousa, M. C., Takeda, S, Wernstedt, C, and Wilbanks, S. M. (1997). Destabilization of peptide binding and interdomain communication by an E543K mutation in the bovine 70-kDa heat shock cognate protein, a molecular chaperone. *The Journal of biological chemistry* 272, 27796–27803.

Hageman, J. and Kampinga, H. H. (2009). Computational analysis of the human HSPH/HSPA/DNAJ family and cloning of a human HSPH/HSPA/DNAJ expression library. *Cell stress & chaperones* 14, 1–21.

Hagn, F., Lagleder, S., Retzlaff, M., Rohrberg, J., Demmer, O., Richter, K., Buchner, J., and Kessler, H. (2011). Structural analysis of the interaction between Hsp90 and the tumor suppressor protein p53. *Nature structural & molecular biology* 18, 1086–1093.

Hainzl, O., Lapina, M. C., Buchner, J., and Richter, K. (2009). The charged linker region is an important regulator of Hsp90 function. *The Journal of biological chemistry* 284, 22559–22567.

Harju, S., Fedosyuk, H., and Peterson, K. R. (2004). Rapid isolation of yeast genomic DNA: Bust n Grab. *BMC biotechnology* 4, 8.

Harris, S. F., Shiau, A. K., and Agard, D. A. (2004). The crystal structure of the carboxy-terminal dimerization domain of htpG, the Escherichia coli Hsp90, reveals a potential substrate binding site. *Structure* 12, 1087–1097.

Harrison, C. J., Hayer-Hartl, M, Di Liberto, M, Hartl, F, and Kuriyan, J (1997). Crystal structure of the nucleotide exchange factor GrpE bound to the ATPase domain of the molecular chaperone DnaK. *Science* 276, 431–435.

Hart, T., Brown, K. R., Sircoulomb, F., Rottapel, R., and Moffat, J. (2014). Measuring error rates in genomic perturbation screens: gold standards for human functional genomics. *Molecular systems biology* 10, 733.

Hartl, F. U., Bracher, A., and Hayer-Hartl, M. (2011). Molecular chaperones in protein folding and proteostasis. *Nature* 475, 324–332.

Haslbeck, M., Weinkauf, S., and Buchner, J. (2019). Small heat shock proteins: Simplicity meets complexity. *The Journal of biological chemistry* 294, 2121–2132.

Havranek, J. J. and Harbury, P. B. (2003). Automated design of specificity in molecular recognition. *Nature structural biology* 10, 45–52.

Hayer-Hartl, M., Bracher, A., and Hartl, F. U. (2016). The GroEL-GroES Chaperonin Machine: A Nano-Cage for Protein Folding. *Trends in biochemical sciences* 41, 62–76.

Hayes, D. B. and Stafford, W. F. (2010). SEDVIEW, Real-time Sedimentation Analysis. *Macromolecular bioscience* 10.7, 731–735.

Hayes, S. A. and Dice, J. F. (1996). Roles of molecular chaperones in protein degradation. *The Journal of cell biology* 132, 255–258.

Hessling, M., Richter, K., and Buchner, J. (2009). Dissection of the ATP-induced conformational cycle of the molecular chaperone Hsp90. *Nature structural & molecular biology* 16, 287–293.

Holmes, W. M., Klaips, C. L., and Serio, T. R. (2014). Defining the limits: Protein aggregation and toxicity in vivo. *Critical reviews in biochemistry and molecular biology* 49, 294–303.

Hong, J. and Gierasch, L. M. (2010). Macromolecular crowding remodels the energy landscape of a protein by favoring a more compact unfolded state. *Journal of the American Chemical Society* 132, 10445–10452.

Horlbeck, M. A. et al. (2016). Compact and highly active next-generation libraries for CRISPR-mediated gene repression and activation. *eLife* 5.

Horwich, A. L., Fenton, W. A., Chapman, E., and Farr, G. W. (2007). Two families of chaperonin: physiology and mechanism. *Annual review of cell and developmental biology* 23, 115–145.

Houry, W. A., Bertrand, E., and Coulombe, B. (2018). The PAQosome, an R2TP-Based Chaperone for Quaternary Structure Formation. *Trends in biochemical sciences* 43, 4–9.

Hua, G., Zhang, Q., and Fan, Z. (2007). Heat shock protein 75 (TRAP1) antagonizes reactive oxygen species generation and protects cells from granzyme M-mediated apoptosis. *The Journal of biological chemistry* 282, 20553–20560.

Huck, J. D., Que, N. L., Hong, F., Li, Z., and Gewirth, D. T. (2017). Structural and Functional Analysis of GRP94 in the Closed State Reveals an Essential Role for the Pre-N Domain and a Potential Client-Binding Site. *Cell reports* 20, 2800–2809.

Hutchison, K. A., Scherrer, L. C., Czar, M. J., Stancato, L. F., Chow, Y. H., Jove, R, and Pratt, W. B. (1993). Regulation of glucocorticoid receptor function through assembly of a receptor-heat shock protein complex. *Annals of the New York Academy of Sciences* 684, 35–48.

Höhfeld, J and Jentsch, S (1997). GrpE-like regulation of the hsc70 chaperone by the anti-apoptotic protein BAG-1. *The EMBO journal* 16, 6209–6216.

Im, C.-N. (2016). Past, present, and emerging roles of mitochondrial heat shock protein TRAP1 in the metabolism and regulation of cancer stem cells. *Cell stress & chaperones* 21, 553–562.

Im, C.-N., Lee, J.-S., Zheng, Y., and Seo, J.-S. (2007). Iron chelation study in a normal human hepatocyte cell line suggests that tumor necrosis factor receptor-associated protein 1 (TRAP1) regulates production of reactive oxygen species. *Journal of cellular biochemistry* 100, 474–486.

Jackson, S. E. (1998). How do small single-domain proteins fold? *Folding & design* 3, R81–R91.

Jaeger, A. M. and Whitesell, L. (2019). HSP90: Enabler of Cancer Adaptation. *Annual review of cancer biology* 3, 275–297.

Jahn, M., Rehn, A., Pelz, B., Hellenkamp, B., Richter, K., Rief, M., Buchner, J., and Hugel, T. (2014). The charged linker of the molecular chaperone Hsp90 modulates domain contacts and biological function. *Proceedings of the National Academy of Sciences of the United States of America* 111, 17881–17886.

Jakob, U and Buchner, J (1994). Assisting spontaneity: the role of Hsp90 and small Hsps as molecular chaperones. *Trends in biochemical sciences* 19, 205–211.

Jakob, U, Lilie, H, Meyer, I, and Buchner, J (1995). Transient interaction of Hsp90 with early unfolding intermediates of citrate synthase. Implications for heat shock in vivo. *The Journal of biological chemistry* 270, 7288–7294.

Jakobsen, B. K. and Pelham, H. R. (1988). Constitutive binding of yeast heat shock factor to DNA in vivo. *Molecular and cellular biology* 8, 5040–5042.

Janke, C. et al. (2004). A versatile toolbox for PCR-based tagging of yeast genes: new fluorescent proteins, more markers and promoter substitution cassettes. *Yeast* 21, 947–962.

Janowska, M. K., Baughman, H. E. R., Woods, C. N., and Klevit, R. E. (2019). Mechanisms of Small Heat Shock Proteins. *Cold Spring Harbor perspectives in biology* 11.

Janson, J, Ashley, R. H., Harrison, D, McIntyre, S, and Butler, P. C. (1999). The mechanism of islet amyloid polypeptide toxicity is membrane disruption by intermediate-sized toxic amyloid particles. *Diabetes* 48, 491–498.

Jarosz, D. F. and Lindquist, S. (2010). Hsp90 and environmental stress transform the adaptive value of natural genetic variation. *Science* 330, 1820–1824.

Jiang, J., Prasad, K., Lafer, E. M., and Sousa, R. (2005). Structural basis of interdomain communication in the Hsc70 chaperone. *Molecular cell* 20, 513–524.

Jiang, J., Maes, E. G., Taylor, A. B., Wang, L., Hinck, A. P., Lafer, E. M., and Sousa, R. (2007). Structural basis of J cochaperone binding and regulation of Hsp70. *Molecular cell* 28, 422–433.

Jiang, Y., Rossi, P., and Kalodimos, C. G. (2019). Structural basis for client recognition and activity of Hsp40 chaperones. *Science* 365, 1313–1319.

Jinek, M., Chylinski, K., Fonfara, I., Hauer, M., Doudna, J. A., and Charpentier, E. (2012). A programmable dual-RNA-guided DNA endonuclease in adaptive bacterial immunity. *Science* 337, 816–821.

Jinek, M., East, A., Cheng, A., Lin, S., Ma, E., and Doudna, J. (2013). RNA-programmed genome editing in human cells. *eLife* 2. Original DateCompleted: 20130207, Original DateCompleted: 20140206, e00471.

Johnson, B. D., Schumacher, R. J., Ross, E. D., and Toft, D. O. (1998). Hop modulates Hsp70/Hsp90 interactions in protein folding. *The Journal of biological chemistry* 273, 3679–3686.

Johnson, J. L. (2012). Evolution and function of diverse Hsp90 homologs and cochaperone proteins. *Biochimica et biophysica acta* 1823, 607–613.

Jolly, C and Morimoto, R. I. (2000). Role of the heat shock response and molecular chaperones in oncogenesis and cell death. *Journal of the National Cancer Institute* 92, 1564–1572.

Jost, M. et al. (2020). Titrating gene expression using libraries of systematically attenuated CRISPR guide RNAs. *Nature biotechnology* 38, 355–364.

Kabani, M. and Martineau, C. N. (2008). Multiple hsp70 isoforms in the eukaryotic cytosol: mere redundancy or functional specificity? *Current genomics* 9, 338–248.

Kalinin, S., Valeri, A., Antonik, M., Felekyan, S., and Seidel, C. A. M. (2010). Detection of structural dynamics by FRET: a photon distribution and fluorescence lifetime analysis of systems with multiple states. *The journal of physical chemistry. B* 114, 7983–7995.

Kamal, A., Thao, L., Sensintaffar, J., Zhang, L., Boehm, M. F., Fritz, L. C., and Burrows, F. J. (2003). A high-affinity conformation of Hsp90 confers tumour selectivity on Hsp90 inhibitors. *Nature* 425, 407–410.

Kampinga, H. H. and Craig, E. A. (2010). The HSP70 chaperone machinery: J proteins as drivers of functional specificity. *Nature reviews. Molecular cell biology* 11, 579–592.

Kampmann, M. (2018). CRISPRi and CRISPRa Screens in Mammalian Cells for Precision Biology and Medicine. *ACS chemical biology* 13, 406–416.

Kampmann, M., Bassik, M. C., and Weissman, J. S. (2013). Integrated platform for genome-wide screening and construction of high-density genetic interaction maps in mammalian cells. *Proceedings of the National Academy of Sciences of the United States of America* 110, E2317–E2326.

Kampmann, M., Bassik, M. C., and Weissman, J. S. (2014). Functional genomics platform for pooled screening and generation of mammalian genetic interaction maps. *Nature protocols* 9, 1825–1847.

Kampmann, M. et al. (2015). Next-generation libraries for robust RNA interference-based genome-wide screens. *Proceedings of the National Academy of Sciences of the United States of America* 112, E3384–E3391.

Kang, B. H., Plescia, J., Dohi, T., Rosa, J., Doxsey, S. J., and Altieri, D. C. (2007). Regulation of tumor cell mitochondrial homeostasis by an organelle-specific Hsp90 chaperone network. *Cell* 131, 257–270.

Karagöz, G. E. and Rüdiger, S. G. D. (2015). Hsp90 interaction with clients. *Trends in biochemical sciences* 40, 117–125.

Karagöz, G. E., Duarte, A. M. S., Ippel, H., Uetrecht, C., Sinnige, T., Rosmalen, M. van, Hausmann, J., Heck, A. J. R., Boelens, R., and Rüdiger, S. G. D. (2011). N-terminal domain of human Hsp90 triggers binding to the cochaperone p23. *Proceedings of the National Academy of Sciences of the United States of America* 108, 580–585.

Karagöz, G. E. et al. (2014). Hsp90-Tau complex reveals molecular basis for specificity in chaperone action. *Cell* 156, 963–974.

Karras, G. I., Yi, S., Sahni, N., Fischer, M., Xie, J., Vidal, M., D'Andrea, A. D., Whitesell, L., and Lindquist, S. (2017). HSP90 Shapes the Consequences of Human Genetic Variation. *Cell* 168, 856–866.e12.

Kekatpure, V. D., Dannenberg, A. J., and Subbaramaiah, K. (2009). HDAC6 modulates Hsp90 chaperone activity and regulates activation of aryl hydrocarbon receptor signaling. *The Journal of biological chemistry* 284, 7436–7445.

Kelley, W. L. (1998). The J-domain family and the recruitment of chaperone power. *Trends in biochemical sciences* 23, 222–227.

Keramisanou, D., Aboalroub, A., Zhang, Z., Liu, W., Marshall, D., Diviney, A., Larsen, R. W., Landgraf, R., and Gelis, I. (2016). Molecular Mechanism of Protein Kinase Recognition and Sorting by the Hsp90 Kinome-Specific Cochaperone Cdc37. *Molecular cell* 62, 260–271.

Kiefhaber, T, Rudolph, R, Kohler, H. H., and Buchner, J (1991). Protein aggregation in vitro and in vivo: a quantitative model of the kinetic competition between folding and aggregation. *Bio/Technology* 9, 825–829.

Kijima, T. et al. (2018). HSP90 inhibitors disrupt a transient HSP90-HSF1 interaction and identify a noncanonical model of HSP90-mediated HSF1 regulation. *Scientific reports* 8, 6976.

Kim, Y. E., Hipp, M. S., Bracher, A., Hayer-Hartl, M., and Hartl, F. U. (2013). Molecular chaperone functions in protein folding and proteostasis. *Annual review of biochemistry* 82, 323–355.

Kimura, Y, Yahara, I, and Lindquist, S (1995). Role of the protein chaperone YDJ1 in establishing Hsp90-mediated signal transduction pathways. *Science* 268, 1362–1365.

Kimura, Y, Rutherford, S. L., Miyata, Y, Yahara, I, Freeman, B. C., Yue, L, Morimoto, R. I., and Lindquist, S (1997). Cdc37 is a molecular chaperone with specific functions in signal transduction. *Genes & development* 11, 1775–1785.

Kirschke, E., Goswami, D., Southworth, D., Griffin, P. R., and Agard, D. A. (2014). Glucocorticoid receptor function regulated by coordinated action of the Hsp90 and Hsp70 chaperone cycles. *Cell* 157, 1685–1697.

Kitagawa, K, Skowyra, D, Elledge, S. J., Harper, J. W., and Hieter, P (1999). SGT1 encodes an essential component of the yeast kinetochore assembly pathway and a novel subunit of the SCF ubiquitin ligase complex. *Molecular cell* 4, 21–33.

Kityk, R., Kopp, J., Sinning, I., and Mayer, M. P. (2012). Structure and dynamics of the ATP-bound open conformation of Hsp70 chaperones. *Molecular cell* 48, 863–874.

Kityk, R., Kopp, J., and Mayer, M. P. (2018). Molecular Mechanism of J-Domain-Triggered ATP Hydrolysis by Hsp70 Chaperones. *Molecular cell* 69, 227–237.e4.

Knarr, G, Gething, M. J., Modrow, S, and Buchner, J (1995). BiP binding sequences in antibodies. *The Journal of biological chemistry* 270, 27589–27594.

Knarr, G, Modrow, S, Todd, A, Gething, M. J., and Buchner, J (1999). BiP-binding sequences in HIV gp160. Implications for the binding specificity of bip. *The Journal of biological chemistry* 274, 29850–29857.

Koren, I., Timms, R. T., Kula, T., Xu, Q., Li, M. Z., and Elledge, S. J. (2018). The Eukaryotic Proteome Is Shaped by E3 Ubiquitin Ligases Targeting C-Terminal Degrons. *Cell* 173, 1622–1635.e14.

Kornbluth, S, Jove, R, and Hanafusa, H (1987). Characterization of avian and viral p60src proteins expressed in yeast. *Proceedings of the National Academy of Sciences of the United States of America* 84, 4455–4459.

Koulov, A. V. et al. (2010). Biological and structural basis for Aha1 regulation of Hsp90 ATPase activity in maintaining proteostasis in the human disease cystic fibrosis. *Molecular biology of the cell* 21, 871–884.

Kravats, A. N., Hoskins, J. R., Reidy, M., Johnson, J. L., Doyle, S. M., Genest, O., Masison, D. C., and Wickner, S. (2018). Functional and physical interaction between yeast Hsp90 and Hsp70. *Proceedings of the National Academy of Sciences of the United States of America* 115, E2210–E2219.

Kundrat, L. and Regan, L. (2010). Balance between folding and degradation for Hsp90-dependent client proteins: a key role for CHIP. *Biochemistry* 49, 7428–7438.

Kurtz, S, Rossi, J, Petko, L, and Lindquist, S (1986). An ancient developmental induction: heat-shock proteins induced in sporulation and oogenesis. *Science* 231, 1154–1157.

Kushnirov, V. V. (2000). Rapid and reliable protein extraction from yeast. *Yeast* 16, 857–860.

Kuzmin, E. et al. (2018). Systematic analysis of complex genetic interactions. *Science* 360.

Laemmli, U. K. (1970). Cleavage of structural proteins during the assembly of the head of bacteriophage T4. *Nature* 227, 680–685.

LaPointe, P., Mercier, R., and Wolmarans, A. (2020). Aha-type co-chaperones: the alpha or the omega of the Hsp90 ATPase cycle? *Biological chemistry* 401, 423–434.

Larkindale, J. and Vierling, E. (2008). Core genome responses involved in acclimation to high temperature. *Plant physiology* 146, 748–761.

Laskey, R. A., Honda, B. M., Mills, A. D., and Finch, J. T. (1978). Nucleosomes are assembled by an acidic protein which binds histones and transfers them to DNA. *Nature* 275, 416–420.

Laue, T, Shah, B, Ridgeway, T, and Pelletier, S (1992). Computer-aided Interpretation of Sedimentation Data for Proteins. In: *Analytical Ultracentrifugation in Biochemistry and Polymer Science*. Royal Society of Chemistry, Cambridge, 90–125.

Laufen, T, Mayer, M. P., Beisel, C, Klostermeier, D, Mogk, A, Reinstein, J, and Bukau, B (1999). Mechanism of regulation of hsp70 chaperones by DnaJ cochaperones. *Proceedings of the National Academy of Sciences of the United States of America* 96, 5452–5457.

Lavery, L. A., Partridge, J. R., Ramelot, T. A., Elnatan, D., Kennedy, M. A., and Agard, D. A. (2014). Structural asymmetry in the closed state of mitochondrial Hsp90 (TRAP1) supports a two-step ATP hydrolysis mechanism. *Molecular cell* 53, 330–343.

Lee, P., Shabbir, A., Cardozo, C., and Caplan, A. J. (2004). Sti1 and Cdc37 can stabilize Hsp90 in chaperone complexes with a protein kinase. *Molecular biology of the cell* 15, 1785–1792.

Lee, S., Fan, C. Y., Younger, J. M., Ren, H., and Cyr, D. M. (2002). Identification of essential residues in the type II Hsp40 Sis1 that function in polypeptide binding. *The Journal of biological chemistry* 277, 21675–21682.

Leskovar, A., Wegele, H., Werbeck, N. D., Buchner, J., and Reinstein, J. (2008). The ATPase cycle of the mitochondrial Hsp90 analog Trap1. *The Journal of biological chemistry* 283, 11677–11688.

Levinthal, C. (1968). Are there pathways for protein folding? *Journal de chimie physique* 65, 44–45.

Levinthal, C. (1969). How to fold graciously. *Mossbauer spectroscopy in biological systems* 67, 22–24.

Li, D., Li, C., Li, L., Chen, S., Wang, L., Li, Q., Wang, X., Lei, X., and Shen, Z. (2016). Natural Product Kongensin A is a Non-Canonical HSP90 Inhibitor that Blocks RIP3-dependent Necroptosis. *Cell chemical biology* 23, 257–266.

Li, J., Richter, K., and Buchner, J. (2011). Mixed Hsp90-cochaperone complexes are important for the progression of the reaction cycle. *Nature structural & molecular biology* 18, 61–66.

Li, J., Soroka, J., and Buchner, J. (2012). The Hsp90 chaperone machinery: conformational dynamics and regulation by co-chaperones. *Biochimica et biophysica acta* 1823, 624–635.

Li, J., Richter, K., Reinstein, J., and Buchner, J. (2013). Integration of the accelerator Aha1 in the Hsp90 co-chaperone cycle. *Nature structural & molecular biology* 20, 326–331.

Li, J. and Sha, B. (2005). Structure-based mutagenesis studies of the peptide substrate binding fragment of type I heat-shock protein 40. *The Biochemical journal* 386, 453–460.

Li, J., Qian, X., and Sha, B. (2003). The crystal structure of the yeast Hsp40 Ydj1 complexed with its peptide substrate. *Structure* 11, 1475–1483.

Li, J., Wu, Y., Qian, X., and Sha, B. (2006). Crystal structure of yeast Sis1 peptide-binding fragment and Hsp70 Ssa1 C-terminal complex. *The Biochemical journal* 398, 353–360.

Li, T., Jiang, H.-L., Tong, Y.-G., and Lu, J.-J. (2018). Targeting the Hsp90-Cdc37-client protein interaction to disrupt Hsp90 chaperone machinery. *Journal of hematology & oncology* 11, 59.

Li, W., Li, Y., Guan, S., Fan, J., Cheng, C.-F., Bright, A. M., Chinn, C., Chen, M., and Woodley, D. T. (2007). Extracellular heat shock protein-90alpha: linking hypoxia to skin cell motility and wound healing. *The EMBO journal* 26, 1221–1233.

Lindquist, S (1986). The heat-shock response. *Annual review of biochemistry* 55, 1151–1191.

Lindquist, S and Craig, E. (1988). The heat-shock proteins. *Annual review of genetics* 22.1, 631–677.

Linke, K., Wolfram, T., Bussemer, J., and Jakob, U. (2003). The roles of the two zinc binding sites in DnaJ. *The Journal of biological chemistry* 278, 44457–44466.

Liu, B. and Li, Z. (2008). Endoplasmic reticulum HSP90b1 (gp96, grp94) optimizes B-cell function via chaperoning integrin and TLR but not immunoglobulin. *Blood* 112, 1223–1230.

Liu, B. et al. (2010). Folding of Toll-like receptors by the HSP90 paralogue gp96 requires a substrate-specific cochaperone. *Nature communications* 1, 79.

Liu, S. J. et al. (2017). CRISPRi-based genome-scale identification of functional long noncoding RNA loci in human cells. *Science* 355.

Liu, X. D., Liu, P. C., Santoro, N, and Thiele, D. J. (1997). Conservation of a stress response: human heat shock transcription factors functionally substitute for yeast HSF. *The EMBO journal* 16, 6466–6477.

Liu, Y. et al. (2019). Multi-omic measurements of heterogeneity in HeLa cells across laboratories. *Nature biotechnology* 37, 314–322.

Lorenz, O. R. et al. (2014). Modulation of the Hsp90 chaperone cycle by a stringent client protein. *Molecular cell* 53, 941–953.

Lotz, G. P., Lin, H., Harst, A., and Obermann, W. M. J. (2003). Aha1 binds to the middle domain of Hsp90, contributes to client protein activation, and stimulates the ATPase activity of the molecular chaperone. *The Journal of biological chemistry* 278, 17228–17235.

Lucas, X. and Ciulli, A. (2017). Recognition of substrate degrons by E3 ubiquitin ligases and modulation by small-molecule mimicry strategies. *Current opinion in structural biology* 44, 101–110.

Mali, P., Yang, L., Esvelt, K. M., Aach, J., Guell, M., DiCarlo, J. E., Norville, J. E., and Church, G. M. (2013). RNA-guided human genome engineering via Cas9. *Science* 339, 823–826.

Mani, R., St Onge, R. P., Hartman, J. L., Giaever, G., and Roth, F. P. (2008). Defining genetic interaction. *Proceedings of the National Academy of Sciences of the United States of America* 105, 3461–3466.

Markus, S. M., Taneja, S. S., Logan, S. K., Li, W., Ha, S., Hittelman, A. B., Rogatsky, I., and Garabedian, M. J. (2002). Identification and characterization of ART-27, a novel coactivator for the androgen receptor N terminus. *Molecular biology of the cell* 13, 670–682.

Martinez-Pastor, M., Marchler, G, Schüller, C, Marchler-Bauer, A, Ruis, H, and Estruch, F (1996). The Saccharomyces cerevisiae zinc finger proteins Msn2p and Msn4p are required for transcriptional induction through the stress response element (STRE). *The EMBO journal* 15.9, 2227–2235.

Martínez-Ruiz, A., Villanueva, L., Orduña, C. González de, López-Ferrer, D., Higueras, M. A., Tarín, C., Rodríguez-Crespo, I., Vázquez, J., and Lamas, S. (2005). S - nitrosylation of Hsp90 promotes the inhibition of its ATPase and endothelial nitric

oxide synthase regulatory activities. *Proceedings of the National Academy of Sciences of the United States of America* 102, 8525–8530.

Masgras, I., Sanchez-Martin, C., Colombo, G., and Rasola, A. (2017). The Chaperone TRAP1 As a Modulator of the Mitochondrial Adaptations in Cancer Cells. *Frontiers in oncology* 7, 58.

Mashaghi, A., Bezrukavnikov, S., Minde, D. P., Wentink, A. S., Kityk, R., Zachmann-Brand, B., Mayer, M. P., Kramer, G., Bukau, B., and Tans, S. J. (2016). Alternative modes of client binding enable functional plasticity of Hsp70. *Nature* 539, 448–451.

Masuda, Y., Shima, G., Aiuchi, T., Horie, M., Hori, K., Nakajo, S., Kajimoto, S., Shibayama-Imazu, T., and Nakaya, K. (2004). Involvement of tumor necrosis factor receptor-associated protein 1 (TRAP1) in apoptosis induced by b-hydroxyisovalerylshikonin. *The Journal of biological chemistry* 279, 42503–42515.

Matsuura, H., Ishibashi, Y., Shinmyo, A., Kanaya, S., and Kato, K. (2010). Genome-wide analyses of early translational responses to elevated temperature and high salinity in Arabidopsis thaliana. *Plant & cell physiology* 51, 448–462.

Matzat, L. H. and Lei, E. P. (2014). Surviving an identity crisis: a revised view of chromatin insulators in the genomics era. *Biochimica et biophysica acta* 1839, 203–214.

Mayer, M. P. and Bukau, B (2005). Hsp70 chaperones: cellular functions and molecular mechanism. *Cellular and molecular life sciences* 62, 670–684.

Mayer, M. P., Schröder, H, Rüdiger, S, Paal, K, Laufen, T, and Bukau, B (2000). Multistep mechanism of substrate binding determines chaperone activity of Hsp70. *Nature structural biology* 7, 586–593.

Mayer, M. P. and Gierasch, L. M. (2019). Recent advances in the structural and mechanistic aspects of Hsp70 molecular chaperones. *The Journal of biological chemistry* 294, 2085–2097.

Mayer, M. P. and Le Breton, L. (2015). Hsp90: breaking the symmetry. *Molecular cell* 58, 8–20.

Mayor, A., Martinon, F., De Smedt, T., Pétrilli, V., and Tschopp, J. (2007). A crucial function of SGT1 and HSP90 in inflammasome activity links mammalian and plant innate immune responses. *Nature immunology* 8, 497–503.

Mayr, C, Richter, K, Lilie, H, and Buchner, J (2000). Cpr6 and Cpr7, two closely related Hsp90-associated immunophilins from Saccharomyces cerevisiae, differ in their functional properties. *The Journal of biological chemistry* 275, 34140–34146.

McCarty, J. S., Buchberger, A, Reinstein, J, and Bukau, B (1995). The role of ATP in the functional cycle of the DnaK chaperone system. *Journal of molecular biology* 249, 126–137.

McLaughlin, S. H., Smith, H. W., and Jackson, S. E. (2002). Stimulation of the weak ATPase activity of human hsp90 by a client protein. *Journal of molecular biology* 315, 787–798.

McLaughlin, S. H., Sobott, F., Yao, Z.-p., Zhang, W., Nielsen, P. R., Grossmann, J. G., Laue, E. D., Robinson, C. V., and Jackson, S. E. (2006). The co-chaperone p23 arrests the Hsp90 ATPase cycle to trap client proteins. *Journal of molecular biology* 356, 746–758.

Melnick, J, Dul, J. L., and Argon, Y (1994). Sequential interaction of the chaperones BiP and GRP94 with immunoglobulin chains in the endoplasmic reticulum. *Nature* 370, 373–375.

Mercier, R., Wolmarans, A., Schubert, J., Neuweiler, H., Johnson, J. L., and LaPointe, P. (2019). The conserved NxNNWHW motif in Aha-type co-chaperones modulates the kinetics of Hsp90 ATPase stimulation. *Nature communications* 10, 1273.

Meyer, P., Prodromou, C., Hu, B., Vaughan, C., Roe, S. M., Panaretou, B., Piper, P. W., and Pearl, L. H. (2003). Structural and functional analysis of the middle segment of hsp90: implications for ATP hydrolysis and client protein and cochaperone interactions. *Molecular cell* 11, 647–658.

Meyer, P., Prodromou, C., Liao, C., Hu, B., Roe, S. M., Vaughan, C. K., Vlasic, I., Panaretou, B., Piper, P. W., and Pearl, L. H. (2004). Structural basis for recruitment of the ATPase activator Aha1 to the Hsp90 chaperone machinery. *The EMBO journal* 23, 1402–1410.

Mickler, M., Hessling, M., Ratzke, C., Buchner, J., and Hugel, T. (2009). The large conformational changes of Hsp90 are only weakly coupled to ATP hydrolysis. *Nature structural & molecular biology* 16, 281–286.

Miller, W. R. and Langdon, S. P. (1997). Steroid hormones and cancer: (III) observations from human subjects. *European journal of surgical oncology* 23, 163–77; quiz 177–8, 183.

Millson, S. H., Truman, A. W., Rácz, A., Hu, B., Panaretou, B., Nuttall, J., Mollapour, M., Söti, C., and Piper, P. W. (2007). Expressed as the sole Hsp90 of yeast, the alpha and beta isoforms of human Hsp90 differ with regard to their capacities for activation of certain client proteins, whereas only Hsp90beta generates sensitivity to the Hsp90 inhibitor radicicol. *The FEBS journal* 274, 4453–4463.

Mimnaugh, E. G., Worland, P. J., Whitesell, L, and Neckers, L. M. (1995). Possible role for serine/threonine phosphorylation in the regulation of the heteroprotein complex between the hsp90 stress protein and the pp60v-src tyrosine kinase. *The Journal of biological chemistry* 270, 28654–28659.

Mishra, P. and Bolon, D. N. A. (2014). Designed Hsp90 heterodimers reveal an asymmetric ATPase-driven mechanism in vivo. *Molecular cell* 53, 344–350.

Mogk, A. and Bukau, B. (2017). Role of sHsps in organizing cytosolic protein aggregation and disaggregation. *Cell stress & chaperones* 22, 493–502.

Mogk, A., Kummer, E., and Bukau, B. (2015). Cooperation of Hsp70 and Hsp100 chaperone machines in protein disaggregation. *Frontiers in molecular biosciences* 2, 22.

Mogk, A., Bukau, B., and Kampinga, H. H. (2018). Cellular Handling of Protein Aggregates by Disaggregation Machines. *Molecular cell* 69, 214–226.

Mogk, A., Ruger-Herreros, C., and Bukau, B. (2019). Cellular Functions and Mechanisms of Action of Small Heat Shock Proteins. *Annual review of microbiology* 73, 89–110.

Mojica, F. J., Díez-Villaseñor, C, Soria, E, and Juez, G (2000). Biological significance of a family of regularly spaced repeats in the genomes of Archaea, Bacteria and mitochondria. *Molecular microbiology* 36, 244–246.

Mollapour, M. and Neckers, L. (2012). Post-translational modifications of Hsp90 and their contributions to chaperone regulation. *Biochimica et biophysica acta* 1823, 648–655.

Mollapour, M., Tsutsumi, S., and Neckers, L. (2010). Hsp90 phosphorylation, Wee1 and the cell cycle. *Cell cycle* 9, 2310–2316.

Momen-Roknabadi, A., Oikonomou, P., Zegans, M., and Tavazoie, S. (2020). An inducible CRISPR-interference library for genetic interrogation of Saccharomyces cerevisiae biology. *bioRxiv*.

Morano, K. A., Santoro, N, Koch, K. A., and Thiele, D. J. (1999). A trans-activation domain in yeast heat shock transcription factor is essential for cell cycle progression during stress. *Molecular and cellular biology* 19, 402–411.

Morimoto, R. I. (1998). Regulation of the heat shock transcriptional response: cross talk between a family of heat shock factors, molecular chaperones, and negative regulators. *Genes & development* 12.24, 3788–3796.

Morra, G., Verkhivker, G., and Colombo, G. (2009). Modeling signal propagation mechanisms and ligand-based conformational dynamics of the Hsp90 molecular chaperone full-length dimer. *PLoS computational biology* 5, e1000323.

Morán Luengo, T., Kityk, R., Mayer, M. P., and Rüdiger, S. G. D. (2018). Hsp90 Breaks the Deadlock of the Hsp70 Chaperone System. *Molecular cell* 70, 545–552.e9.

Morán Luengo, T., Mayer, M. P., and Rüdiger, S. G. D. (2019). The Hsp70-Hsp90 Chaperone Cascade in Protein Folding. *Trends in cell biology* 29, 164–177.

Munro, S and Pelham, H. R. (1987). A C-terminal signal prevents secretion of luminal ER proteins. *Cell* 48, 899–907.

Murphy, P. J. M., Morishima, Y., Kovacs, J. J., Yao, T.-P., and Pratt, W. B. (2005). Regulation of the dynamics of hsp90 action on the glucocorticoid receptor by acetylation/deacetylation of the chaperone. *The Journal of biological chemistry* 280, 33792–33799.

Mühlhofer, M., Berchtold, E., Stratil, C. G., Csaba, G., Kunold, E., Bach, N. C., Sieber, S. A., Haslbeck, M., Zimmer, R., and Buchner, J. (2019). The Heat Shock Response in Yeast Maintains Protein Homeostasis by Chaperoning and Replenishing Proteins. *Cell reports* 29, 4593–4607.e8.

Müller, L., Schaupp, A., Walerych, D., Wegele, H., and Buchner, J. (2004). Hsp90 regulates the activity of wild type p53 under physiological and elevated temperatures. *The Journal of biological chemistry* 279, 48846–48854.

Nagata, Y, Anan, T, Yoshida, T, Mizukami, T, Taya, Y, Fujiwara, T, Kato, H, Saya, H, and Nakao, M (1999). The stabilization mechanism of mutant-type p53 by

impaired ubiquitination: the loss of wild-type p53 function and the hsp90 association. *Oncogene* 18, 6037–6049.

Nathan, D. F. and Lindquist, S (1995). Mutational analysis of Hsp90 function: interactions with a steroid receptor and a protein kinase. *Molecular and cellular biology* 15, 3917–3925.

Nathan, D. F., Vos, M. H., and Lindquist, S (1997). In vivo functions of the Saccharomyces cerevisiae Hsp90 chaperone. *Proceedings of the National Academy of Sciences of the United States of America* 94, 12949–12956.

Neckers, L. and Workman, P. (2012). Hsp90 molecular chaperone inhibitors: are we there yet? *Clinical cancer research* 18, 64–76.

Obermann, W. M., Sondermann, H, Russo, A. A., Pavletich, N. P., and Hartl, F. U. (1998). In vivo function of Hsp90 is dependent on ATP binding and ATP hydrolysis. *The Journal of cell biology* 143, 901–910.

Ohgushi, M and Wada, A (1983). 'Molten-globule state': a compact form of globular proteins with mobile side-chains. *FEBS letters* 164, 21–24.

Ohtsuka, K and Hata, M (2000). Mammalian HSP40/DNAJ homologs: cloning of novel cDNAs and a proposal for their classification and nomenclature. *Cell stress & chaperones* 5, 98–112.

Onuchic, J. N., Luthey-Schulten, Z, and Wolynes, P. G. (1997). Theory of protein folding: the energy landscape perspective. *Annual review of physical chemistry* 48, 545–600.

Onuchic, J. N. and Wolynes, P. G. (2004). Theory of protein folding. *Current opinion in structural biology* 14, 70–75.

Onuoha, S. C., Coulstock, E. T., Grossmann, J. G., and Jackson, S. E. (2008). Structural studies on the co-chaperone Hop and its complexes with Hsp90. *Journal of molecular biology* 379, 732–744.

Oroz, J. et al. (2018). Structure and pro-toxic mechanism of the human Hsp90 / PPIase / Tau complex. *Nature communications* 9, 4532.

Oroz, J., Blair, L. J., and Zweckstetter, M. (2019). Dynamic Aha1 co-chaperone binding to human Hsp90. *Protein science* 28, 1545–1551.

Osterlehner, A., Simmeth, S., and Göpfert, U. (2011). Promoter methylation and transgene copy numbers predict unstable protein production in recombinant Chinese hamster ovary cell lines. *Biotechnology and bioengineering* 108, 2670–2681.

Pace, C. N., Shirley, B. A., McNutt, M, and Gajiwala, K (1996). Forces contributing to the conformational stability of proteins. *FASEB journal* 10, 75–83.

Panaretou, B, Prodromou, C, Roe, S. M., O'Brien, R, Ladbury, J. E., Piper, P. W., and Pearl, L. H. (1998). ATP binding and hydrolysis are essential to the function of the Hsp90 molecular chaperone in vivo. *The EMBO journal* 17, 4829–4836.

Panaretou, B. et al. (2002). Activation of the ATPase activity of hsp90 by the stress-regulated cochaperone aha1. *Molecular cell* 10, 1307–1318.

Papapetrou, E. P. and Schambach, A. (2016). Gene Insertion Into Genomic Safe Harbors for Human Gene Therapy. *Molecular therapy* 24, 678–684.

Park, S. J., Kostic, M., and Dyson, H. J. (2011a). Dynamic Interaction of Hsp90 with Its Client Protein p53. *Journal of molecular biology* 411, 158–173.

Park, S. J., Borin, B. N., Martinez-Yamout, M. A., and Dyson, H. J. (2011b). The client protein p53 adopts a molten globule-like state in the presence of Hsp90. *Nature structural & molecular biology* 18, 537–541.

Parnas, O. et al. (2015). A Genome-wide CRISPR Screen in Primary Immune Cells to Dissect Regulatory Networks. *Cell* 162, 675–686.

Parsell, D. A., Kowal, A. S., Singer, M. A., and Lindquist, S (1994). Protein disaggregation mediated by heat-shock protein Hsp104. *Nature* 372, 475–478.

Parsell, D. A., Taulien, J., and Lindquist, S. (1993). The role of heat-shock proteins in thermotolerance. In: *Molecular chaperones*. Springer, 23–30.

Partridge, J. R., Lavery, L. A., Elnatan, D., Naber, N., Cooke, R., and Agard, D. A. (2014). A novel N-terminal extension in mitochondrial TRAP1 serves as a thermal regulator of chaperone activity. *eLife* 3.

Patwardhan, C. A., Fauq, A., Peterson, L. B., Miller, C., Blagg, B. S. J., and Chadli, A. (2013). Gedunin inactivates the co-chaperone p23 protein causing cancer cell death by apoptosis. *The Journal of biological chemistry* 288, 7313–7325.

Pearl, L. H. and Prodromou, C. (2006). Structure and mechanism of the Hsp90 molecular chaperone machinery. *Annual review of biochemistry* 75, 271–294.

Pelham, H. R. (1986). Speculations on the functions of the major heat shock and glucose-regulated proteins. *Cell* 46, 959–961.

Pellecchia, M, Montgomery, D. L., Stevens, S. Y., Vander Kooi, C. W., Feng, H. P., Gierasch, L. M., and Zuiderweg, E. R. (2000). Structural insights into substrate binding by the molecular chaperone DnaK. *Nature structural biology* 7, 298–303.

Perales-Calvo, J., Muga, A., and Moro, F. (2010). Role of DnaJ G/F-rich domain in conformational recognition and binding of protein substrates. *The Journal of biological chemistry* 285, 34231–34239.

Picard, D, Khursheed, B, Garabedian, M. J., Fortin, M. G., Lindquist, S, and Yamamoto, K. R. (1990). Reduced levels of hsp90 compromise steroid receptor action in vivo. *Nature* 348, 166–168.

Picard, D. (2006). Chaperoning steroid hormone action. *Trends in endocrinology and metabolism* 17, 229–235.

Pick, E., Kluger, Y., Giltnane, J. M., Moeder, C., Camp, R. L., Rimm, D. L., and Kluger, H. M. (2007). High HSP90 expression is associated with decreased survival in breast cancer. *Cancer research* 67, 2932–2937.

Polier, S., Dragovic, Z., Hartl, F. U., and Bracher, A. (2008). Structural basis for the cooperation of Hsp70 and Hsp110 chaperones in protein folding. *Cell* 133, 1068–1079.

Potting, C. et al. (2018). Genome-wide CRISPR screen for PARKIN regulators reveals transcriptional repression as a determinant of mitophagy. *Proceedings of the National Academy of Sciences of the United States of America* 115, E180–E189.

Pratt, W. B. and Dittmar, K. D. (1998). Studies with Purified Chaperones Advance the Understanding of the Mechanism of Glucocorticoid Receptor-hsp90 Heterocomplex Assembly. *Trends in endocrinology and metabolism* 9, 244–252.

Pratt, W. B. and Toft, D. O. (1997). Steroid receptor interactions with heat shock protein and immunophilin chaperones. *Endocrine reviews* 18, 306–360.

Pratt, W. B., Morishima, Y, Murphy, M, and Harrell, M (2006). Chaperoning of glucocorticoid receptors. *Handbook of experimental pharmacology*, 111–138.

Pratt, W. B. and Toft, D. O. (2003). Regulation of signaling protein function and trafficking by the hsp90/hsp70-based chaperone machinery. *Experimental biology and medicine* 228, 111–133.

Prodromou, C, Roe, S. M., O'Brien, R, Ladbury, J. E., Piper, P. W., and Pearl, L. H. (1997). Identification and structural characterization of the ATP/ADP-binding site in the Hsp90 molecular chaperone. *Cell* 90, 65–75.

Prodromou, C, Siligardi, G, O'Brien, R, Woolfson, D. N., Regan, L, Panaretou, B, Ladbury, J. E., Piper, P. W., and Pearl, L. H. (1999). Regulation of Hsp90 ATPase activity by tetratricopeptide repeat (TPR)-domain co-chaperones. *The EMBO journal* 18, 754–762.

Prodromou, C, Panaretou, B, Chohan, S, Siligardi, G, O'Brien, R, Ladbury, J. E., Roe, S. M., Piper, P. W., and Pearl, L. H. (2000). The ATPase cycle of Hsp90 drives a molecular 'clamp' via transient dimerization of the N-terminal domains. *The EMBO journal* 19, 4383–4392.

Prodromou, C. (2016). Mechanisms of Hsp90 regulation. *The Biochemical journal* 473, 2439–2452.

Pérez-González, A. and Caro, E. (2019). Benefits of using genomic insulators flanking transgenes to increase expression and avoid positional effects. *Scientific reports* 9, 8474.

Qi, L. S., Larson, M. H., Gilbert, L. A., Doudna, J. A., Weissman, J. S., Arkin, A. P., and Lim, W. A. (2013a). Repurposing CRISPR as an RNA-guided platform for sequence-specific control of gene expression. *Cell* 152, 1173–1183.

Qi, R. et al. (2013b). Allosteric opening of the polypeptide-binding site when an Hsp70 binds ATP. *Nature structural & molecular biology* 20, 900–907.

Qu, B. H., Strickland, E. H., and Thomas, P. J. (1997). Localization and suppression of a kinetic defect in cystic fibrosis transmembrane conductance regulator folding. *The Journal of biological chemistry* 272, 15739–15744.

Queitsch, C., Sangster, T. A., and Lindquist, S. (2002). Hsp90 as a capacitor of phenotypic variation. *Nature* 417, 618–624.

Quintana-Gallardo, L., Martín-Benito, J., Marcilla, M., Espadas, G., Sabidó, E., and Valpuesta, J. M. (2019). The cochaperone CHIP marks Hsp70- and Hsp90-bound substrates for degradation through a very flexible mechanism. *Scientific reports* 9, 5102.

Rabindran, S. K., Haroun, R. I., Clos, J., Wisniewski, J., and Wu, C. (1993). Regulation of heat shock factor trimer formation: role of a conserved leucine zipper. *Science* 259.5092, 230–234.

Radli, M. and Rüdiger, S. G. D. (2018). Dancing with the Diva: Hsp90-Client Interactions. *Journal of molecular biology* 430, 3029–3040.

Radons, J. (2016). The human HSP70 family of chaperones: where do we stand? *Cell stress & chaperones* 21, 379–404.

Randow, F and Seed, B (2001). Endoplasmic reticulum chaperone gp96 is required for innate immunity but not cell viability. *Nature cell biology* 3, 891–896.

Ratzke, C, Hellenkamp, B, and Hugel, T (2014). Four-colour FRET reveals directionality in the Hsp90 multicomponent machinery. *Nature communications* 5, 4192.

Ratzke, C., Nguyen, M. N. T., Mayer, M. P., and Hugel, T. (2012). From a ratchet mechanism to random fluctuations evolution of Hsp90's mechanochemical cycle. *Journal of molecular biology* 423, 462–471.

Rebeaud, M. E., Mallik, S., Goloubinoff, P., and Tawfik, D. S. (2020). On the evolution of chaperones and co-chaperones and the exponential expansion of proteome complexity. *bioRxiv*. eprint: `https://www.biorxiv.org/content/early/2020/06/09/2020.06.08.140319.full.pdf`.

Reed, S. I. (1980). The selection of S. cerevisiae mutants defective in the start event of cell division. *Genetics* 95, 561–577.

Rehn, A. et al. (2020). A methylated lysine is a switch point for conformational communication in the chaperone Hsp90. *Nature communications* 11, 1219.

Reidy, M. and Masison, D. C. (2020). Mutations in the Hsp90 N Domain Identify a Site that Controls Dimer Opening and Expand Human Hsp90alpha Function in Yeast. *Journal of molecular biology*.

Reidy, M., Kumar, S., Anderson, D. E., and Masison, D. C. (2018). Dual Roles for Yeast Sti1/Hop in Regulating the Hsp90 Chaperone Cycle. *Genetics* 209, 1139–1154.

Retzlaff, M., Stahl, M., Eberl, H. C., Lagleder, S., Beck, J., Kessler, H., and Buchner, J. (2009). Hsp90 is regulated by a switch point in the C-terminal domain. *EMBO reports* 10, 1147–1153.

Retzlaff, M., Hagn, F., Mitschke, L., Hessling, M., Gugel, F., Kessler, H., Richter, K., and Buchner, J. (2010). Asymmetric activation of the hsp90 dimer by its cochaperone aha1. *Molecular cell* 37, 344–354.

Richter, K. and Buchner, J. (2006). hsp90: twist and fold. *Cell* 127, 251–253.

Richter, K., Muschler, P., Hainzl, O., Reinstein, J., and Buchner, J. (2003). Sti1 is a non-competitive inhibitor of the Hsp90 ATPase. Binding prevents the N-terminal dimerization reaction during the atpase cycle. *The Journal of biological chemistry* 278, 10328–10333.

Richter, K., Walter, S., and Buchner, J. (2004). The Co-chaperone Sba1 connects the ATPase reaction of Hsp90 to the progression of the chaperone cycle. *Journal of molecular biology* 342, 1403–1413.

Richter, K., Moser, S., Hagn, F., Friedrich, R., Hainzl, O., Heller, M., Schlee, S., Kessler, H., Reinstein, J., and Buchner, J. (2006). Intrinsic inhibition of the Hsp90 ATPase activity. *The Journal of biological chemistry* 281, 11301–11311.

Richter, K., Soroka, J., Skalniak, L., Leskovar, A., Hessling, M., Reinstein, J., and Buchner, J. (2008). Conserved conformational changes in the ATPase cycle of human Hsp90. *The Journal of biological chemistry* 283, 17757–17765.

Richter, K., Haslbeck, M., and Buchner, J. (2010). The heat shock response: life on the verge of death. *Molecular cell* 40, 253–266.

Riggs, D. L., Roberts, P. J., Chirillo, S. C., Cheung-Flynn, J., Prapapanich, V., Ratajczak, T., Gaber, R., Picard, D., and Smith, D. F. (2003). The Hsp90-binding peptidylprolyl isomerase FKBP52 potentiates glucocorticoid signaling in vivo. *The EMBO journal* 22, 1158–1167.

Riggs, D. L., Cox, M. B., Tardif, H. L., Hessling, M., Buchner, J., and Smith, D. F. (2007). Noncatalytic role of the FKBP52 peptidyl-prolyl isomerase domain in the regulation of steroid hormone signaling. *Molecular and cellular biology* 27, 8658–8669.

Ritossa, F. (1962). A new puffing pattern induced by temperature shock and DNP in drosophila. *Experientia* 18, 571–573.

Rivera-Calzada, A., Pal, M., Muñoz-Hernández, H., Luque-Ortega, J. R., Gil-Carton, D., Degliesposti, G., Skehel, J. M., Prodromou, C., Pearl, L. H., and Llorca, O. (2017). The Structure of the R2TP Complex Defines a Platform for Recruiting Diverse Client Proteins to the HSP90 Molecular Chaperone System. *Structure* 25, 1145–1152.e4.

Rizzolo, K. et al. (2017). Features of the Chaperone Cellular Network Revealed through Systematic Interaction Mapping. *Cell reports* 20, 2735–2748.

Rizzolo, K., Kumar, A., Kakihara, Y., Phanse, S., Minic, Z., Snider, J., Stagljar, I., Zilles, S., Babu, M., and Houry, W. A. (2018). Systems analysis of the genetic interaction network of yeast molecular chaperones. *Molecular omics* 14, 82–94.

Rodina, A. et al. (2016). The epichaperome is an integrated chaperome network that facilitates tumour survival. *Nature* 538, 397–401.

Roe, S. M., Prodromou, C, O'Brien, R, Ladbury, J. E., Piper, P. W., and Pearl, L. H. (1999). Structural basis for inhibition of the Hsp90 molecular chaperone by the antitumor antibiotics radicicol and geldanamycin. *Journal of medicinal chemistry* 42, 260–266.

Roe, S. M., Ali, M. M. U., Meyer, P., Vaughan, C. K., Panaretou, B., Piper, P. W., Prodromou, C., and Pearl, L. H. (2004). The Mechanism of Hsp90 regulation by the protein kinase-specific cochaperone p50(cdc37). *Cell* 116, 87–98.

Rohner, N., Jarosz, D. F., Kowalko, J. E., Yoshizawa, M., Jeffery, W. R., Borowsky, R. L., Lindquist, S., and Tabin, C. J. (2013). Cryptic variation in morphological evolution: HSP90 as a capacitor for loss of eyes in cavefish. *Science* 342, 1372–1375.

Romei, M. G. and Boxer, S. G. (2019). Split Green Fluorescent Proteins: Scope, Limitations, and Outlook. *Annual review of biophysics* 48, 19–44.

Rosenzweig, R., Moradi, S., Zarrine-Afsar, A., Glover, J. R., and Kay, L. E. (2013). Unraveling the mechanism of protein disaggregation through a ClpB-DnaK interaction. *Science* 339, 1080–1083.

Rosenzweig, R., Sekhar, A., Nagesh, J., and Kay, L. E. (2017). Promiscuous binding by Hsp70 results in conformational heterogeneity and fuzzy chaperone-substrate ensembles. *eLife* 6.

Rosenzweig, R., Nillegoda, N. B., Mayer, M. P., and Bukau, B. (2019). The Hsp70 chaperone network. *Nature reviews. Molecular cell biology* 20, 665–680.

Rowlands, M. G., Newbatt, Y. M., Prodromou, C., Pearl, L. H., Workman, P., and Aherne, W. (2004). High-throughput screening assay for inhibitors of heat-shock protein 90 ATPase activity. *Analytical biochemistry* 327, 176–183.

Rudiger, S., Freund, S. M. V., Veprintsev, D. B., and Fersht, A. R. (2002). CRINEPT-TROSY NMR reveals p53 core domain bound in an unfolded form to the chaperone Hsp90. *Proceedings of the National Academy of Sciences of the United States of America* 99, 11085–11090.

Rutherford, S. L. and Lindquist, S (1998). Hsp90 as a capacitor for morphological evolution. *Nature* 396, 336–342.

Rutz, D. A., Luo, Q., Freiburger, L., Madl, T., Kaila, V. R. I., Sattler, M., and Buchner, J. (2018). A switch point in the molecular chaperone Hsp90 responding to client interaction. *Nature communications* 9, 1472.

Röhl, A., Tippel, F., Bender, E., Schmid, A. B., Richter, K., Madl, T., and Buchner, J. (2015a). Hop/Sti1 phosphorylation inhibits its co-chaperone function. *EMBO reports* 16, 240–249.

Röhl, A. et al. (2015b). Hsp90 regulates the dynamics of its cochaperone Sti1 and the transfer of Hsp70 between modules. *Nature communications* 6, 6655.

Rüdiger, S, Germeroth, L, Schneider-Mergener, J, and Bukau, B (1997). Substrate specificity of the DnaK chaperone determined by screening cellulose-bound peptide libraries. *The EMBO journal* 16, 1501–1507.

Rüdiger, S, Schneider-Mergener, J, and Bukau, B (2001). Its substrate specificity characterizes the DnaJ co-chaperone as a scanning factor for the DnaK chaperone. *The EMBO journal* 20, 1042–1050.

Sabbagh, J. J. et al. (2018). Targeting the FKBP51/GR/Hsp90 Complex to Identify Functionally Relevant Treatments for Depression and PTSD. *ACS chemical biology* 13, 2288–2299.

Sager, R. A., Woodford, M. R., and Mollapour, M. (2018). The mTOR Independent Function of Tsc1 and FNIPs. *Trends in biochemical sciences* 43, 935–937.

Sager, R. A. et al. (2019). Post-translational Regulation of FNIP1 Creates a Rheostat for the Molecular Chaperone Hsp90. *Cell reports* 26, 1344–1356.e5.

Sahasrabudhe, P., Rohrberg, J., Biebl, M. M., Rutz, D. A., and Buchner, J. (2017). The Plasticity of the Hsp90 Co-chaperone System. *Molecular cell* 67, 947–961.

Saibil, H. R., Fenton, W. A., Clare, D. K., and Horwich, A. L. (2013). Structure and allostery of the chaperonin GroEL. *Journal of molecular biology* 425, 1476–1487.

Salminen, A., Ojala, J., Kaarniranta, K., Hiltunen, M., and Soininen, H. (2011). Hsp90 regulates tau pathology through co-chaperone complexes in Alzheimer's disease. *Progress in neurobiology* 93, 99–110.

Sarge, K. D., Murphy, S. P., and Morimoto, R. I. (1993). Activation of heat shock gene transcription by heat shock factor 1 involves oligomerization, acquisition of DNA-binding activity, and nuclear localization and can occur in the absence of stress. *Molecular and cellular biology* 13, 1392–1407.

Sato, S, Fujita, N, and Tsuruo, T (2000). Modulation of Akt kinase activity by binding to Hsp90. *Proceedings of the National Academy of Sciences of the United States of America* 97, 10832–10837.

Savitski, M. M. et al. (2018). Multiplexed Proteome Dynamics Profiling Reveals Mechanisms Controlling Protein Homeostasis. *Cell* 173, 260–274.e25.

Sawarkar, R., Sievers, C., and Paro, R. (2012). Hsp90 globally targets paused RNA polymerase to regulate gene expression in response to environmental stimuli. *Cell* 149, 807–818.

Scheibel, T, Neuhofen, S, Weikl, T, Mayr, C, Reinstein, J, Vogel, P. D., and Buchner, J (1997). ATP-binding properties of human Hsp90. *The Journal of biological chemistry* 272, 18608–18613.

Scheufler, C, Brinker, A, Bourenkov, G, Pegoraro, S, Moroder, L, Bartunik, H, Hartl, F. U., and Moarefi, I (2000). Structure of TPR domain-peptide complexes: critical elements in the assembly of the Hsp70-Hsp90 multichaperone machine. *Cell* 101, 199–210.

Schmid, A. B. et al. (2012). The architecture of functional modules in the Hsp90 co-chaperone Sti1/Hop. *The EMBO journal* 31, 1506–1517.

Schmidpeter, P. A. M. and Schmid, F. X. (2015). Prolyl isomerization and its catalysis in protein folding and protein function. *Journal of molecular biology* 427, 1609–1631.

Schneider, C. A., Rasband, W. S., and Eliceiri, K. W. (2012). NIH Image to ImageJ: 25 years of image analysis. *Nature methods* 9, 671–675.

Schopf, F. H., Biebl, M. M., and Buchner, J. (2017). The HSP90 chaperone machinery. *Nature reviews. Molecular cell biology* 18, 345–360.

Schopf, F. H. et al. (2019). The Co-chaperone Cns1 and the Recruiter Protein Hgh1 Link Hsp90 to Translation Elongation via Chaperoning Elongation Factor 2. *Molecular cell* 74, 73–87.e8.

Schrimpf, W., Barth, A., Hendrix, J., and Lamb, D. C. (2018). PAM: A Framework for Integrated Analysis of Imaging, Single-Molecule, and Ensemble Fluorescence Data. *Biophysical journal* 114, 1518–1528.

Schuck, P (2000). Size-distribution analysis of macromolecules by sedimentation velocity ultracentrifugation and lamm equation modeling. *Biophysical journal* 78, 1606–1619.

Schuldiner, M. et al. (2005). Exploration of the function and organization of the yeast early secretory pathway through an epistatic miniarray profile. *Cell* 123, 507–519.

Schulte, T. W. et al. (1999). Interaction of radicicol with members of the heat shock protein 90 family of molecular chaperones. *Molecular endocrinology* 13, 1435–1448.

Scroggins, B. T. and Neckers, L. (2007). Post-translational modification of heat-shock protein 90: impact on chaperone function. *Expert opinion on drug discovery* 2, 1403–1414.

Scroggins, B. T. et al. (2007). An acetylation site in the middle domain of Hsp90 regulates chaperone function. *Molecular cell* 25, 151–159.

Sekhar, A., Rosenzweig, R., Bouvignies, G., and Kay, L. E. (2015). Mapping the conformation of a client protein through the Hsp70 functional cycle. *Proceedings of the National Academy of Sciences of the United States of America* 112, 10395–10400.

Sekhar, A., Rosenzweig, R., Bouvignies, G., and Kay, L. E. (2016). Hsp70 biases the folding pathways of client proteins. *Proceedings of the National Academy of Sciences of the United States of America* 113, E2794–E2801.

Sekhar, A., Velyvis, A., Zoltsman, G., Rosenzweig, R., Bouvignies, G., and Kay, L. E. (2018). Conserved conformational selection mechanism of Hsp70 chaperone substrate interactions. *eLife* 7.

Sepehrnia, B, Paz, I. B., Dasgupta, G, and Momand, J (1996). Heat shock protein 84 forms a complex with mutant p53 protein predominantly within a cytoplasmic compartment of the cell. *The Journal of biological chemistry* 271, 15084–15090.

Shannon, P., Markiel, A., Ozier, O., Baliga, N. S., Wang, J. T., Ramage, D., Amin, N., Schwikowski, B., and Ideker, T. (2003). Cytoscape: a software environment for integrated models of biomolecular interaction networks. *Genome research* 13.11, 2498–2504.

Sharma, D. and Masison, D. C. (2009). Hsp70 structure, function, regulation and influence on yeast prions. *Protein and peptide letters* 16, 571–581.

Shelton, L. B., Koren, J., and Blair, L. J. (2017). Imbalances in the Hsp90 Chaperone Machinery: Implications for Tauopathies. *Frontiers in neuroscience* 11, 724.

Shen, Y. and Bax, A. (2013). Protein backbone and sidechain torsion angles predicted from NMR chemical shifts using artificial neural networks. *Journal of biomolecular NMR* 56, 227–241.

Shiau, A. K., Harris, S. F., Southworth, D. R., and Agard, D. A. (2006). Structural Analysis of E. coli hsp90 reveals dramatic nucleotide-dependent conformational rearrangements. *Cell* 127, 329–340.

Shiber, A. and Ravid, T. (2014). Chaperoning proteins for destruction: diverse roles of Hsp70 chaperones and their co-chaperones in targeting misfolded proteins to the proteasome. *Biomolecules* 4. Original DateCompleted: 20140719, 704–724.

Sidera, K., Samiotaki, M., Yfanti, E., Panayotou, G., and Patsavoudi, E. (2004). Involvement of cell surface HSP90 in cell migration reveals a novel role in the developing nervous system. *The Journal of biological chemistry* 279, 45379–45388.

Siligardi, G., Panaretou, B., Meyer, P., Singh, S., Woolfson, D. N., Piper, P. W., Pearl, L. H., and Prodromou, C. (2002). Regulation of Hsp90 ATPase activity by the co-chaperone Cdc37p/p50cdc37. *The Journal of biological chemistry* 277, 20151–20159.

Siligardi, G., Hu, B., Panaretou, B., Piper, P. W., Pearl, L. H., and Prodromou, C. (2004). Co-chaperone regulation of conformational switching in the Hsp90 ATPase cycle. *The Journal of biological chemistry* 279, 51989–51998.

Sima, S. and Richter, K. (2018). Regulation of the Hsp90 system. *Biochimica et biophysica acta. Molecular cell research* 1865, 889–897.

Sinha, H. et al. (2008). Sequential elimination of major-effect contributors identifies additional quantitative trait loci conditioning high-temperature growth in yeast. *Genetics* 180, 1661–1670.

Skarra, D. V., Goudreault, M., Choi, H., Mullin, M., Nesvizhskii, A. I., Gingras, A.-C., and Honkanen, R. E. (2011). Label-free quantitative proteomics and SAINT analysis enable interactome mapping for the human Ser/Thr protein phosphatase 5. *Proteomics* 11, 1508–1516.

Smith, D. F., Sullivan, W. P., Marion, T. N., Zaitsu, K, Madden, B, McCormick, D. J., and Toft, D. O. (1993). Identification of a 60-kilodalton stress-related protein, p60, which interacts with hsp90 and hsp70. *Molecular and cellular biology* 13, 869–876.

Soga, S., Shiotsu, Y., Akinaga, S., and Sharma, S. V. (2003). Development of radicicol analogues. *Current cancer drug targets* 3, 359–369.

Solis, E. J., Pandey, J. P., Zheng, X., Jin, D. X., Gupta, P. B., Airoldi, E. M., Pincus, D., and Denic, V. (2016). Defining the essential function of yeast Hsf1 reveals a compact transcriptional program for maintaining eukaryotic proteostasis. *Molecular cell* 63.1, 60–71.

Sondermann, H, Scheufler, C, Schneider, C, Hohfeld, J, Hartl, F. U., and Moarefi, I (2001). Structure of a Bag/Hsc70 complex: convergent functional evolution of Hsp70 nucleotide exchange factors. *Science* 291, 1553–1557.

Song, H. Y., Dunbar, J. D., Zhang, Y. X., Guo, D, and Donner, D. B. (1995). Identification of a protein with homology to hsp90 that binds the type 1 tumor necrosis factor receptor. *The Journal of biological chemistry* 270, 3574–3581.

Sorger, P. K. and Pelham, H. R. (1988). Yeast heat shock factor is an essential DNA-binding protein that exhibits temperature-dependent phosphorylation. *Cell* 54, 855–864.

Sorger, P. K., Lewis, M. J., and Pelham, H. R. (1987). Heat shock factor is regulated differently in yeast and HeLa cells. *Nature* 329, 81–84.

Soroka, J., Wandinger, S. K., Mäusbacher, N., Schreiber, T., Richter, K., Daub, H., and Buchner, J. (2012). Conformational switching of the molecular chaperone Hsp90 via regulated phosphorylation. *Molecular cell* 45, 517–528.

Southworth, D. R. and Agard, D. A. (2008). Species-dependent ensembles of conserved conformational states define the Hsp90 chaperone ATPase cycle. *Molecular cell* 32, 631–640.

Staron, M., Yang, Y., Liu, B., Li, J., Shen, Y., Zúñiga-Pflücker, J. C., Aguila, H. L., Goldschneider, I., and Li, Z. (2010). gp96, an endoplasmic reticulum master chaperone for integrins and Toll-like receptors, selectively regulates early T and B lymphopoiesis. *Blood* 115, 2380–2390.

Stephanou, A, Amin, V, Isenberg, D. A., Akira, S, Kishimoto, T, and Latchman, D. S. (1997). Interleukin 6 activates heat-shock protein 90 beta gene expression. *The Biochemical journal* 321 (Pt 1), 103–106.

Stevens, S. Y., Cai, S., Pellecchia, M., and Zuiderweg, E. R. P. (2003). The solution structure of the bacterial HSP70 chaperone protein domain DnaK(393-507) in complex with the peptide NRLLLTG. *Protein science* 12, 2588–2596.

Stiegler, S. C., Rübbelke, M., Korotkov, V. S., Weiwad, M., John, C., Fischer, G., Sieber, S. A., Sattler, M., and Buchner, J. (2017). A chemical compound inhibiting the Aha1-Hsp90 chaperone complex. *The Journal of biological chemistry* 292, 17073–17083.

Storer, C. L., Dickey, C. A., Galigniana, M. D., Rein, T., and Cox, M. B. (2011). FKBP51 and FKBP52 in signaling and disease. *Trends in endocrinology and metabolism* 22, 481–490.

Studier, F. W. (2005). Protein production by auto-induction in high density shaking cultures. *Protein expression and purification* 41, 207–234.

Suh, W. C., Burkholder, W. F., Lu, C. Z., Zhao, X, Gottesman, M. E., and Gross, C. A. (1998). Interaction of the Hsp70 molecular chaperone, DnaK, with its cochaperone DnaJ. *Proceedings of the National Academy of Sciences of the United States of America* 95, 15223–15228.

Suh, W. C., Lu, C. Z., and Gross, C. A. (1999). Structural features required for the interaction of the Hsp70 molecular chaperone DnaK with its cochaperone DnaJ. *The Journal of biological chemistry* 274, 30534–30539.

Sullivan, W, Stensgard, B, Caucutt, G, Bartha, B, McMahon, N, Alnemri, E. S., Litwack, G, and Toft, D (1997). Nucleotides and two functional states of hsp90. *The Journal of biological chemistry* 272, 8007–8012.

Sullivan, W. P., Owen, B. A. L., and Toft, D. O. (2002). The influence of ATP and p23 on the conformation of hsp90. *The Journal of biological chemistry* 277, 45942–45948.

Suren, T., Rutz, D., Mößmer, P., Merkel, U., Buchner, J., and Rief, M. (2018). Single-molecule force spectroscopy reveals folding steps associated with hormone binding and activation of the glucocorticoid receptor. *Proceedings of the National Academy of Sciences of the United States of America* 115, 11688–11693.

Suzuki, H., Noguchi, S., Arakawa, H., Tokida, T., Hashimoto, M., and Satow, Y. (2010). Peptide-binding sites as revealed by the crystal structures of the human Hsp40 Hdj1 C-terminal domain in complex with the octapeptide from human Hsp70. *Biochemistry* 49, 8577–8584.

Swain, J. F., Dinler, G., Sivendran, R., Montgomery, D. L., Stotz, M., and Gierasch, L. M. (2007). Hsp70 chaperone ligands control domain association via an allosteric mechanism mediated by the interdomain linker. *Molecular cell* 26, 27–39.

Swingle, M. R., Honkanen, R. E., and Ciszak, E. M. (2004). Structural basis for the catalytic activity of human serine/threonine protein phosphatase-5. *The Journal of biological chemistry* 279, 33992–33999.

Szabo, A, Langer, T, Schröder, H, Flanagan, J, Bukau, B, and Hartl, F. U. (1994). The ATP hydrolysis-dependent reaction cycle of the Escherichia coli Hsp70 system DnaK, DnaJ, and GrpE. *Proceedings of the National Academy of Sciences of the United States of America* 91, 10345–10349.

Taipale, M., Jarosz, D. F., and Lindquist, S. (2010). HSP90 at the hub of protein homeostasis: emerging mechanistic insights. *Nature reviews. Molecular cell biology* 11, 515–528.

Taipale, M., Krykbaeva, I., Koeva, M., Kayatekin, C., Westover, K. D., Karras, G. I., and Lindquist, S. (2012). Quantitative analysis of HSP90-client interactions reveals principles of substrate recognition. *Cell* 150, 987–1001.

Taipale, M., Tucker, G., Peng, J., Krykbaeva, I., Lin, Z.-Y., Larsen, B., Choi, H., Berger, B., Gingras, A.-C., and Lindquist, S. (2014). A quantitative chaperone interaction network reveals the architecture of cellular protein homeostasis pathways. *Cell* 158, 434–448.

Takayama, S, Xie, Z, and Reed, J. C. (1999). An evolutionarily conserved family of Hsp70/Hsc70 molecular chaperone regulators. *The Journal of biological chemistry* 274, 781–786.

Tavaria, M, Gabriele, T, Kola, I, and Anderson, R. L. (1996). A hitchhiker's guide to the human Hsp70 family. *Cell stress & chaperones* 1, 23–28.

Teng, X, Cheng, W.-C., Qi, B, Yu, T.-X., Ramachandran, K, Boersma, M. D., Hattier, T, Lehmann, P. V., Pineda, F. J., and Hardwick, J. M. (2011). Gene-dependent cell death in yeast. *Cell death & disease* 2, e188.

Tenge, V. R., Zuehlke, A. D., Shrestha, N., and Johnson, J. L. (2015). The Hsp90 cochaperones Cpr6, Cpr7, and Cns1 interact with the intact ribosome. *Eukaryotic cell* 14, 55–63.

Tesic, M., Marsh, J. A., Cullinan, S. B., and Gaber, R. F. (2003). Functional interactions between Hsp90 and the co-chaperones Cns1 and Cpr7 in Saccharomyces cerevisiae. *The Journal of biological chemistry* 278, 32692–32701.

Theodoraki, M. A. and Caplan, A. J. (2012). Quality control and fate determination of Hsp90 client proteins. *Biochimica et biophysica acta* 1823, 683–688.

Thul, P. J. et al. (2017). A subcellular map of the human proteome. *Science* 356.

Tian, R. et al. (2019). CRISPR Interference-Based Platform for Multimodal Genetic Screens in Human iPSC-Derived Neurons. *Neuron* 104, 239–255.e12.

Tong, A. H. et al. (2001). Systematic genetic analysis with ordered arrays of yeast deletion mutants. *Science* 294, 2364–2368.

Tong, A. H. Y. and Boone, C. (2006). Synthetic genetic array analysis in Saccharomyces cerevisiae. *Methods in molecular biology* 313, 171–192.

Trepel, J., Mollapour, M., Giaccone, G., and Neckers, L. (2010). Targeting the dynamic HSP90 complex in cancer. *Nature reviews. Cancer* 10, 537–549.

Tsutsumi, S., Mollapour, M., Prodromou, C., Lee, C.-T., Panaretou, B., Yoshida, S., Mayer, M. P., and Neckers, L. M. (2012). Charged linker sequence modulates eukaryotic heat shock protein 90 (Hsp90) chaperone activity. *Proceedings of the National Academy of Sciences of the United States of America* 109, 2937–2942.

Tyanova, S., Temu, T., Sinitcyn, P., Carlson, A., Hein, M. Y., Geiger, T., Mann, M., and Cox, J. (2016). The Perseus computational platform for comprehensive analysis of (prote)omics data. *Nature methods* 13, 731–740.

Vartholomaiou, E., Echeverría, P. C., and Picard, D. (2016). Unusual Suspects in the Twilight Zone Between the Hsp90 Interactome and Carcinogenesis. *Advances in cancer research* 129, 1–30.

Vaughan, C. K. et al. (2008). Hsp90-dependent activation of protein kinases is regulated by chaperone-targeted dephosphorylation of Cdc37. *Molecular cell* 31, 886–895.

Verba, K. A., Wang, R. Y.-R., Arakawa, A., Liu, Y., Shirouzu, M., Yokoyama, S., and Agard, D. A. (2016). Atomic structure of Hsp90-Cdc37-Cdk4 reveals that Hsp90 traps and stabilizes an unfolded kinase. *Science* 352, 1542–1547.

Verghese, J., Abrams, J., Wang, Y., and Morano, K. A. (2012). Biology of the heat shock response and protein chaperones: budding yeast (Saccharomyces cerevisiae) as a model system. *Microbiology and molecular biology reviews* 76, 115–158.

Verma, M., Vats, A., and Taneja, V. (2015). Toxic species in amyloid disorders: Oligomers or mature fibrils. *Annals of Indian Academy of Neurology* 18, 138–145.

Voellmy, R. and Boellmann, F. (2007). Chaperone regulation of the heat shock protein response. In: *Molecular Aspects of the Stress Response: Chaperones, Membranes and Networks*. Springer, 89–99.

Vogel, M., Mayer, M. P., and Bukau, B. (2006). Allosteric regulation of Hsp70 chaperones involves a conserved interdomain linker. *The Journal of biological chemistry* 281, 38705–38711.

Wakabayashi, Y. et al. (2006). A protein associated with toll-like receptor 4 (PRAT4A) regulates cell surface expression of TLR4. *Journal of immunology* 177, 1772–1779.

Walsh, P., Bursać, D., Law, Y. C., Cyr, D., and Lithgow, T. (2004). The J-protein family: modulating protein assembly, disassembly and translocation. *EMBO reports* 5, 567–571.

Wandinger, S. K., Suhre, M. H., Wegele, H., and Buchner, J. (2006). The phosphatase Ppt1 is a dedicated regulator of the molecular chaperone Hsp90. *The EMBO journal* 25, 367–376.

Wang, H., La Russa, M., and Qi, L. S. (2016). CRISPR/Cas9 in Genome Editing and Beyond. *Annual review of biochemistry* 85, 227–264.

Wang, X. et al. (2006). Hsp90 cochaperone Aha1 downregulation rescues misfolding of CFTR in cystic fibrosis. *Cell* 127, 803–815.

Wayne, N. and Bolon, D. N. (2007). Dimerization of Hsp90 is required for in vivo function. Design and analysis of monomers and dimers. *The Journal of biological chemistry* 282, 35386–35395.

Weaver, A. J., Sullivan, W. P., Felts, S. J., Owen, B. A., and Toft, D. O. (2000). Crystal structure and activity of human p23, a heat shock protein 90 co-chaperone. *The Journal of biological chemistry* 275, 23045–23052.

Wegele, H., Wandinger, S. K., Schmid, A. B., Reinstein, J., and Buchner, J. (2006). Substrate transfer from the chaperone Hsp70 to Hsp90. *Journal of molecular biology* 356, 802–811.

Weikl, T, Abelmann, K, and Buchner, J (1999). An unstructured C-terminal region of the Hsp90 co-chaperone p23 is important for its chaperone function. *Journal of molecular biology* 293, 685–691.

Weikl, T, Muschler, P, Richter, K, Veit, T, Reinstein, J, and Buchner, J (2000). C-terminal regions of Hsp90 are important for trapping the nucleotide during the ATPase cycle. *Journal of molecular biology* 303, 583–592.

Werner-Washburne, M and Craig, E. A. (1989). Expression of members of the Saccharomyces cerevisiae hsp70 multigene family. *Genome* 31, 684–689.

Whitesell, L and Cook, P (1996). Stable and specific binding of heat shock protein 90 by geldanamycin disrupts glucocorticoid receptor function in intact cells. *Molecular endocrinology* 10, 705–712.

Whitesell, L, Sutphin, P. D., Pulcini, E. J., Martinez, J. D., and Cook, P. H. (1998). The physical association of multiple molecular chaperone proteins with mutant p53 is altered by geldanamycin, an hsp90-binding agent. *Molecular and cellular biology* 18, 1517–1524.

Whitmore, L. and Wallace, B. A. (2008). Protein secondary structure analyses from circular dichroism spectroscopy: methods and reference databases. *Biopolymers* 89, 392–400.

Wiech, H, Buchner, J, Zimmermann, R, and Jakob, U (1992). Hsp90 chaperones protein folding in vitro. *Nature* 358, 169–170.

Wilkinson, B. and Gilbert, H. F. (2004). Protein disulfide isomerase. *Biochimica et biophysica acta* 1699, 35–44.

Wong, D. S. and Jay, D. G. (2016). Emerging Roles of Extracellular Hsp90 in Cancer. *Advances in cancer research* 129, 141–163.

Woo, H.-J., Jiang, J., Lafer, E. M., and Sousa, R. (2009). ATP-induced conformational changes in Hsp70: molecular dynamics and experimental validation of an in silico predicted conformation. *Biochemistry* 48, 11470–11477.

Woodford, M. R., Dunn, D., Miller, J. B., Jamal, S., Neckers, L., and Mollapour, M. (2016a). Impact of Posttranslational Modifications on the Anticancer Activity of Hsp90 Inhibitors. *Advances in cancer research* 129, 31–50.

Woodford, M. R. et al. (2016b). The FNIP co-chaperones decelerate the Hsp90 chaperone cycle and enhance drug binding. *Nature communications* 7, 12037.

Woodford, M. R. et al. (2017). Tumor suppressor Tsc1 is a new Hsp90 co-chaperone that facilitates folding of kinase and non-kinase clients. *The EMBO journal* 36, 3650–3665.

Workman, P., Burrows, F., Neckers, L., and Rosen, N. (2007). Drugging the cancer chaperone HSP90: combinatorial therapeutic exploitation of oncogene addiction and tumor stress. *Annals of the New York Academy of Sciences* 1113, 202–216.

Wu, H., Hyun, J., Martinez-Yamout, M. A., Park, S. J., and Dyson, H. J. (2018). Characterization of an Hsp90-Independent Interaction between Co-Chaperone p23 and Transcription Factor p53. *Biochemistry* 57, 935–944.

Wu, S., Hong, L., Wang, Y., Yu, J., Yang, J., Yang, J., Zhang, H., and Perrett, S. (2020). Kinetics of the conformational cycle of Hsp70 reveals the importance of the dynamic and heterogeneous nature of Hsp70 for its function. *Proceedings of the National Academy of Sciences of the United States of America* 117, 7814–7823.

Wu, Y., Li, J., Jin, Z., Fu, Z., and Sha, B. (2005). The crystal structure of the C-terminal fragment of yeast Hsp40 Ydj1 reveals novel dimerization motif for Hsp40. *Journal of molecular biology* 346, 1005–1011.

Wu, Z., Gholami, A. M., and Kuster, B. (2012). Systematic identification of the HSP90 candidate regulated proteome. *Molecular & cellular proteomics* 11, M111.016675.

Xie, L. and Jakob, U. (2019). Inorganic polyphosphate, a multifunctional polyanionic protein scaffold. *The Journal of biological chemistry* 294, 2180–2190.

Xu, W., Marcu, M., Yuan, X., Mimnaugh, E., Patterson, C., and Neckers, L. (2002). Chaperone-dependent E3 ubiquitin ligase CHIP mediates a degradative pathway for c-ErbB2/Neu. *Proceedings of the National Academy of Sciences of the United States of America* 99, 12847–12852.

Xu, Y and Lindquist, S (1993). Heat-shock protein hsp90 governs the activity of pp60v-src kinase. *Proceedings of the National Academy of Sciences of the United States of America* 90, 7074–7078.

Xu, Y, Singer, M. A., and Lindquist, S (1999). Maturation of the tyrosine kinase c-src as a kinase and as a substrate depends on the molecular chaperone Hsp90. *Proceedings of the National Academy of Sciences of the United States of America* 96, 109–114.

Yan, M., Li, J., and Sha, B. (2011). Structural analysis of the Sil1-Bip complex reveals the mechanism for Sil1 to function as a nucleotide-exchange factor. *The Biochemical journal* 438, 447–455.

Yan, W and Craig, E. A. (1999). The glycine-phenylalanine-rich region determines the specificity of the yeast Hsp40 Sis1. *Molecular and cellular biology* 19, 7751–7758.

Yang, Y., Liu, B., Dai, J., Srivastava, P. K., Zammit, D. J., Lefrançois, L., and Li, Z. (2007). Heat shock protein gp96 is a master chaperone for toll-like receptors and is important in the innate function of macrophages. *Immunity* 26, 215–226.

Yoshida, S. et al. (2013). Molecular chaperone TRAP1 regulates a metabolic switch between mitochondrial respiration and aerobic glycolysis. *Proceedings of the National Academy of Sciences of the United States of America* 110, E1604–E1612.

Young, J. C. (2010). Mechanisms of the Hsp70 chaperone system. *Biochemistry and cell biology* 88, 291–300.

Yu, H. Y., Ziegelhoffer, T., and Craig, E. A. (2015a). Functionality of Class A and Class B J-protein co-chaperones with Hsp70. *FEBS letters* 589, 2825–2830.

Yu, H. Y., Ziegelhoffer, T., Osipiuk, J., Ciesielski, S. J., Baranowski, M., Zhou, M., Joachimiak, A., and Craig, E. A. (2015b). Roles of intramolecular and intermolecular interactions in functional regulation of the Hsp70 J-protein co-chaperone Sis1. *Journal of molecular biology* 427, 1632–1643.

Yu, Y., Hamza, A., Zhang, T., Gu, M., Zou, P., Newman, B., Li, Y., Gunatilaka, A. A. L., Zhan, C.-G., and Sun, D. (2010). Withaferin A targets heat shock protein 90 in pancreatic cancer cells. *Biochemical pharmacology* 79, 542–551.

Zhang, F., Snead, C. M., and Catravas, J. D. (2012). Hsp90 regulates O-linked b-N-acetylglucosamine transferase: a novel mechanism of modulation of protein O-linked b-N-acetylglucosamine modification in endothelial cells. *American journal of physiology. Cell physiology* 302, C1786–C1796.

Zhang, M., Botër, M., Li, K., Kadota, Y., Panaretou, B., Prodromou, C., Shirasu, K., and Pearl, L. H. (2008). Structural and functional coupling of Hsp90- and Sgt1-centred multi-protein complexes. *The EMBO journal* 27, 2789–2798.

Zhao, R. and Houry, W. A. (2007). Molecular interaction network of the Hsp90 chaperone system. *Advances in experimental medicine and biology* 594, 27–36.

Zhao, R. et al. (2005). Navigating the chaperone network: an integrative map of physical and genetic interactions mediated by the hsp90 chaperone. *Cell* 120, 715–727.

Zhao, R. et al. (2008). Molecular chaperone Hsp90 stabilizes Pih1/Nop17 to maintain R2TP complex activity that regulates snoRNA accumulation. *The Journal of cell biology* 180, 563–578.

Zheng, M., Cierpicki, T., Burdette, A. J., Utepbergenov, D., Janczyk, P. L., Derewenda, U., Stukenberg, P. T., Caldwell, K. A., and Derewenda, Z. S. (2011). Structural features and chaperone activity of the NudC protein family. *Journal of molecular biology* 409, 722–741.

Zheng, X., Krakowiak, J., Patel, N., Beyzavi, A., Ezike, J., Khalil, A. S., and Pincus, D. (2016). Dynamic control of Hsf1 during heat shock by a chaperone switch and phosphorylation. *eLife* 5.

Zhu, X, Zhao, X, Burkholder, W. F., Gragerov, A, Ogata, C. M., Gottesman, M. E., and Hendrickson, W. A. (1996). Structural analysis of substrate binding by the molecular chaperone DnaK. *Science* 272, 1606–1614.

Zhu, X.-J., Liu, X., Jin, Q., Cai, Y., Yang, Y., and Zhou, T. (2010). The L279P mutation of nuclear distribution gene C (NudC) influences its chaperone activity and lissencephaly protein 1 (LIS1) stability. *The Journal of biological chemistry* 285, 29903–29910.

Zierer, B. K., Rübbelke, M., Tippel, F., Madl, T., Schopf, F. H., Rutz, D. A., Richter, K., Sattler, M., and Buchner, J. (2016). Importance of cycle timing for the function of the molecular chaperone Hsp90. *Nature structural & molecular biology* 23, 1020–1028.

Zuehlke, A. D. and Johnson, J. L. (2012). Chaperoning the chaperone: a role for the co-chaperone Cpr7 in modulating Hsp90 function in Saccharomyces cerevisiae. *Genetics* 191, 805–814.

Zuehlke, A. D. et al. (2017). An Hsp90 co-chaperone protein in yeast is functionally replaced by site-specific posttranslational modification in humans. *Nature communications* 8, 15328.

Zuehlke, A. D., Moses, M. A., and Neckers, L. (2018). Heat shock protein 90: its inhibition and function. *Philosophical transactions of the Royal Society of London. Series B, Biological sciences* 373.

Zuiderweg, E. R. P., Hightower, L. E., and Gestwicki, J. E. (2017). The remarkable multivalency of the Hsp70 chaperones. *Cell stress & chaperones* 22, 173–189.

Zwanzig, R, Szabo, A, and Bagchi, B (1992). Levinthal's paradox. *Proceedings of the National Academy of Sciences of the United States of America* 89, 20–22.

Zúñiga, R. A., Gutiérrez-González, M., Collazo, N., Sotelo, P. H., Ribeiro, C. H., Altamirano, C., Lorenzo, C., Aguillón, J. C., and Molina, M. C. (2019). Development of a new promoter to avoid the silencing of genes in the production of recombinant antibodies in chinese hamster ovary cells. *Journal of biological engineering* 13, 59.

Acknowledgements

This thesis was prepared at the Technical University of Munich at the Chair for Biotechnology under the supervision of Prof. Dr. Johannes Buchner.

I would like to thank Prof. Dr. Johannes Buchner for giving me the opportunity to prepare my PhD thesis in his group, for offering me these very exciting projects and for his excellent scientific and personal support as well as the pleasant working atmosphere. I am also grateful for Johannes establishing and promoting a very successful research cooperation with the Martin Kampmann lab in San Francisco and making it possible for me to work there for several months in two research visits. This has been a unique personal and scientific experience. Additionally, I would like to thank him for the opportunity to attend the Hsp90 conference in 2016 and 2018, the EMBO conference in 2017 and the SFB conference in 2018.

I want to thank Prof. Dr. Martin Kampmann from the UCSF for mentoring my thesis with exceptional advice. Additionally, I would like to thank him for inviting me to work in his lab over the course of several months and giving me access to excellent scientific equipment and knowledge.

Moreover, I would like to thank Dr. Florent Delhommel, Dr. Abraham Lopez and Prof. Dr. Michael Sattler from the TU Munich, Dr. Ofrah Faust and Dr. Rina Rosenzweig from the Weizmann Institute in Israel as well as Ganesh Agam and Prof. Dr. Don Lamb from the LMU Munich for the excellent collaboration.

Additionally, I want to thank all technicians and the secretary staff of the group for their constant scientific and organizational support.

I would like to thank all my colleagues from the Kampmann lab for their help and the pleasant working atmosphere. Additionally, I want to thank my colleagues at the Buchner lab for making the last four years a great experience. In particular, I want to thank Chris, Tuan and Georg for our many fruitful discussions.

Lastly, I would like to thank my family and my wife for constantly supporting me and being there for me.

Declaration of Authorship

I, Maximilian Michael BIEBL, hereby declare that this thesis was prepared independently using only the references and resources stated herein. This work has not been presented to any examination board, yet. Parts of the work have been submitted or published in scientific journals.

Ich, Maximilian Michael BIEBL, erkläre an Eides statt, dass ich die vorliegende Arbeit selbstständig verfasst und keine anderen als die angegebenen Quellen und Hilfsmittel verwendet habe. Ich habe die Dissertation in dieser oder ähnlicher Form in keinem anderen Prüfungsverfahren als Prüfungsleistung vorgelegt. Teile dieser Arbeit wurden zur Veröffentlichung in wissenschaftlichen Journalen eingereicht.

Signed:

Date: